P
2

NASA TECHNICAL TRANSLATION NASA TT F-15,236

FLOW VISUALIZATION: OPTICAL METHODS OF ANALYZING FLUID FLOWS

R. Řezníček

Translation of Visualisace proudení: Optické metody vyšetřování proudění tekutin, Prague, "Academia" Press, 1972, 177 pages

(NASA-TT-F-15236) FLOW VISUALIZATION: OPTICAL METHODS OF ANALYZING FLOWS (Kanner (Leo) Associates) 195 p HC $11.75 CSCL 20D N74-15967 Unclas G3/12 27516

NATIONAL AERONAUTICS AND SPACE ADMINISTRATION
WASHINGTON, D.C. 20546 FEBRUARY 1974

STANDARD TITLE PAGE

1. Report No.	2. Government Accession No.	3. Recipient's Catalog No.
NASA TT F-15,236		

4. Title and Subtitle FLOW VISUALIZATION: OPTICAL METHODS OF ANALYZING FLUID FLOWS

5. Report Date February 1974

6. Performing Organization Code

7. Author(s)

R. Řezníček

8. Performing Organization Report No.

10. Work Unit No.

9. Performing Organization Name and Address

Leo Kanner Associates
Redwood City, California 94063

11. Contract or Grant No. NASw-2481

13. Type of Report and Period Covered Translation

12. Sponsoring Agency Name and Address

National Aeronautics and Space Administration, Washington, D.C. 20546

14. Sponsoring Agency Code

15. Supplementary Notes

Translation of Visualisace proudení: Optickémetody vyšetřovaní proudění tekutin, Prague, "Academia" Press, 1972, 177 pages

16. Abstract

A review is presented of all the methods of studying fluid flows which make it possible to obtain an optical recording, or image, of the properties of a flowfield and their development in time. The methods discussed include those based on the introduction of particles into a fluid which have properties differing from those of the fluid, methods in which observations are made of the changes occurring in a special coating applied to the surface of a body in a fluid flow, and methods which take advantage of natural changes occurring in the optical properties of a fluid during flow.

17. Key Words (Selected by Author(s))

18. Distribution Statement

Unclassified-Unlimited

19. Security Classif. (of this report)	20. Security Classif. (of this page)	21. No. of Pages	22. Price
Unclassified	Unclassified		

Preface

The main impetus for writing this study was the fact that so far no publication exists either in Czech or in other languages which discusses comprehensively and in sufficient breadth all methods used to study fluid flows which can optically record the image of the properties of the flow field and their development.

The majority of the methods that were mentioned belong to the group of experimental procedures called "flow visualization" ("making visible"). This nomenclature, especially the Czech term "making visible," no longer adequately describes their possibilities. It does not take into account the fact that when these methods are used, not only the image, the flow visualization, but quantitative data are required on an ever increasing scale, unlike in the first applications. In foreign languages, the term "visualization" (flow visualization, "visualitsatsiya potokov," "visualisation des écoulements") is used, whose meaning also includes the quantitative possibilities of the above-mentioned methods. In this book, we will use the term visualization as the basic term, and along with it the not altogether appropriate Czech synonym "making visible."

The extent, use and significance of visualization methods have increased to such an extent that the methods which are subsumed under the term "flow visualization" are treated as an independent field in the experimental mechanics of fluids. The need for and importance of these methods was also appreciated by the members of the American Society of Mechanical Engineers who organized, in 1960 in New York, a symposium on flow visualization. The hundreds of literature sources in which the use of these methods is mentioned also attest to their importance.

Flow visualization methods are extremely important auxiliaries in the experimental mechanics of fluids and recently became indispensible in the study of complex flow cases. The results that can be obtained with the aid of these methods are discussed in the introduction. The significance of these methods is that they help to clarify the physical basis of processes which occur in various flow cases and thus facilitate the setting up of a physical model which is a good approximation of the real process and the required basis for a theoretical analysis. The importance of these methods in machine building, agricultural and health technology follows from the above. In these fields many problems exist which are connected with the flow of fluids which cannot be solved without using flow visualization. Examples of these problems are the design of new pipes for water, steam and gas turbines, combustion chambers in steam generators and engines, parts of airplanes, ships and rockets, pneumatic and hydraulic haulage, separation of particles with different densities, capillary lifts of fluids in porous substances, heating, ventilation, cooling, preparation of spray aerosols and the motion of their particles in the atmosphere, the flow of underground water, the activity of protective wind belts, etc. The theoretical solution of problems in the fields that were mentioned is extremely difficult or practically impossible in most cases, so that designers must rely on many years of experience and technical intuition. Using flow visualization, they will be able to grasp the problem in greater depth and to obtain new bases for the design and thus improve the technical level of their work. Many films which record the flow in various technical and elementary cases with the aid of visualization methods were made abroad for this purpose.

The book was written for technical and scientific workers engaged in the field of flows and in many other fields in which problems connected with the flow of fluids occur, examples of which were given in the previous paragraph. The purpose of the book is to acquaint workers in these fields with all known flow visualization methods, to enable them to select the appropriate visualization method, and to provide the basic directives for its use. Naturally, the book can also be used for instruction purposes, especially to conceptually acquaint the students with the basic images which occur in flows around bodies.

The book was written as a reference monograph, on a level which makes the theoretical part accessible to workers with a university education, i.e. to the higher level technical and scientific staff. However, it can also be understood by lower grade technical workers provided they are interested in their field and continue their education in it. The remaining parts of the book, which are technical directives for the assembly of measuring devices and their use, can be understood by all technical workers.

Writing the book, I used the available literature sources and my own laboratory work and studies.

The standard arrangement and numbering system will hopefully ensure good referencing. The book is divided into three parts, numbered 1, 2 and 3. The parts are divided into sections, referred to by two numbers (for example, 2.1 is the first section in Part 2); whenever necessary the sections are divided into chapters referred to by three numbers (for example, 3.2.1 is the first chapter in Section 3.2), and, as needed, letters are used to denote further subdivisions within chapters. The methods discussed in individual parts, sections or chapters of the book are concisely referred to by the same number as the corresponding part, section or chapter (for example, by the methods in group 3 we shall mean concisely the methods described in Part 3, the methods in group 3.2.6 are the methods described in Chapter 3.2.6, etc.). The equations in the entire book are numbered sequentially. The bibliographical references are arranged on the basis of the subjects in conformity with the contents of individual chapters.

With regard to individual methods or groups of methods, first, the principle of the method is always discussed briefly with a subsequent analysis of its physical basis and the requirements on assembling the necessary equipment. Finally, the information necessary for the technical application of the method and a brief evaluation of the method are given. Generally, some concrete cases of its use are given as examples for each method. The reader is referred to literature sources for other applications published in the specialized literature. To provide the reader with an extensive base, the bibliographical references are very detailed and contain, in my opinion, all important special studies from the world literature dealing with the subject discussed. In all other respects, the emphasis is on generality in introducing the information, since this will enable the technical worker to apply the knowledge gained on the widest scale and most creatively and propose the most suitable equipment for the given case.

Finally, I would like to thank Prof. Engineer Dr. Rudolf Peskov, Doctor of Science, associate member, Czechoslovak Academy of Sciences, and Prof. Engineer Dr. Vaclav Smolar, Doctor of Science, for their interest in this book and for their valuable comments. My thanks are also due to Jan Chlumsky to whom I am grateful for his help in preparing the manuscript for publication. Thanks are also due to Josef Kadrmas for his help in preparing the illustrations.

Table of Contents

Page

FLOW VISUALIZATION: OPTICAL METHODS OF ANALYZING FLUID FLOWS

R. Řezníček

0. Introduction /11*

By flow visualization we mean optical methods used to analyze the flow of fluids which make it possible to obtain an optical recording, the image of the properties of the flow field. This is a field in the experimental mechanics of flows, whose goal is to obtain optically, in a short time interval, data which are used as the basis for determining the different characteristics of flows in a chosen region.

The significance of the various flow visualization methods is that they provide an image of the flow on the basis of which it is possible to form primarily a qualitative opinion about the manner of flow. Further, these methods help to clarify the physical basis of processes occurring in various cases of flow and thus facilitate the setting up of a physical model for the process which is a good approximation of the real process and the necessary basis for a theoretical analysis. In many cases visualization methods can be used to obtain quantitative data directly, without influencing the flow in most cases by foreign bodies, for example, measuring sensors. For example, if a motion picture camera is used to record changing processes during visualization, the results are free of the inaccuracies resulting from the inertia of the measuring instruments. Finally, some visualization methods are very important for instruction and pedagogical purposes.

A brief summary of the results which can be obtained by means of visualization will best illustrate the significance and importance of this field. Visualization methods make it possible to determine:

- the velocity field,
- the image of the flow around bodies,
- the shape of the streamlines,
- the velocity profiles,
- the downwash angle of the flow past the streamlined body,
- the circulation value,
- the wake and whirling regions and the manner of the flow in them,
- the mechanism for the formation of vortices, their type and properties,

---

* Numbers in the margin indicate pagination in the foreign text.

laminar flow regions,
the boundaries or transition zones of the boundary layer,
the separation of the laminar and turbulent boundary layers,
the reverse flow in the boundary layer,
the thickness of the boundary layer,
the direction, type, position and motion of shock and pressure waves, /12
the pressure distribution on the surface of the streamlined body,
the mixing behavior during the flow.

Visualization methods are mostly used to study various cases of two-dimensional flows. Sometimes these methods can also be used to study three-dimensional flows.

The flow medium, the fluid, which is either a liquid or a gas, can be considered as a continuous medium, a continuum, whose individual parts are small (we will call such small parts the particles of the fluid), which have the same physical properties as the entire medium, so that their motion or clusters cannot be recorded in most cases by the naked eye. This can be overcome by means of visualization methods which we will classify into three basic groups (groups 1, 2 and 3). The methods in group 1 are based on observing particles introduced into the fluid flow where the particles have different properties than the fluid. The methods in group 2 use coatings which are applied to the surface of the streamlined body. The methods in group 3 take advantage of the natural changes in the optical properties of the fluid which arise during the flow.

1. Methods Based on the Introduction of Particles into the Fluid Flow Where These Particles Have Different Properties Than the Flow /13

1.0. Basic Considerations

In the methods from this group, visualization is achieved with the aid of particles whose properties are different from those of the fluid flow, which are introduced into the flow either from the outside or are obtained by artificially changing the properties of some particles of the fluid flow. These particles may be in any state (gaseous, liquid, solid), and their dimensions, shape, density (specific mass), and concentration must be selected in different cases so that they follow the local direction of the flow, and gravity or inertia do not have a great effect on their motion, so that when they are present in the flow the basic character of the flow is not changed.

The particles may form in the fluid either a continuous trail, a a continuous region, or a system of trails, or they can be introduced into the flow individually in a particular geometric configuration and in equal time intervals or randomly in time or possibly also without any geometric configurations.

When the fluid flow is illuminated, these particles are visible as a result of absorption, scatter, reflection, or light refraction, and their motion can be observed either by the naked eye or with the aid of optical equipment which raises the observation sensitivity. For various purposes the recording can be obtained with the aid of a camera or any ordinary or high-speed motion picture camera. Stereoscopic photographs, stroboscopic records and high-speed snapshots can also be obtained.

During visualization with the aid of particles, images of the particle trajectories are obtained most frequently. If we chose the size and density of the visualization particles appropriately, we will determine with a certain accuracy the trajectory of the particles of the fluid. The trajectory of one particle can be recorded, for example, by a motion picture camera, or for a sufficiently long exposure time, with the aid of a camera. If interrupted illumination is used, it is possible to determine from the length of the tracks (trajectory sectors) the velocity of the particle, provided we know the frequency with which the light is interrupted.

Besides the trajectories, the streamlines must be determined, which are, by definition, the vector lines of the velocity field. This means that the streamline is the line at each point of which at the given instant the velocity has the direction of its tangent. If we are dealing with a stationary flow, i.e. a steady-state flow over time, the shape of the streamline does not /14 vary with time and the streamlines are identical with the trajectories of the particles of the fluid. On the other hand, during nonstationary flow, the above statement is not valid except in some special cases. During nonstationary flow, we obtain, for example, the streamlines by connecting the tracks (small trajectory sectors) of a large number of particles. However, the tracks must be recorded simultaneously, for example, by means of photography with a short exposure time.

To prove the above statement that during stationary flow the streamlines coincide with the trajectories we use the differential equation of the streamline:

$$\mathbf{v} \times \delta \mathbf{s} = \mathbf{o}. \tag{1}$$

In this equation

$$\mathbf{v} = \mathbf{v}(x, y, z, t) \tag{2}$$

is the velocity of the particle at the instant t at the point with coordinates x, y, z and $\delta\mathbf{s}$ is an elementary sector of the streamline which passes through this point at the instant t. The zero magnitude of the vector cross product $\mathbf{v} \times \delta\mathbf{s}$ expresses the fact that the direction of the velocity $\mathbf{v}$ is the same as the direction of the tangent of the streamline. In the proof which will be presented, we will assume that the vector function $\mathbf{v}(x,y,z,t)$ which expresses the velocity vector as a function of the coordinates and time is known, which is equivalent to knowing the three scalar functions

$$\left.\begin{aligned} v_x &= v_x(x, y, z, t), \\ v_y &= v_y(x, y, z, t), \\ v_z &= v_z(x, y, z, t), \end{aligned}\right\} \tag{3}$$

which express the velocity components of $\mathbf{v}$ as a function of the coordinates and time. In the case of stationary flow, the right members of equation (2) and (3) do not involve the time t.

From the vector differential equation (1) we obtain a system of two equations:

$$\frac{\delta x}{v_x} = \frac{\delta y}{v_y} = \frac{\delta z}{v_z}, \tag{4}$$

in which δx, δy, δz are components of the vector $\delta \mathbf{s}$, where we assumed tacitly, without loss of generality, that v_x, v_y and v_z are different from zero. Now if we denote the derivatives with respect to the variable x by primes (i.e. $\delta y/\delta x \equiv y'$, $\delta z/\delta x \equiv z'$), it is clear that equations (4) are a system of two differential equations

$$y' = f_1(x, y, z, t), \qquad z' = f_2(x, y, z, t), \tag{5}$$

where

$$f_1(x, y, z, t) \equiv \frac{v_y(x, y, z, t)}{v_x(x, y, z, t)}, \qquad f_2(x, y, z, t) \equiv \frac{v_z(x, y, z, t)}{v_x(x, y, z, t)}$$

are, by hypothesis, known functions. In equations (5) the time t is a parameter, so that they will be solved for a fixed arbitrarily chosen t. To obtain the solution means to determine y, z, which are unknown functions of the variable x and the parameter t in equations (5). We will obtain the general solution in implicit form:

$$g_1(x, y, z, t, C_1, C_2) = 0, \qquad g_2(x, y, z, t, C_1, C_2) = 0, \tag{6}$$

where C_1, C_2 are integration constants.

If we want to determine concretely the streamline which, at the chosen instant $t = t_0$, passes through the point with coordinates x_0, y_0, z_0, we first set in (6) $t = t_0$, $x = x_0$, $y = y_0$, and $z = z_0$, and calculate the constants C_1, C_2 from the two equations that were obtained. Generally, their values will depend on the chosen initial conditions, i.e. /15

$$C_1 = C_1(x_0, y_0, z_0, t_0), \qquad C_2 = C_2(x_0, y_0, z_0, t_0).$$

We then substitute the calculated values in (6) for C_1, C_2 and set $t = t_0$ and leave x, y, z expressed in general form. Each of the equations obtained:

$$g_1(x, y, z, t_0, C_1, C_2) = 0, \qquad g_2(x, y, z, t_0, C_1, C_2) = 0 \tag{7}$$

describes a plane. The unknown streamline is determined as the intersection of two planes.

In the case of a stationary flow, the time t, or its chosen value t_0, is eliminated from all previous relations. In particular, the two planes described by equations (7) will not depend on t_0; hence, their intersection will also not depend on t_0, and the streamline passing through the point with the arbitrarily selected coordinates x_0, y_0, z_0 will not change its shape with time.

With regard to the trajectories of the particles of the fluid, we obtain them from the three equations which define the velocity components of **v**:

$$v_x = \frac{dx}{dt}, \quad v_y = \frac{dy}{dt}, \quad v_z = \frac{dz}{dt}. \tag{8}$$

Here dx, dy, dz are the components of an elementary sector ds of the trajectory of a particle of the fluid. If we denote the derivatives with respect to time by a dot (i.e. $dx/dt \equiv \dot{x}$, $dy/dt \equiv \dot{y}$, $dz/dt \equiv \dot{z}$) and substitute for v_x, v_y, v_z the functions in the right members of equations (3) which are assumed to be known, equations (8) become the system of three differential equations:

$$\dot{x} = v_x(x, y, z, t), \qquad \dot{y} = v_y(x, y, z, t), \qquad \dot{z} = v_z(x, y, z, t), \tag{9}$$

in which x, y, z are unknown functions of time t.

Generally the solution of this system is obtained in implicit form:

$$\begin{aligned} \varphi_1(x, y, z, t, C_1, C_2, C_3) &= 0, \\ \varphi_2(x, y, z, t, C_1, C_2, C_3) &= 0, \\ \varphi_3(x, y, z, t, C_1, C_2, C_3) &= 0, \end{aligned} \tag{10}$$

where C_1, C_2, C_3 are integration constants which are determined from the initial condition that, at the instant $t = t_0$, the particle is at the point with coordinates x_0, y_0, z_0, i.e. the values of the constants C_1, C_2, C_3 generally depend on the initial conditions:

$$C_1 = C_1(x_0, y_0, z_0, t_0), \quad C_2 = C_2(x_0, y_0, z_0, t_0), \quad C_3 = C_3(x_0, y_0, z_0, t_0). \tag{11}$$

Eliminating from equations (10) the time t, we obtain the two equations:

$$\varphi_1(x, y, z, C_1, C_2, C_3) = 0, \qquad \varphi_2(x, y, z, C_1, C_2, C_3) = 0, \tag{12}$$

each of which describes a plane. The unknown trajectory is the intersection of these planes.

We note that the planes (12) are independent of t, but do depend, because of the relations (11), on t_0. Only in a stationary flow when the right members of equations (9) do not involve the variable t, t and t_0 are also eliminated in the general case from the relations (10), (11), and (12), so that the shape of the trajectory will be independent of time, and all particles which pass through the point with coordinates x_0, y_0, z_0 (at any instant) will have the same trajectory.

Having analyzed the question of the streamlines and of the trajectories in complete generality, we will finally prove that they are identical in a stationary flow. It suffices to know that, if the right members of equations (3) do not involve the variable t, we obtain for the flow lines instead of (5), the system of equations: /16

$$y' = F_1(x, y, z), \qquad z' = F_2(x, y, z), \tag{13}$$

in which

$$F_1(x, y, z) \equiv \frac{v_y(x, y, z)}{v_x(x, y, z)}, \qquad F_2(x, y, z) \equiv \frac{v_z(x, y, z)}{v_x(x, y, z)} \tag{14}$$

are known functions. Next, when the trajectories are determined, the time t need not be eliminated from relations (10), but can already be eliminated from equations (9) through division. Since

$$\frac{\dot{y}}{\dot{x}} = \frac{\frac{\mathrm{d}y}{\mathrm{d}t}}{\frac{\mathrm{d}x}{\mathrm{d}t}} = \frac{\mathrm{d}y}{\mathrm{d}x} \equiv y', \qquad \frac{\dot{z}}{\dot{x}} = \frac{\frac{\mathrm{d}z}{\mathrm{d}t}}{\frac{\mathrm{d}x}{\mathrm{d}t}} = \frac{\mathrm{d}z}{\mathrm{d}x} \equiv z',$$

we obtain, using the notation introduced for relations (14), a system of differential equations for the trajectories

$$y' = F_1(x, y, z), \qquad z' = F_2(x, y, z), \tag{15}$$

which is identical to the system (13) used to determine the streamlines. This proves that in a stationary flow, the trajectories and the flow lines are identical.

The criteria for the selection of the type of visualization particles in a concrete case are based on the equation of motion of these particles in the fluid flow. When we derive this equation below, we will use the following notation:

m = mass
ρ = density } of visualization particle
V = volume
d = characteristic linear dimension of visualization particle in direction perpendicular to its relative velocity u with respect to the surrounding medium (when the particle is spherical d is its diameter)
p = pressure
ρ' = density } of fluid
ν = kinematic viscosity coefficient
g = acceleration due to gravity.

We will associate with the acceleration **a** and the velocity **v** the subscript P or T depending on whether the magnitude refers to the visualization particle P or a particle of the fluid flow T. Consequently,

$$\mathbf{u} = \mathbf{v}_P - \mathbf{v}_T$$

will denote the relative velocity of the visualization particle P with respect to the surrounding medium T. The magnitude of the relative velocity **u** will be denoted by u.

The following forces are acting on the particle P in the fluid flow:

1. its weight **G**:

$$G = mg = \rho V g, \tag{16}$$

2. the resultant **F** of the pressure forces exerted by the surrounding fluid on the particle P[1]: /17

---

[1] In a fluid at rest the force F is identical with the so-called upward pressure, known from the Law of Archimedes.

$$F = -V \operatorname{grad} p, \tag{17}$$

3. the hydrodynamic force H:

$$H = -\varrho' \frac{Vu}{d} f\left(\frac{ud}{\nu}\right) u, \tag{18}$$

where the function f takes on only positive values. The argument of the function f is dimensionless, it is the so-called Reynolds number $Re \equiv ud/\nu$, and the value of the function f is dimensionless, so that here the function f is a coefficient which varies in accordance with the Reynolds number.

According to Newton's Second Law we have:

$$G + F + H = m a_P. \tag{19}$$

When we rearrange this equation so that the right member is zero, we have, in the left member, the expression $-ma_P$, which is often called inertia. After substitution of the relations (16), (17), (18) and division by the expression $-V$, the equation of motion (19) for the particle P in the fluid flow will take on the form

$$\varrho\, a_P - \varrho g + \operatorname{grad} p + \varrho' \frac{u}{d} f\left(\frac{ud}{\nu}\right) u = 0. \tag{20}$$

On the other hand, for a particle T of the fluid, we obtain analogously the equation of motion

$$\varrho' a_T - \varrho' g + \operatorname{grad} p = 0. \tag{21}$$

Subtracting this equation from the previous equation we obtain, after modification, the relation

$$\varrho\, a_P - \varrho' a_T = -\varrho' \frac{u}{d} f\left(\frac{ud}{\nu}\right) u + (\varrho - \varrho') g. \tag{22}$$

The equations that were presented can often be simplified. Thus, when the relative velocity $u = v_P - v_T$ is sufficiently small, the hydrodynamic force $\mathbf{H}$ is directly proportional to the relative velocity $\mathbf{u}$, so that we can write, instead of (18)

$$H = -mKu, \tag{23}$$

where K is a coefficient whose dimension is s^{-1}, which is always positive and depends on the viscosity of the fluid, the shape and dimensions of the particle P. Using this expression instead of equation (18), we obtain, instead of (22), the equation

$$\varrho a_P - \varrho' a_T = -\varrho K u + (\varrho - \varrho')g. \tag{24}$$

In the study of fluid flows it is always possible to find visualization particles whose density ρ is approximately equal to the density of the fluid ρ'. For $\rho = \rho'$, the previous equation becomes /18

$$a_P - a_T = -Ku,$$

i.e., the equation

$$\frac{du}{dt} = -Ku,$$

which has the solution

$$u = u_0 e^{-Kt},$$

where $\mathbf{u}_0$ is the relative velocity at time $t = 0$ and $K > 0$ as was already mentioned. When $\mathbf{u}_0$ is small, which must be assumed since the original relations (23) and (24) are only valid for small relative velocities, the relative velocity $\mathbf{u}$ decreases exponentially with time for $\rho = \rho'$, so that $\mathbf{v}_P \rightarrow \mathbf{v}_T$ and the trajectories of the visualization particles P which satisfy the condition $\rho = \rho'$ almost do not differ from the trajectories of the particles of the fluid. For example, for a spherical visualization particle P with diameter $d = 10^{-4}$ m in water at a temperature of 18°C we find, with the aid of the well known Stokes formula, that $K = 1800\ s^{-1}$, so that in this case, when the density of the particles is approximately equal to the density of water, the ratio u/u_0 drops already in approximately $2.5 \cdot 10^{-3}$ sec to the value $0.01 = 1\%$.

If solid particles are used to visualize the flow of a gas, the possibility of a simplification follows from the fact that the gas (fluid) has a much smaller density than the visualization particles, so that the term $\rho' \mathbf{g}$ compared to the term $\rho \mathbf{g}$ can be ignored in equation (22). Further, if we restrict ourselves to the case of small relative velocities $\mathbf{u}$, when the velocities $\mathbf{v}_P$, $\mathbf{v}_T$ are of the same order of magnitude and hence, the accelerations $\mathbf{a}_P$, $\mathbf{a}_T$ are also of the same order of magnitude, we can also ignore the term $\rho' \mathbf{a}_T$ compared to the term $\rho \mathbf{a}_P$. In addition we can again use equation (23) instead of (18) as the expression for the hydrodynamic force $\mathbf{H}$. Finally, if the term $\mathbf{g}$ can also be ignored relative to $\mathbf{a}_P$, we obtain the equation

$$\mathbf{a}_P = K(\mathbf{v}_T - \mathbf{v}_P), \qquad (25)$$

which we write as two equations in the components, chosing the axes in the direction of the tangent (the direction of $\mathbf{v}_P$) and the principal normal to the trajectory of the particle P. After division of the first equation by the velocity $v_P = ds_P/dt$, where ds_P is an element of length of the trajectory of the particle P, we obtain

$$\left.\begin{aligned} \frac{\mathrm{d}v_P}{\mathrm{d}s_P} &= \frac{K(v_T \cos\alpha - v_P)}{v_P}; \\ \frac{v_P^2}{R_P} &= K\, v_T \sin\alpha; \end{aligned}\right\} \qquad (26)$$

where α is the angle subtended by the vectors $\mathbf{v}_P$, $\mathbf{v}_T$, and R_P is the radius of curvature of the trajectory at the point under consideration. Using the notation /19

$$\frac{v_P - v_T}{v_P} = \lambda, \qquad (27)$$

the equations can be modified to

$$\left.\begin{aligned} (1-\lambda)\cos\alpha &= 1 + \frac{1}{K}\frac{\mathrm{d}v_P}{\mathrm{d}s_P}, \\ (1-\lambda)\sin\alpha &= \frac{1}{K}\frac{v_P}{R_P}. \end{aligned}\right\} \qquad (28)$$

Among the quantities which occur in the relations that have just been derived, v_P, R_P and dv_P/ds_P can be measured from photographs. The magnitude of the velocity v_P of the visualization particle is easily determined from the photograph when interrupted illumination is used with a known frequency. Physically, dv_P/ds_P is the change in the magnitude of the velocity v_P of the particle P during a displacement of unit length along the trajectory. With regard to the constant K of the given visualization particles in the given gas, it can be determined by an independent experiment in which we observe the motion of the visualization particles (powder) in a very slow rising vertical gas flow or the velocity at which they drop in a gas at rest.

When the values R_P, v_P, dv_P/ds_P and K are known, we can calculate the values of the parameters α and λ, which characterize the visualization fidelity of the flow of the gas under consideration from equations (28), since α is the angle of error of the trajectory of the visualization particle P and the trajectory of the gas (flow) particle T, which, in the absence of the particle P, was at the same point. According to (27) λ is the relative difference in the magnitudes of their velocities at this point. Visualization fidelity will clearly be achieved if the values of α and $|\lambda|$ are small. For small α and $|\lambda|$, equations (28) can be simplified:

$$\left.\begin{aligned} \lambda &= -\frac{1}{K}\frac{dv_P}{ds_P}, \\ \alpha &= \frac{1}{K}\frac{v_P}{R_P}. \end{aligned}\right\} \qquad (29)$$

where α is in radians.

It should also be emphasized that the values of α, λ refer to the given point in the flow field, so that to evaluate the visualization fidelity in the entire flow region under consideration, it is necessary to determine (for the known K) R_P, v_P, dv_P/ds_P at a sufficient number of points in this region, and thus find both for α and λ the interval of their values. For example, for $K = 50{,}000\ \mathrm{sec}^{-1}$, which corresponds to very fine aluminum power in air and for $v_P \leq 100$ m/sec, $R_P \geq 8\cdot10^{-2}$ m and /20
$|dv_P/ds_P| \leq 500\ \mathrm{sec}^{-1}$, we obtain: $\alpha \leq 1.5°$, $|\lambda| \leq 0.01 = 1\%$. On the basis of the required accuracy of the results we must decide whether the visualization fidelity achieved is acceptable. If it is not acceptable, i.e. if we require that the limiting values for α and $|\lambda|$ be smaller than the values that we obtained, equations (28) or (29) together with the intervals of values for R_P, v_P, dv_P/ds_P can be used to determine the required K, i.e. they can be used as a guide to find more appropriate visualization particles (powder) [98, 112].

1.1. Use of Methods from Group 1 for the Visualization of Fluid Flows

1.1.1. Methods Based on the Use of Particles Forming Continuous Trails or Relatively Large Continuous Regions

(The use of various dyes. Use of chemical reactions with color effects. Electrolytic method.)

Various fluids, especially dyes introduced into the flow by thin tubes, nozzles, can be used to form colored trails. For example, malachite green, methylene blue, with a bit of Bismark blue, fuchsin, indigo, methylene violet, ponceau (bright red) or any aniline dye, first mixed with a small amount of alcohol and then with a sufficient amount of water can be used. Next, india ink, ink, milk, an aqueous solution of potassium permanganate, and oil dyed black by fat-free nigrisine can also be used. Oil is particularly suitable for experiments in which it is necessary to retain the trail on a long, relatively thin path, since, in comparison with highly concentrated dyes, it diffuses much less in the medium [1]. The density of the selected visualization fluid must first be brought to the required value by mixing it with another fluid. During the photography, visualization fluids which absorb the blue end of the spectrum are advantageous, since the photographic material is most sensitive at these wavelengths of light.

Electrolysis is also used to form trails [1, 27]. The source for particles with different properties than those of the fluid flow (electrolyte) in which these particles form trails is the electrode (or several electrodes), which may also be part of the model (the streamlined body). When the fluid flow is an appropriate electrolyte (often ordinary water from the faucet can be used) and the current circuit between this electrode and the next electrode with opposite polarity is closed, the electrolysis products on the electrode can be eliminated in the form of a gas, whose small bubbles are carried by the fluid flow and form the required trails,, or these products can acquire, as a result of /21
secondary reactions with the electrolyte, a color which is different from the color of the electrolyte, forming colored strips in the electrolyte flow. Similar results can be achieved with the aid of electrochemoluminescence (see below).

Similarly, the chemical reaction which manifests itself as a change in the color of the fluid flow as a result of the effect of light can be used [39, 40]. The original yellow-green solution [39] acquires a blue color at the spot where it is illuminated as a result of a light flash of high intensity. Thus it is possible to obtain in the fluid flow regions (for example), strips of different colors without disturbing the flow by parts (tubes, wires, elctrodes) which introduce the dye into the flow. For example, using this method the development of the velocity profile above the streamlined body can be well observed.

Among the methods which use particles forming connected regions in the fluid flow various methods for visualizing the mixing processes (mixing) during the flow must also be mentioned. These include primarily the use (of one or several) fluids of different colors, which are introduced into the colored or colorless fluid whose flow is being studied, which mix with each other and with the fluid flow, forming color shades, which characterize the manner in which they mix. For the same purpose, various visualization fluids are used, in particular, dyes which are introduced into the flow through a nozzle, which considerably change the color when they react with an acid, a base or an appropriate dissolved salt introduced with the aid of another nozzle. Sometimes it is convenient if such a reaction is relatively slow and occurs with a certain time lag whose value can be influenced by choosing the reacting substances so that a pronounced change in the color occurs only at a certain distance from the place where the reacting substances mix [63]. Finally, if an analysis of mixing processes must determine the boundaries of turbulent mixed flow, it is advantageous to apply a thick color coating to the surface of the streamlined body which dissolves in the fluid flow around the body. The intensity of its discoloration marks well the mixing boundaries.

A three-dimensional flow can also be studied with the aid of trails of different colors which are introduced into the fluid flow. Thus, if the fluid flows primarily in the direction of the X axis, we introduce into the flow in several planes parallel to the XY plane colored trails in such a way that the trails introduced in the same plane have the same color and a different color in each plane. These trails are deformed in the flow. When the flow is three-dimensional, generally every trail acquires the shape of a three-dimensional curve. If we take simultaneously two colored photographs, one in the direction of the Y axis, and the other in the direction of the Z axis, we can determine the velocity field from the change in the shape of the trails. From the first photograph we find the velocity components in the XZ plane, and from the second, the components in the XY plane [33].

The experimental equipment for applying the methods that were mentioned is extremely simple. It consists of a hydraulic channel or tunnel or only of transparent pipes and of the illuminating and recording equipment (camera, motion picture camera). The design of a simple hydraulic channel is illustrated in Fig. 2. The hydraulic channels which are usually used have a closed circuit and their design and equipment are outlined in Figs. 1, 3 and 4. /22

The requirements on the illumination when these methods are used are also not particularly demanding. The light source used are bulbs, arc lamps, and high performance discharge tubes. The direction of the ray is usually perpendicular to the plane of flow (in a two-dimensional flow). It is desirable that the observed field be uniformly illuminated with the aid of a condenser and an appropriate reflector or a plane illuminating body. The observation or recording are usually carried out on the look-through part of the tunnel which is opposite to the light source. Hence, extinction (absorption and scattering) of the light by visualization particles is used predominantly.

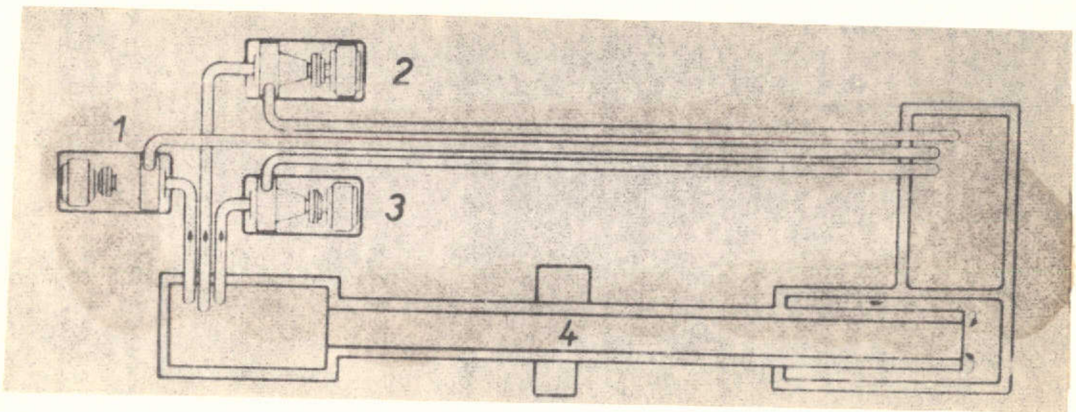

Fig. 1. Schematic diagram of hydraulic channel (1, 2, 3 -- pumps; 4 -- observation space with glass side walls).

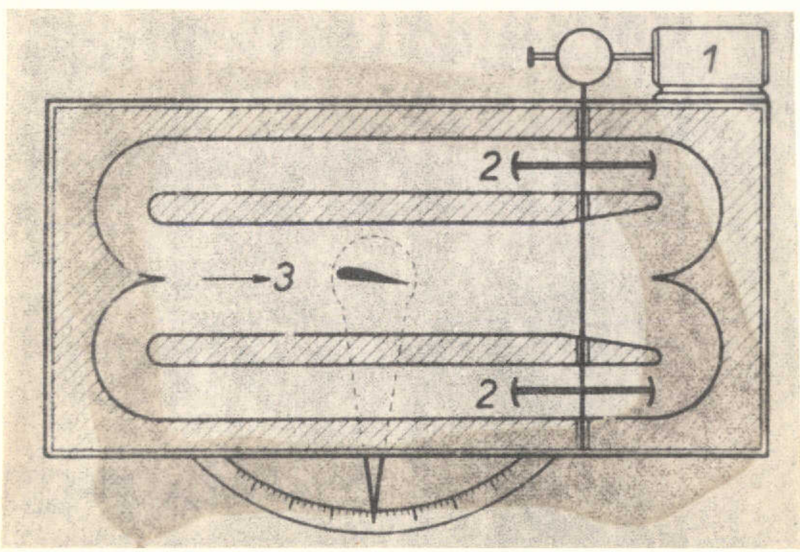

Fig. 2. Schematic diagram of hydraulic channel (1 -- motor; 2 -- bladed wheels; 3 -- observation space).

In some cases, mainly when the electrolytic method is used, ordinary illumination and the methods from group 1.1.2 are used. This illumination is illumination through a slit, where the "plane" of rays (the plane pencil of rays) is parallel to the plane of the flow. The observation or photography direction is perpendicular to the plane of the flow. /23

We will now give a number of concrete cases where the method that were discussed are applied. We will start with Reynolds' method for analyzing the character of a flow in pipes [24]. In this case the /24

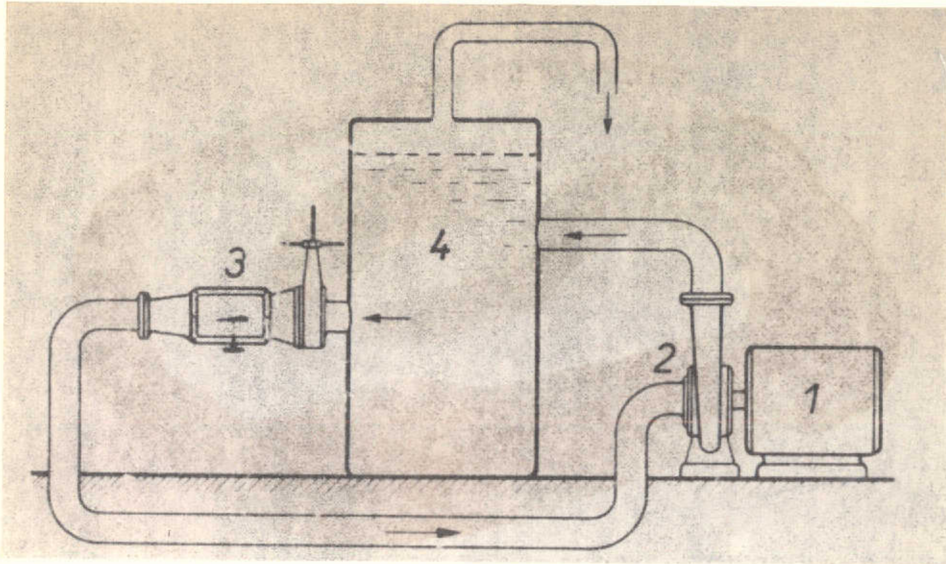

Fig. 3. Schematic diagram of hydraulic channel (1 -- motor; 2 -- pump; 3 -- observation space; 4 -- reservoir).

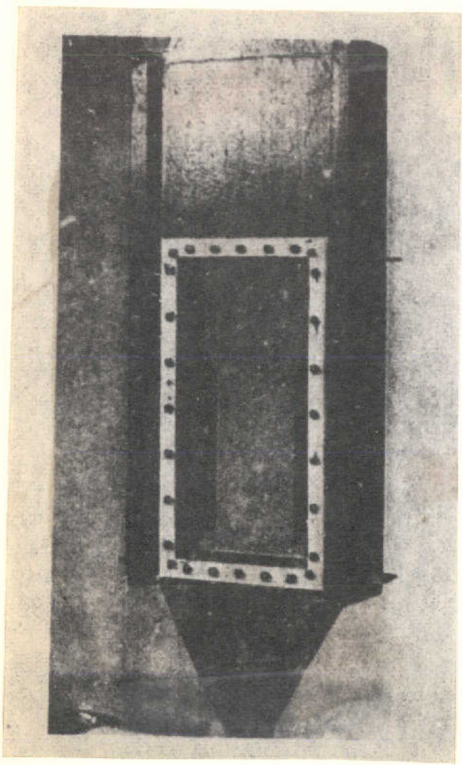

Fig. 4. Hydraulic channel observation space [10].

visualization is used to determine the transition from laminar flow to turbulent flow, and quantitative data are also obtained, for example, the critical value of Reynolds number. Reynolds' experimental equipment consists of a vessel with the fluid in which the level is held constant. A replaceable measuring tube with a sleeve is inserted in the vessel. The flow rate in the tube is regulated by a cock. The dye is brought from the small tank into the tube with the aid of a thin nozzle. In a laminar flow, the dye forms a thin trail which does not mix with the remaining fluid. In a turbulent flow, the colored trail disappears, and the dye spreads gradually into the entire fluid flow. The results obtained are shown in photographs 5 [5]. The photographs of vortices formed during flow around a cylinder and sphere were obtained in a similar manner (Fig. 6) [10].

Another example which must not be omitted is the so-called Hele-Shaw analogy [25, 26] in which the flow of a /25

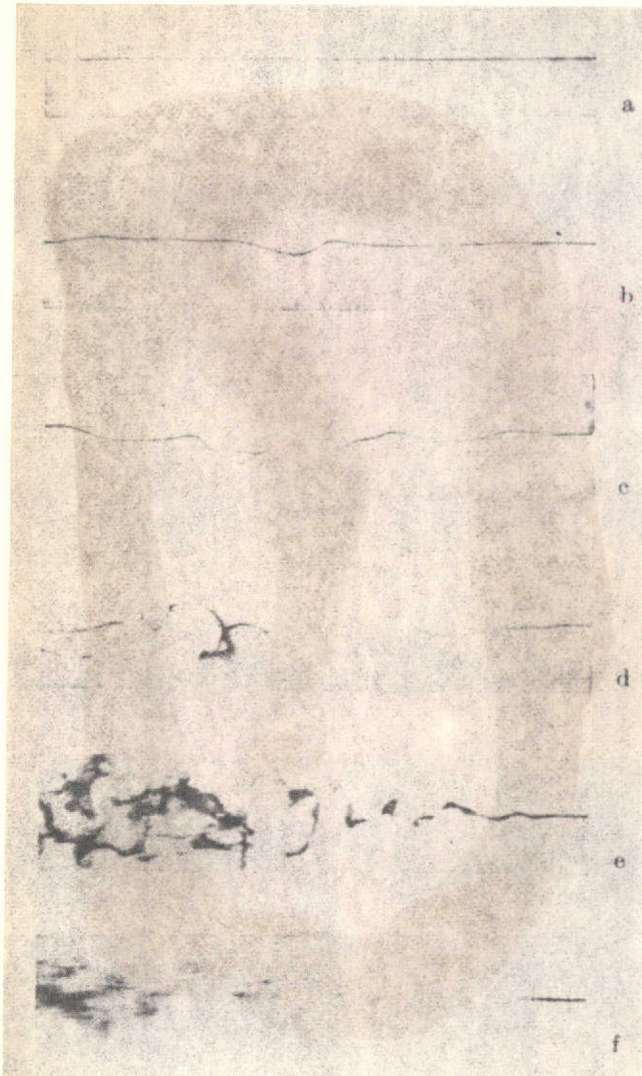

Fig. 5. Photograph of colored trail during Reynolds experiment. Photographs 5 a through 5 f show the transition from laminar flow to turbulent flow [10].

viscous fluid between two walls (plates) which are very close is visualized. Using the appropriate equipment, very clear images of the flow are obtained, which are a very good aid in teaching. However, originally this method served as the analogy for a two-dimensional steady-state potential flow of an incompressible fluid, which is possible when the distance between the plates is very small and the fluid has a sufficiently high viscosity. A sketch of the original equipment is given in Fig. 7a. The flow takes place between two glass plates at a negligible distance from each other, so that the viscosity forces dominate considerably the inertial forces. The distance between the plates is ensured by a metallic packing, and the plates are pressed toward each other by clamps. The section through the body around which the flow must be studied is cut out from a metallic sheet of the same thickness as the metallic packing and is inserted between the glass plates. Preferably,
the model and the glass plates /26
used in the experiment should be assembled under the water so that no air bubbles are left in the observation space. The streamlines are visualized by the dye which is introduced through several openings and can be observed by the naked eye, or they can be photographed, or possibly projected on a screen with the aid of a diascope. In the original experiment, the fluid flow was glycerine (the distance between the plates was 0.127 mm and the pressure needed for the glycerine flow between them was 7-15 atm) and the dye used for the

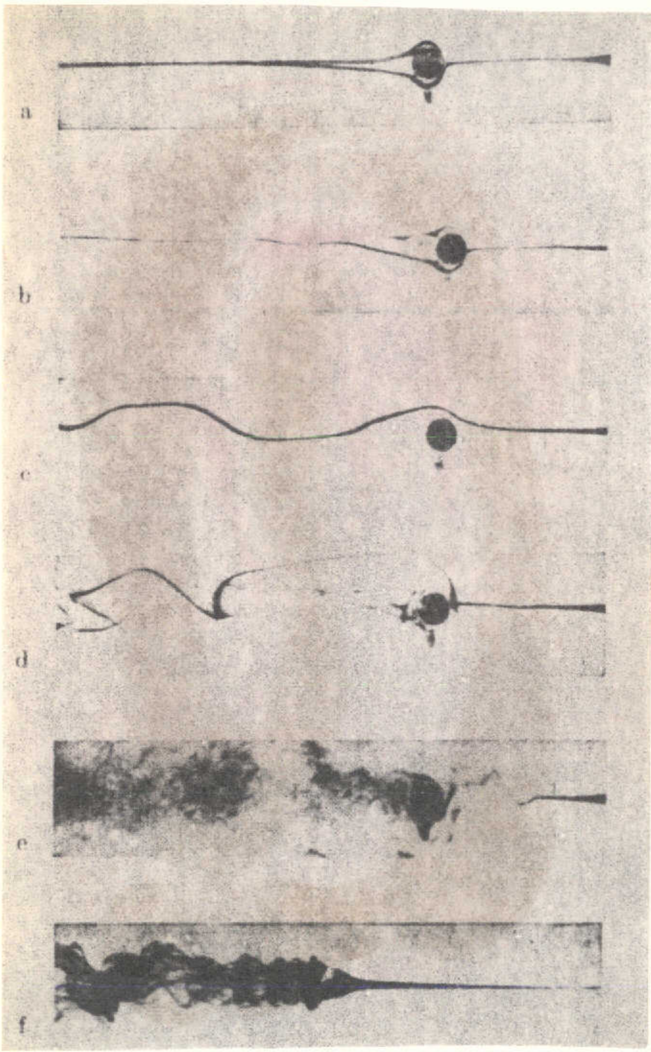

Fig. 6. Photograph of colored trail during the flow around a cylinder (6 a to 6 e) and sphere (6 f) in a small hydraulic channel [10].

visualization was a mixture of pyrogallol-carbonic acid and iron monosulfide neutralized with ammonia. However, water can also be used with good results, and a solution of potassium permanganate as the dye, which must be filtered to prevent the clogging of the inlet openings. The pressure in the horizontal pipes is adequate for the flow of the water between the plates, and the flow rate can be regulated by a cock at the water supply. The potassium permanganate solution is forced into the flowing water by the small overpressure which is obtained by placing the vessel with the solution at the appropriate height. The equipment that was described makes it possible, in addition to visualizing the flow around bodies of different shapes, to also obtain the images of the flow past a depression and the source, by drilling in one of the glass plates a hole and letting in or pumping /27
out the fluid flow through this hole. The wake region can also be visualized distinctly with it, since in this region in which the fluid is at rest, the dye will remain for a certain period after the supply of the dye was stopped so that the remaining fluid flow around the analyzed model is no longer discolored. See Fig. 8.

Another method of using colored trails to visualize the flow around a delta wing and the vortices at the edges of a delta wing (Figs. 9, 10) was applied in a hydraulic tunnel. The dye used was milk which was introduced into the stream through openings in the model whose surface was coated with a black dull paint [29].

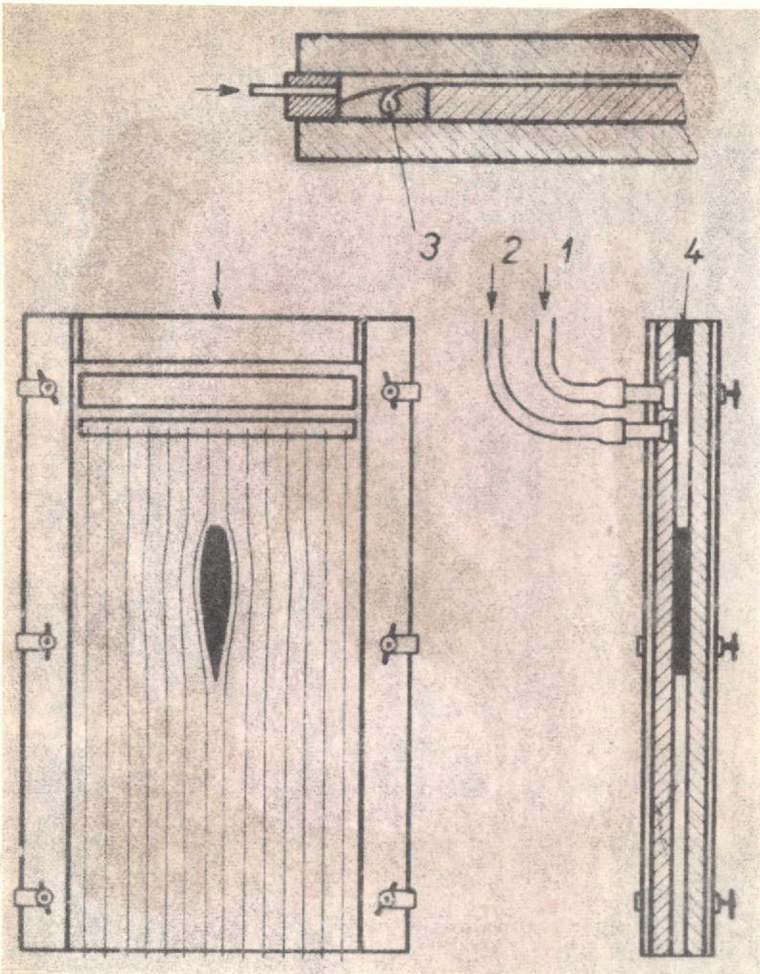

Fig. 7 a. Schematic diagram of equipment according to Hele-Shaw (1. water supply; 2. colored fluid inlet; 3. detail in colored fluid outlet and seal).

To illustrate the electrolytic method we first mention the method used by Wortmann [27], which also provides quantitative data during laminar flow. In this method the cathode is a tellurium wire, the anode can be made from any metal and the electrolyte is the water flow (water from a pipe, i.e. water which is not chemically pure). According to Wortmann, after the current is switched on, as a result of superposition of a number of physical-chemical processes, the ions are discharged from the tellurium cathode and then during the secondary reactions are converted into colloidal elementary tellurium (tellurium atoms) forming black clusters in the water which descend at a rate less than 10^{-4} m/sec, and whose diffusion rate does not exceed 10^{-6} m/sec. When the wire cathode is placed across the flow and covered with an insulating coating which was damaged in several equally spaced spots, black colloidal /28
tellurium clusters are formed during the passage of the current only in the exposed spots, which are carried by the water flow forming black trails in it. On the other hand, when the development of the velocity profile is studied, it is more convenient if the colloidal tellurium is formed along the entire cathode placed across the flow in certain equal time intervals, which is achieved with the aid of short current pulses whose duration is on the order of 10^{-3} sec. During each pulse a thin black colloidal tellurium trail is formed at the cathode which is transversal to the direction of the flow, and the train of pulses forms a sequence of such trails. The trails that are formed are carried by the fluid flow and the change in their shape indicates the development of the velocity profile (see Fig. 11 a, which shows the flow at the bottom of a bent channel, and Fig. b on which,

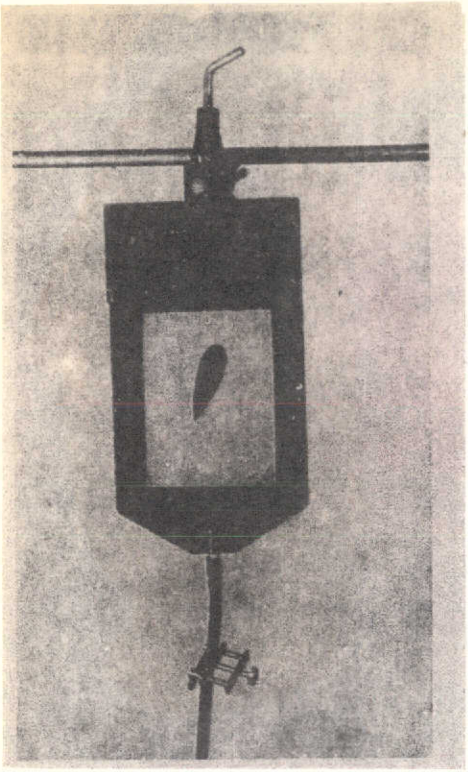

Fig. 7b. Photograph of simple apparatus for visualizing the flow according to the Hele-Shaw method. The reservoirs for both fluids are attached to the top part of the apparatus. The observation space is arranged so that it can be inserted in the projector instead of the diapositive. It is a product of the firm Phylatex, German Democratic Republic.

in addition to the velocity profile, visualized by one trail, a part of another trail formed earlier can be seen at the bottom near the wall W). An ordinary camera can be used for the photography with an exposure time greater than $2 \cdot 10^{-3}$ sec, and for the illumination a projector lamp with a gas discharge tube.

Another useful electrolytic method uses as the electrolyte a treated aqueous solution of thymol blue in a 0.01 weight % concentration [44]. The solution is first mixed with a small amount of sodium hydroxide, through which it acquires a deep blue color, and then hydrochloric acid is added until the /29
titration stop is exceeded and the color of the solution changes from blue to yellow. After the current is turned on, the solution in the immediate vicinity of the anode turns blue again, which can be used, analogously as in the Wortmann method, to obtain colored trails in the electrolyte stream. The best results were achieved with electrodes made from platinum wires with a 0.05 mm diameter and a current intensity of 5 mA. When the electrode is made from a wire mesh and placed /31
perpendicularly to the dominant direction of the flow, the colored trails that are obtained can also be used to observe well a three-dimensional flow.

The method that was described is only suitable for the study of flows with very small velocities (up to 5 cm/sec), since at greater velocities the colored trails are no longer distinct. The advantage of the method is that the electrochemical reaction on the anode does not lead to a change in specific gravity, so that that part of the fluid which turned blue as a result of this reaction has the same specific gravity as the original solution. This makes it possible to visualize the spontaneous flow caused in the fluid by the difference in the specific gravities which arise, for example, as a result of nonuniform heating. The method, like Wortmann's method, also provides quantitative data. Specifically,

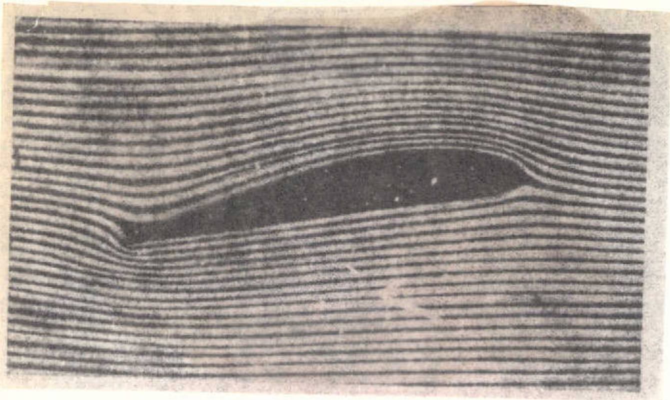

Fig. 8a. Photograph of flow around a profile obtained using the equipment in Fig. 7 a [5].

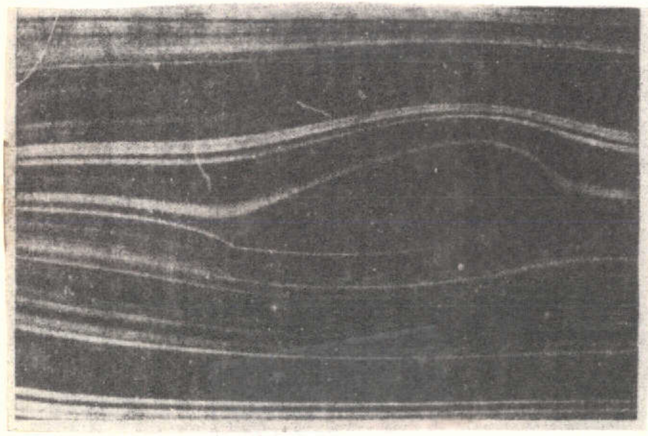

Fig. 8b. Photograph of a flow around a profile obtained using the equipment in Fig. 7b [10].

instead of a direct current, current pulses can be used in it and the local velocities of the flow can be obtained from the photographs [44]. Yellow or orange filters can be used conveniently in the photography and a sodium discharge tube is suitable for the illumination.

Fig. 12 can be used to illustrate the electrolytic methods, which shows the visualization trails formed by the oxygen bubbles obtained by water electrolysis [64].

Recently, as we already mentioned, electrochemoluminescence was also used for visualizing the flow [37, 38, 45]. When this method is used, two electrodes are immersed in a specially prepared solution [37]. When there is a current between them, a bluish glow appears on the anode whose intensity depends on the mass transfer between the electrolyte and the anode. This glow reaches a distance which is smaller than the thickness of the laminar boundary layer. When the voltage is increased above a certain limiting value, it is detached from the anode and it moves with the fluid flow. However, the images that are formed are neither streamlines nor trajectories. According to the arrangement in [37], this limiting value is 1.5 V. The method can be used, for example, to study flow around bodies of various shapes at various Reynolds numbers and to determine the boundary layer separation. The prepared anode has the shape of the streamlined body and the best results were achieved with a platinum or platinum-coated anode. The cathode /32
can be made, for example, from aluminum and it must be placed near the anode in such a way that the flow of the solution is not disturbed.

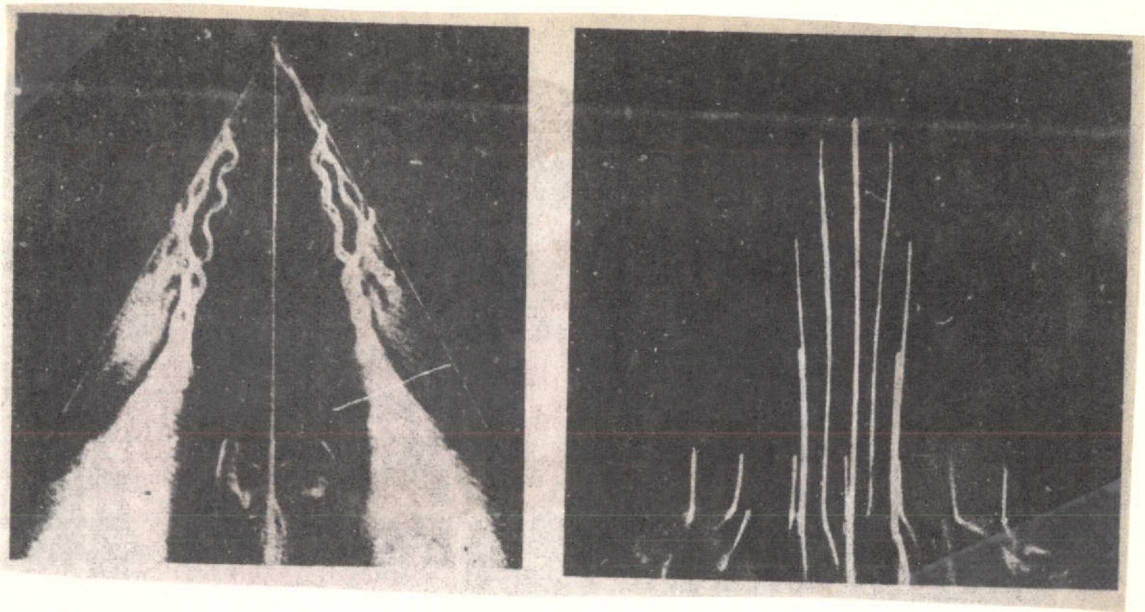

Fig. 9. Flow around a delta wind in a hydraulic channel. The dye used is milk introduced into the flow through holes in the model. The surface of the model is coated with dull black paint [29].

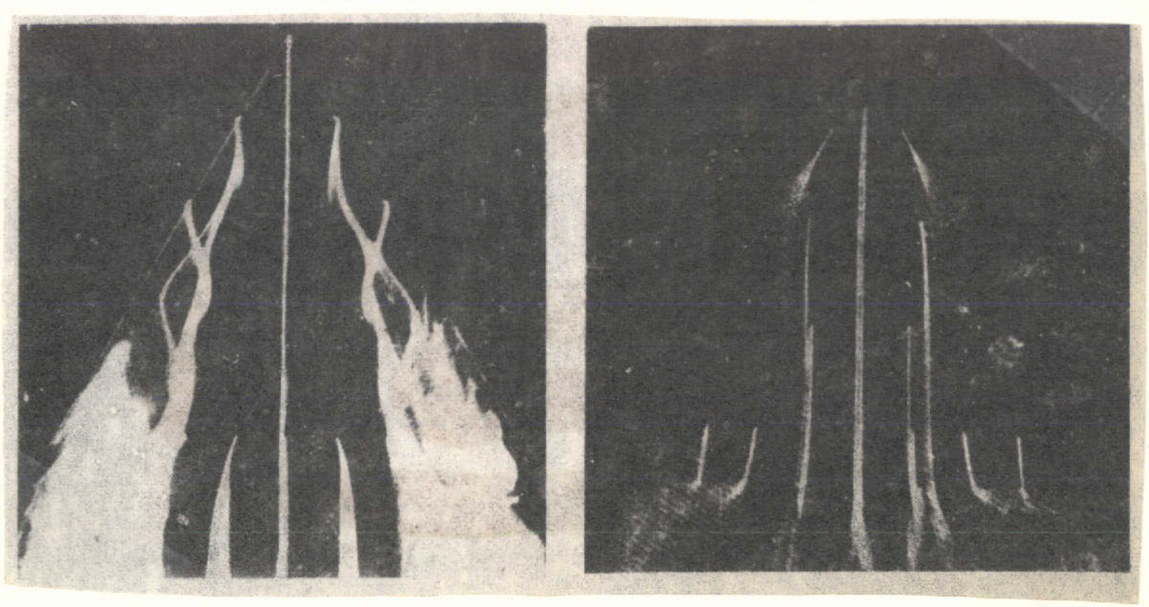

Fig. 10. Flow around a delta wing [29].

Finally, we will point out certain concrete possibilities of visualizing mixing processes. These possibilities, as we already mentioned, are furnished especially by the color effect which accompanies the reaction of acids and bases with dyes. The most appropriate dye is phenolphthalein, which, when it reacts

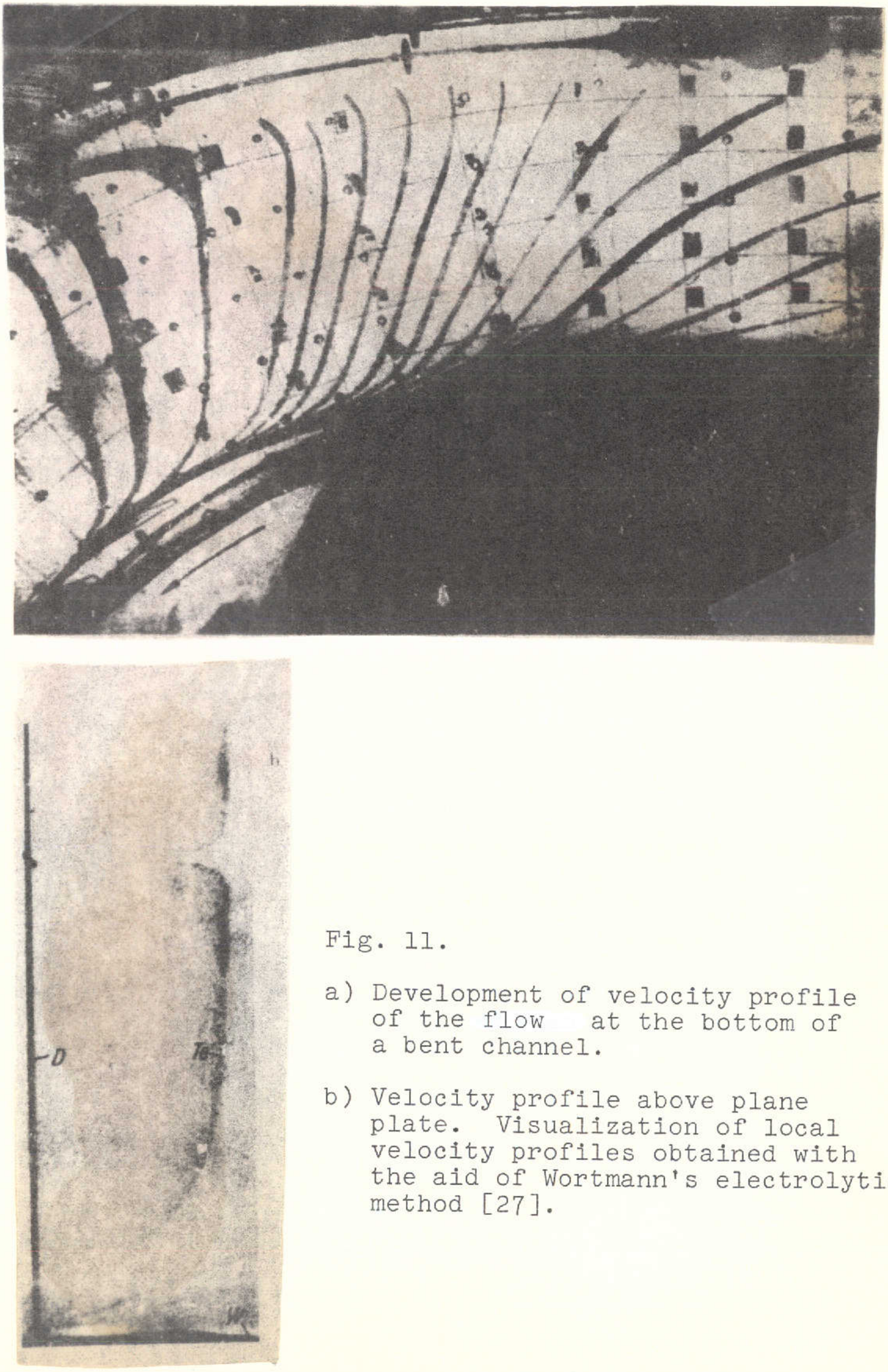

Fig. 11.

a) Development of velocity profile of the flow at the bottom of a bent channel.

b) Velocity profile above plane plate. Visualization of local velocity profiles obtained with the aid of Wortmann's electrolytic method [27].

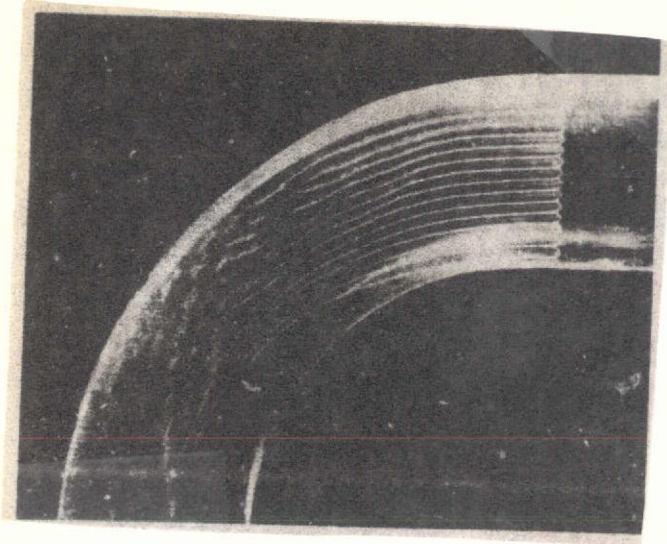

Fig. 12. Visualization trails formed by hydrogen bubbles obtained by water electrolysis.

with an acid, gives a colorless solution, and with a base a reddish-violet solution. By adding an acid in an amount which is slightly greater than that needed for neutralization, this solution can again be made colorless. The change from the reddish-violet basic solution to a colorless solution will occur practically instantaneously due to the very high neutralization rate, so that the mixing of the basic phenolphthalein solution with the required amount of acid is indicated immediately by the loss of color. Similarly, by adding an appropriate amount of the base to the acidic phenolphthalein solution, a red-violet color can be obtained. For example, if the fluid, whose flow is analyzed is a colorless solution of phenolphthalein with an acid and if the base is introduced into the flow with the aid of a nozzle, red-violet trails are formed which again disappear and become colorless at a certain distance due to additional mixing with the acidic solution flow. The place where the trails disappear can be changed by introducing acid through another appropriately placed nozzle. Similarly, many other dyes can be used like phenolphthalein. For example, metacresol red, thymol blue, orthoxylene blue, which have a red color when mixed with an acid, and turn yellow in a neutral solution when they react with a base, the first becomes purple and the other two turn blue. Sodium pyrosulfite with potassium iodide, sodium thiosulfate and starch also turned out to be useful.

1.1.2. Methods Based on the Use of Particles Which Do Not Form Continuous Trails or Relatively Large Continuous Regions

(The use of sawdust, metallic powder, oil drops and air bubbles in the fluid. Spraying of the surface with aluminum powder or lycopodium.)

When isolated particles are introduced into the flow to visualize it, they must have in the fluid approximately the same density as the fluid flow. For example, sawdust, small mica particles and a fine metallic powders, for instance, aluminum powder are used. This powder is mixed with the fluid and on its particles whose linear dimension is approximately 0.02 mm, air bubles are intercepted, so that some of the dust particles rise in the fluid. Small solidified polystyrene drops or other artificial resins are also used as well as tiny oil drops. The type of oil must be selected taking into consideration the density of the fluid into which the oil is introduced. The oil is introduced into the fluid flow, for example, by means of capillary nozzles with an internal diameter of 0.15 mm, or, if the model moves in a quiescent fluid, the oil emulsion is mixed into the fluid before the experiment. Besides oils, other fluids can be used, for example, a mixture of carbon tetrachloride with xylene, olive oil with nitrobenzene or ethylene dibromide and carbon tetrachloride with benzene. Small air bubles which can be introduced into the flow by means of the following two methods are also useful: either the air is blown through small openings into the vicinity of the streamlined body, or the water flow enters the observation space from a closed reservoir where a low air pressure is maintained by means of a vacuum pump, so that it is saturated with very fine air bubbles released from the water. Isolated bubble-particles can also be obtained using the electrolytic method, either by an appropriate adjustment of the current intensity, or with the aid of current pulses. Finally, filament probes can also be used, which will be described in Chapter 1.2.2. /33

Individual particles are frequently used, especially to visualize the flow on the surface of the fluid. The surface of the fluid is sprayed, for example, with balsa wood or aluminum powder or possibly lycopodium. The fluid used to fill the trough or channel is water and the condition for success is that it be absolutely pure. During the motion of the model through the originally quiescent fluid, the sprayed particles form the image of the flow on its surface.

All methods discussed in group 1.1.2 give qualitative results and were often used, mainly the last ones, for instruction purposes. However, quantitative conclusions can also be drawn on the basis of these methods. The required hydraulic experimental equipment is basically the same as in the previous group 1.1.1. It consists of a hydraulic channel or tunnel. Only in the last method, the motion of the model inside the channel is used more frequently.

With the exception of the last method that was mentioned, it is most convenient to illuminate the observation space by a plane pencil of rays emanating from the slit, since by changing the position of the pencil across the stream also a three-dimensional flow can be recorded, for example, the flow around solids of revolution with the axis in the direction of the flow. Such illumination is obtained with the aid of a slit diaphragm mounted behind the condenser of the light source, or with the aid of one or two illumination bodies in the shape of a prism or cylinder which is 3-4 m long and blackened inside with a 0.5-1 mm wide slit on one base and with the high-intensity light source (bulb, arc lamp, discharge tube) on the opposite base. The observation direction or the axis of the camera or motion picture camera is perpendicular to the plane of the light beam. The arrangement is illustrated more clearly in Fig. 13.

In the illumination and observation methods that were just described, advantage is taken of the light scattered on the visualization particles. Therefore, tiny mica or aluminum powder grains should not be introduced into the fluid when this method is used, since they reflect the light, and the reflected light may also illuminate particles which are outside the space illuminated by the plane pencil of rays used. This, of course, leads to incorrect conclusions when the recorded three-dimensional flow is evaluated.

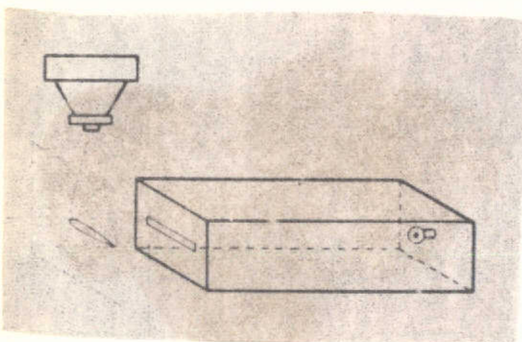

Fig. 13. Illumination and photography method.

Naturally, the illumination, /34 observation and recording methods commonly used in the preceding group 1.1.1 can also be used, or slanted illumination, when the axis of the three-dimensional pencil of parallel rays is neither perpendicular nor parallel to the plane of flow, and the light reflected from the visualization particles is used during the observation or recording.

With regard to the last method of visualizing the flow on the surface of the fluid with the aid of sprayed particles, the reflectors illuminate the surface of the fluid in the vicinity of the model and move together with the model. In this case, the photographic equipment or the motion picture camera usually moves along with the model, while in the remaining methods in group 1.1.2, the camera is usually fixed when the photographs are taken. The situation is reversed in the case when we are not interested in the state of the flow around the streamlined body, but in the motion of a certain region of the fluid, for example, in the study of vortices carried by the flow.

Quantitative data can also be obtained from photographic records on the basis of the length and orientation of the track of the visualization particle, the exposure time and the image enlargement. For example, the velocity field is determined in this way.

The first concrete case in which methods from this group are used, which will be described in greater detail, is the widely used visualization method with the aid of particles on the surface of the water flow [51 through 58]. The equipment used for this purpose includes a trough (vessel) in the shape of a parallelopiped. Rails are attached to the upper edges of the vessel for a carriage driven by an electric motor. The camera or motion picture camera is mounted on the top part of the carriage and the bottom part of the carriage carries the model (Fig. 14 a, b) [58]. The visualization is achieved by spraying the water surface with a fine powder. The best powder turned out to be lycopodium. When the results obtained are evaluated, it must be assumed that the water surface flows in the same manner as the other layers which are paralell to the surface which are in contact with the model, i.e. that the flow whose image is obtained is two-dimensional. Absolute purity of the water will help to satisfy this assumption.

The disadvantage of this method is that the velocity of motion of the model must be limited, since at higher velocities surface waves are formed around it. These waves are formed in an undisturbed water flow at a velocity of 23.3 cm/sec, and, during flow around a cylinder with a circular cross section, the maximum admissible velocity is half this magnitude without taking into account the diameter of the cylinder. For a cylinder with a 5 cm diameter, the maximum attainable Reynolds number will have approximately /35 the value 5500. Since the critical value of the Reynolds number during flow around a cylinder, depending on the degree of turbulence and many other factors, is on the order of 10^5, we must clearly restrict ourselves only to the subcritical (laminar) flow region around the cylinder. Another disadvantage is the capillary lift of the water on the walls of the tested model caused by the surface tension, which prevents the particles from arriving to the immediate vicinity of the model. This disadvantage can be eliminated by coating the model with a thin paraffin layer.

The method that was described was used, among other things, in the quantitative analysis of vortices formed behind a cylinder moving in the fluid and the results that were obtained served as the basis for theoretical studies [57]. The cylinder which was attached to the carriage was drawn through the channel and the Karman vortex path formed behind the cylinder was visualized by spraying the surface with aluminum powder and photographed with two cameras placed above the channel at different distances behind the cylinder, i.e. at different /36 distances in the direction of the flow. The photographs that are obtained make it possible to determine from the length and orientation of the particle tracks and from the visualization scale and exposure time the magnitude and direction of the velocity of the particles at each point, and also the vortex development process. Assuming that the aluminum particles complete the same motion during the observation time as the particles on the surface of the fluid, we obtain the velocity field of the flow. For an illustration, see Fig. 15 [57].

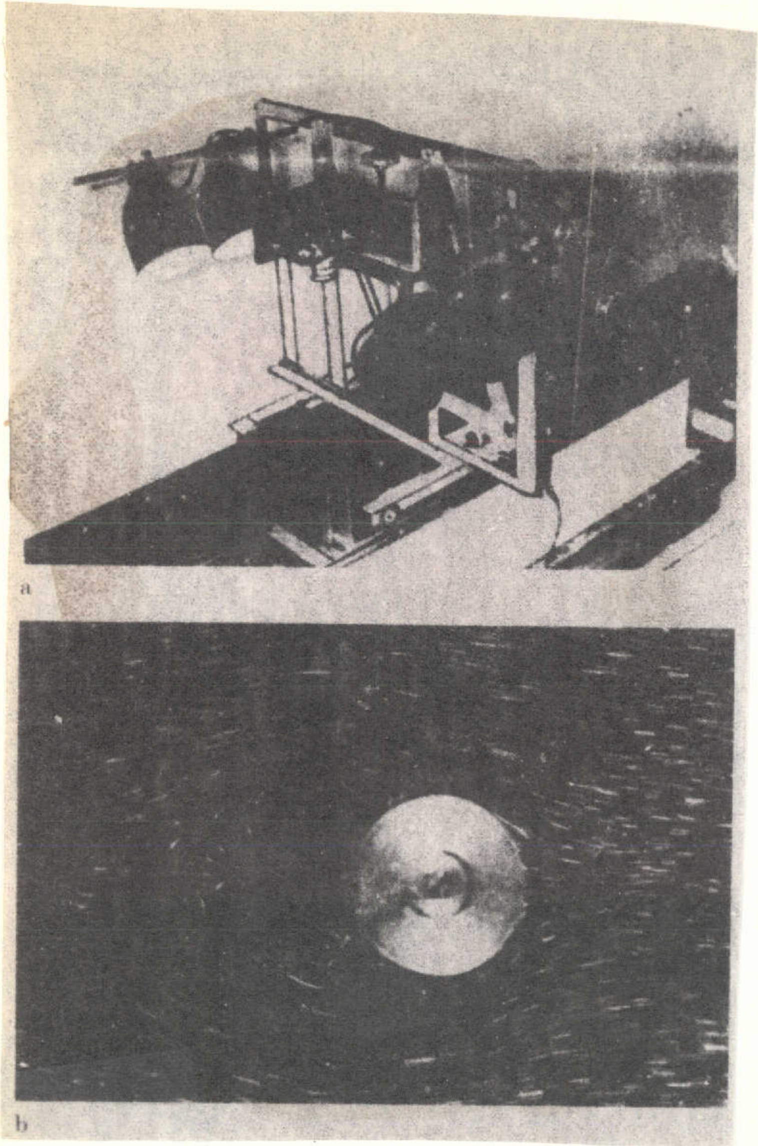

Fig. 14. a) Hydraulic bath with carriage for the study of a flow around bodies based on visualizing the flow on the surface; b) Visualization of flow around cylinder [58].

The method can be modified so that instead of the fluid (water) in the vessel in which the height of the surface layer from the bottom is on the order of several centimeters to tens of centimeters, a thin layer (film) of a fluid is used which adheres to a horizontal plane plate and is sprayed with a visualizing powder. For visual observation, the fluid layer need not move and the model around which the flow is studied is pulled along the plate with the aid of a sling (thread). When photographs must be taken we use the arrangement in which the plate is mounted on the carriage and moves. Together with it, the fluid layer moves and flows around the model which is attached to the fixed base, the track of the carriage. The camera is mounted on the fixed base above the model (Fig. 16). The method can also be used to obtain a model /37 of a potential flow when the viscosity is sufficiently high and the thickness of the fluid layer is sufficiently small (see Fig. 17 a, which shows the flow of water around a cylinder; the thickness of the water is approximately 1 mm, visualized by lycopodium). Some additional results obtained in this manner are illustrated in Figs. 17 b (visualized flow of a wavy surface), 17 c and 17 d (flow in a labyrinth seal) where, in the last two cases, the fluid is set in motion by inclining the plate, which can be done for a greater thickness of the fluid layer (for water at a thickness of 2-3 mm) [10].

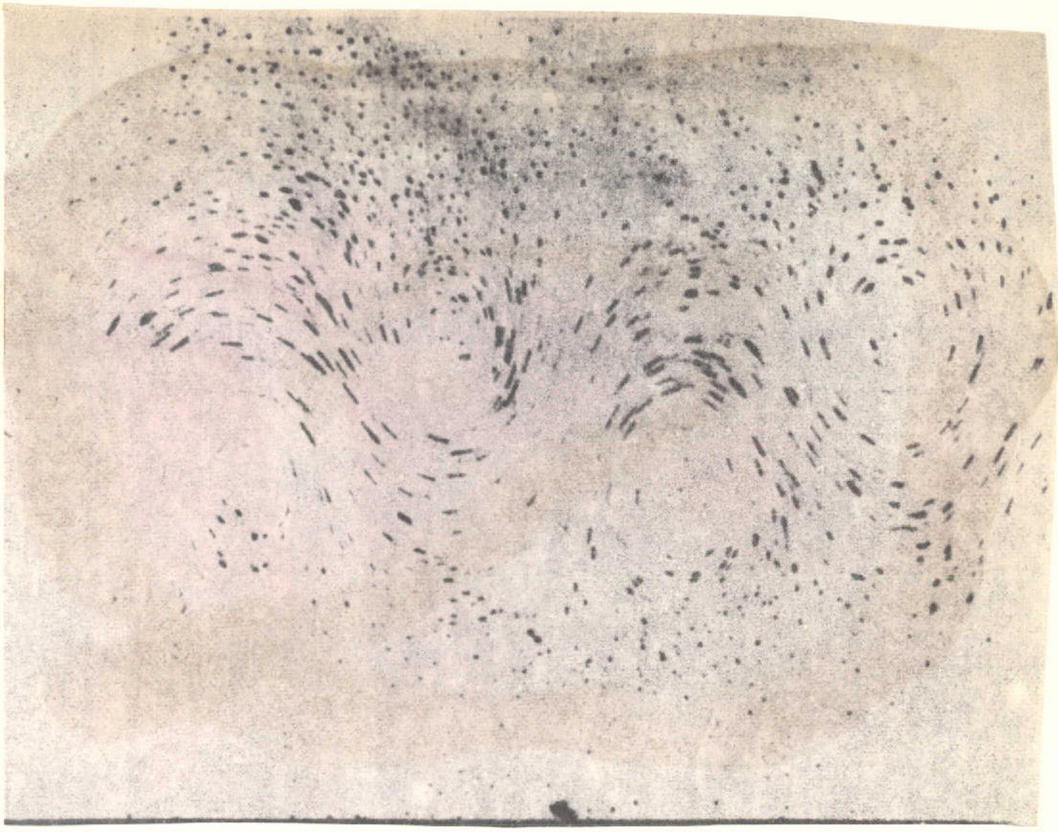

Fig. 15 a, b. Visualization of vortices behind a streamlined cylinder. c, d. Graphs of circumferential velocities. The velocities were determined from photographs as in Fig. 15 a [57].
[Fig. 15 c, d on following page.]

Particles sprayed on the surface of the fluid can also be used to visualize the flow in hydraulic channels when the model is at rest and the fluid flows around or through the model. Hydraulic channels with an open observation space which is not covered and a free surface are suitable for this purpose (see, for example, the schematic diagrams in Figs. 1 and 2). In this case, the camera is in a fixed position above the model and the surface is illuminated at an angle in such a way that the light sources reflected from the surface do not interfere in the photographs. An example of the results obtained using this method is given in Fig. 18, in which the flow in the separation mechanism of a threshing machine is visualized (with a short exposure time (a), a longer exposure time (b) and the image of the streamlines is drawn according to the photographs (c)). /41

With regard to the use of visualization particles inside the fluid flow, certain concrete results are illustrated in Figs. 19 a, b [30]. These were obtained using a hydraulic channel whose /42

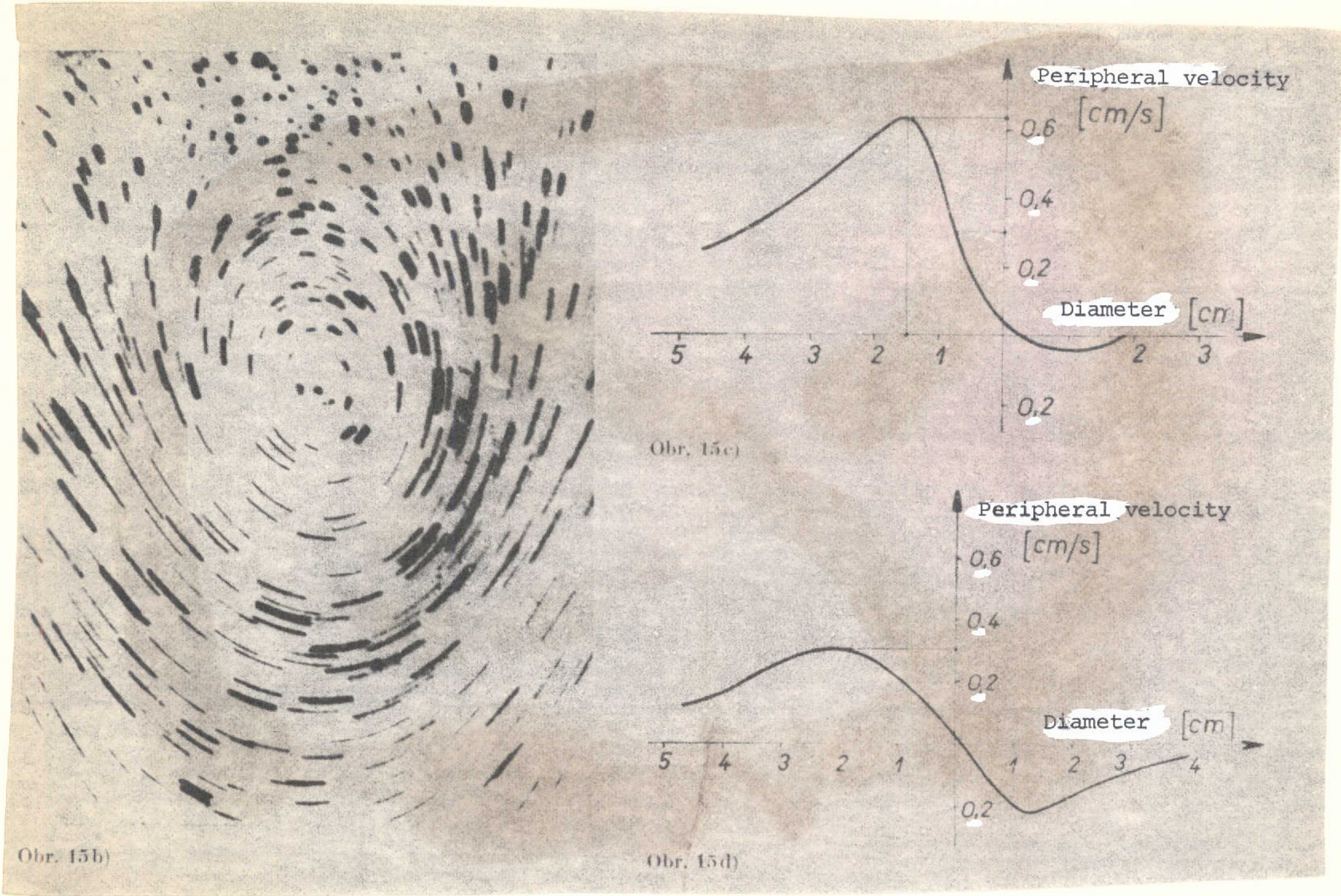

Fig. 15 c, d. Graphs of circumferential velocities. The velocities were determined from photographs as in Fig. 15 a [57].

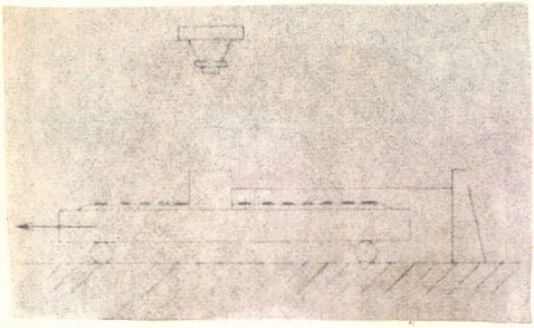

Fig. 16. Schematic diagram of equipment for visualization using a thin fluid film.

observation space had a 22 × 22 cm cross section and whose length was 70 cm. Small solidified polystyrene drops with a 0.5-2 mm diameter were used for the visualization. Small air bubbles can be used in a similar way.

Also in this case, quantitative results can be obtained. The procedure used is either the method described on p. 27, or, using the same camera, two photographs of the flow field visualized by the particles are taken and the time interval between both exposure is determined exactly. The photographs are superimposed on one other so that the boundaries of the measured area coincide. They are lit though and the motion of the particles in the time which elapsed between the two exposures is measured, for example, by a measuring microscope. It is also possible to have two exposures on one

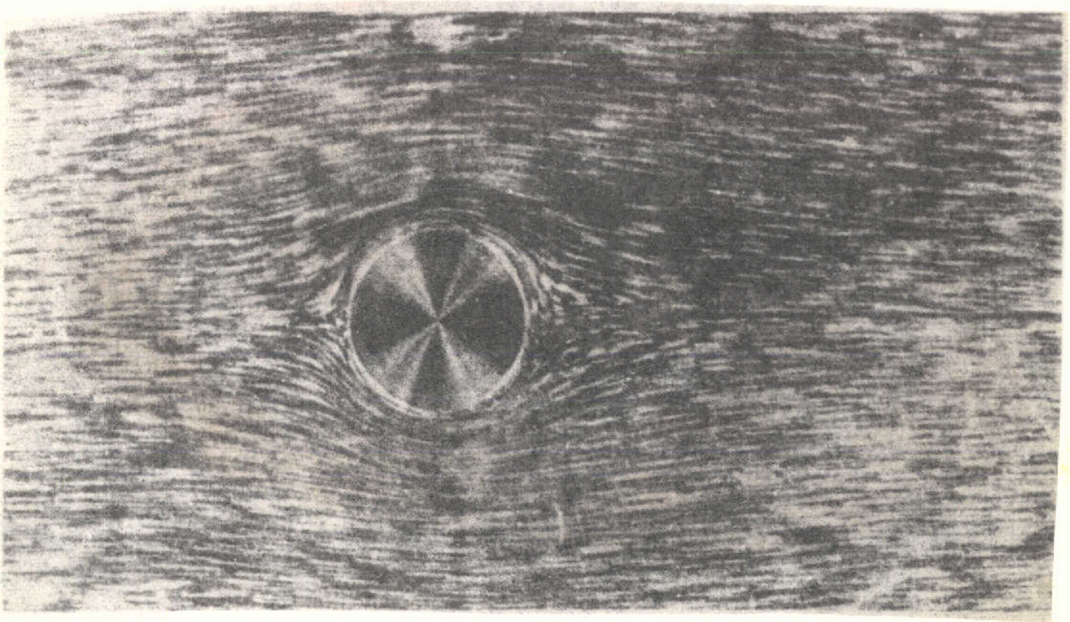

Fig. 17 a, b. Flow around a cylinder and surface rippled by a thin fluid film (the thickness of the water layer is approximately 1 mm, visualized by lycopodium) [10].

c, d. Flow in labyrinth seal visualized with the aid of a thin fluid film sprayed with visualizing powder.

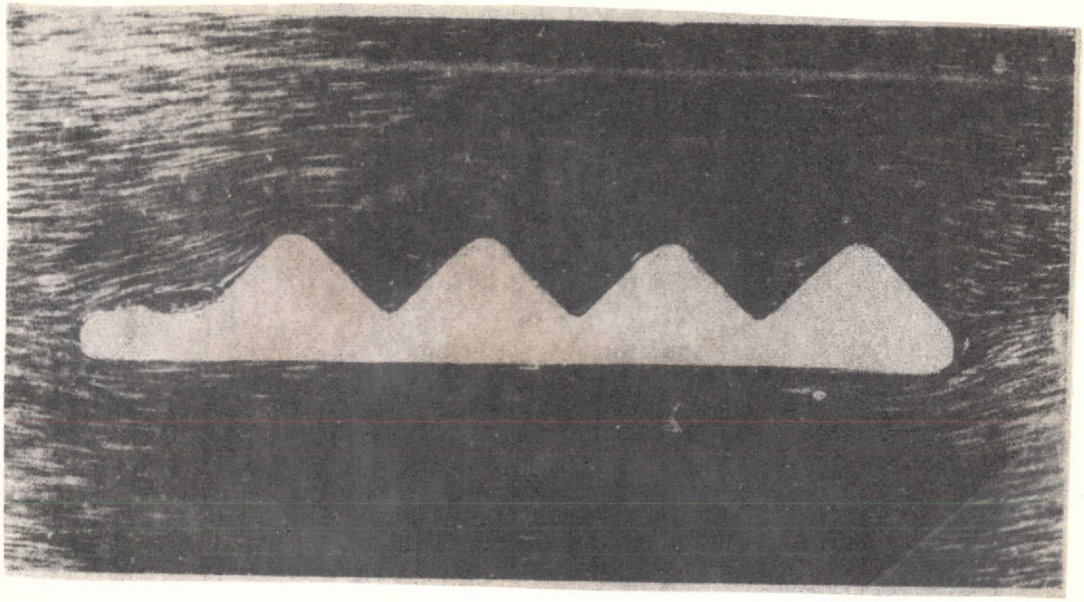

Fig. 17 b.

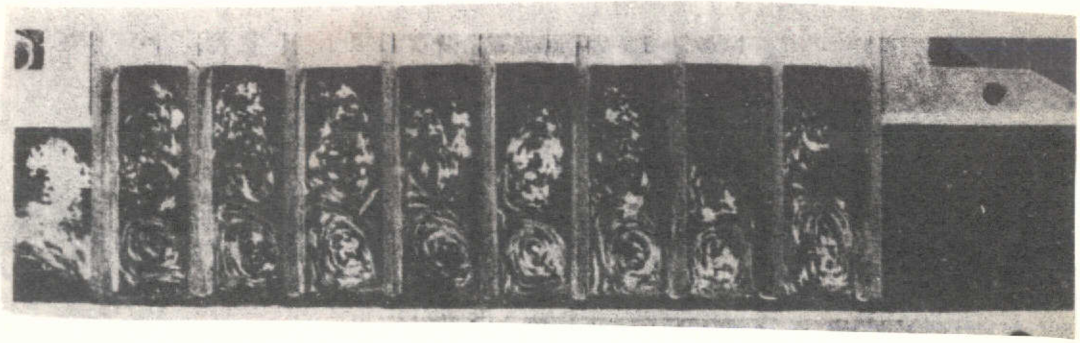

Fig. 17 c.

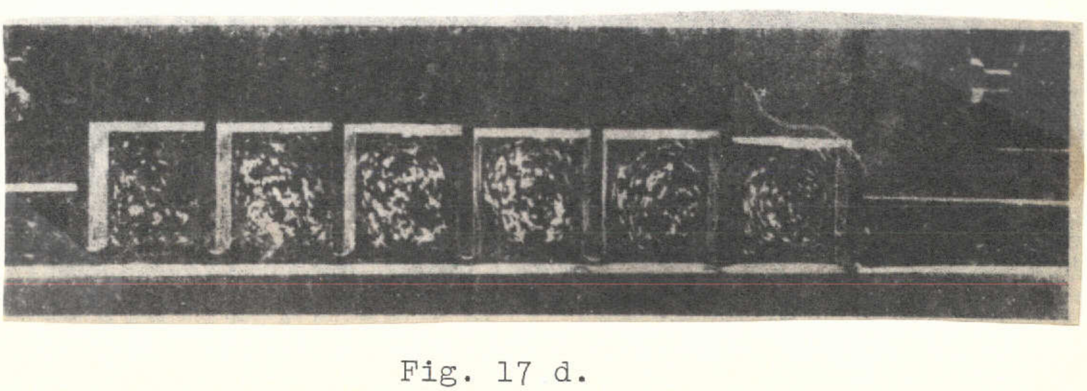

Fig. 17 d.

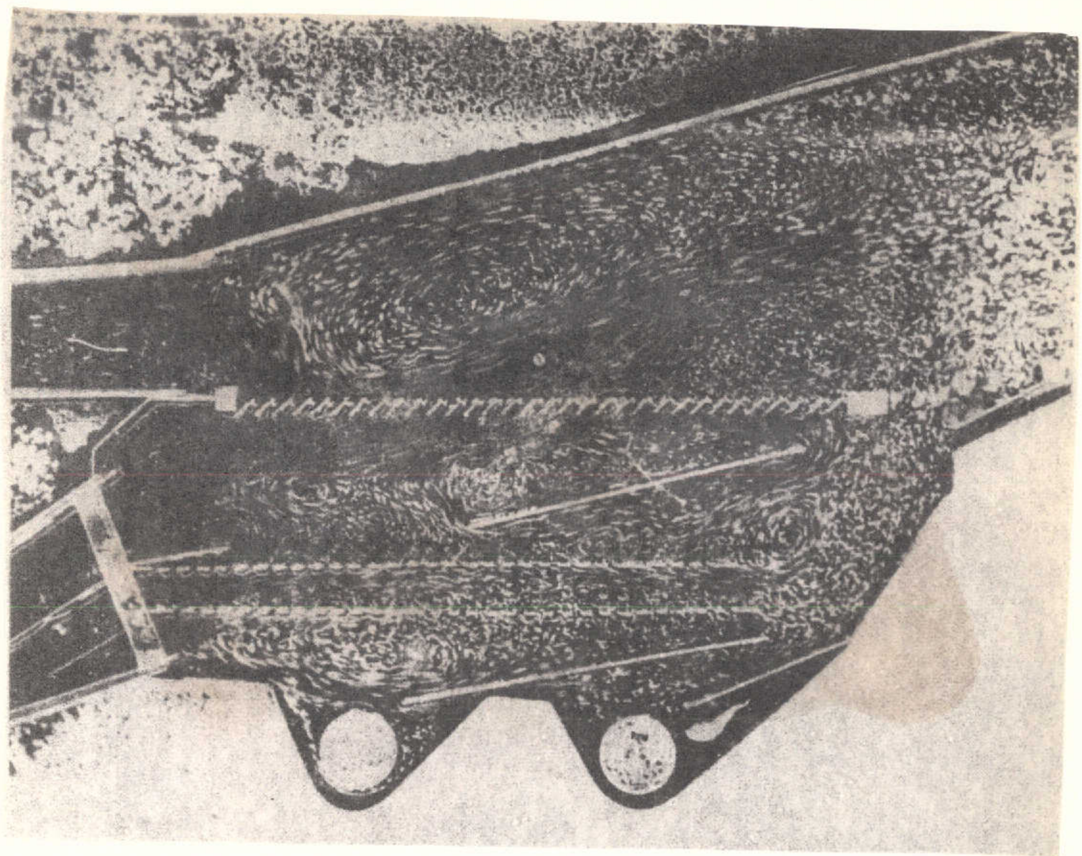

Fig. 18 a. Flow in the separation mechanism of a threshing machine. Short exposure time [10].

photograph. This method was used in the quantitative analysis of velocity fields in water caused by the introduction of a solid body [59]. Here, the visualization particles were small air bubbles whose source was a thick-walled soft rubber hose with a 1 cm diameter in which holes with a 0.25 mm diameter were punched at regular intervals with a needle. When air with an overpressure of about 1 atm is brought into such a hose, which is immersed in water, air bubbles with a 0.2-2 mm diameter rise from the hose in still water in a chosen roughly vertical plane. Now, if the body is introduced into the vessel with the water, the motion of the bubbles changes, and this change is used as the basis for determining the velocity field. If the time between exposures is Δt and the displacement of the bubble in this time is Δs, the magnitude v of the average local velocity $\mathbf{v}$ is given by the ratio $v = \Delta s/\Delta t$. Usually, one proceeds so that the flow, which is generally three-dimensional, is lit through in one plane (with the aid of a light source with a slit) and photographed in the perpendicular direction to this plane. The average local velocity $\mathbf{v}$ in this plane is determined in this manner at individual points of the plane that was lit

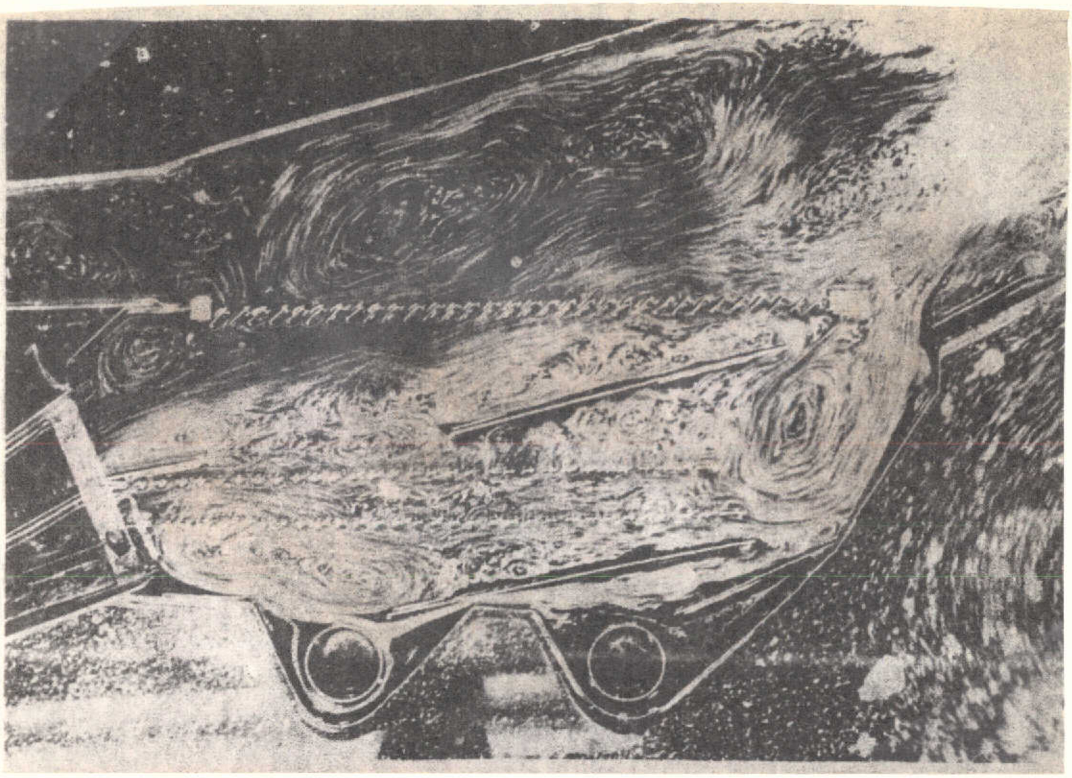

Fig. 18 b. Flow in separation mechanism of threshing machine. Longer exposure time [10].

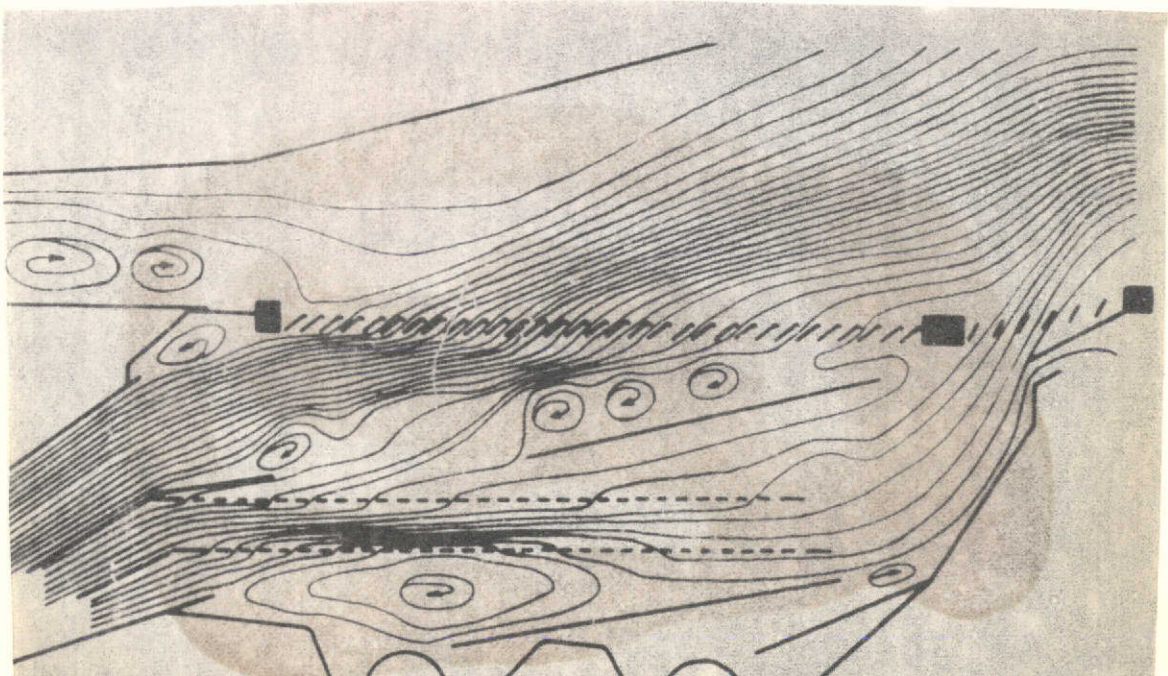

Fig. 18 c. Image of streamlines drawn according to photographs 18 a, b [10].

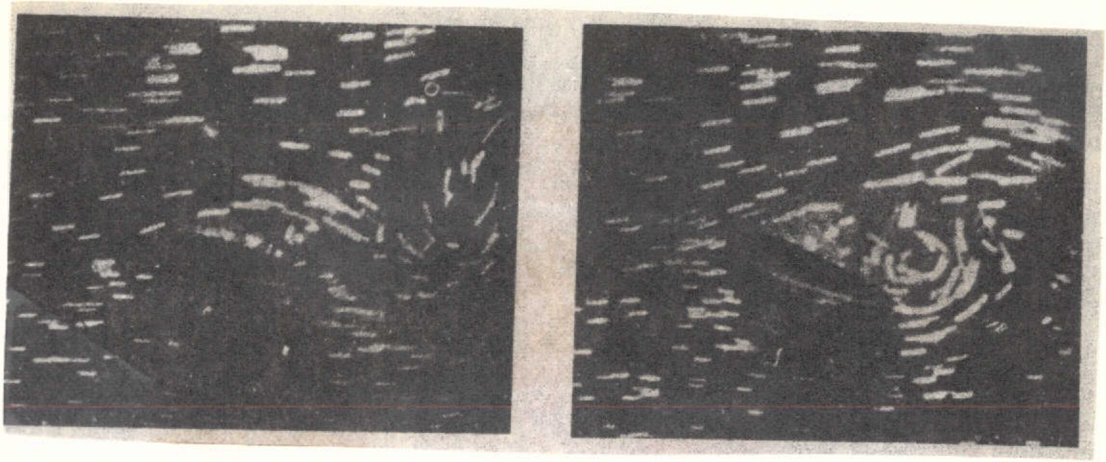

Fig. 19. Flow around a profile in a hydraulic channel. Small solidified polystyrene drops with a 0.5-2 mm diameter are used for the visualization [30].

a) flow at small angle of incidence; b) flow at large angle of incidence.

through. The three-dimensional flow can then be analyzed by passing light successively through the flow in different planes. However, corrections for the rise velocity of the bubbles, the effect of the walls of the vessel, etc. must be introduced into the data obtained. Similarly, instead of air bubbles, oil drops or hexane drops can be used. In this case, a metallic tube with 0.05-0.5 mm diameter holes or an injection needle are more suitable than a hose.

Oil drops in water can also be used to obtain quantitative data in a different way [48]. A model which moves in still water is used for this purpose, and two glass plates which are parallel to the plane of flow formed by the motion of the model are inserted in the appropriate place before the experiment. An oil emulsion is poured between them (olive oil + ethylene dibromide + water). The drops which form in it, the oil dissolved in dibromide, must have approximately the same density as water, which is achieved using the proper oil to dibromide ratio. The glass plates are then removed, the layer with the oil drops is illuminated by the source with the slit (Fig. 13) and the body (model) is set in motion. The direction of photography is perpendicular to the plane of light rays and to the plane of flow. The exposure time is regulated by the shutter, consisting of the rotating diaphragm. The velocity of the flow is determined from the length of the particle tracks on the film which are measured by a microscope. /43

1.2. Use of Methods from Group 1 for Visualizing the Flow of Gases

1.2.1. Methods Based on the Use of Particles Forming Continuous Trails or Larger Continuous Regions

(Use of mottle trails, smoke and mist. The method of hot wires. Method using electric discharges. Luminescent methods. The method of a mist screen for visualizing a shock wave.)

A. The first method in group 1.2.1 is the introduction of a burning gas flame into the airflow by means of a thin nozzle. The flame that is introduced must have a small diameter and it must be long. The method is suitable for analyzing local turbulence, and it can also be used to determine sufficiently well the wake boundaries when the nozzle is inserted in the separated flow region, the wake.

A system of trails can also be used. These are obtained by introducing into the flow burning gas with the aid of a tube-shaped torch with a series of openings (Fig. 20). If the mottle trails are long and thin, illumination is not needed in certain cases, and the observations can be carried out or the photographs can be taken with a dark background.

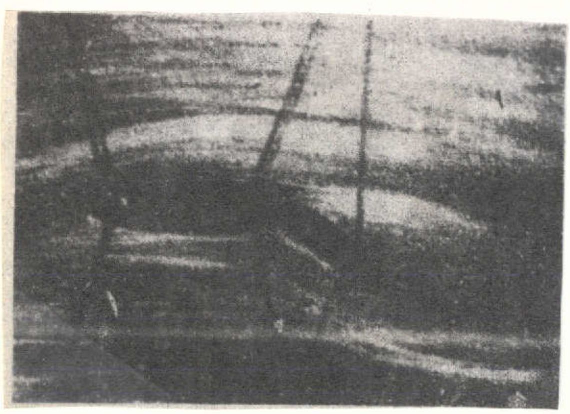

Fig. 20. Visualization of flow around profile with the aid of mottle trails.

B. The second method in group 1.2.1 uses smoke and mist trails. Smoke and mist are aerosols and therefore are classified as dispersive systems. Here, the dispersing agent is a gas, for example, air. When solid particles are dispersed in it, smokes and fumes are formed and the dispersed liquid particles form the mists.

The aerosol, the smoke or mist, is introduced into the stream by a comb [sic] nozzle, a simple nozzle through an opening in the streamlined body, etc., depending /44
on the type of problem studied and the type of aerosol. The condition is that the aerosol leaving the nozzle have the same velocity as the surrounding flow medium. The velocity of the flow must be selected so that the aerosol trails do not liquify. The aerosol can also enter the stream directly from the surface of the streamlined body where it is formed by the chemical reaction of the flow medium

with the appropriate coating substance applied to the surface of the streamlined body.

The methods for obtaining the aerosols belong to two different basic groups:

a) smoke or mist resulting from the chemical reaction of an appropriate substance (usually a liquid) with the flow medium.

b) the smoke which was already generated or the mist that was formed are introduced into the flow medium:

b_1) through a chemical reaction or
b_2) combustion and vaporization.

A. a) The simplest method among these methods is using smoke generated by water-soluble salts, for example, by titanium chloride or stannous chloride. The smoke is generated when these substances bond with the water vapors contained in the air and, in the cases mentioned, it consists of the metallic oxide particles (for example, TiO_2) and the hydrogen chloride. The smoke that is generated is thick, white and it can be seen easily. Its particles sometimes contain large drops of water so that at low flow velocities they tend to drop; however, at sufficiently high flow velocities, the drop does not manifest itself noticeably.

The salts that were mentioned are in the liquid state, and their reaction during contact with air, the hydrolysis with the water vapor, is vigorous, and large amounts of smoke are generated during it. One drop of the fluid at the end of a glass rod gives an amount of smoke which is sufficient for several minutes of the experiment. However, the disadvantage is that deposits are formed on the streamlined bodies.

To observe the flow around the streamlined body, it is sufficient if several drops of the fluid are placed on the surface of the body, and, in the second case, it is more advantageous to use a mixture of the two salts that were mentioned in the ratio 1:1 to prevent clogging of the openings [1, 5]. For observation in other parts of the flow field, a glass rod which was first immersed in a smoke-producing fluid can be used as the source for the smoke trails.

Since the smoke contains hydrochloric acid, the smoke is corrosive and generally harmful. Therefore, smokes of this type are not suitable for use in tunnels that were not specially designed for this purpose. Wood was mainly used in the construction of such special tunnels [77]. The acidic chatacter of the smoke must be neutralized after it leaves the tunnel. Hence, for a number of reasons, smokes of this type are used only seldomly.

A.b_1) Another method uses ammonium chloride-salmiak vapors. Apparatus consisting of three flasks is used to generate the smoke. The first flask with the hydrochloric acid passes through the air and carries with it the vapors of this acid which react /45 with the ammonium hydroxide in the second flask. The reaction

$$HCl + NH_4OH = NH_4Cl + H_2O$$

occurs during which the salmiak is obtained in the form of white smoke. The third flask is used as a separator [1].

A.b_2) Group b_2 also uses chlorine, bromine and iodine vapors which, however, are damaging to health, and strict hygiene measures must be observed while working with them.

Smokes of various colors from smoke generator can also be used advantageously without volatile chemical component substances (especially in studies dealing with room ventilation).

However, aerosols obtained by burning wood, tobacco and other organic substances (for example, also straw) are used most frequently or aerosols obtained through vaporization or possibly the burning of oils [66 through 76]. We will therefore now describe certain concrete methods by which they are obtained.

One of the simplest smoke generators is outlined in Fig. 21 [73]. The tobacco smoke in it is obtained by burning a cigar soaked in oil.

A very convenient smoke which is nonpoisonous and noncorrosive (used by beekeepers) is obtained by burning rotten wood (so-called loose rot). The smoke from the combustion chamber passes through the cooler and then through a filter in which the tar and also larger particles which clog the nozzles and form deposits on the streamlined bodies are collected. The layout for the smoke generator of this type is given in Fig. 22 [66]. The smoke supply to the tunnel is regulated by the bypass which releases most of the smoke generated into the atmosphere, so that the generator can operate with the same capacity regardless of the amount of smoke drawn off. The disadvantage of this method of obtaining the smoke is the long time needed to put the generator in operation. In addition to this, the smoke contains large amounts of particles which do not trace well the surrounding medium, form deposits on /46 the streamlined bodies, and disturb the flow that is studied.

The disadvantages that were mentioned are reduced considerably when an oil generator is used which also provides aerosols in larger concentrations. The aerosol here is mist, which is formed through the collision of the vaporized oil in the form

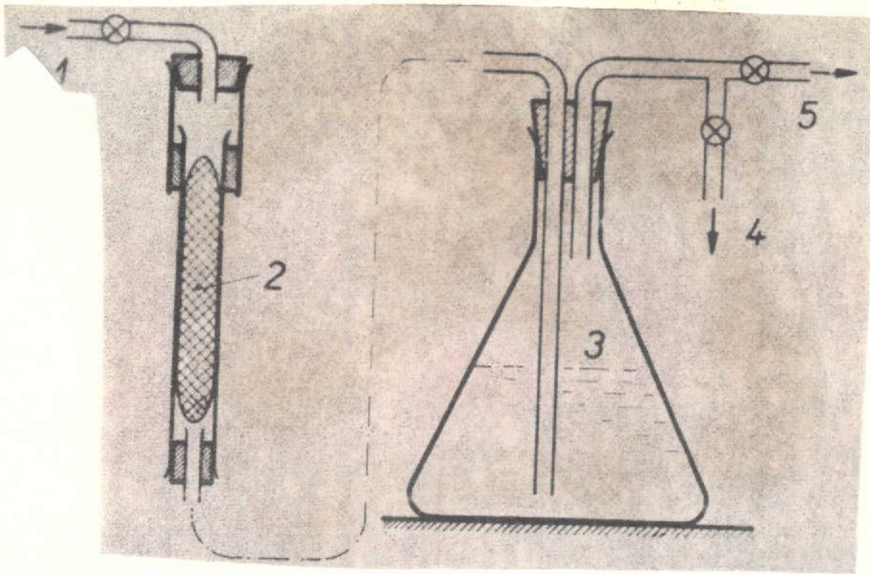

Fig. 21. Schematic diagram of very simple smoke generator (1. air supply with slight overpressure of approximately 0.1 atm; 2. burning cigar soaked in oil; 3. separator-filter; 4. bypass; 5. nozzle inlet).

of a small drop with a cold air current [76, 69]. Since the mist consists of tiny drops, deposits are not formed on the body or in the pipes. The generator can be put in operation in 5 min and it can operate for an unlimited period, it has small dimensions and the quality and amount of mist supplied can be regulated well. When mineral oil is used, kerosene and paraffin oil have especially good properties for these purposes. The mist obtained is not corrosive, it is not poisonous, and it does not have an unpleasant odor, even when the concentrations are high. When it is used, the very slight probability of an explosion cannot be eliminated altogether, but in the usual cases the proportion of oil in the air is such that the danger of an explosion can be discounted.

A simple type of oil generator is outlined in Fig. 23 a. Most of its parts are made from glass. The oil is supplied from the oil tank to the vaporizing chamber (boiler tube) around which a heating coil is wound with a maximum power of approximately 200 W, which is wrapped in several layers of asbestos twines [76]. The current in the heating coil and the /47
heating of the oil can be regulated by a rheostat, and the passage of the current is indicated by a control box. The heating coil heats the oil in the boiler tube which is vaporized, and the vapors are let into the mixing chamber through a small opening to which the air is supplied through the small tubes on the side.

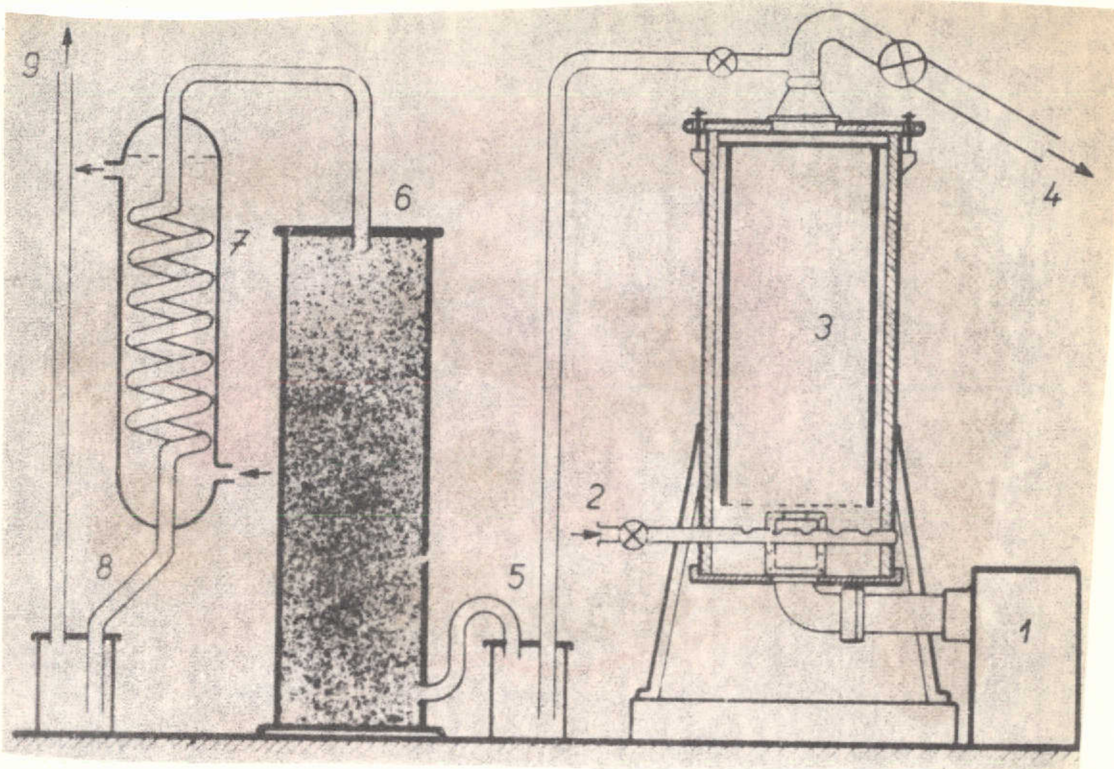

Fig. 22. Schematic diagram of apparatus for generating smoke by burning wood [66] (1. ventilator; 2. gas supply to burner; 3. area for burned wood; 4. bypass; 5 and 8. water filter; 6. coke filter; 7. cooler; 9. nozzle inlet).

indicated by the number 5 in Fig. 23 a. The mist that is formed is conducted to the mist reservoir and its supply to the tunnel or the bypass is regulated with the aid of valves.

After the generator is put in operation, the oil reservoir is placed in such a position that the oil level in the boiler tube is approximately at one-half of its lenth. After the heat is turned on, the oil is heated slowly, and only after a certain time the oil reservoir is lifted so that the level in the boiler tubes rises somewhat, but does not reach the outlet opening. This is necessary since the interior of the mixing chamber must always be dry. If a relatively large amount of oil is condensed in it, the oil level in the boiler tube must be lowered. /48

The regulation of the amount of mist needed in the oil generator that was described in ensured by the bypass, and the quality (concentration) of the mist by the rheostat of the heater. To avoid raising the position of the oil reservoir in

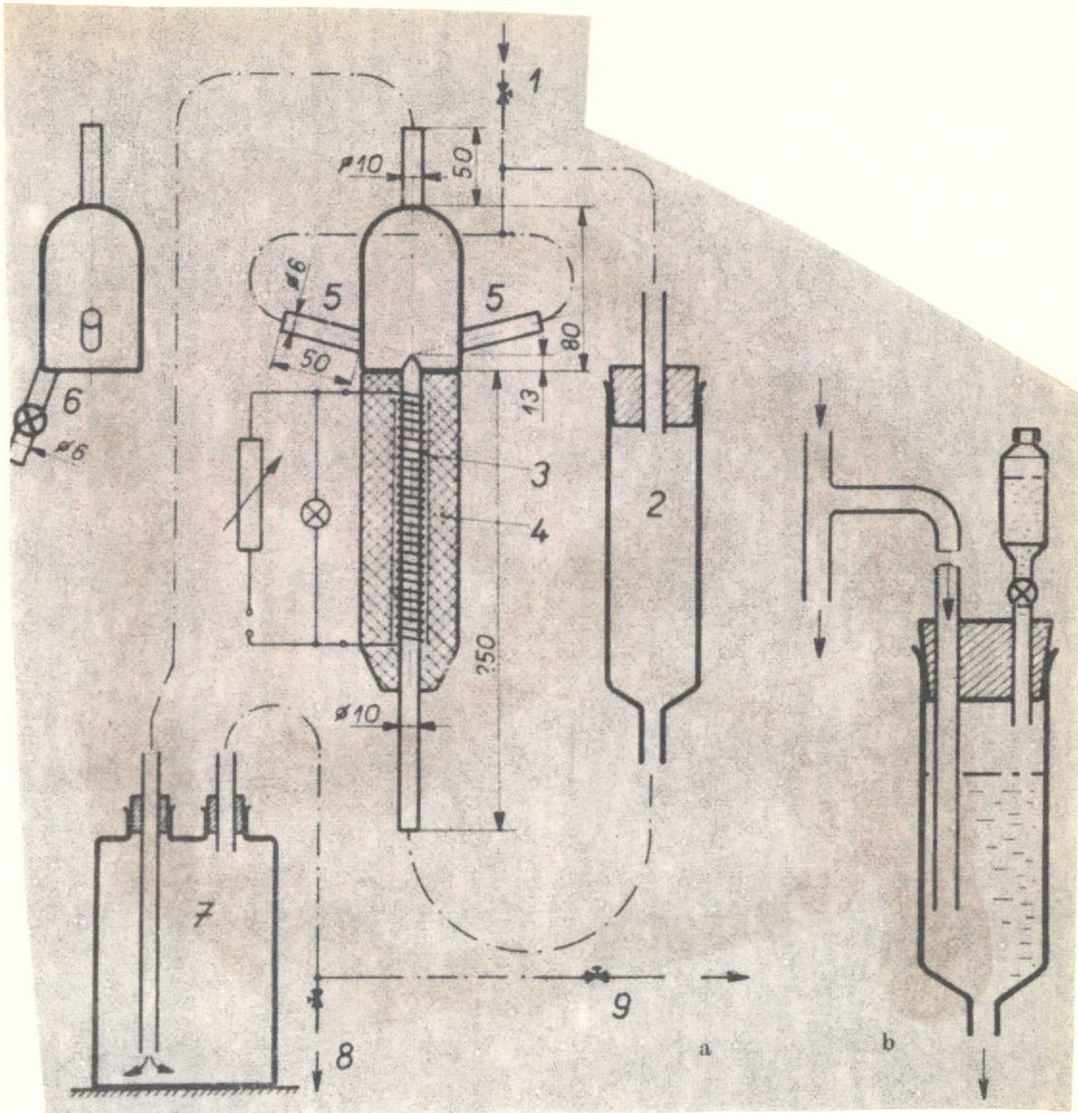

Fig. 23. Schematic diagram of smoke generator with oil vaporization [76].
a) (1. air supply with slight overpressure of approximately 0.1 atm; 2. oil reservoir; 3. electric heating winding; 4. asbestos heating insulation; 5. air nozzles; 6. condensed oil outlet; 7. separator and smoke reservoir; 8. bypass; 9. smoke supply for nozzles).
b) Different layout of oil reservoir.

operation, the additional oil can be supplied in the manner shown in Fig. 23 b.

To generate a larger amount of mist, a generator with a larger number of air nozzles and nozzles for the oil vapors was designed on the same principle [69]. Another advantage of this generator is its greater strength when it is serviced, since most of its parts are metallic.

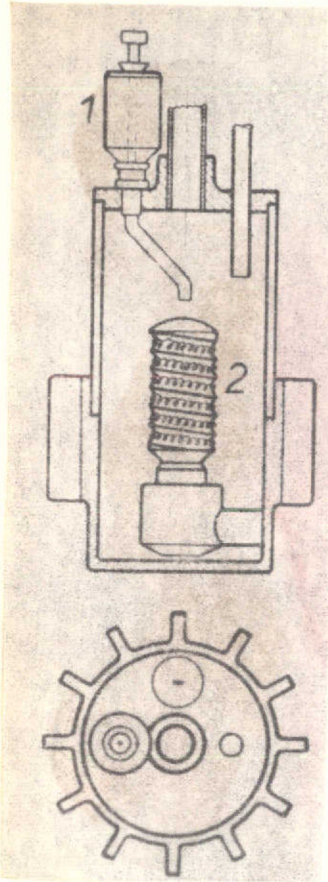

Fig. 24. Schematic diagram of smoke generator with oil combustion and vaporization (1. oil reservoir; 2. heating body).

Before generators of the type that was mentioned had been designed, the commonly used oil smoke generators were based on a slightly different principle (see Fig. 24). In these, the oil from the reservoir drops onto the heater where it is partially vaporized and a part is burned. The vapors condense in the air current into small drops as they enter the cooler parts of the generator apparatus and form with the solid particles obtained through the burning the aerosol needed for the visualization. However, the aerosol obtained using this method does not have high concentration and the advantageous /49 optical properties as that obtained from the oil generators that were described. In addition to this, its regulation is less flexible.

Another method of generating an oil mist which is especially suitable when it is intermittently introduced into the current is worth mentioning. Basically, it is a L-shaped tube with a piece of cotton soaked in oil at the inlet to the shorter arm. The heating wire, preferably a platinum wire, passes through it and is connected with the electric current source with the aid of lead-ins with outlets at the other end of the tube. An air current carries the small mist drops formed by the precipitation of the oil vapors. Fig. 25 gives an outline of such a spout intended for letting out a single aerosol filament.

The tunnels for smoke and mist visualization differ from the usual wind tunnels mainly by their high inlet branch taper ratio (up to 1:48) and by the equipment used to reduce turbulence. Their design must satisfy the following requirements. The flow in the observation space must be the same in the entire cross section, and it must have a low turbulence value. To prevent the smoke from filling the tunnel, the most suitable type of tunnel is a tunnel with an open circuit. The velocity of the flow must not be too low so that the smoke trails do not descend, i.e. the effect of gravity must not be felt. In this respect, vertical tunnels have certain advantages. The method for designing appropriate tunnels is illustrated in Figs. 26 a, b, c and Fig. 27.

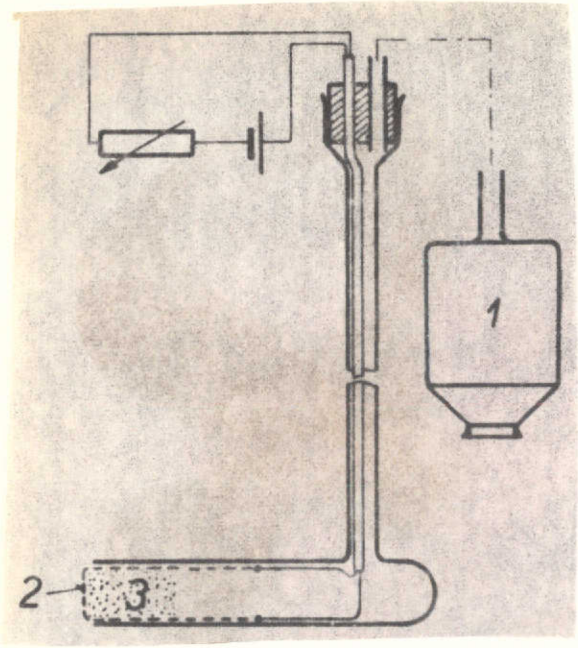

Fig. 25. Tube for generating a single smoke trail (1. oil reservoir; 2. heating winding; 3. cotton with oil).

The literature [70, 93] describes the two most sophisticated smoke tunnels. The first tunnel was designed for the study of two-dimensional flows. Its taper ratio is 1:20, and the dimensions of the measurement space are 1 × 1.7 m with a depth of 5 cm. The three walls (upper, bottom and one side wall) are made from pure glass plates. The walls are transparent. The images obtained in this tunnel are shown in Fig. 28.

The second tunnel is used /51
to observe three-dimensional flow. Otherwise, both tunnels have a great deal in common. Thus, quiescent flow is obtained in both cases by several screens of various types located immediately behind the inlet opening of the tunnel. For example, in one design [83], altogether 13 screens were used, seven bronze screens whose linear dimension was approximately 1.6 mm and six nylon screens whose linear dimension was approximately 1.3 mm. The /52
mist is introduced by a comb nozzle placed in front of the body at the tapering area or immediately before it. The outer shape

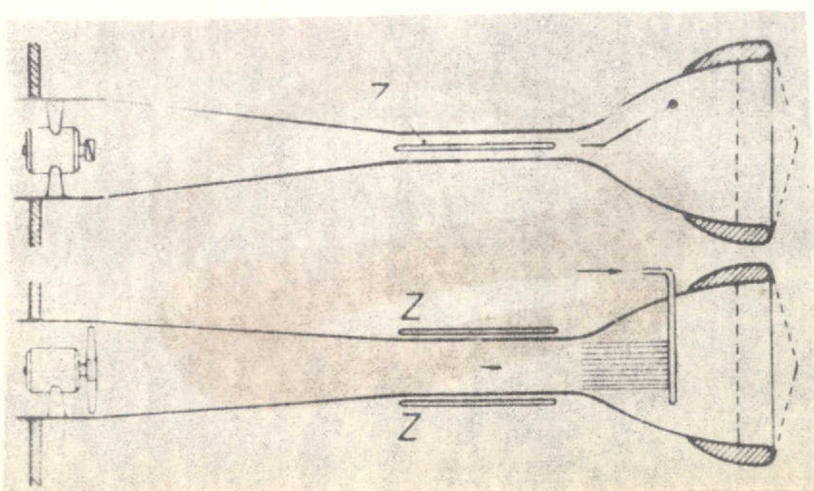

Fig. 26 a. Schematic diagram of smoke tunnel [5] (Z -- light source).

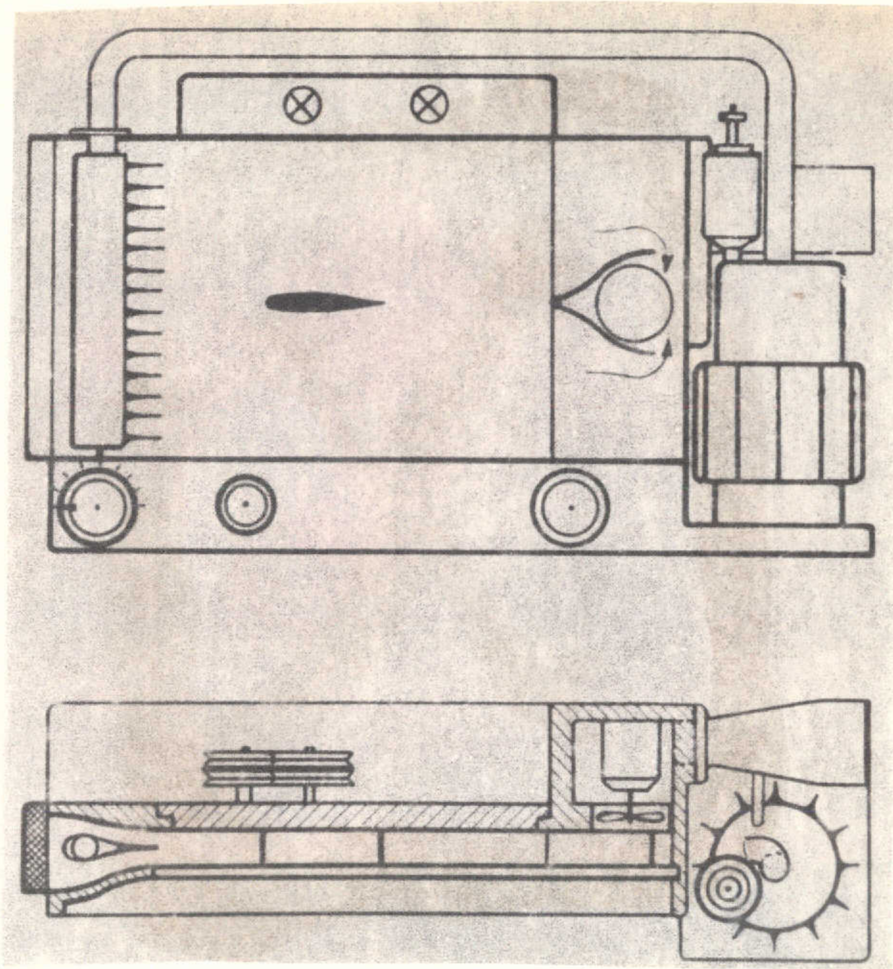

Fig. 26 b. Schematic diagram of small smoke tunnel.

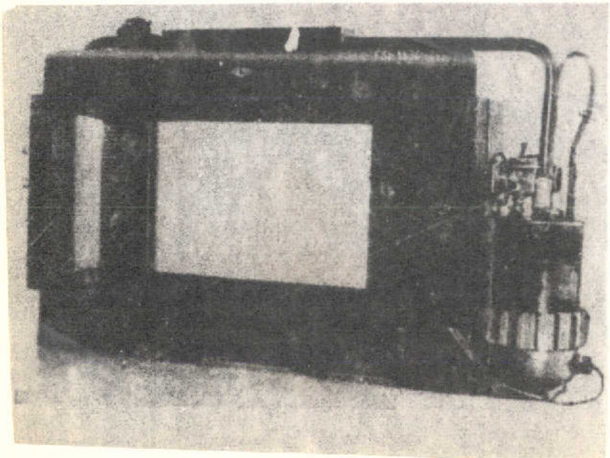

Fig. 26 c. Small smoke tunnel.

of the comb nozzle has the form of a wing of constant depth and the smoke is let out through the individual holes in the trailing edge. When the boundary layer is studied, the mist is let out, in most cases, from the streamlined body, for example, immediately behind the leading edge.

Smoke tunnels operate at relatively low velocities. The maximum velocity of a free stream is about 30 m/sec. Higher velocities can be attained

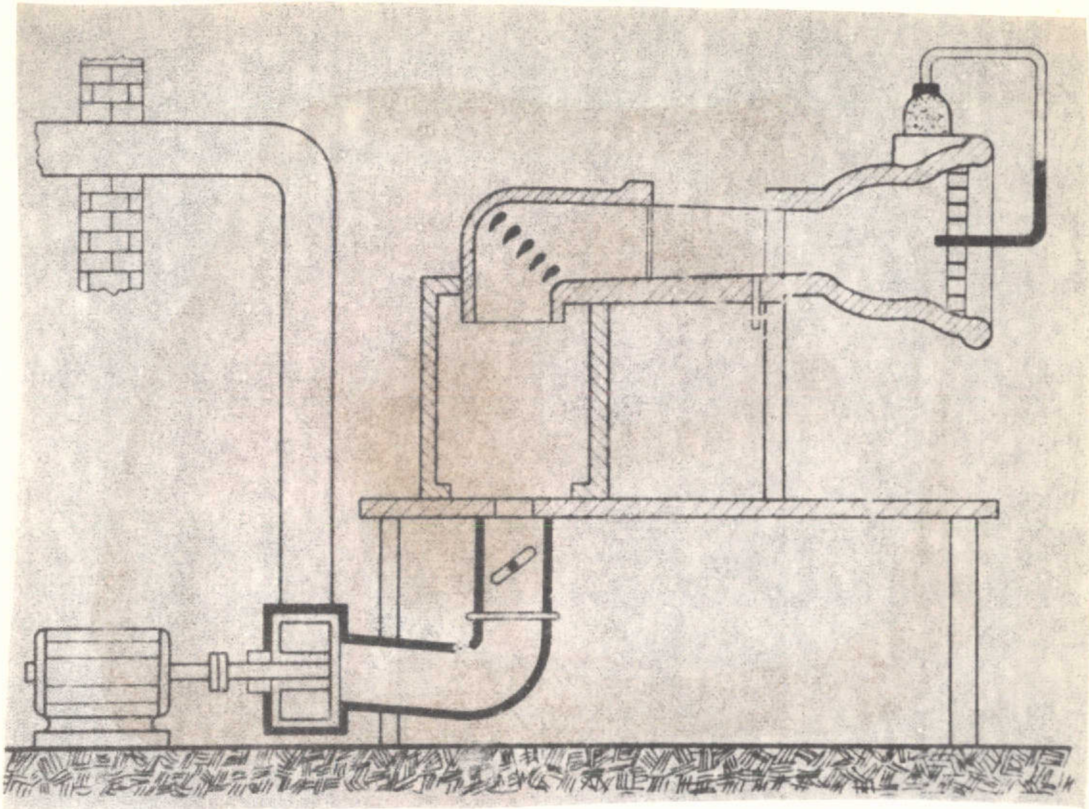

Fig. 27. Schematic diagram of smoke tunnel using smoke obtained with the aid of titanium chloride.

when the taper ratios are very high and the flow is laminar without liquifying the smoke trails.

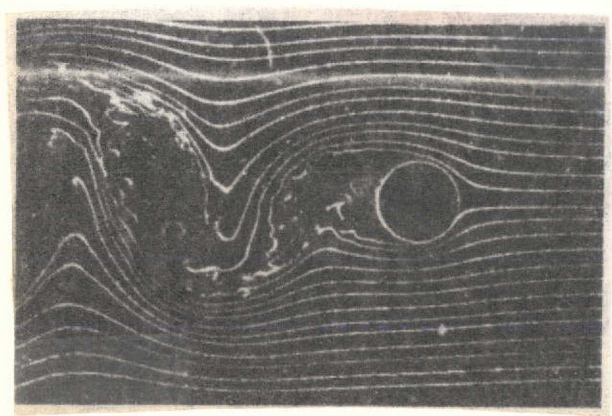

Fig. 28. Photograph obtained in perfect smoke tunnel [93].

The illumination method is outlined in the sketch in Fig. 26a. The observation space is illuminated from above and from below and the axis of the photographic equipment is perpendicular to the plane of flow (in three-dimensional flow studies). The rear wall of the tunnel is covered by black velvet (black background). When the tunnel is used to study three-dimensional flow and flow in the boundary layer, the illumination and photography direction depend on the type of problem that is studied. For certain purposes, illumination by a plane pencil of rays is adequate (see p. 23). The illumination requires high-intensity sources, whose input in the tunnel is usually greater than the input needed for the blower drive (for example, [83] the tunnel motor works with a 1.5 k input, and the input of the light sources is 26 kW = 35 k).

In addition to the usual recording methods that were already mentioned, experiments were made with high-speed motion picture cameras (up to 3000 pictures per minute). These records were used to study unstable processes during the flow. Light sources with a high input, for example, 38 discharges each 700 W, had to be used for this recording method.

The results obtained in modern smoke tunnels can also be used, among others (see below), in the quantitative evaluation of the velocity field around the streamlined body on the basis of the group of smoke trails that were determined which have the shape of the streamline in a stationary flow. The following images of the flow will best illustrate the many ways in which smoke methods can be used (see Figs. 29 through 35).

C. The third method in group 1.2.1 is based on the use of hot wires and heated surfaces [85, 86, 87]. Trails, layers or regions with properties other than those of the flow medium (gas) are obtained here by artificially changing the properties of the medium. A thin wire heated by electric current is used for this purpose. A layer of the medium (gas, as a rule, air) is formed which has a different temperature and hence a different density and a different refractive index than the surrounding parts of the flow medium so that for a proper illumination, a darker strip is formed on the screen which represents, for example, the streamline. Several wires placed parallel above one another across the flow can also be used, which makes it possible to visualize the system of streamlines. The changes in the properties of the flow medium in a certain region can also be achieved by heating the surface or part of the surface of the streamlined body. More sensitive observation in all these cases can be achieved with the optical refraction method (simple refraction method, diaphragm refraction method) described in Part 3. /53 /54

When the method was applied, 1 to 3 cm long platinum wires with a diameter of approximately 0.05 mm were used, which were heated by current from batteries. Rheostats were used to regulate the current [85, 86]. The wire must be heated until it has a dark red glow and a current intensity of roughly 1 A is needed for the wires that were mentioned when the velocity of the flow is about 10 m/sec. Instead of a platium wire, another material can also be used. Alternating current can also be used for the heating. /55 /58

Combined with a stroboscope, the methods can also be used to observe transient and periodic processes. They are also suitable

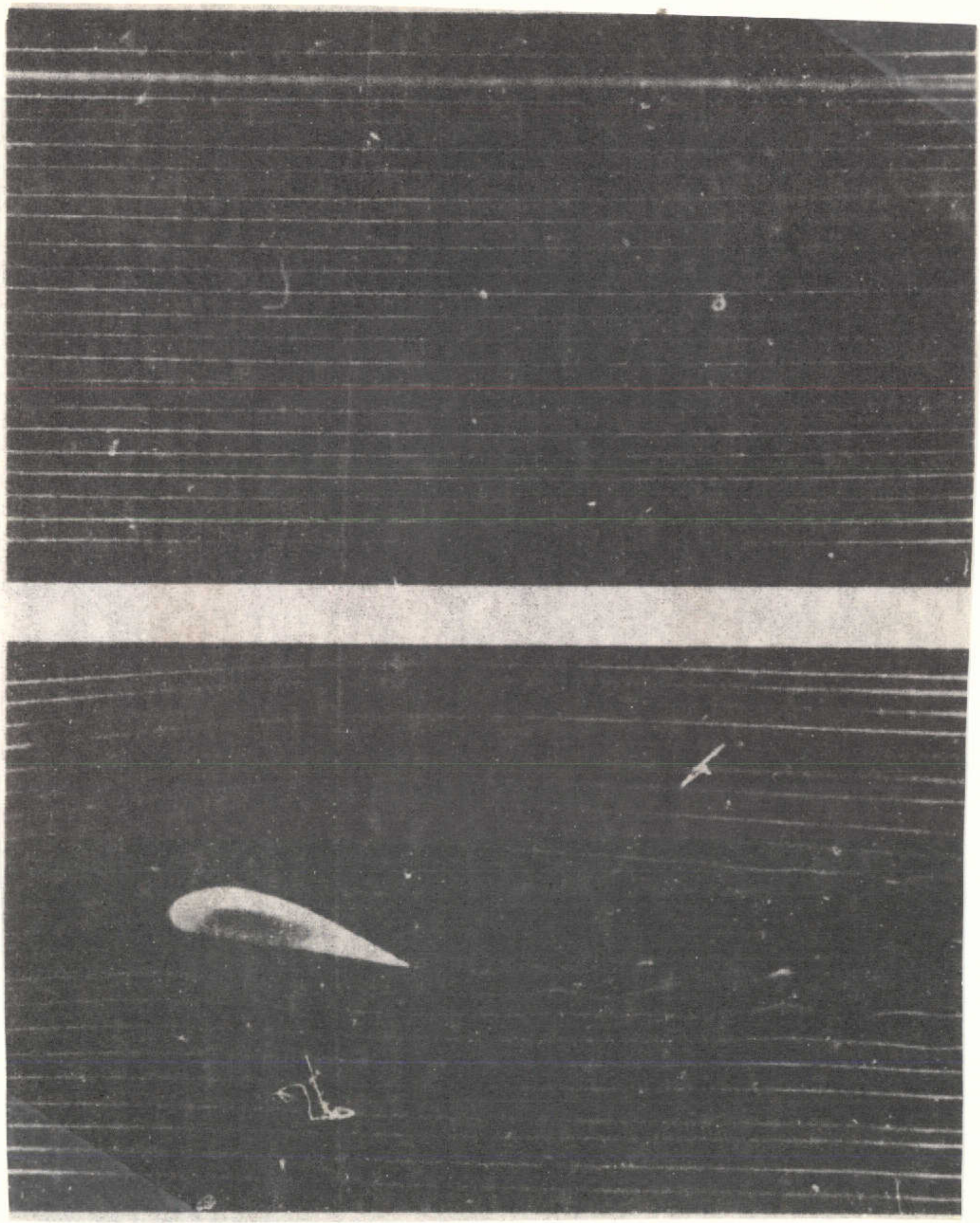

Fig. 29. Photographs [10] obtained using the smoke tunnel plotted in Fig. 26b. a) smoke trails in unperturbed flow in homogeneous velocity field.

for the study of three-dimensional flows when illumination with a slit is used as described on p. 23.

The wind tunnel must have similar properties as the smoke tunnels described in B (low velocities, low turbulence). Any light source level can be used together with the optical equipment which will ensure that a pencil of approximately parallel light rays will pass through the observed place.

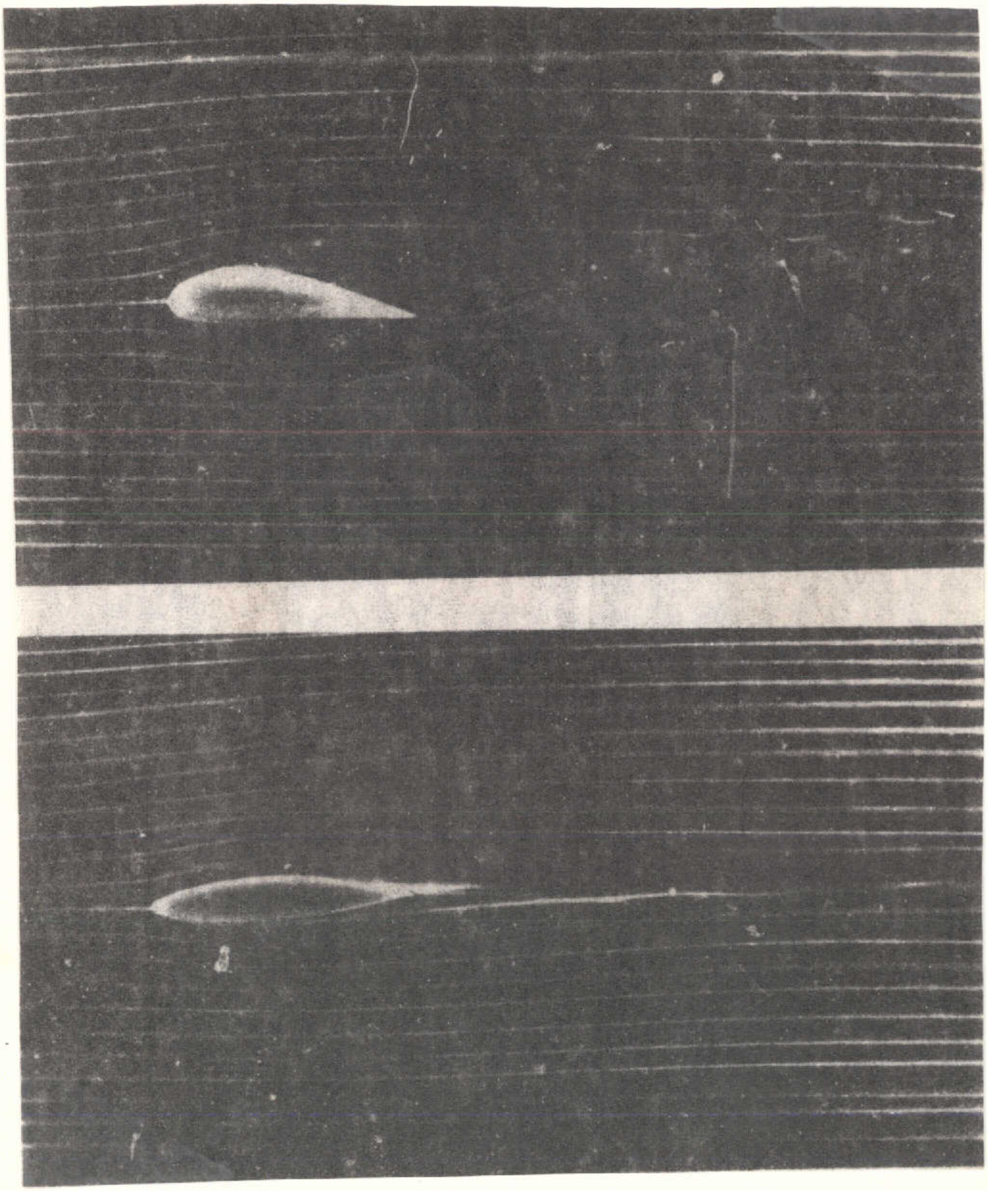

Fig. 29. b, c) Image of flow around classical profile; d) Image of flow around laminar profile.

When this method is used, the velocity of the flow is bounded above and below. The maximum velocity that can be used is about 20 m/sec, at high velocities the trails liquify rapidly as a result of the higher viscosity. The lower velocity boundary is due to the rate of rise of the heated gas (air) as a result of its smaller density. The effect of this rate of rise no longer manifests itself noticeably at velocities above 2 m/sec.

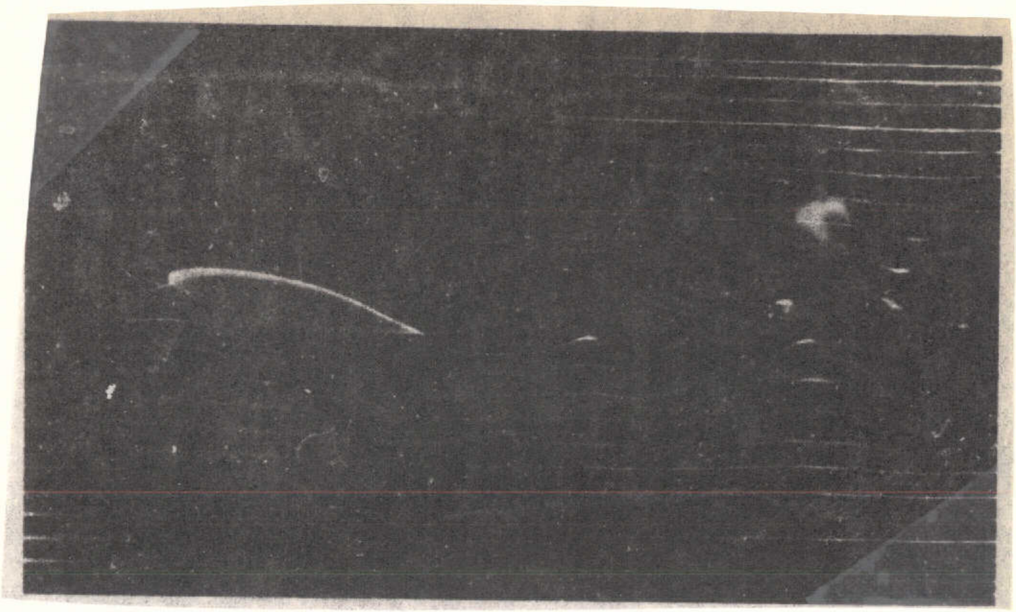

Fig. 29 e. Image of flow around a laminar profile.

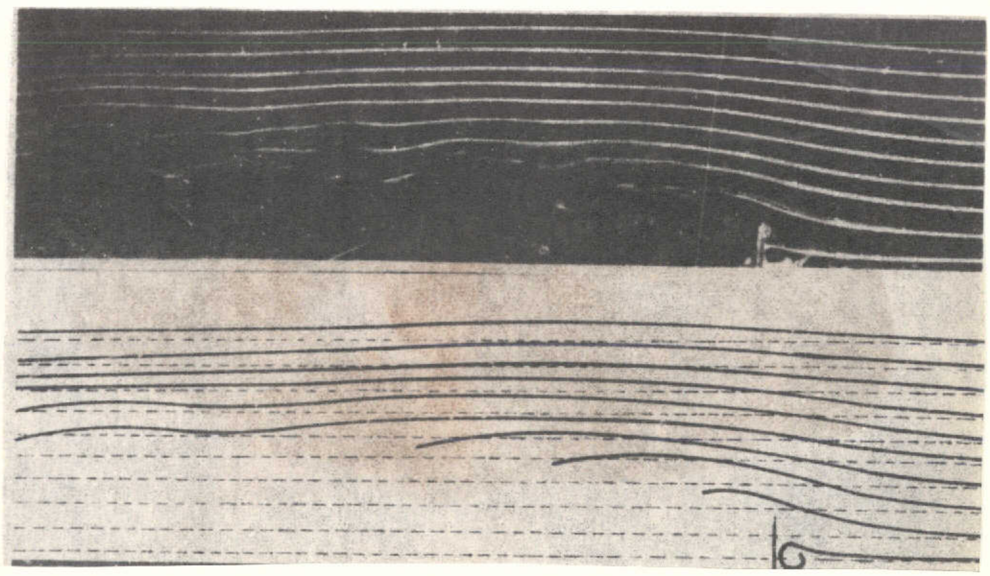

Fig. 30. Photograph obtained using the small smoke tunnel drawn in Fig. 26b. a) Flow around an impenetrable obstacle.

The advantages of the method are the simplicity of the equipment, the short time needed to prepare the experiment and also that it is not necessary to introduced other substances into the flow, since the introduction of other substances into the flow medium can have an effect on the type of flow in certain cases. The

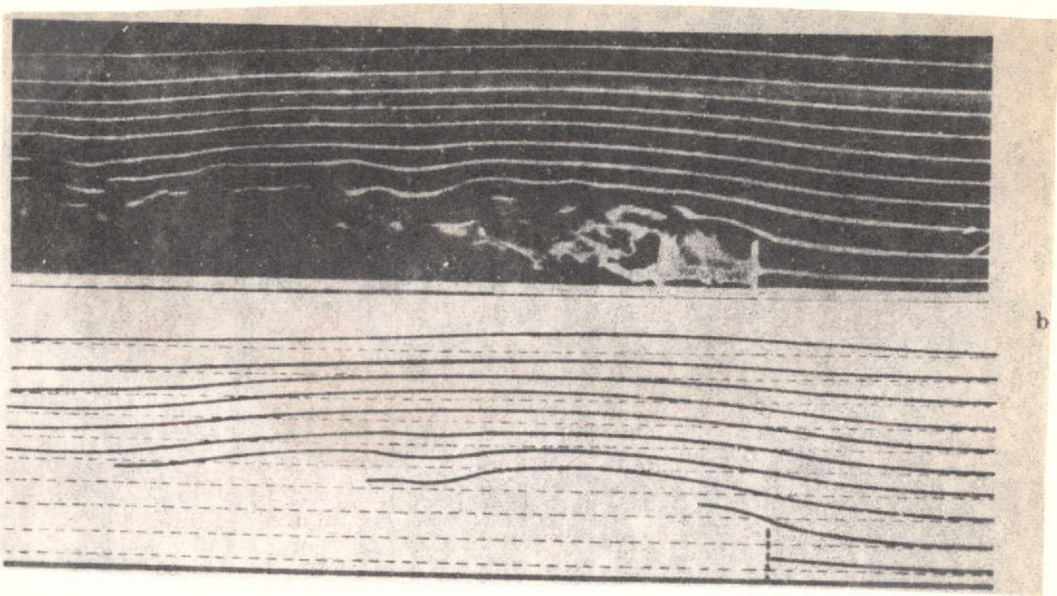

Fig. 30 b. Flow around a penetrable obstacle.

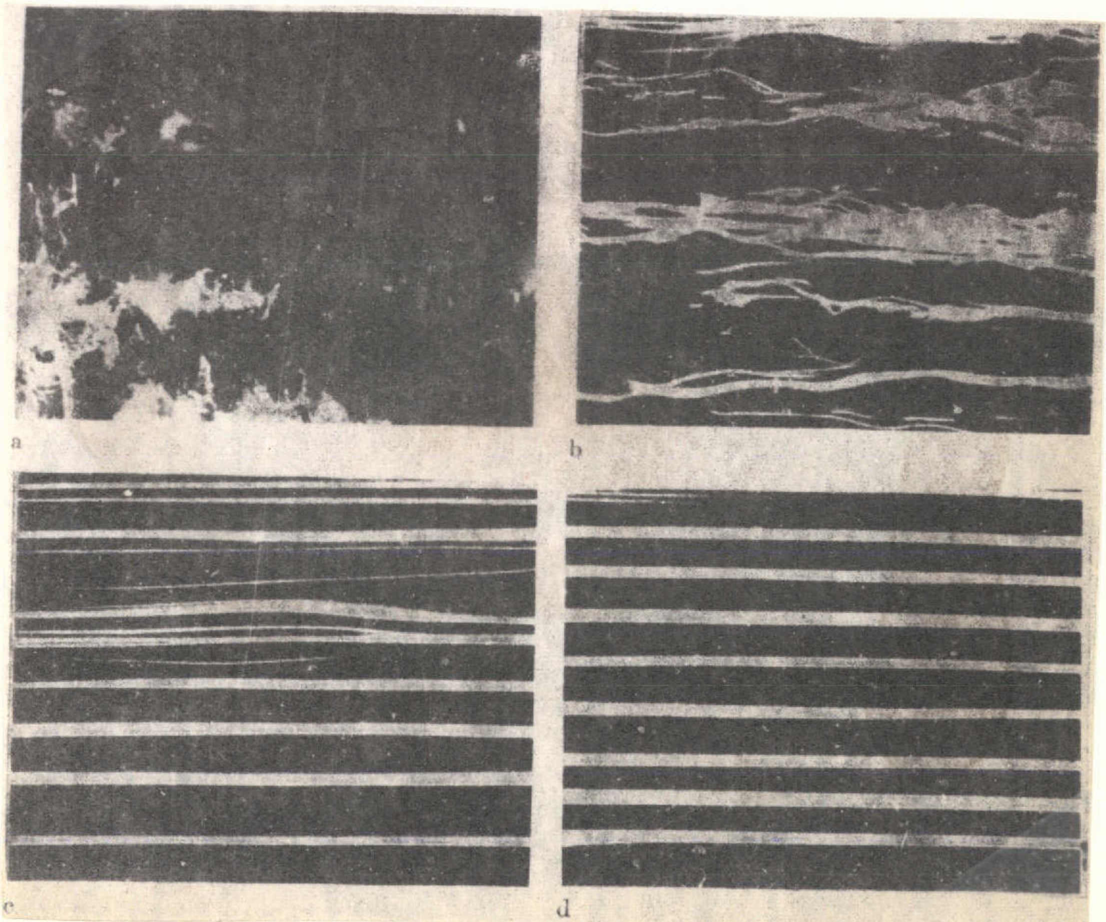

Fig. 31. Effect of tranquilization screens in inlet branch of smoke tunnel [72]. a) Without screens, b) Two screens, c) Five screens, d) Twelve screens.

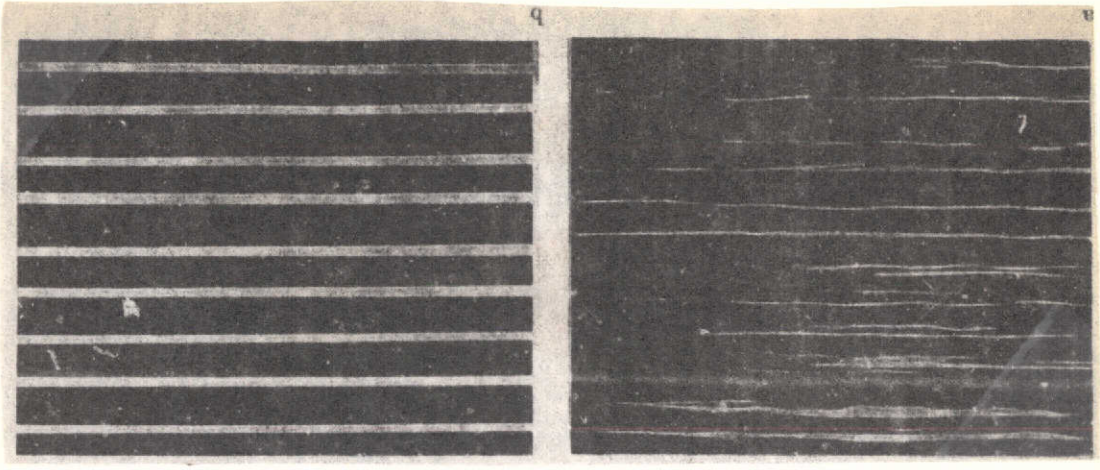

Fig. 32. Effect of tapering inlet branch of smoke tunnel [72]. a) Tapering 12:1, b) Tapering 24:1.

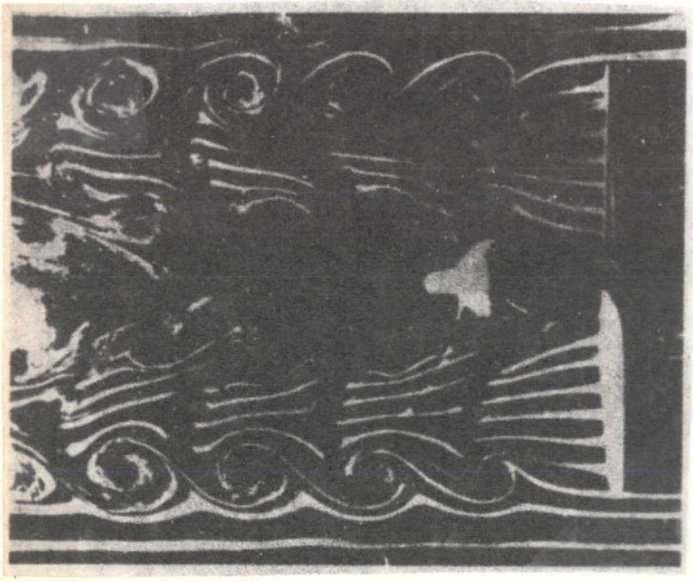

Fig. 33. Image of flow behind propeller [72].

disadvantage of the method is that the vortices behind the streamlined model cannot be observed in the wake, since as a result of the effect of the vortical motion the warm air trails liquify rapidly, i.e. they mix with the surrounding cold air. As a result of this the method is mainly suitable for visualizing the flow in front of the model and around it. /59

Fig. 36 shows the photograph of a two-dimensional flow around a wing obtained with the aid of this method. Fig. 37 shows the results obtained from using a heated surface to visualize the flow around a sphere. The brass sphere was heated by a burner flame before it was inserted in the tunnel [87]. The velocity of the flow around the body when heated surfaces are used must be selected properly, i.e. it must be sufficiently high so that the spontaneous flow caused by the differences in the temperatures can be ignored.

A small volume of air can also be heated with a high-current electrical discharge. For example, to determine the velocity profile in the boundary layer and its development on the plate,

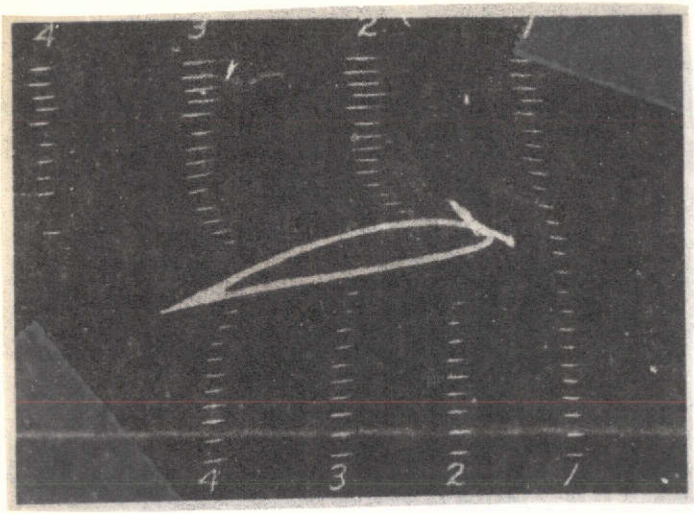

Fig. 34. Visualization of flow around a profile by smoke introduced in pulses [93].

Fig. 35. Visualization of vortices behind vibrating wing. The smoke is conducted by two tubes: one above the wind and the other below it [5].

one can use the changes in the shape of the heated air trail which was originally perpendicular to the plate and heated by the discharge between the plate and the tip placed above the plate [104].

The method which uses light spark discharges in the gas flow, usually air, is based on a similar principle [94, 95]. When it is used, electric pulses are supplied to the electrodes inserted in the flowing air which have such properties that a spark discharge of very short duration is generated between the electrodes (roughly 60 kV, duration on the order of 10^{-6} sec). The highly ionized plasma cylinder formed by the first spark is carried by the current. The subsequent light spark discharges which repeat themselves in short time intervals no longer follow the trajectory of the first spark, but pass through the plasma cylinder formed by the previous discharge which was displaced by the flow, since the plasma cylinder has a much higher conductivity than the air which is not ionized. The light discharges can not only be observed directly, but can also be photographed with an ordinary camera in which the objective must be open from the instant when the first spark was formed until the time when the plasma cylinder is carried by the flow to the end of the part of the flow that is studied. When the pulse frequency causing the spark discharges is f, the images of the individual positions of the plasma cylinder obtained in the photograph are shifted through distances corresponding to the path $s = v/f$ in the flow, where v is the local velocity of the flow. /60
Fig. 38 gives a diagram for the arrangement of the electrodes for various cases of flow and Figs. 39 and 40, the photographs of

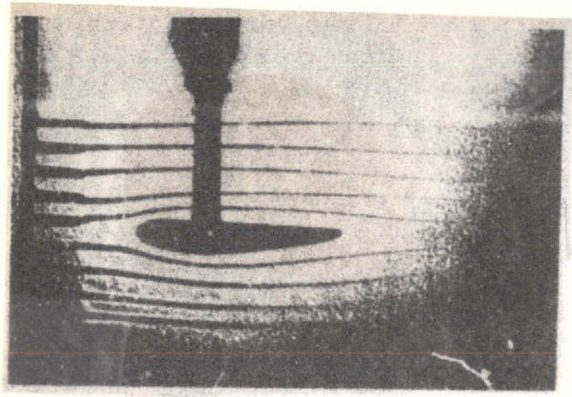

Fig. 36. Visualization of flow around a wing with the aid of the method of hot wires [87].

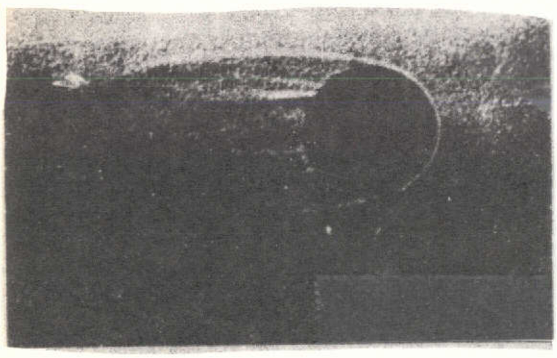

Fig. 37. Visualization of flow around a sphere using the method of heating the surface [87].

two flow fields in widening pipes visualized by light spark discharges.

To obtain the required electric pulses, the authors of article [95] used the equipment manufactured as the source for a discharge tube of a stroboscope (Strobokin Hochfrekvenzblitzgerät). The electric power from the pulse capacitor of the lamp is sup- /61 plied to the high voltage pulse transformer. Exactly regulated high-voltage pulses up to 250 kV can be obtained in this manner. The width of the pulse can be adjusted by choosing the transformer values and modified with the aid of damping resistances. With regard to the frequency of the pulses using the equipment that was described, a value of 70 kHz can be attained and, in a special version, up to 140 kHz. However, for the study of gas flows, frequencies on the order of 10^3 Hz = 1 kHz must be used. The highest frequency that can be used must be determined mainly by the velocity of the flow and its transverse velocity gradient. However, the time during which the discharge glows must also be taken into account, since it has an effect on the sharpness of the discharge images on the photographs, and the transverse dimensions of the discharge, the discrimination possibilities on the photograph, and finally also the sensitivity of the photographic material must be taken into account.

The use of the method described in aerodynamics is limited both by the maximum attainable dimensions of the flow field which are on the order of several centimeters and also by the shape of the electrodes. Correct results can actually only be obtained in the case when electrodes with the smallest possible dimensions are used in the direction of the flow. In the case of long

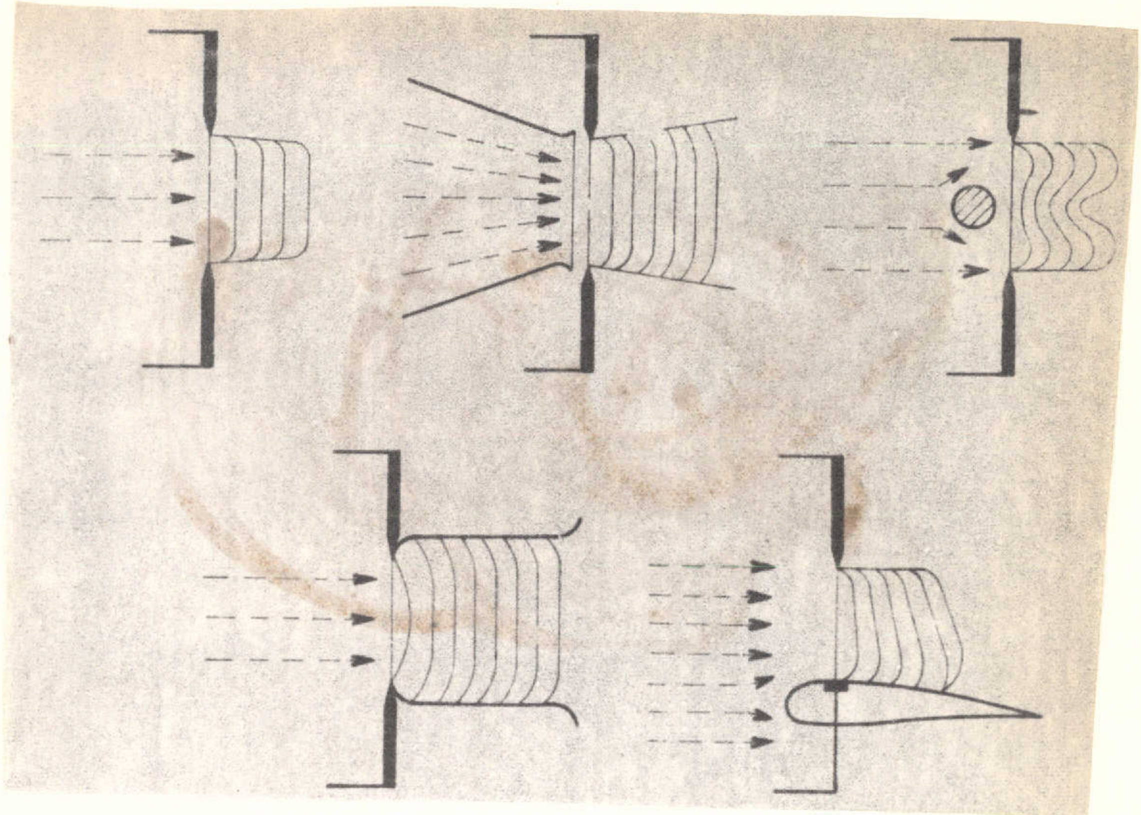

Fig. 38. Schematic diagram for the arrangement of electrodes for the method of light spark discharges.

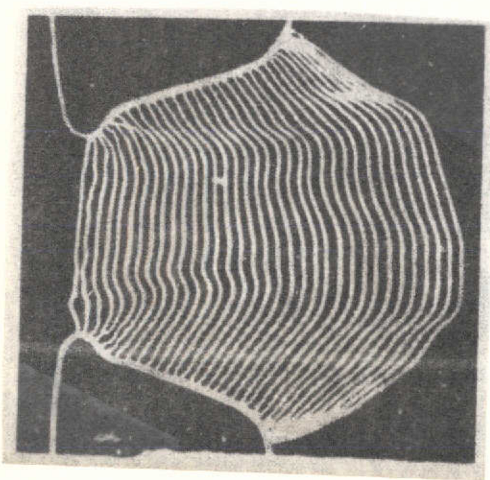

Fig. 39. Photograph of successive light spark discharges in widening pipes [95].

electrodes forming the boundaries of the flow field, the incorrect conclusion follows from the record that the velocity of the flow near the surface of the electrode, i.e. the flow around the wall, has /62 the same order of magnitude as the velocity in the flow. Similarly, when the flow field behind an obstacle is studied where the plasma cylinders acquire deep curvatures as a result of the great differences in velocities (as in the previous case, near the walls), it may happen that the spark discharge no longer follows the trajectory of the previous plasma cylinder but follows the relatively shortest path between the electrodes. The results subsequently obtained are incorrect.

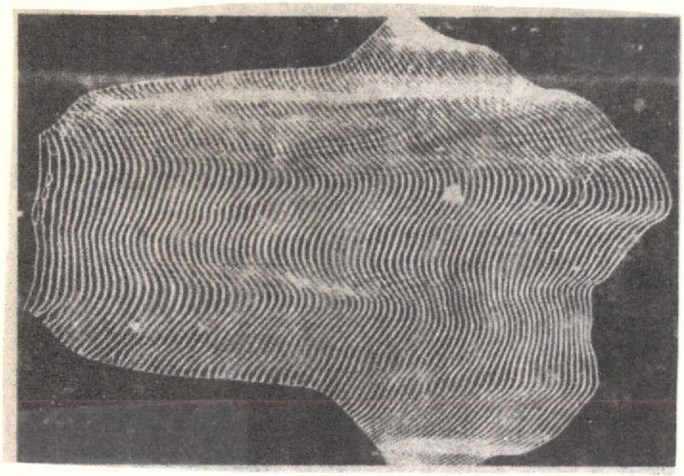

Fig. 40. Photograph of successive light spark discharges in an expanding pipe.

Next, disturbances caused by the high temperature of the discharge and pressure waves which accompany may occur, although this possibility is improbable because of the very small amounts of energy per discharge. From everything that was mentioned, it follows that, although the method is effective, it can only be used for a qualitative analysis of certain simple cases of flow where the dimensions of the flow field are on the order of several centimeters.

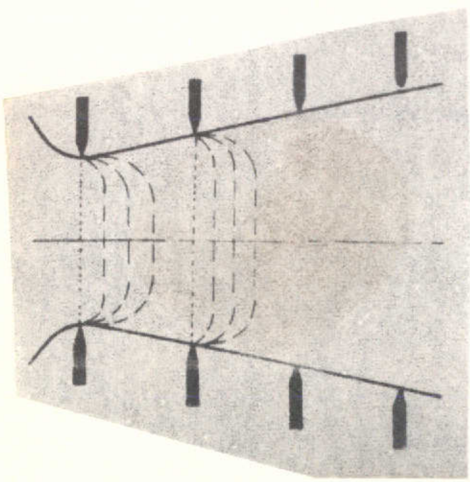

Fig. 41. Schematic diagram for the arrangement of a larger number of electrodes.

A certain improvement can be achieved by introducing a larger number of electrodes of small dimensions placed pairwise opposite to one another in the electrically non-conductive walls which limit the flow field (Fig. 41). A train of several pulses (two to five) must be supplied to these electrodes simultaneously in a way which will ensure that each discharge between a particular pair of electrodes follows the plasma cylinder of the previous discharge displaced by the flow between the same pair of electrodes, so that the plasma cylinder belonging to the discharge between a certain pair of electrodes will not have an effect on the shape of the plasma cylinders from discharges between neighboring pairs of electrodes. A record like that in Fig. 41 is obtained (the dots indicate the trajectory of the discharge from the first pulse, the dashes from the second, third, and fourth pulses). However, this modification would require from the source of the pulses an electric power which is several times larger.

D. The fourth method in group 1.2.1 uses a glow discharge in a gas and gas luminescence at low pressures.

The glow discharge causing changes in the entire flow region used for its visualization can also be used to study the gas let out from the nozzle into a medium at a very low pressure on the order of several torr, which is convenient, since at these low pressures, the usual refraction and interferometric methods which will be described in Part 3 are not suitable. The gas flow is visualized so that its atoms are excited by the high frequency voltage and the glow determines the region of the flow and also the strong pressure changes in it. The disadvantage is that also the surrounding gas which was left in the space into which the gas that is studied flows, also glows. However, since the incoming gas has a higher pressure than the still gas in the chamber, its glow has a higher intensity, so that this disadvantage does not cause excessive difficulties.

A Tesla transformer, which gives a high frequency alternating voltage of about 40 kV can be used as the current source. An outline of the experimental equipment is given in Fig. 42. Fig. 43 shows the flow of argon from a nozzle with a 1 mm diameter into a chamber in which the pressure is 1 torr. The pressure drop on the nozzle was 20 torr [88].

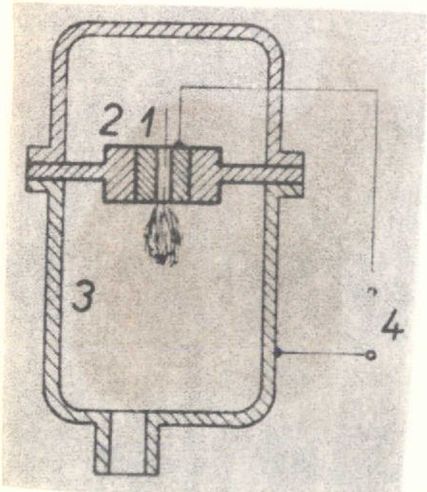

Fig. 42. Chamber for the study of gas let out from a nozzle with the aid of a glowing discharge (1. nozzle from electrically conductive material; 2. partition from insulating material; 3. chamber from conductive material with transparent windows; 4. high voltage supply source).

A bundle of electron beams bombarding the gas flow can be used instead of the high-frequency alternating current to excite the atoms of the gas flow. /63

Similarly as in the discharge, to visualize the flow at very low frequencies (on the order of several tenths of a torr) luminescence can be used (see Figs. 44 and 45). The gas atoms are excited by the strong high-frequency alternating electric field before they enter the nozzle, and when they are let out from the nozzle and enter the medium with the lower pressure they glow, and also outline directly the shape (outline, contour) of the flow and also by their different intensities, the pressure differences in the flow [89, 19, 146, 146a]. In comparison with discharges during luminescence, the atoms continue to glow for a certain time after excitation.

Luminescence has also been used in tunnels to study the flow of nitrogen and air at very low pressures. The experiments with pure nitrogen were carried out in the pressure range from 0.1 to 60 torr. When a strong electric discharge passes in this state through /65

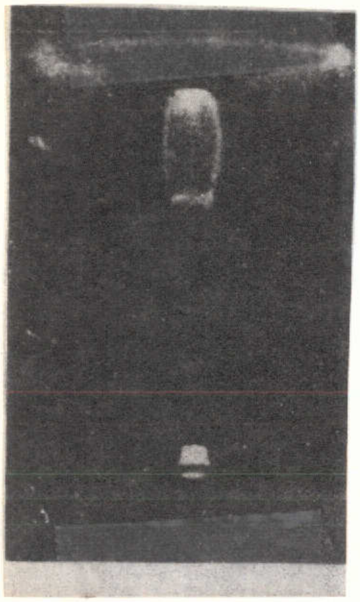

Fig. 43. Argon flow from nozzle with a 1 mm diameter into the space where the pressure is 1 torr visualized by glowing discharge [88].

pure nitrogen it may induce in it a luminescent glow which lasts for a certain period (several tenths of a second) after the discharge ends. The wavelengths and the relative luminance (relative to the green line at wavelength 5371 Å) of the strongest spectral lines of this radiation are given in the following table:

Red	6251 Å	0.345
Yellow	5802 Å	0.940
Green	5371 Å	1.000

The intensity of this glow increases (in the range of pressures under consideration) with the pressure. If the nitrogen contains oxygen and carbon dioxide remnants, these substances have an effect on the color of the luminescent glow which changes with the pressure, so that the density of the gas can also be inferred on the basis of the color of the glow.

In air, the luminescence was observed in the pressure range from 0.02 to 10 torr. Similarly, as in nitrogen, also here the intensity of this glow increases with the pressures (in the given range of pressures).

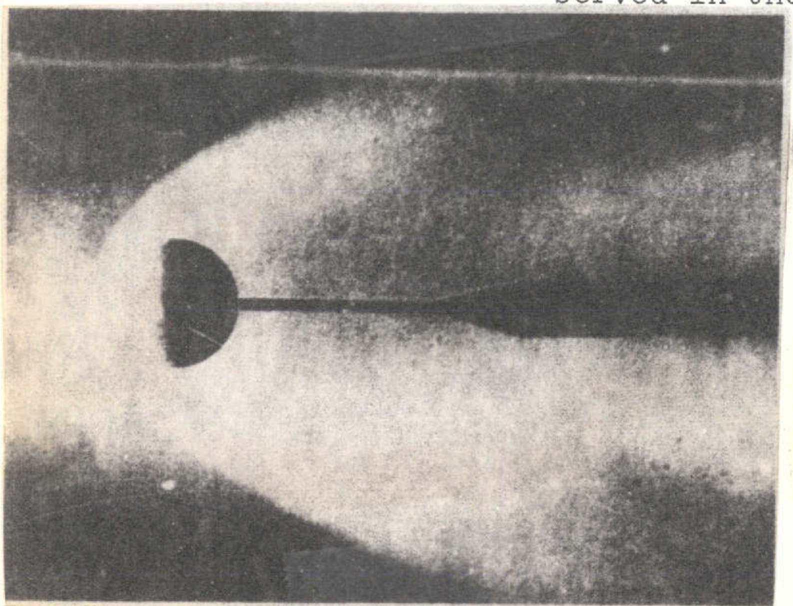

Fig. 44. Use of gas luminescence at low pressure for visualizing flow around a sphere [89].

Compression waves can be visualized well in the gas flow with the aid of luminescence. A comparison with photographs of the flow obtained with the aid of the diaphragm refraction method which was described in Part 3 shows that the position of shock waves can be determined correctly by the luminescence method.

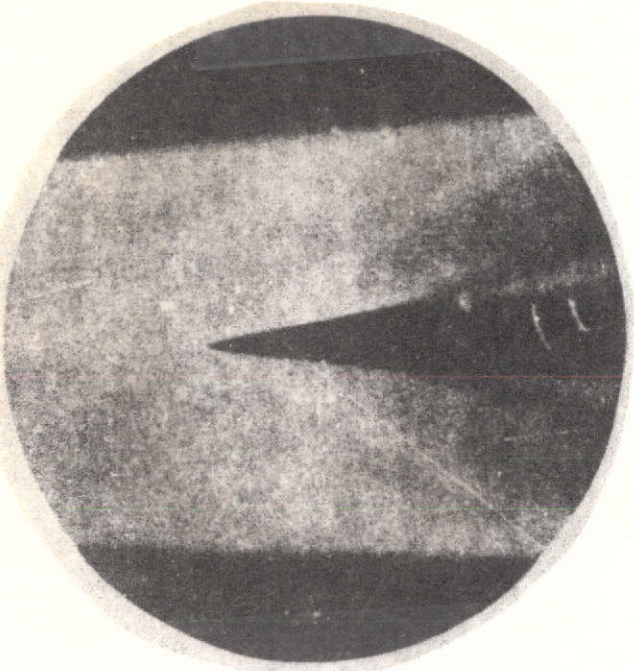

Fig. 45. Visualization of flow around rhombic profile using luminescence of excited gas [89, 146].

We also note that both methods are suitable for visualizing supersonic flow at very low pressures, which is becoming a topical problem.

E. Group 1.2.1 also includes the following method for obtaining images of shock waves in humid air or in air with smoke. In places in which the air pressure is much higher than the pressure in the undisturbed medium (i.e. in places occupied, for example, by the shock wave), an increase in the concentration of the admixture particles in the air (smoke, water) occurs or possibly condensation of water vapors, so that these places can be distinguished from the surrounding medium by the naked eye due to the greater absorption and scattering of the light. It is convenient if the observation space is illuminated in the direction of the flow and the wave is observed approximately in its direction. Using this method it is also possible to determine the three-dimensional wave pattern. Vortices and wakes which appear in passing light as darker spots in the observation field can be visualized in a similar manner [96, 97].

1.2.2. <u>Methods Based on the Use of Particles Not Forming Coherent Trails or Relatively Large Coherent Regions</u> /66

(Use of aluminum powder, fine balsa dust, sparks. Townend's method of heated air particles. Filament probes, direction probes.)

The following methods are used to visualize gas flows with the aid of individual particles:

A. For relatively low velocities (to 100 m/sec) aluminum powder or fine balsa powder can be introduced advantageously into the flow [99 through 102]. These two methods are used most frequently; however, fine cork powder, elder pith powder, etc. have also been used. The condition under which the particles that were introduced trace well the flow that is being examined were mentioned on p. 12.

Balsa dust is very advantageous because its particles have a low density and reflect light well. They are obtained by grinding the balsa wood across the grain on fine emery paper. The dust that is obtained is sieved twice on a sieve whose linear dimension is approximately 1.4 mm. Its particles fall in an atmosphere at rest at an average velocity of 30 cm/sec [100].

Other suitable particles of a floccular character can be obtained by sublimating solid metaldehyde which is a polymerized acetaldehyde. The piece of metal which is heated until it is red is pressed to a Meta fuel block (so-called solid alcohol). This leads to the sublimation of the polymerized acetaldehyde.

Other suitable particles are sparks which can also be used at higher velocities [11, 12]. Sparks obtained from coal dust, tinder or through grinding on a grinding disk are used.

The usual types of wind tunnels and the illumination method described on pp. 14 and 25 are suitable for all these methods. Observation by the naked eye, photography or motion picture recording do not cause any difficulties. The problems connected with the illumination were solved theoretically in study [102].

Quantitative data can also be obtained (for example, the velocity field during flow around bodies) and the corresponding method is called the chronophotographic method [98, 112]. One of the three following basic methods can be used. The first method is based on photographing the flow fields with the particles with a certain known exposure time, and subsequently determining the velocities of the flow at the appropriate points from the lengths of the particle tracks. In the second method, two exposures are taken on the same photograph with a known time interval and the velocities are determined from the change in the position of the visualized particles. Both exposure times are sufficiently short, so that in each exposure the trace of the particle is nearly a point. Both these methods have already been mentioned earlier. The third method uses interrupted flash illumination and a large number of exposures of the flow field are taken on the same photograph. Thus, we obtain, on the photograph, dashed trajectories of the particles. The direction of the dashes determines the direction of the velocity of the flow and the magnitude of the velocity is determined from their spacing and the frequency with which the light is interrupted. The basic difference in this method compared to the first two methods is that the third method yields the actual trajectories, whereas /68
in the first two methods we obtain the trajectories by connecting the tracks formed by different particles.

Examples of the concrete use of individual particles are given in Fig. 46 (flow through the model of a helicopter rotor, balsa dust was used) and Figs. a, b (flow around the model of a roof and cylinder, aluminum powder). Interrupted illumination was used which was obtained with the aid of the continuous light of an arc lamp and a screen (a disk with cutouts) rotating with a variable number of revolutions. Another method is to construct the source of interrupted light with the aid of an electronic stroboscope where a discharge arc is used as the light source, or advantage is taken of the natural oscillations of a carbon arc lamp. The equipment that was used for the photographic studies whose photographs are given in Figs. 47 a, b is described in detail in article [48].

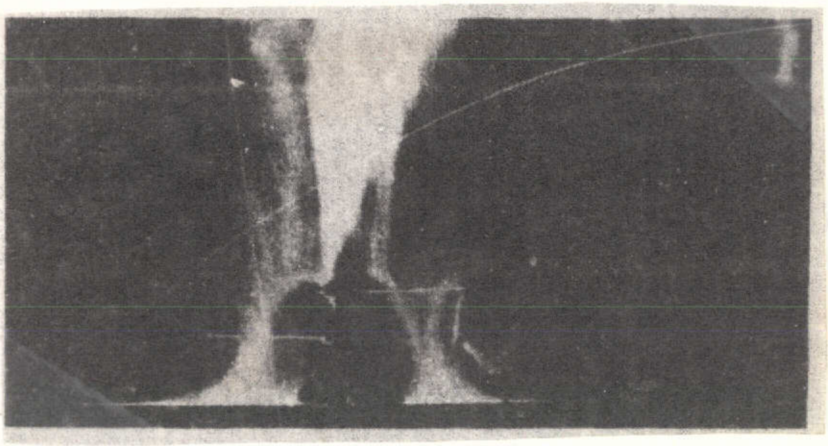

Fig. 46. Image of flow through model of helicopter rotor. Balsa dust used for visualization.

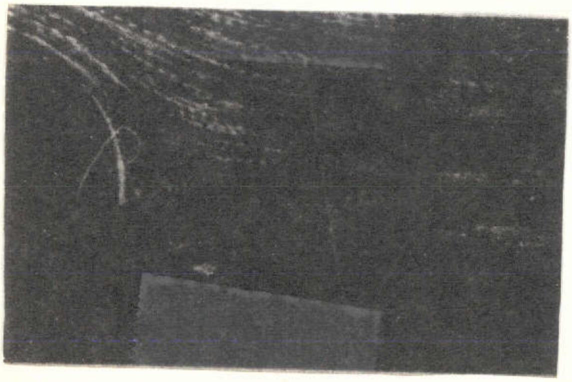

Fig. 47 a. [See caption on following page]

Individual particles in the flow can also be used to obtain a stereoscopic image of the flow. A certain section through the three-dimensional velocity field which is lit through by the light source with the slit is photographed by two cameras with nonparallel axes. We obtain the stereoscopic image of this flow through the optical composition of the pair of photographs that were obtained.

B. The second method in group 1.2.2 uses to visualize the flow the property that the small volume

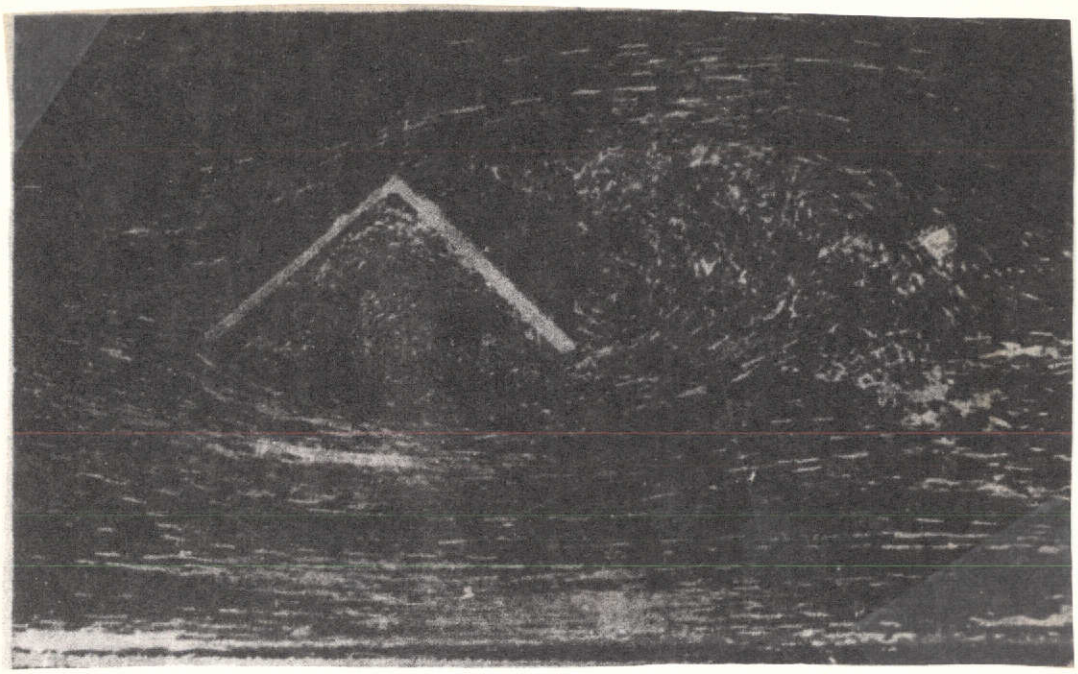

Fig. 47 a, b. Photographs obtained with the aid of the chronophotographic method [98].

of the medium flow heated by the spark (the gas, generally air) has different properties, in particular a different refractive index than the surrounding unheated medium flow [103-107]. During the practical application, repeated electric discharges occur at several spark gaps placed next to one another across the flow. The line connecting the spark gap electrodes is perpendicular to the plane of flow. From each pair of electrodes forming one spark gap, a series of small volumes of the flowing gas moves with the flow, which are connected as a result of the thermal inertia of the electrodes by thin filaments of the heated gas (the entire series can be compared to a filament which has "bubbles" at certain distances). Because there are several such spark gaps, a set of such series is formed. If the flow is stationary, images of the flow lines can be obtained. In addition, if the discharges occur at the spark gaps in equal time intervals whose length is known, the local velocity of the flow can be determined from the heated volumes ("bubbles" on the filaments).

The observations are carried out using the same equipment as in the method of hot wires (see p. 46). The sparks can be generated with the aid of an induction coil and an interruptor or with the aid of an alternator. For example, a 150-V alternator with an output of 0.5 k at 2500 rpm was used successfully. The current that was obtained was regulated by rheostats and after it was raised 1:100 by the transformer, it was supplied to the spark gap. The appropriate distance between the two electrodes forming the spark gap was approximately 1 cm [103 through 105]. Fig. 48 a, b shows the visualized flow around a wing obtained using this method. The diaphragm refraction method described in Part 3 was used for observation [105].

C. Another appropriate method is using a probe with tufts, for example, the probe can be a rod to which several tufts are attached at equal distances (possibly only one tuft whose /69 ends are frayed or have a small piece of feather attached to them. If such a probe is inserted in the current, the form of the particle trajectories in the flowing medium can be inferred from the orientation of the tufts. The characterof the flow around the body can be determined with the aid of the probe when it is inserted close to it. During quiescent flow, the tufts will acquire such a shape that they will be oriented along the surface of the body. In the region where the flow is separated, the tufts will move in jumps. Regions of reverse flow or the downwash angle behind the model of a wing or around an airplane can be determined in a similar manner. However, the results obtained are only qualitative and it must be kept in mind that the flow is disturbed considerably by such probes.

More accurate results during the measurement of the downwash angle are obtained with the aid of probes suspended on a thin wire in the appropriate place. The probes are small balsa or metallic bodies (several types of such probes are shown in Fig. 49) which maintain in a flow in a given direction relatively steadily their direction and position. If we measure the direction and position (for example, by a theodolite), we can determine from the measured /70 values the necessary data about the direction of the flow [13, 114, 115, 109].

Quantitative data can be obtained with the aid of a probe with tufts using a grid [108]. The tufts are attached to a wire mesh whose linear dimension is about 25-50 mm at the points where the wires of the mesh cross. When such a mesh is placed behind the streamlined body perpendicularly to the direction of the flow, the flow in the wake and its range behind the body can be studied on the basis of the orientation of the tufts on the mesh. A mesh with an appropriate opening can also be pulled over the streamlined body and the region in which the flow of the medium around the body is affected by the presence of the streamlined body can be visualized with the aid of tufts Such a study in carried out at different depths of the body.

If all the tufts on the grid probe have the same length (in the case under consideration, wool tufts are used) it is possible to determine from the horizontal and vertical projections of their images on the photograph obtained by a

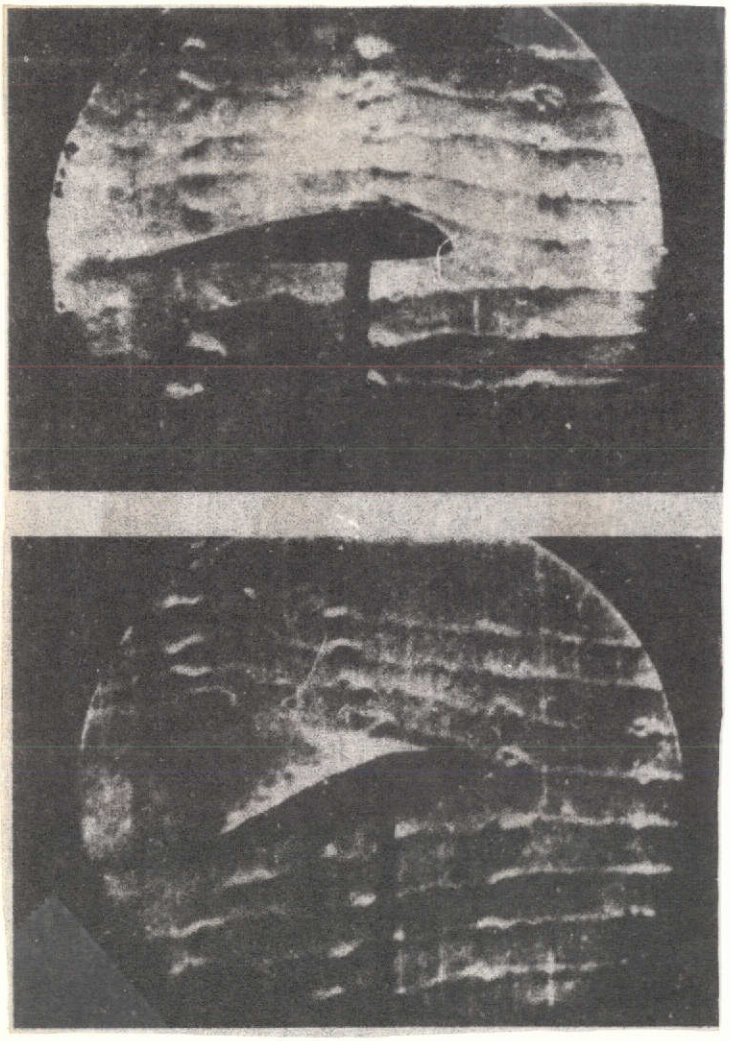

Fig. 48, a, b. The visualization of flow around a wing with the aid of Townend's spark method [103].

camera placed behind the mesh on the axis of symmetry of the streamlined body the deflection angles of the streamlines in the vertical and horizontal direction. From the angles that were determined from the photograph, the angles subtended by the axis of the camera and the lines connecting the points where the tufts are attached and the center of the objective of the camera must be subtracted. In a steady flow, using this method, the unknown angles can be determined with an accuracy of ±0.5°. /71

If the mesh moves with the opening for the wing along the chord of the wing, the origin and development of trailing vortices can also be observed. By integrating the tangential velocity of the vortices which is determined from the projections of the tufts on the photographs, the relative intensity of the vortices can be determined [108].

Fig. 50 shows a grid with tufts, placed at a distance of 60 cm behind the model of a delta wing with a sweepback of 60° at an angle of attack of 20° and an angle of yaw of 10°. The span of the wing is 90 cm and the velocity of the undisturbed flow is 27 m/sec.

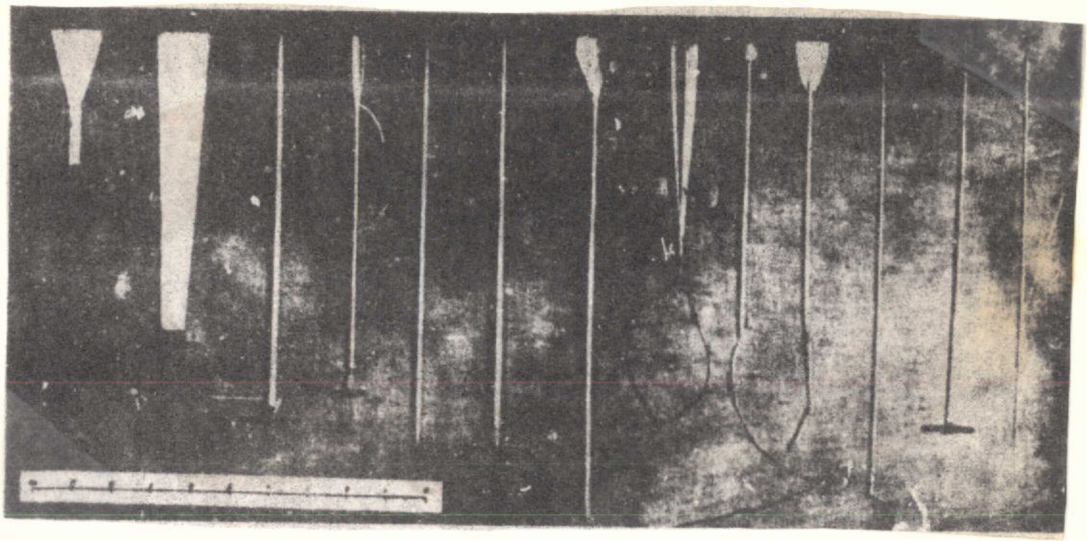

Fig. 49. Indicators of direction of flow [13].

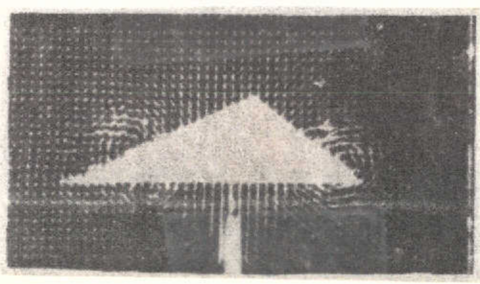

Fig. 50. Visualization of flow behind the model of a delta wing using a grid with tuft probes [108].

Part 2. Methods in Which Changes in the Specially Treated Surface of the Streamlined Bodies are Analyzed /72

Group 2 includes methods in which visualization is achieved by an appropriate treatment of the surface of the streamlined bodies in which the fluid flow causes changes and from which certain characteristics of the flow can be determined. These changes are observed either by the naked eye or they are photographed or possibly filmed. Methods based on the principle that was mentioned can be classified into three groups:

a) Chemical methods in which the chemical reaction of the fluid flow with an appropriate substance applied in a thin layer to the surface of the streamlined body is used. Areas on the surface of the streamlined body where this reaction occurs faster or more intensely acquire, as a result of the reaction, a different color shade or an entirely different color than the remaining surface. The reaction occurs faster during turbulent flow around a body and the regions of turbulent flow and the transition boundaries are also visualized.

b) Physical methods based on the principle of sublimation, vaporization or dissolution of the surface coating of the streamlined body in the fluid flow. Also in this case, as a result of the effect of the more vigorous mixing during turbulent flow, the physical processes that were mentioned occur faster and the laminar and turbulent flow can be distinguished by the different properties of the surface (a different refractive index and a different color hue).

c) Mechanical methods which are based on mechanical processes, such as a change in the position or shape of tiny particles placed on the surface of the streamlined body, a change in the thickness of the layer of an appropriate fluid applied to the surface, or the settling of particles scattered in the flow on the treated surface of the body.

The materials for the coatings used in these methods must not be poisonous and damaging to the human organism when handled, they must not cause corrosion or otherwise disturb the surface finish of the model.

Generally, the characteristics of the flow on the surface of bodies are obtained with these methods, both in models and in objects with real dimensions. The local direction of the flow on the surface of the body, the laminar and turbulent flow regions and the transition regions can be determined.

2.1. Use of Methods from Group 2 to Visualize Fluid Flows /73

The methods based on chemical reactions are not used frequently to visualize fluid flows since the liquid used usually is water and since it is difficult to find a substance which is satisfactory in all respects and reacts with the water in the required manner.

On the other hand, the methods that belong to the group of physical methods are used. The following substances which are the base of the indicator coatings have been used: acetoacetanilide, exalgin, acetanilide, phenacetine, hydroquinone diacetate, etc. [116]. The surface coating is obtained through dry spraying with the aid of a spray gun, which means that most of the solvent must vaporize before the substance which is dissolved in it impinges on the surface of the body. The thickness of the sprayed layer which is 5-12 μm must be smooth and it must not form unevennesses on the surface. The surface of the model must have a dark color. Usually, the sprayed layer has a light color. During turbulent flow, the layer dissolves faster than during laminar flow so that the laminar flow region is indicated by the light color of the remaining sprayed indication substance, whereas in turbulent flow regions, the dominant color on the surface of the model is dark, since in those regions the layer dissolves faster as a result of the effect of the more vigorous mixing motion. The most convenient solvent that can be used is acetone, or light oil fractions with a 4-5% concentration of the indication substance. A 5% solution of hydroquinone acetate with acetone or a 4-5% solution of acetanilide dissolved in a mixture of acetone and oil are most suitable for finding the transition region. The local unevennesses on the surface of the streamlined body cause the local disturbance of the flow, wakes which leave in the region of laminar flow on the surface of a streamlined body dark strips which can be used to determine the direction of the flow on the surface of the body [116, 117].

When these methods are used to visualize the the fluid flow on the surface of streamlined bodies, which we call mechanical methods, the methods used to treat the surface are very simple and not demanding with regard to the arrangements. For example, a thick coat of an oil paint is applied to the body which is inserted into the fluid flow before the paint dries. Fine scratches are formed in the coat which determine the direction of the local flow on the surface. Using the same method, separation regions can also be determined because the grooves disappear in this region. The following method in which the body is covered before the experiment by drops of oil paint and inserted in the flow which spreads (wet) drops in the direction of the flow is similar. The paint drops used must have the proper consistency in order that they spread only after a certain time period rather than immediately. The lines that are formed on the surface of the body in this manner provide good information about the flow on the surface of the body. Certain tuft probes attached to the surface of the body can also be used (see p. 69).

2.2. The Use of Methods in Group 2 To Visualize the Flow of Gases /74

We will again consider first chemical methods. The first method is such that a coating containing a lead compound is applied to the streamlined body and a hydrogen monosulfide filament is brought through an opening in the surface to its immediate vicinity. When it makes contact with the body, the hydrogen monosulfide blackens the flow. In turbulent flow regions the hydrogen monosulfide diffuses very rapidly in the surrounding medium so that blackening does not occur in these regions. Since both substances are damaging to health, it is better to use mercury chloride for the coating and supply ammonia to the immediate vicinity of the surface. The method that was described, compared with the methods based on the use of smoke trails (see p. 46), can be used well to study a boundary layer also at higher velocities. At higher velocities the trails partially liquify which makes observation impossible when smoke trails are used. Liquification at higher velocities also occurs in an ammonia filament; however, in this case, this does not matter very much, since an ammonia filament in a sufficiently low concentration can also cause the reaction.

In the next chemical method, ozalid paper is glued to the tested body (collotype paper) and using thin nozzles ammonia filaments are introduced in front of the streamlined body which bring forth dark strips on the ozalid paper having the direction of the local flow on the surface.

Another chemical method uses an iodide starch (potassium iodide + starch) coating. A small amount of chlorine is mixed into the current which reacts with the iodide in the surface coating, primarily in the turbulent flow region, since during turbulent flow the chlorine makes contact with the surface coating more frequently than in the laminar flow region as a result of the more vigorous mixing. One of the consequences of this reaction is a change in the color of the coating, the coating acquires a purple color. The chlorine liberates the iodine from the potassium iodide and the free iodine stains the starch. This method is not very suitable for work in a tunnel since chlorine is harmful to health. However, it was used during the flight of an airplane. The airplane flies through a cloud of air which is enriched by chlorine let out from another airplane, from a factory chimney, or from nozzles in the airplane that is studied [1, 5, 5a].

Among the physical methods we will first mention the sublimation method, which is based on the fact that the coating from the appropriate material which covers the surface of the

streamlined body sublimates more strongly in the turbulent boundary layer region than in the laminar boundary layer region. The basic requirement is that the color of the coating differ from the color of the surface of the streamlined body. Then it is possible to determine the transition line (boundary) which appears as the boundary between the surface without a coating, i.e. that part of the surface on which the coating substance already passed into the medium flow as a result of sublimination, and the surface on which the coating is still left (see Fig. 51). However, in some cases the difference between these two parts of the surface is not sufficiently marked, and it only stands out better under intense slanted illumination [121]. The following substances are mainly used for the coatings: hexachloroethane, naphthalene, diphenyl, acenaphthene, hydro- /75
quinone, diethyl ether, fluorene, camphor, and borneol [116]. The surface of the object studied is sprayed dry by these substances, and, if necessary, with the aid of a solvent, for example, acetone, light paraffin, benzene or xylene fractions. The type of surface finish must be taken into account when the solvent is selected to prevent damage to the surface by the solvent.

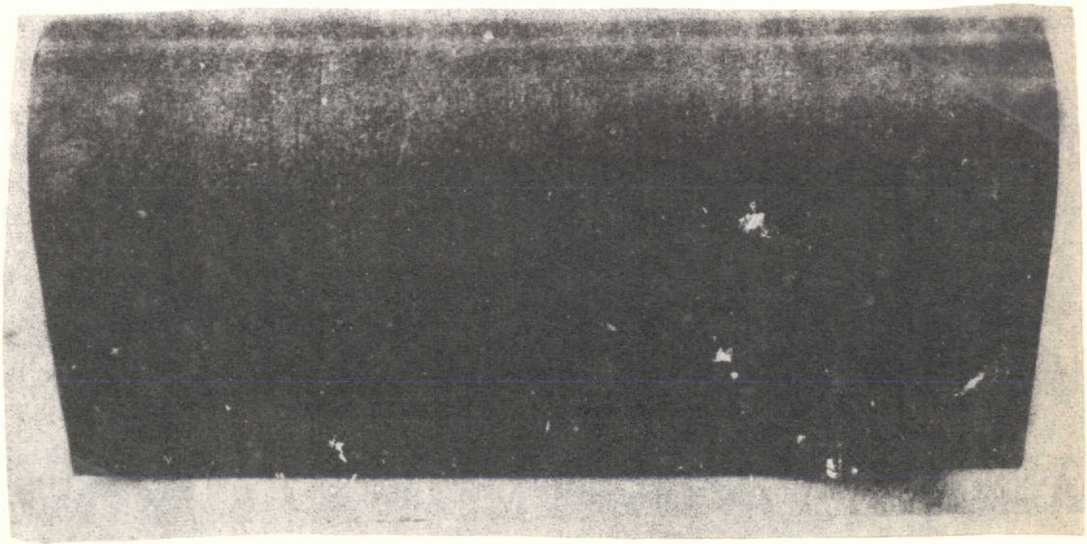

Fig. 51. Visualization of transition region of flow with the aid of sublimation of naphthalene coating [10].

With regard to practical use, hexachlorethane is most suitable for a quick laboratory study of transition regions and wakes. A 10% solution can be used for the spraying. The coating that is formed has a white dull color, so that the surface of the streamlined body must be black. At velocities of 50-130 km/hour a clear boundary is obtained for 30-120 sec which is preserved approximately for 2-3 min after the model is removed from the tunnel. Naphthalene, diphenyl and acenaphthene are good indication substances for velocities from 150 to 700 km/ /hour. Acenaphthene can also be used to indicate the transition at supersonic velocities, for example, at a velocity of 1900 km/ /hour the clear boundary was formed in 10 min. When a thick azobenzene layer was used, a satisfactory image was also obtained in 90 min at velocities of 2000 km/hour. Diethyl ether was used for tests during flights on airplanes at low velocities (200 km/hour). The image was developed in 10 to 45 min, depending on the atmospheric temperature and the altitude of the flight. Acenaphthene and fluorene were used for velocities from 400 to 800 km/hour and the development time for the image was in the range 8-30 min [116, 119, 120].

The other physical method, the so-called vaporization methods, are similar with regard to the method of observation and their use to mark the transition boundaries. In particular, good results are obtained by a simple method called the method of kaolin coatings [121, 122]. When this method is used, the black coated surface of the streamlined body is covered by a kaolin layer, for example a sprayed kaolin suspension. The appropriate suspension is obtained from 100 ml of colorless /76 frigilene + 100 ml butylacetate + 100 ml butylalcohol + 50 ml xylene + 100 g kaolin [5, 5a]. When the sprayed layer dries it must be ground by fine emery paper to eliminate unevennesses in the kaolin layer. After this, the layer is sprayed with a volatile fluid; for low velocities of about 100 m/sec, nitrobenzene is used, and for high subsonic velocities, ethyl benzoate, methyl salicylate and isosafrole are used. As a result of this, the original kaolin layer, which appeared as a dull white, due to the diffusive reflection of the light, becomes glossy, i.e. the light reflected on the layer is now regular and the layer which is illuminated in a certain direction appears as dark. When air is blown on the model which was prepared in this manner, the sprayed volatile fluid vaporizes much faster in the turbulent boundary layer region as a result of the vigorous mixing of particles than in the laminar flow region. Therefore, the surface region were the flow is turbulent becomes dull, i.e. again lighter due to the diffusive reflection of light, whereas the laminar region is still glossy and darker in the appropriate illumination [121, 118]. The advantage of this method is that the basic kaolin layer can be used many times. However, sometimes this layer may affect (reduce) the unevennesses on the surface.

The next vaporization method, the method of fluid layers, which is simpler than the method of kaolin coatings, is similar. However, the contrasts in the results are not as great [5, 5a, 123]. When this method is used, the surface of the object is covered by a thin layer of a volatile fluid, for example, by means of spraying or coating. Some of the volatile fluids that are used have already been mentioned when the previous method was described. During the flow around the body, the volatile fluid vaporizes much faster in the turbulent boundary layer region than in the laminar region, so that after a certain time the fluid layer disappears behind the transition boundary, i.e. vaporizes completely. The surface of the body should be covered by a black dull paint to increase the contrast. The advantage of this method is that the fluid layer which is very thin has no effect on the unevennesses on the surface. The method was also used at supersonic flow velocities [123, 131 through 134].

Among the methods which we called mechanical methods, the frequently used method of fiber probes attached to the surface of the streamlined body which is used to visualize the flow near the surface should be mentioned first [1, 5, 5a, 124]. Two centimeter long silk fibers frayed at one end whose second end is attached to the surface of the body are usually used in wind tunnels (Fig. 52). Fiber probes attached to the trailing edge of a wing are conveniently used to visualize trailing edge vortices [58]. The directions of the local velocities on the surface of the body can be determined on the basis of the orientation of the fibers. The character of the flow can also be inferred. When the fibers are still, they are in the laminar boundary layer, if they oscillate gently they are in the turbulent boundary layer, and if their motion is violent and jerky, they are in the turbulent separation region. The method can be used both in a tunnel and in a real airplane in flight. However, it must be kept in mind that the appropriate finish on the surface which is often used does affect somewhat the character of the flow.

In the next method to visualize the flow, the surface of the body is coated by a mixture of soot and paraffin. When air is blown on the surface, the paraffin vaporizes and flows in the direction of the flow [125]. The soot is arranged in the direction of the flow on the surface by the paraffin stream. The transition regions and separation regions can be determined very well by this simple method. Certain other oils can also be used besides paraffin. /77

Another method in which the surface of the body is covered by oil and sprayed relatively thickly with a fine powder, for example, sulfur powder is also used. If highly humid air is used as the flow medium, the precipitated water drops settle on the body and form series as a result of the effect of the surrounding flow which have the direction of the stream on the surface [11].

Fig. 52. Visualization of flow on the surface of a wing with the aid of fiber probes [5].

The body can also be coated by oil and finely ground floating chalk can be added uniformly to the gas flow around the body. The chalk settles on those areas on the surface where strong turbulence occurs. The turbulent boundary layer region and the turbulent separation region are determined in this manner, and in the last case the chalk is introduced into the wake and it is brought to the surface of the body by the reverse flow [126, 129, 130].

A fine powder, this time lycopodium, which in light is a yellow powder with grains whose linear dimension is about 0.04 mm can also be used for visualization in the following manner. The lycopodium is dried and the surface of the model from which grease was removed which was polished and coated by a dark paint is sprayed by it. Next, the blower is turned on in the tunnel and the powder remains on the surface of the model onto which the air is blown at those places where the velocity of the air in the layer adjacent to the model whose thickness is approximately equal to the dimension of the grains is not sufficiently high to blow away the powder. Hence, the powder remains in a relatively thick laminar boundary layer; however, it is blown away from the leading edge where the /78 laminar boundary layer is thin, and also from places where the boundary layer is turbulent, so that the velocity gradient near the surface is large. The method is suitable for velocities approximately up to 30 m/sec. At higher velocities the laminar boundary layer is too thin [118].

Recently a method has been applied successfully in which the surface of the streamlined body is coated by an oil layer which has a fluorescence effect in ultraviolet radiation. During the flow around the body, the thickness of the oil film that is formed is affected by the tangential stress on the surface of the body caused by the flowing air. The oil is spread along the surface and vaporized, so that the oil layer has a shape which is related to the magnitude and direction of the tangential stress on the surface. The differences in the thickness of the oil layer can be distinguished well when it is irradiated with ultraviolet rays in which the oil fluoresces, since theplaces where the oil layer is thicker emanate more intense light. Since the thickness of the oil film which is affected by the flow is maintained for a certain period which depends on the viscosity of the oil used, the model can be removed from the tunnel and photographed under ultraviolet radiation even after the flow is interrupted.

To use the method successfully it is necessary that the surface of the model have a white non-fluorescing color and that it not absorb the oil used. The surface must be white or glossy, since it reflects both the incident ultraviolet radiation and the fluorescent radiation that is induced, which strengthens the observed effect.

The method is very suitable for visualizing the regions of laminar and turbulent flow, reverse flow and flow separation. It can also be used to determine the positions of pressure maxima and shock waves. It can also be used at high velocities, for example, Fig. 53 shows the visualization of a row of vortices in the boundary layer during supersonic flow around a plate (M = 3).

When transverse flow in the boundary layer must be studied, it is more advantageous to place the oil on the surface of the streamlined body in small separate drops or in longitudinal strips. The direction of the tangential stress on the surface can then be determined well from the changes in their shape. /79

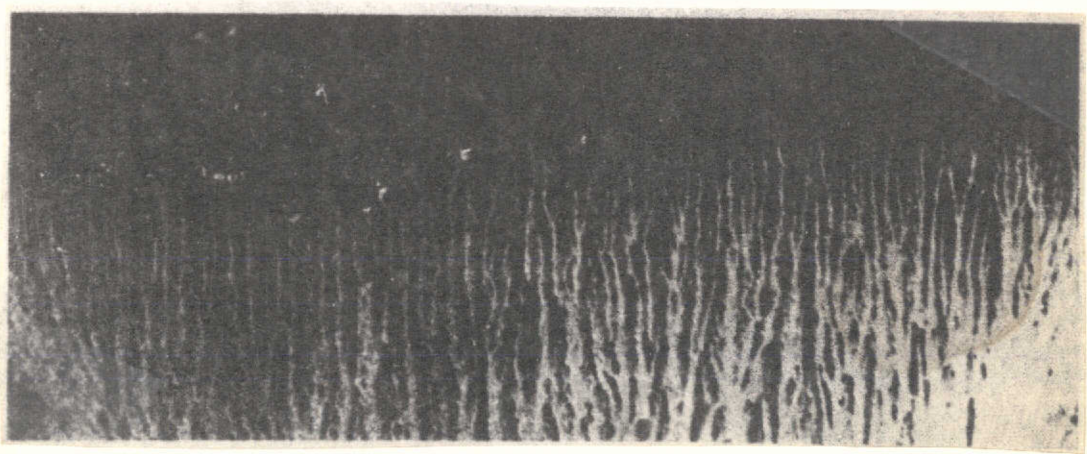

Fig. 53. Visualization of vortex rows on the surface of a wing using an oil film. Photograph in ultraviolet light [135].

The selection of the oil is based on its viscosity on which the capacity of the oil layer to adapt to the flow, the time during which the oil will adhere to the model in a sufficiently thick layer and the time during which the oil layer will remain in the transformed form after the flow is interrupted depend.

Since these two effects of the viscosity of the oil are in conflict from the standpoint of the method under consideration, it is necessary that a preliminary test be made in each case to select an oil with the appropriate viscosity. It is also necessary that the selected oil wet easily the surface of the model. At low velocities of the flow basically oils with a smaller viscosity are adequate; at higher velocities, oils with greater viscosities must be used. Ordinary motor oils can be used [135, 136, 137].

The thickness of the fluid film on the surface of the body affected by the airflow around it can be measured on the basis of the light interference in this thin layer [128]. When the light is reflected from the thin layer, the rays reflected from the top surface of the layer interfere with the rays reflected from the bottom surface of the layer. At those points of the layer where its thickness t satisfies the condition for the vanishing of the light as a result of interference dark fringes are formed. These are the points where one ray passing through the layer is delayed so that it encounters the other ray reflected from the top layer of the surface in the antiphase [15, 16]. In order that the rays encounter in the opposite phase, it is necessary that the path covered by the first ray inside the layer be an odd multiple of half the wavelength λ_v, which is the wavelength of the light used in the fluid forming the layer. Hence, when the incident monochromatic parallel light waves are approximately perpendicular to the fluid layer, dark fringes are formed at the points where the thickness of the layer d satisfies the condition

$$2d = (2k+1)\frac{\lambda_v}{2}, \quad \text{where} \quad k = 0, 1, 2, 3, \ldots \tag{30}$$

If the incident monochromatic light has wavelength λ in vacuum, its wavelength λ_v in the fluid forming the layer is

$$\lambda_v = \frac{\lambda}{n}, \tag{13}$$

where n is the absolute refractive index of the fluid forming the layer. Hence, condition (30) can be modified to

$$d = (2k+1)\frac{\lambda}{4n}, \quad \text{where} \quad k = 0, 1, 2, 3, \ldots, \tag{32}$$

so that the dark fringes are formed at points at which the thickness d of the layer is equal to one of the values $\lambda/4n$, $3\lambda/4n$, $5\lambda/4n$, ...

If the thickness of the layer varies with time, the interference fringes move and the number of interference fringes passing through a selected point on the surface of the streamlined body per unit time will be proportional to the change in the thickness of the layer over time. /80

The methods that were described can also be used to determine quantitatively the skin friction. It is assumed that the change with time (reduction) in the thickness of the layer is proportional to the local value of the skin friction [128].

The fluid used to form the layer must thoroughly wet the surface of the model and it must vaporize at the appropriate rate (relative to the velocity of the airflow around it). For example, ethyl alcohol, methyl alcohol, iso-octane and xylene are good wetting agents, but vaporize slowly, while toluene, benzene, isosafrole, cyclohexanol, isoamyl alcohol and water vaporize well, but do not wet so well [128].

Part 3. Methods Based on the Use of Natural in the Optical Properties of the Fluid Formed During the Flow /81

The third basic group of methods for visualizing the flow are methods which are based on the use of natural changes in the optical properties formed in the fluid during the flow. The advantage of these methods is that no other particles besides those forming the medium flow or foreign bodies which could possibly have an effect on the flow are introduced into the flow.

3.1. Methods in Group 3 Which Are Suitable for Visualizing the Flow of Fluids

(Use of temporary birefringence during the flow.)

The temporary birefringence during the flow can be used to visualize the flow of fluids [145]. This phenomenon can be observed in many types of colloidal and pure fluids, for example, in aqueous solutions solutions of clays such as halloysite, bentonite, aqueous solutions of gels, and also dissolved anhydroglucose, vanadium dioxide , etc.

Transient birefringence is a phenomenon during which some substance which is otherwise optically isotropic becomes optically anisotropic and birefringent when a certain field of force acts on it. Hence, in such a case the substances acquires optical properties found in certain crystals, for example, limestone, which are polarized in mutually perpendicular planes, whose propagation velocity in the birefringent substance under consideration can be different, so that each of the two rays has a different refractive index. The difference Δn in the refractive indices associated with these two rays can be considered as a datum which determines the birefringence value. For example, Δn can be determined with the aid of a compensator when the birefringent substance that is studied is observed between the crossed nicols.

The field of force which can cause temporary birefringence in the fluids may be an electric field (the Kerr effect), a magnetic field (the Cotton-Mouton effect) and also the hydrodynamic field of force formed in the fluid during the flow as a result of internal friction. The last phenomenon that was mentioned was detected by Maxwell [145] already in 1873 during his study of the flow of Canada balsam in an annular layer. This phenomenon was later observed, as we already mentioned in many types of colloidal solution and pure fluids.

The mechanism by which temporary birefringence is formed during the flow depends on the type of particles suspended in the fluid flow, or possibly, in the case of a pure fluid, on the molecules of the fluid flow. All cases can be classified into two basic groups. /82

In the first case, the particles suspended in the fluid flow /83 approach by their properties and shape solid undeformed rods or plates with dimensions on the order of 10^3-10^5 Å. These particles themselves are birefringent; however, in a fluid which is not subjected to the effect of the appropriate field of force, the solution will appear to be optically isotropic as a result of the disordering caused by the rotational brownian motion of these particles. A certain region of the fluid becomes birefringent only when the particles are statistically ordered in the fluid as a result of the effect of the tangential stresses. The effect of the tangential stresses on the ordering of the particles is of course disturbed by the brownian motion of these particles, so that the resulting statistical ordering is the result of the effect of the tangential stresses in the fluid and the brownian motion of the particles. Hence, the ordering is not static, but we have the case when the direction in which the particles are oriented on the average, and hence also the direction of the optical axis of the fluid layer formed by these particles are given by the direction of the longer axes of the particles at the instant when the angular velocity of the particles is a minimum. The degree of orientation can be characterized by the parameter $\alpha = G/\Phi$, where G is the velocity gradient and Φ is the rotational diffusion constant. Φ is a measure of the intensity of the Brownian motion and it depends on the dimensions and shape of the particles in the fluid. To each velocity gradient G corresponds a certain distribution of the orientation directions of the rod-shaped particles. As the gradient G (or the parameter α) increases, this distribution narrows, and the birefringence value increases. The first group includes, for example, the tobacco mosaic virus, clays such as halloysite, bentonite, and also various proteins.

The second group includes polymers. Their particles can be replaced for theoretical considerations by a spherical or a dumbbell model. However, these particles are deformed in the fluid flow as a result of the effect of the tangential stresses (similarly as in the photoelastic phenomenon), for example, spheres are deformed into ellipsoids, resulting in their optical anisotropy. In the entire fluid region subjected to the effect of forces, the birefringence value is also affected by the orientation of the deformed particles. We can also include in this group pure fluids in which the direction of the statistical orientation of the molecules almost does not vary with the magnitude of the velocity gradient G, so that for them the birefringence formed depends mainly on the deformation of the molecules.

In addition to the birefringence value, another datum must be known for practical application, i.e. the so-called orientation angle (extinction angle) χ, which is defined as the angle subtended by the principal optical axis of the fluid layer at a certain point and the direction of the flow at this point. By measuring Δn and χ at the selected point of the two-dimensional fluid flow layer, we can determine from these data under certain assumptions (see p. 81) the magnitudes of the velocity gradient G and the local direction of the flow, since for all groups of fluids it was determined that Δn and χ are functions of the velocity gradient G (see Fig. 54):

$$\Delta n = f(G), \tag{33}$$

$$\chi = g(G). \tag{34}$$

To determine the experimental values of the quantities Δn and χ for the relations (33) and (34), equipment called, according to Cvetkov [139], a dynamooptimeter is used. This equipment is based on the principle of a rotary viscosity meter. It consists of two coaxial cylinders, one of which can be rotated. The measured fluid in the space between the two cylinders is observed with the aid of a polariscope.

The use of temporary birefringence to obtain characteristics of the flow is based on the fundamental relations (33) and (34). This means that by measuring the birefringence value at various points of the fluid flow region it is possible to determine, on the basis of relation (33), at these points the magnitude of the velocity gradient G, and from it, with the aid of the orientation angle χ additional data without disturbing the flow by any measuring sensor. Also it is necessary to determine for the fluid used the behavior of the functions f(G) and g(G) which can be done, for example, with the aid of the dynamooptimeter that was mentioned. Of course, those fluids for which f(G) is linear in the required range of velocity gradients and χ is nearly constant in the same range are most suitable. (The proper fluids and their use for hydrodynamic purposes were studied by Weller [140]).

Since the flow when the behavior of the functions f(G) and g(G) is determined with the aid of the dynamooptimeter is a flow where the direction of the velocity gradient is perpendicular to the direction of the flow, when the method is applied to other cases the question arises whether this condition must be preserved. A reliable use of the temporary birefringence to obtain characteristics of the flow in more complex cases would require that the question be answered and that the assumption that the direction of the velocity gradient in colloidal solutions can be determined on the basis of the value of the orientation angle χ be confirmed. However, so far, the necessary experimental and theoretical prerequisites are not yet available. /84

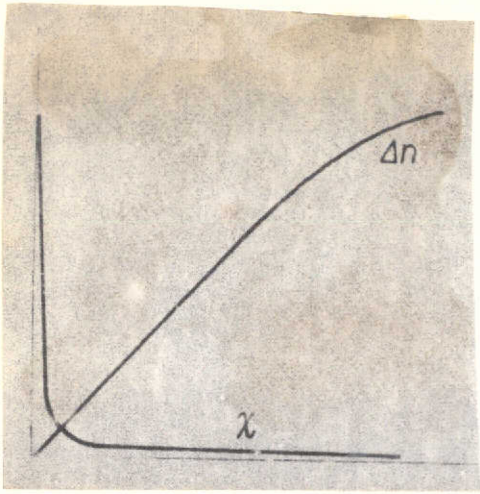

Fig. 54. Birefringence and extinction angle versus velocity gradient.

The experimental equipment which takes advantage of temporary birefringence to study the flow consists of a channel in which the flow must be studied or into which objects are inserted, the flow around which interests us. The bounding surfaces of the channel which are parallel to the plane of two-dimensional flow which is studied in the channel consists of plane-parallel glass plates. The channel is attached to a unit which ensures the passage of the fluid and the entire set forms the hydraulic tunnel. Basically, two layouts are possible. One is a gravitational tunnel, a combination in which the fluid flows out from the reservoir of the channel under the effect of its own weight. This tunnel can also be equipped so that the fluid that flows out is brought back to the reservoir in which a constant level is maintained. The second combination is a circulation tunnel, a closedhydraulic circuit in which a pump ensures the circulation of the fluid. The disadvantage of this layout is that the character of the flow can be affected by the vibrations caused in the fluid by the pump, which is a disadvantage, especially when transient phenomena are observed. This basic hydraulic unit has a companion optical equipment unit, a polariscope, which is entirely analogous to the polariscopes used in photoelasticimetry. It consists of two polarization filters (or nicols), a light source, and possibly also of a quarter-wave plate and compensator.

Two methods can be used during the measurements. We can either measure individual points in the channel or observe the entire measurement space simultaneously. The first method is time consuming, but it is useful in cases when it is necessary to determine the birefringence values in a small part of the channel (for example, in the boundary layer), especially when a low-sensitivity fluid is used or when the flow has a small velocity gradient. The cover glass of the channel has a mesh, and with the aid of the polarization equipment, the birefringence values are measured by the compensator at the points which correspond to the intersections of the mesh, or the entire polariscope is mounted on a slide bed with the aid of which the axis of the polariscope can be set in the desired position. When small parts of the channel are measured using single-ray equipment, very small changes in the position of the ray can be obtained with the aid of a rotary glass plane-parallel plate inserted in the path of the ray before the inlet to the channel. During such exact measurements, of course, it is necessary to take into account the effect of the birefringence of the cover glasses on the values that are obtained. The basic schematic diagram of the equipment for the case when nicols and the Babinet-Soleil compensator are used, is given in Fig. 55. However, a polariscope with polarization filters can also be used and the birefringence value can be measured using a goniometric compensator, which is common practice in photoelasticimetry. /85

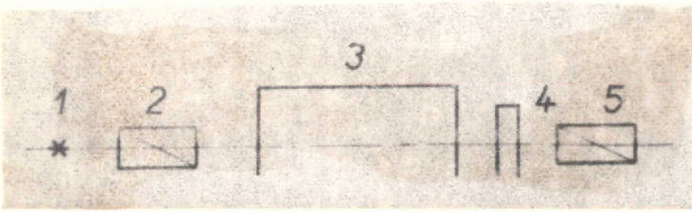

Fig. 55. Single-ray polariscope (1. light source; 2. nicol polarizer; 3. analyzed fluid; 4. compensator; 5. nicol analyzer).

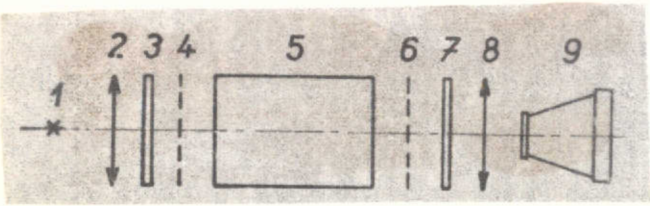

Fig. 56. Polariscope for the analysis of a flow field of relatively large dimensions (1. light source; 2. condenser; 3. polarizing filter polarizer; 4 and 6. quarter-wave plate; 5. analyzed fluid layer; 7. polarizing filter analyzer; 8. objective; 9. camera).

Another method can also be used in cases when the velocity gradient and the sensitivity of the fluid are such that in the flow region analyzed birefringence occurs whose value causes a phase shift of the split rays which corresponds to several times the wavelength of the light used. Interference fringes are then formed behind the analyzer which can be photographed or plotted, and the required characteristics of the flow can then be determined from them. The schematic diagram of the optical part of the equipment used for this method is given in Fig. 56. These methods are suitable in both versions for the study of cases of plane flow. Therefore, the rays of light that are used must be perpendicular to the plane of flow during their passage through the channel.

The origin of interference fringes, for example, in fluids with undeformable particles (these fluids which have a high sensitivity are most suitable for visualization of flow using the method under consideration) can be explained as follows. The particles which have birefringent properties are arranged in the two-dimensional fluid flow by the tangential forces into rows (in the sense of their orientation distribution). A row of such oriented particles behaves like a crystal from the standpoint of optical properties and splits the incident ray of linearly polarized light into two linearly polarized rays whose vibration directions are mutually perpendicular and lie in the orientation plane (i.e. in the plane given by the statistical orientation direction of the longer axes of the oriented particles) and in the plane perpencidular to it. The refractive index for the two vibration directions is not the same. Therefore, the split rays propagate through the fluid at different velocities c_1 and c_2 and leave it with a shift in phase. Both rays require different times for passage through a fluid layer of thickness t:

$$\tau_1 = \frac{t}{c_1} = \frac{t}{c} n_1, \qquad \tau_2 = \frac{t}{c_2} = \frac{t}{c} n_2;$$

where c is the velocity of light in vacuum, and n_1 and n_2 are the absolute refractive indices of the two rays under consideration in the fluid forming the layer. Hence, the time difference is

$$\Delta\tau = \frac{t}{c} \Delta n,$$

which corresponds to a phase shift /86

$$\varepsilon = 2\pi \frac{\Delta\tau}{\frac{\lambda}{c}} = 2\pi \frac{t}{\lambda} \Delta n. \tag{35}$$

The analyzer, whose polarizing plane is perpendicular to the polarizing plane of the polarizer, are the two rays which have the same frequency and amplitude and are oriented in the same vibration direction so that they can interfere. The conditions which determine when the dark interference fringes will be formed follow from the follow following expression (36). From the graphical representation (see Fig. 57) it follows for the amplitude A_r of the emanating light that

$$A_r^2 = A_0^2 \cdot \sin^2 2\gamma \cdot \sin^2 \frac{\varepsilon}{2},$$

where A_0 is the original amplitude of each of the two rays, and the meaning of the angle γ is obvious from Fig. 57 (s_p denotes the direction of the flow). Since the intensity of the light is proportional to the square of the amplitude, we obtain for the ratio of the intensity J_0 of the ray entering the fluid under consideration to the intensity J_r of the ray leaving the analyzer the relation

$$\frac{J_r}{J_0} = \frac{A_r^2}{A_0^2} = \sin^2 2\gamma \cdot \sin^2 \frac{\varepsilon}{2} = \sin^2 2\gamma \cdot \sin^2 \left(\pi \frac{t}{\lambda} \Delta n\right). \tag{36}$$

where we did not take into account light absorption.

Hence, the light will vanish (dark fringes) in the following cases (we assume of course that $J_0 \neq 0$):

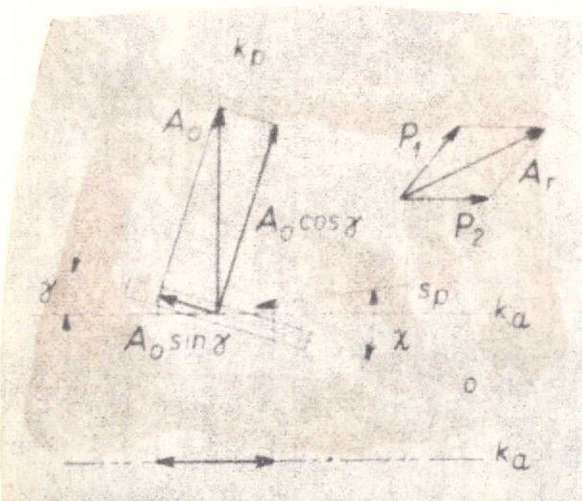

a) for $\gamma = 0°$ or $\gamma = 90°$, i.e. when the optical axis of the fluid layer has the same direction as the vibration direction of the analyzer or polarizer. The dark lines in the field of view corresponding to these conditions are called isocline lines, with the aid of which the statistical orientation direction of the particles can be determined. The isocline lines vanish when circular polarized light is used, which is obtained from linearly polarized light with the aid of quarter-wavelength plates. /87

b) the next case when the intensity of the emanating light drops to zero is given by the condition $\sin \varepsilon/2 = 0$. This condition is only satisfied when $\Delta n = 0$, i.e. when the velocity gradient $G = 0$. Thus those points in the field of view will be dark where the velocity gradient is zero. By analogy with the terminology used in photoelasticimetry, these points can be called singular points or possibly lines.

The condition $\sin \varepsilon/2 = 0$ can also be satisfied according to (35) when

$$\pi \frac{t}{\lambda} \Delta n = i\pi, \quad \text{where} \quad i = 1, 2, 3, 4, \ldots$$

87a

The points in the fluid flow where such condition is satisfied appear as dark only when observed in monochromatic light. In white light, these fringes resulting from interference at a particular wavelength become a bundle of colored interference fringes corresponding to the wavelenths of the white light components. These fringes are called isochromatic lines. Since they satisfy $\Delta n = i(\lambda/t) = \text{const}$, they are actually the locus of the points in the plane of flow at which Δn has the same value.

Assuming that relations (33) and (34), which are found experimentally in the case when the velocity gradient is perpendicular to the direction of the flow (see p. 76) can be used for the general case of flow, it is possible to determine from the isoclinic lines with the aid of the orientation angle χ the direction of the flow.

If we select a fluid for which $\Delta n = kG$, where k is a constant, the isochromatic lines connect the points with a constant velocity gradient G, since in this case $G = i(\lambda/kt) = \text{const}$ along the isochromatic line. $i = 1$ is associated with the isochromatic line which is closest to the singular line; therefore, it is called a first-order isochromatic line and the velocity gradient has the same magnitude $G = 1(\lambda/kt) = \lambda/kt$ at all points on the line; $i = 2$ is associated with the next isochromatic line (second-order isochromatic line), and the magnitude of the velocity gradient at its points is $G = 2(\lambda/kt)$.

Thus, for example, for a completely developed laminar flow between parallel plane plates, we obtain the image of the isochromatic lines in the form of a system of parallel dark fringes at equal distances from one another (see Fig. 58 a) which corresponds to a parabolic velocity profile. In the subsequent photographs (Fig. 58 b, c) are interference images obtained during the flow around a cylinder between parallel walls at a very low Reynolds number [144]. /88

Since the magnitudes of the gradient can be determined on the perimeter of the streamlined bodies, the magnitudes of the frictional resistance can also be determined. During turbulent flow, the sharpness and connectedness of the fringes disappears, so that although they cannot be used to determine quantitatively the characteristics of the flow in the sense that was mentioned, they can be used to analyze transition phenomena [142].

The photographs of the interference images that are presented were made with the aid of equipment whose basic hydraulic unit consists of a simple gravitational tunnel. The channel is bounded by parallel walls. The passage from the reservoir to the channel is designed continuously by bending these walls. The sides of the transverse rectangular cross section of the channel /89

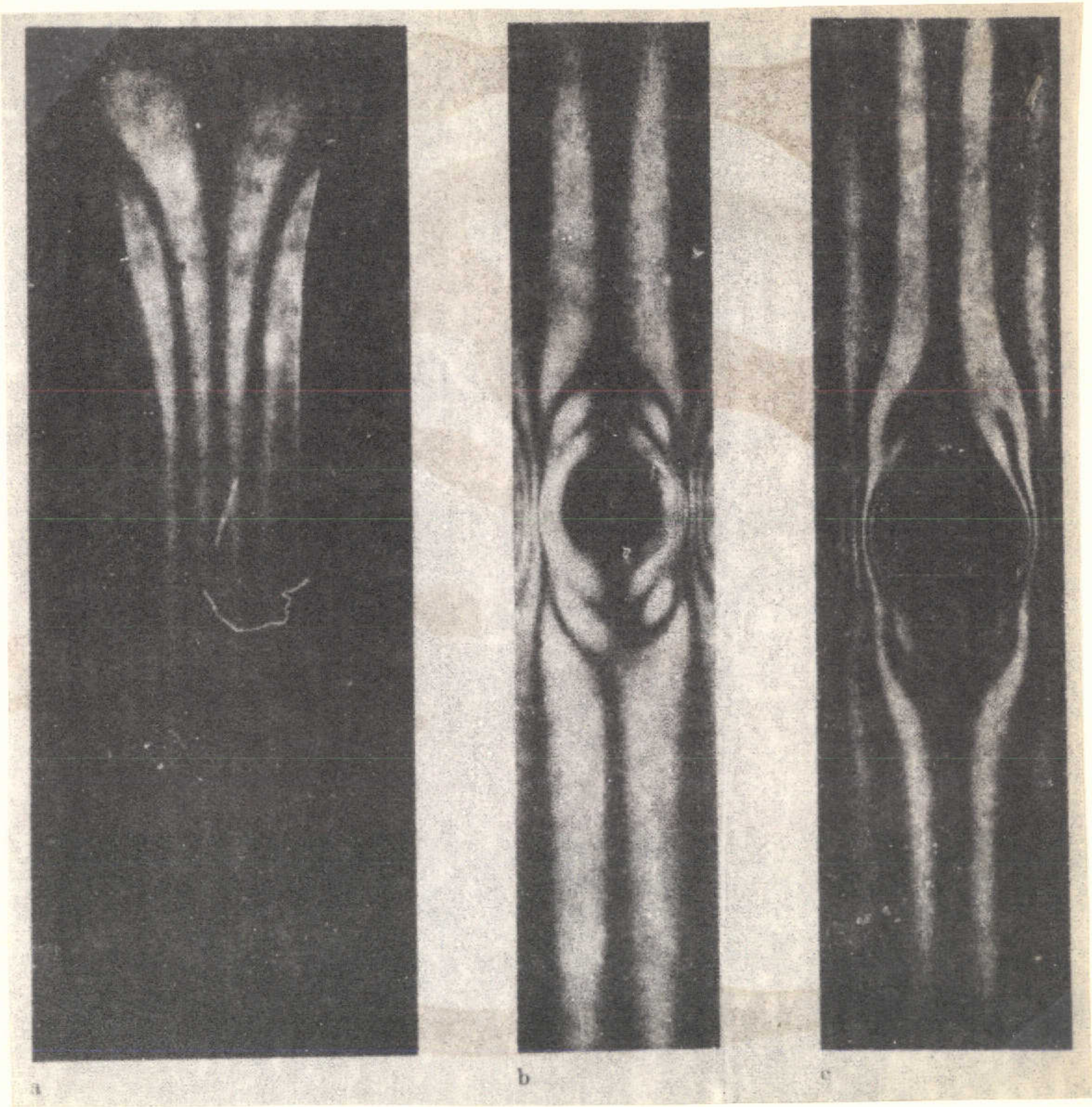

Fig. 58. Interference images obtained using the birefringence method during the flow [144]: a) flow between parallel plane plates; b), c) flow around a cylinder at a very low Reynolds number.

are: width 2 cm, depth t = 15 cm. Hence, the ratio of the depth to the width is 7.5. The selected ratio must be sufficiently high to suppress the effect of the forces exerted by the transparent walls of the channel on the fluid. These walls are perpendicular to the direction of the rays of the light used and parallel to the plane of the model of the two-dimensional flow which must be obtained. However, a high value of this ratio leads to difficulties during photography. The fluid that was used was a gelatin solution in the initial gelatinized state. Hence, the motion of the gel in the channel was very slow [144].

3.2. Methods in Group 3 Which Are Suitable to Visualize the Flow of Gases

Some methods from group 3 are very often used to visualize the flow of gases, since they provide quantitative data in certain cases and are also suitable for studying flows with high (supersonic) velocities. The compressibility of gases is the property without which these methods could not be used. When these methods are used, advantage is taken of the changes in the refractive index of the gas flow caused by pressure changes and thus also changes in the density or possibly temperature. Since these changes in the refractive index cannot be seen by the naked eye, in most cases various optical apparatus is used for their visualization, and the associated methods can be classified into several main groups. In the first three groups, light refraction is the basic phenomenon which makes visualization possible. Therefore, we will call all these methods refraction methods. They are also call schlieren methods (from the German word "die Schliere"). The next two groups take advantage of light interference. Finally, the last groups include methods based on taking advantage of the dependence of the attenuation of various types of electromagnetic and corpuscular radiation on the density of the gas through which this radiation passes.

Hence, in Section 3.2 we will discuss the following methods or groups of methods:

1. the shadow method
2. diaphragm schlieren methods
3. diaphragm schlieren method with a colored image
4. interferometric methods
5. phase contrast method
6. methods based on taking advantge of the attenuation of electromagnetic or corpuscular radiation during passage through the gas flow.

These methods will be discussed in detail in Sections 3.2.1 through 3.2.6, and whenever necessary, these numbers will also be used to describe them, i.e. for example, diaphragm schlieren methods with a colored image will be called methods in group 3.2.3, etc.

In all methods from group 3.2 the information about the flow /90 is basically obtained from the local changes in the illumination of the field of view of the observation equipment, for example, from the changes in the state when the medium is at rest. When we observe a ray of light passing through the gas layer that is analyzed (see Fig. 59) we find that if the layer is homogeneous the particle is incident to the screen S at the point P at the instant t in the direction Θ (characterized, for example, by the three corresponding direction cosines), whereas if there are inhomogeneities in the layer, the ray is incident at a point P^* at the instant t^* in the direction Θ^*, which results in a local change in the illumination of the screen. Using optical apparatus, it is possible to obtain on the screen either a record of the phase shift corresponding to the time difference $\tau = t^* - t$ (methods in group 3.2.4) or a record of the deviation $\varepsilon = \Theta^* - \Theta$ (methods in group 3.2.2) or a record of the displacement of the track $\Delta P = \overline{P^*P}$ (methods in group 3.2.1) or possibly a combination of these records. The corresponding τ, ε and ΔP must then be found from the records, and from these the local values of the absolute refractive index $n = n(x,y,z)$ of the object through which the rays pass. From the values n that were found, the local density values of the object can be calculated, and from these, subsequently, other data.

To obtain results which will aid in evaluating quantitatively the images of the flow obtained by the methods in group 3.2, we will use the following arguments.

Suppose that a bundle of parallel rays passes through a medium which is bounded by the two parallel planes 1 and 2 at a distance $x_2 - x_1$ from one another. The incident rays are perpendicular to plane 1, which is closer to the light source, and they are parallel to the direction of the X axis of a rectangular Cartesian coordinate system. The optical properties of the medium are characterized by the absolute refractive index n of the light used. Suppose that the medium has such inhomogeneities that n changes continuously in the planes which are perpendicular to the X axis and does not change in the directions which are parallel to the X axis, hence, we have a plane field, i.e. $n = f(y,z)$. The shape of the ray of light in such a medium is described by the Fermat principle, according to which the optical path of the ray is extremal. The optical path covered by the rays between two points which will be denoted by 1 and 2 since concretely we /91
assumed that the first point lies in the plane 1 and the second in the plane 2, is given by the expression

$$\int_1^2 n \, ds, \tag{37}$$

where ds is an elementary arc of the trajectory of the ray. This expression is a functional, i.e. generally it takes on different values on each curve connecting the points 1 and 2. According to Fermat's principle, the actual trajectory is the

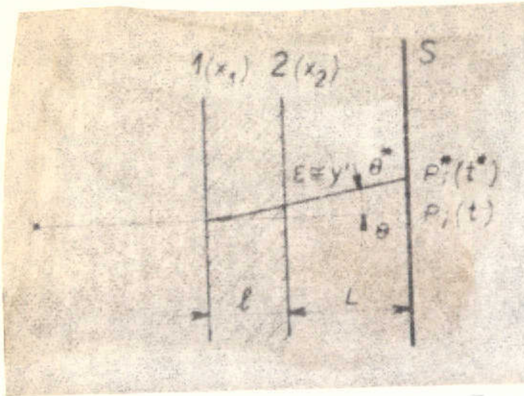

Fig. 59.

curve on which the functional (37) has an extremum. Since the necessary condition for the extremum of the functional is that its first variation vanish [20], the relation

$$\delta \int_1^2 n \, \mathrm{d}s = 0. \tag{38}$$

must hold on the actual trajectory.

Expressing the trajectory of the the ray as the intersection of cylindrical surfaces

$$y = f_1(x), \qquad z = f_2(x). \tag{39}$$

we have

$$\mathrm{d}s = \sqrt{\mathrm{d}x^2 + \mathrm{d}y^2 + \mathrm{d}z^2} = \mathrm{d}x \sqrt{1 + \left(\frac{\mathrm{d}y}{\mathrm{d}x}\right)^2 + \left(\frac{\mathrm{d}z}{\mathrm{d}x}\right)^2} = \sqrt{1 + y'^2 + z'^2}\,\mathrm{d}x$$

Hence relation (38) can be written in the form

$$\delta \int_1^2 n \sqrt{1 + y'^2 + z'^2} \, \mathrm{d}x = 0. \tag{40}$$

It has been proved in the calculus of variations [20] that the function (39) for which the functional (37) has an extremum, i.e. the function satisfying condition (40), must be the solution of a system of so-called Euler differential equations. In our case, the Euler equations have the form:

$$\begin{aligned} &\frac{\partial n}{\partial y} \sqrt{1 + y'^2 + z'^2} - \frac{\mathrm{d}}{\mathrm{d}x}\left(n \frac{y'}{\sqrt{1 + y'^2 + z'^2}}\right) = 0, \\ &\frac{\partial n}{\partial z} \sqrt{1 + y'^2 + z'^2} - \frac{\mathrm{d}}{\mathrm{d}x}\left(n \frac{z'}{\sqrt{1 + y'^2 + z'^2}}\right) = 0. \end{aligned} \tag{41}$$

The expressions $y' = dy/dx$, $z' = dz/dx$ are the angular deflections of the passing light from the original direction, which was parallel to the direction of the X axis. These deflections are very small in the usual cases that will be discussed, so that their squares can be ignored in comparison with unity. (This and additional simplifications lead to errors in the quantitative evaluation, since they do not take into account the already existing deflection of the ray from the original direction in the layer that is studied. This is further compounded by the effect of the glass covers of the measurement space on the flow. The boundary layer on these walls is responsible for the fact that in concrete cases the flow in the tunnel is not exactly planar. If very accurate results must be obtained in the evaluation, these errors must be limited by means of various corrections which complicates the calculation [146, 146a]). /92

Ignoring y'^2 and z'^2 compared to one, equations (41) take on the form

$$\begin{aligned} \frac{\partial n}{\partial y} &= \frac{\mathrm{d}}{\mathrm{d}x}(ny'), \\ \frac{\partial n}{\partial z} &= \frac{\mathrm{d}}{\mathrm{d}x}(nz'). \end{aligned} \tag{42}$$

In these equations n is independent of x, since we assumed a plane field $n = n(y,z)$, and consequently the partial derivatives $\partial n/\partial y$ and $\partial n/\partial z$ are also independent of x. However, the quantities y' and z' depend on x. Integrating each equation in (42) with respect to the variable x from $x = x_1$ to $x = x_2$, we obtain:

$$\begin{aligned} \frac{\partial n}{\partial y}(x_2 - x_1) &= n[y'(x_2,y,z) - y'(x_1,y,z)], \\ \frac{\partial n}{\partial z}(x_2 - x_1) &= n[z'(x_2,y,z) - z'(x_1,y,z)]. \end{aligned} \tag{43}$$

The relations that were obtained can be further simplified formally. As a consequence of the assumption that the incident, rays are perpendicular to plane 1 (the plane $x = x_1$), $y'(x_1,y,z) = 0$, $z'(x_1,y,z) = 0$. Therefore, without making an error we will write henceforth, for brevity, y' instead of $y'(x_2,y,z)$ and similarly z' instead of $z'(x_2,y,z)$. Of course, we must remember that y', z' now mean the angular deflections of the ray passing through plane 2 (the plane $x = x_2$) at the point with the coordinates x_2, y, z, from the direction of the X axis.

Using the notation that was just introduced, from equations (43) we obtain the relations

$$\frac{\partial n}{\partial y} = \frac{ny'}{x_2 - x_1},$$
$$\frac{\partial n}{\partial z} = \frac{nz'}{x_2 - x_1}, \qquad (44)$$

from which the $\partial n/\partial y$, $\partial n/\partial z$ can be determined, i.e. the y-th and z-th component of the gradients of the refractive index (the x-th component is zero, since by assumption n is independent of x) at any point of the field, provided we know from the experiment the angular deflections of the rays when they leave the layer whose thickness is $x_2 - x_1$. Although theoretically we must always substitute the local value $n = n(y,z)$ of the refractive index (which is unknown and for which we try to prove that it can be determined at least approximately), we can substitute the refractive index n_0 instead of n (in cases that will be discussed below) of the substance forming the medium flow in the case when the flow does not cause inhomogeneities in it. Hence, for example, the refractive index of the medium flow outside the inhomogeneous region that is examined can be substituted. This procedure can be justified by the fact that the value of the refractive index varies insignificantly from point to point in comparison with the change in the gradient of the refractive index. /93

If n_0 is the refractive index of the medium flow at the point with coordinates x, y_0, z_0, i.e. $n_0 = n(y_0,z_0)$, the relations

$$n(y, z_0) = n_0 + \int_{y_0}^{y} \frac{\partial n}{\partial y} \, dy,$$
$$n(y_0, z) = n_0 + \int_{z_0}^{z} \frac{\partial n}{\partial z} \, dz, \qquad (45)$$

hold, since by assumption the refractive index is independent of x. These relations are derived without any physical considerations, only on the basis of a simple mathematical argument. The relations show that if the components of the gradient of the refractive index have already been determined (on the basis of experimental data) according to (44), by integrating them the values of the refractive index can be determined at any point of the field. In practice, of course, the corresponding integration must be a numerical or graphical integration, since the components $\partial n/\partial y$, $\partial n/\partial z$ of the gradient of the refractive index determined from the experimental data are obviously only known numerically, not analytically.

In was already mentioned that the corresponding local changes in the density of the medium flow can be inferred from the local changes in its refractive index. The relation

$$\frac{n^2-1}{n^2+2}\frac{1}{\varrho} = \text{const} \tag{46}$$

is valid, where n is the absolute refractive index and ρ is the density of the transparent medium under consideration. This relation expresses the fact that, during a change in the density of the transparent medium caused, for example, by the effect of pressure, the specific refraction does not change (the Lorenz-Lorentz law). Further if the absolute index of the medium under consideration differs very little from one, for example, as in air, the left member in equation (46) can be modified approximately as follows: /94

$$\frac{n^2-1}{n^2+2} = \frac{(n+1)(n-1)}{n^2+2} \approx \frac{2(n-1)}{3},$$

so that (46) takes on, in this case, the form:

$$\frac{n-1}{\varrho} = K, \tag{47}$$

where K is a constant, giving the Gladstone-Dale relation.

The value of the constant K can be determined by substituting the corresponding values for ρ and n. Thus, for example, under normal conditions (0°C, 760 torr) for sodium light at wavelength $\lambda = 0.589$ µm, air has a refractive index $n_0 = 1.000292$, and the density of the air is $\rho_0 = 1.293$ kg·m^{-3}, hence for air the value of the constant K is $K_0 = 2.26 \cdot 10^{-4}$ kg^{-1}·m^3.

Equation (47) implies:

$$\frac{\partial n}{\partial y} = K \frac{\partial \varrho}{\partial y},$$

$$\frac{\partial n}{\partial z} = K \frac{\partial \varrho}{\partial z}, \qquad (48)$$

hence it is obvious that using equations (48) and (44) the density gradient or the density at an arbitrary point of the field can be determined directly from the values of y', z' that were determined experimentally[4, 5, 5a, 147, 156, 162].

Let n_0 be the refractive index of air (or another gas) in the layer whose thickness is $x_2 - x_1$, and let ρ_0 be the density. If the density of the air in the layer changes to the value ρ, the refractive index of air changes to the value n. If n is greater than n_0, the time needed for the passage of the ray through the layer in the second case (for the refractive index n) is greater than in the first case (for the refractive index n_0) by the time

$$\tau = \frac{x_2 - x_1}{c} (n - n_0), \qquad (49)$$

where c is the velocity of light in a vacuum. After it leaves the layer, the ray enters in both cases the same surrounding medium in which the velocity of the light is c', its density is ρ, and the absolute refractive index is $n' = c/c'$. In this surrounding medium, the displacement

$$\Delta s = c'\tau = \frac{n - n_0}{n'} (x_2 - x_1). \qquad (50)$$

along the trajectory corresponds to the time shift τ. If we determine τ or Δs from the results of the experiment, we can determine the difference between the change in the refractive index n of air, for example, during flow, and the original refractive index n_0 of air, for example, when it was quiescent in the layer studied. /95

The necessary experimental data are obtained with the aid of various optical devices which will now be described together with a more detailed analysis of the individual methods.

3.2.1. Shadow Method

The simple refractive method uses the simplest equipment. This method is based on a phenomenon which was observed during the passage of light through transparent objects (glass objects, gas layers) with local inhomogeneities [161]. The pencil of rays entering the object at all points of its cross section with the same intensity impinges after the passage through the object on the screen with local changes in the intensity, and subsequently points with greater and smaller illumination corresponding to the inhomogeneities on the object appear on the screen (turbidities, schlieren, from the German "die Schlieren"). Certain characteristics of the flow can be determined on the basis of similar changes in the screen illuminated by the pencil of rays that passed through an airflow layer (or another gas). For example, the region occupied by the wake, the shape and type of shock wave, the local Mach number, the region of turbulent flow, etc. can be determined from their image on the screen.

The local relative change $\Delta A/A$ in the illumination A of the screen corresponding to the inhomogeneities in the air layer depends on the changes in the gradient of the refractive index at the corresponding points of the layer. This relation can be expressed approximately by expression (57) below which is derived using the following argument:

We introduce in the plane of the screen whose distance from the layer is L rectangular Cartesian coordinates y, z (we are still using the same coordinate systems and the same notation as on pages 84-89). The illumination A of the screen by the light rays passing through a layer without inhomogeneities will be described by the function $A = A(y,z)$. Now let us study the ray (Fig. 59) which is incident to the screen the point $P(y,z)$ (when there are no inhomogeneities in the layer). If there are inhomogeneities in the layer, the same ray will be incident at some point P^* with the coordinates

$$y^* = \varphi_1(y, z), \qquad z^* = \varphi_2(y, z). \tag{51}$$

Assuming that the functions ϕ_1, ϕ_2 are continuous, all rays which after passage through the layer without inhomogeneities were incident at an element of area dS of the screen which includes the point P, will be incident after passage through an inhomogeneous layer at a certain element of area dS^* of the screen, which includes the point P^*. Hence, by the definition /96 of illumination we will have, for the ratio of the illumination, $A^*(y^*,z^*)$ by the rays passing through the inhomogeneous layer at the point P* (on the area dS*) of the screen to the original illumination A(x,y) at the point P (on the area dS)

$$\frac{A^*(y^*, z^*)}{A(y, z)} = \frac{\mathrm{d}S}{\mathrm{d}S^*}. \tag{52}$$

The ratio dS/dS* can be expressed, as is well known, with the aid of the Jacobian of the image (51). During its calculation we will apply similar simplifying assumptions as on p. 85, i.e. we will assume that the differences $\Delta y \equiv y^* - y$, $\Delta z \equiv z^* - z$ are small, and that their first derivatives are small compared to 1, so that the products of these derivatives can be ignored. In this case we obtain, for the Jacobian J, using the identities $y^* = y + \Delta y$, $z^* = z + \Delta z$

$$J = \begin{vmatrix} \frac{\partial y^*}{\partial y} & \frac{\partial z^*}{\partial y} \\ \frac{\partial y^*}{\partial z} & \frac{\partial z^*}{\partial z} \end{vmatrix} = \begin{vmatrix} 1 + \frac{\partial(\Delta y)}{\partial y} & \frac{\partial(\Delta z)}{\partial y} \\ \frac{\partial(\Delta y)}{\partial z} & 1 + \frac{\partial(\Delta z)}{\partial z} \end{vmatrix} \approx 1 + \frac{\partial(\Delta y)}{\partial y} + \frac{\partial(\Delta z)}{\partial z}; \tag{53}$$

The expression that we obtained is obviously positive, since we assumed that the partial derivatives in it are small compared to 1, so that $|J| = J$ holds. Since $dS/dS^* = 1/|J|$ holds for the ratio dS/dS* in relation (52), we can write (52) in the form

$$\frac{A}{A^*} = |J| = 1 + \frac{\partial(\Delta y)}{\partial y} + \frac{\partial(\Delta z)}{\partial z}. \tag{54}$$

Finally, we also note that

$$\Delta y = Ly', \qquad \Delta z = Lz', \tag{55}$$

holds, where L is the distance of the screen from the layer, and y', z' are interpreted as on p. 85, so that their expressions given by equations (44) can be substituted for them. We will use such an expression for y', z' but we will write it formally differently. If, in the step from equations (42) to equations (43), the integrals in the left members are only

expressed symbolically, i.e. not evaluated, equations (44) can be written /97
formally somewhat differently, namely so that we obtain from them the expressions

$$y' = \frac{1}{n}\int_{x_1}^{x_2} \frac{\partial n}{\partial y}\,\mathrm{d}x, \qquad z' = \frac{1}{n}\int_{x_1}^{x_2} \frac{\partial n}{\partial z}\,\mathrm{d}x. \tag{56}$$

for y' and z'. If we also set in these relations $n = n_0$, a possibility we discussed on p. 88 and substitute these in relations (55) which in turn are substituted again in (54), we obtain finally the sought expression for the relative change in the illumination (the so-called contrast)

$$\begin{aligned} \frac{\Delta A}{A} = \frac{A - A^*}{A^*} = \frac{A}{A^*} - 1 = |J| - 1 = \frac{\partial(\Delta y)}{\partial y} + \frac{\partial(\Delta z)}{\partial z} = \\ = \frac{L}{n_0}\int_{x_1}^{x_2} \left(\frac{\partial^2 n}{\partial y^2} + \frac{\partial^2 n}{\partial z_2}\right)\mathrm{d}x, \end{aligned} \tag{57}$$

where the first equality is valid by the definition of the contrast.

However, the use of expression (57) for a quantitative evaluation of the density field is laborious and it is not used in practice except in a few exceptional cases. See also the remarks about the results obtained using the simple refraction method on p. 96.

It follows from equation (57) that the change in the illumination on the screen occurs at those points which correspond to the points of the layer at which $[(\partial^2 n/\partial y^2) + (\partial^2 n/\partial z^2)]$ is different from zero. To simplify the discussion, let us assume for a moment that n is only a function of y, i.e.

$n = f(y)$. Then $\dfrac{\Delta A}{A} = \dfrac{L}{n_0}\displaystyle\int_{x_1}^{x_2} \frac{\partial^2 n}{\partial y^2}\,\mathrm{d}x$, so that a change in the illumination will not occur when $\partial^2 n/\partial y^2 = 0$, i.e. when the gradient of the refractive index is either 0 (homogeneous field) or constant $[(\partial n/\partial y) = \text{const}]$. In the first case the rays will

not change their direction, and in the second case all rays of the pencil will be deflected from the original direction which they had before the layer when they leave the layer, but always by the same angle, so that the illumination on the screen will again be uniform. If, at some point of the layer, the relative change in the gradient of the refractive index is positive $[(\partial^2 n/\partial y^2) > 0]$, the rays passing through the layer at the point corresponding to the larger y are more deflected when they leave the layer than the rays passing through the point corresponding to the smaller y, and the illumination in the corresponding region of the screen will be smaller than in the case when the layer has no inhomogeneities. Conversely, if the /98
relative change in the gradient of the refractive index is negative $[(\partial^2 n/\partial y^2) < 0]$, the illumination at the corresponding point on the screen will be increased (see Fig. 60) [5, 5a]. When we take into account equations (48) it is obvious that dark points correspond to a positive relative change in the density gradient (an increasing density gradient) and lighter points to a negative relative change in the gradient. Thus, for example, the image of a shock wave (for a comparison with the previous argument we assume that the wave propagates in the direction of the positive y axis, see also Fig. 61) obtained by this method, is formed by two fringes, a dark fringe in the front part of the wave and a light fringe in the rear part of the wave.

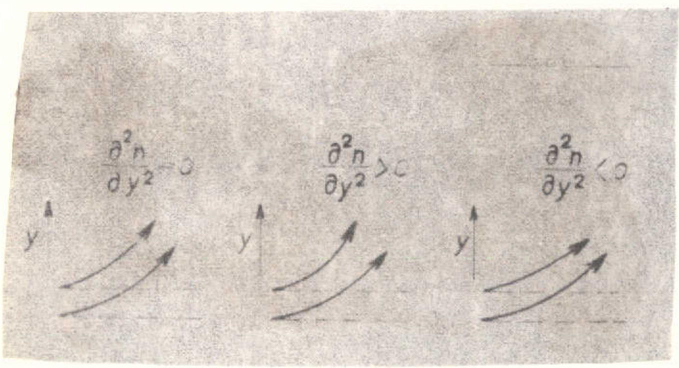

Fig. 60.

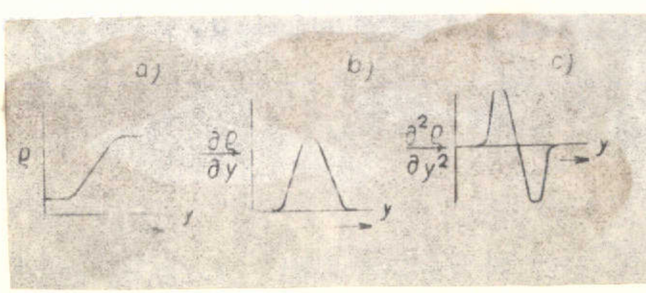

Fig. 61.

The changes in the illumination are naturally greater during greater relative changes in the density gradient. Therefore, this method can be used advantageously for high subsonic and supersonic velocities when relatively great changes in the density gradient induced by observable changes in the illumination can occur.

The optical equipment needed to apply the method is usually arranged in two ways: a) with a divergent pencil of rays in the measurement space, b) with a parallel pencil of rays.

The first method does not require any lenses or mirrors. In the simplest case it consists of a high intensity point light source, a screen or possibly a camera (Fig. 62). The light sources used most often are high-pressure, high-performance discharge tubes. Optically, a spark discharge was used as the source, which was obtained by discharging the condenser through the spark gap, which is still used successfully (therefore this method is also called the spark method and the photographs that are obtained, spark photographs). This method was used to obtain images of the flow around projectiles in flight [162]. Spark illumination is still the most convenient means for the study of projectiles in flight, and it can also be used to study the motion of unstable pressure waves. Other light sources can also be used, such as arc lamps, bulbs and discharge tubes [146, 146a, 154, 155].

When a divergent beam of light is used, a magnified image is obtained. The best results were achieved with enlargements not exceeding 1.5 [153]. For small objects, for /99
example, bullets from a rifle, a satisfactory distance of the screen or the film from the object is 15 cm, and of the spark, the light souce, from the object, it is 1.2 m. However, the last distance can be up to 5 m when relatively large measurement spaces in tunneld are lit through. Besides the advantages that can be obtained with the aid of enlargement, it is limited in all respects by the divergent rays, only to the use on objects and a field with a small span in the direction of the rays (projectiles, airplane bodies, propeller tips, etc. whose longer side is perpendicular to the direction of the rays).

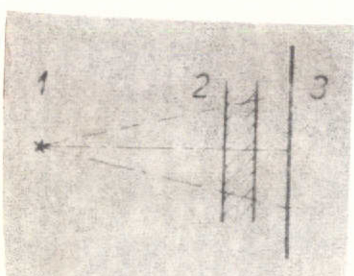

Fig. 62. Schematic diagram of simplest equipment for shadow method with divergent beam of light (1. light source; 2. analyzed gas layer; 3. screen).

To obtain images of the two-dimensional flow, the observed layer of air must be lit through by a parallel pencil of rays. To the previous version, one lens or concave mirror is added (Fig. 63) and the light source is placed at their focus. The selected focal length should be as short as possible, to obtain with the given light source a high illumination on the screen. However, this must be done without detriment to the uniformity of the initial illumination on the screen and the sharpness of the images of the inhomogeneities. A reduction in the sharpness depends indirectly on the focal length f_1, directly on the distance L of the inhomogeneity from the screen or film, and also directly on the diameter d of the light souce [174]. The sensitivity depends directly on the distance L. Since d cannot be reduced without limit, f_1 must be selected taking into consideration these factors. In some cases, it is advantageous to focus on the screen or the photographic plate (film) some plane inside the measurement space with the aid of another lens.

The lenses or mirrors used must be of first-class quality and defects in them must be corrected to prevent nonuniform illumination of the screen. Nevertheless, an instrument with cheap Fresnel lenses pressed from organic glass has been constructed. In some special cases, satisfactory results were obtained with the aid of this instrument [150].

Figs. 64 through 67 show photographs that were obtained by the shadow method.

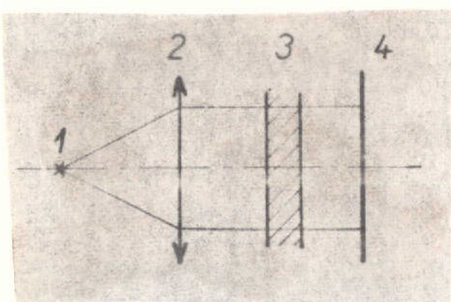

Fig. 63. Schematic diagram of equipment for shadow method with parallel light beam (1. light source; 2. lens; 3. analyzed gas layer; 4. screen).

This method was used subsequently to study the shape of three-dimensional shock waves and to obtain data about the processes that occur in them [165]. It is also used together with the so-called method of hot wires and other similar methods (see pp. 46 and 59). It was also used to obtain images of the flow around parts of an airplane during flight [168] and also to determine the state of the boundary layer and of the transition regions [159, 164]. Sometimes a very thin layer of volatile oil is applied to the surface of the streamlined body for this purpose [146a]. The oil vaporizes faster in the region of turbulent flow than in the laminar flow region, and the vaporized oil changes the refractive index more substantially in the turbulent boundary layer whose image is therefore clearer. /100

The oscillations of shock waves can be studied with the aid of an interrupted light source (stroboscope) [154, 158]. Although obtaining quantitative data about the distribution of the density in the observed field on the basis of photographic measurements or photographs is not sufficiently reliable and requires a great deal of care and caution during the technical photographic work, data about the distribution of the density near the front of a shock wave can be obtained [146, 162, 156].

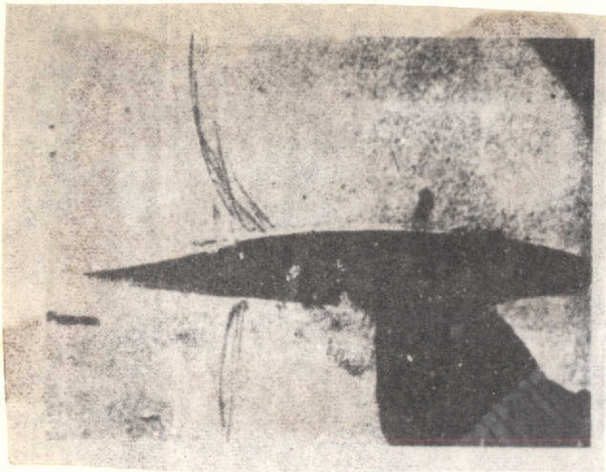

Fig. 64. Photograph obtained using shadow method during flow around a wing [5].

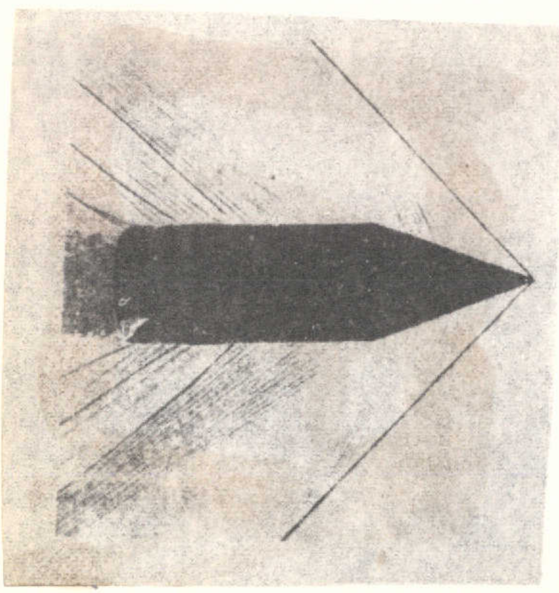

Fig. 65. Shadow image obtained during the study of the flow field around a projectile [146].

In other experiments that were carried out to obtain quantitative data about the density distribution in the entire observed layer a two-dimensional mesh (with square openings) is placed in front of the observed object in the direction of the light rays and the distortion in its image on the screen behind the observed object is used as the basis to determine the inhomogeneities in the object [162]. /102

The shadow method can also yield certain quantitative data about turbulence. When the turbulent layer is lit through, the local changes in the density have a similar effect on the passing, originally parallel rays as small converging and diverging lenses. The field with the local differences in the illumination is obtained on the screen placed immediately behind the layer in this manner (Fig. 68). The continuity of this illumination field and the density field have been described by mathematical relations, whose analysis makes it possible to determine certain statistical properties of the fluctuations in the density in the layer that is examined [146, 166].

A method for the study of three-dimensional flow has also been developed [170, 165].

3.2.2. Diaphragm Schlieren Methods

In addition to the qualitative data similar to those obtained by the previous method, it is possible to obtain more easily and better quantitative data about the distribution of the density in the entire region under consideration, i.e. for

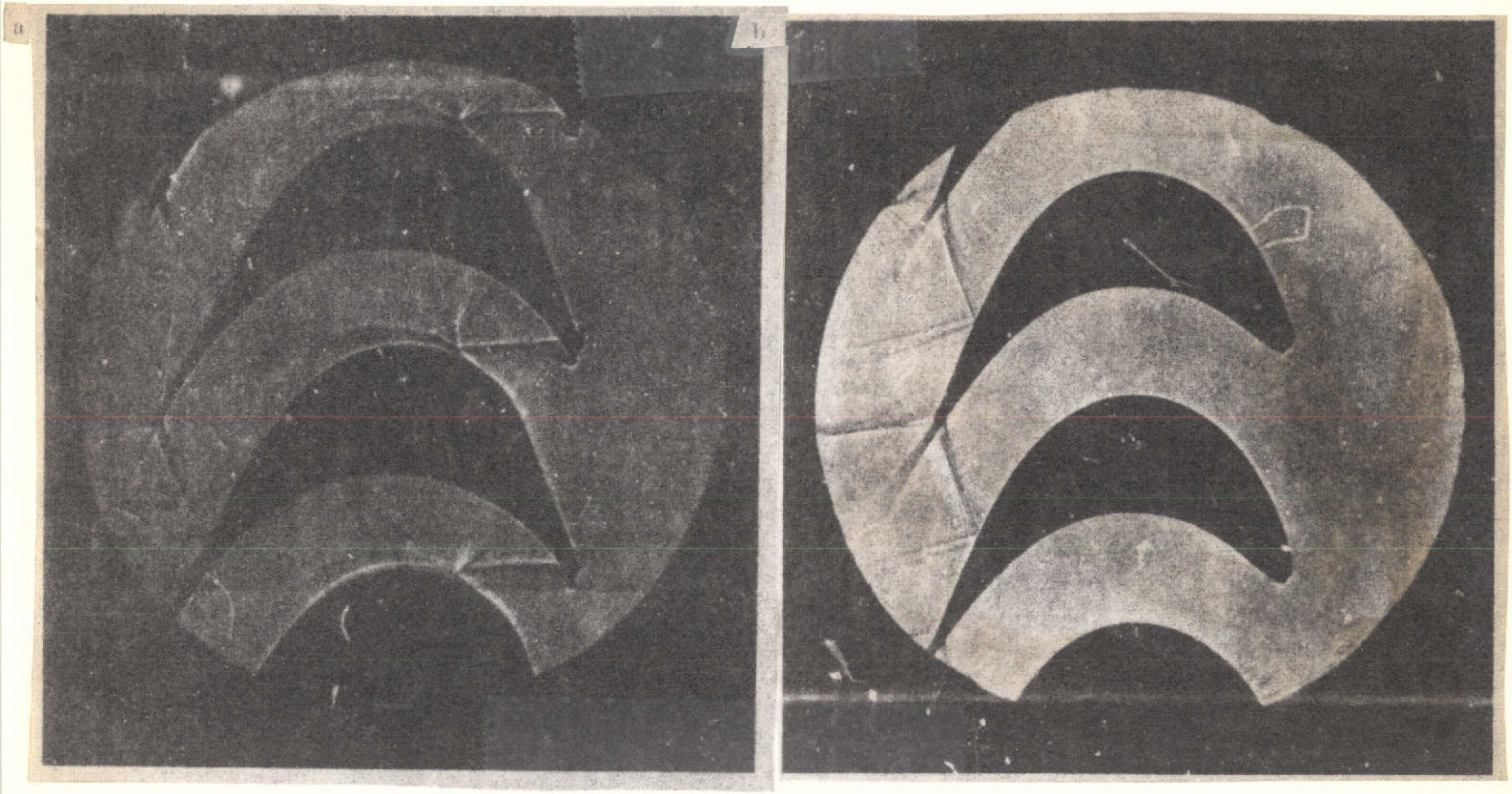

Fig. 66. Shadow image of flow field in cascade. The photographs were included with the kind permission of the author [164].

example, to determine the density field in a two-dimensional gas flow layer, by using various versions of diaphragm schlieren methods. The method used most frequently to set up the optical apparatus is evident from Figs. 69 and 70. It is the so-called Toepler principle [173]. From the photographs obtained with the aid of diaphragm schlieren methods, it is possible to determine y' and z' by measuring the blackening (see p. 85) and subsequently from this the density gradient and the density field. However, diaphragm methods are used more frequently only to obtain basic data about the flow, mainly about shock waves, expansion and wake regions, and about the boundary layer. /103

A high-intensity light source, whose dimensions are small, is used. The source is placed in the focal plane of the first lens or mirror (Fig. 69), (or the source is lit through by the condenser at the slit at the focus of the first lens, in which case the light area of the slit is considered as the source).

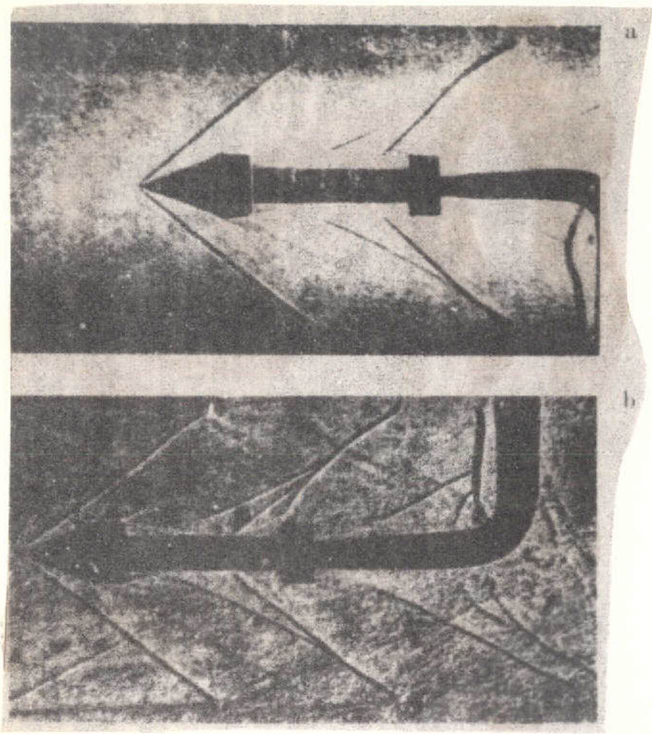

Fig. 67. Effect of exposure time during the shadow method [1]: a) exposure time 1/300 sec; b) exposure time 10^{-5} sec. The unstable oscillating character of the shock waves can be inferred from the sharper images of the shock waves in b) (during a very low exposure time).

If the layer is homogeneous a pencil of straight parallel rays passes through the layer that is examined (the measurement space in the tunnel). Then the second lens placed behind the measurement space forms the image of the light source in its own focal plane and the image of the measurement space which contains, for example, the studied model is obtained on the screen or the camera film. Lens C_3 is used to form the image. If the source has the same luminance at any point, the illumination on the screen where the rays impinge will be the same at all points. Now if, for example, a knife diaphragm (a diaphragm with a straight edge) is placed in the focal plane of the second lens in such a way that it intercepts a part of the rays incident to the screen or film, their illumination is reduced, but is again the same at all points on the illuminated area of the screen. The reduction in the illumination depends on how large the part of the image of the light source is shaded by the diaphragm, i.e. (see Fig. 69) on the distance a of the edge of the diaphragm from the vertical axis of the equipment. /104

If the examined layer has inhomogeneities, the rays passing through these points are bent, and the corresponding part of the image of the source is displaced from the original point through a distance Δs. This of course changes the illumination at the corresponding point on the screen. We will now analyze, with the aid of Fig. 69, this case in greater detail [171, 174]. /105

We will consider a light source with a slit whose width is b, whose height is h with luminance E, placed in the focal plane of the lens C_1 with focal length f_1. If the area of the lens C_1 illuminated by the source is S, we derive easily, on the basis

Fig. 68. Shadow image of wake [146].

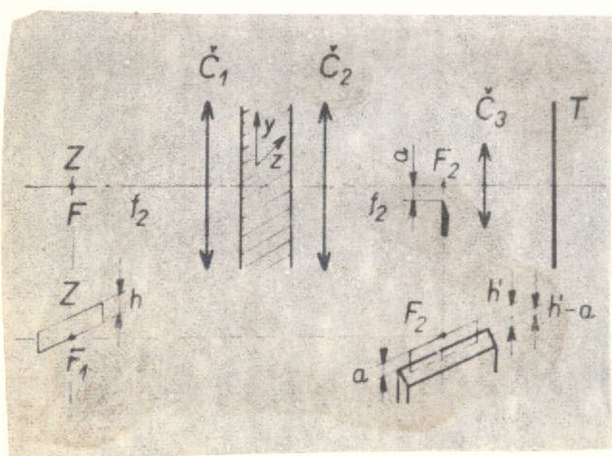

Fig. 69. Schematic diagram of equipment for diaphragm schlieren method.

of the definition of the luminance of the source for the approximate value Φ of the luminous flux incident at the lens C_1 the expression

$$\Phi = \frac{EbhS}{f_1^2}. \tag{58}$$

If we ignore the effect of the losses and take into consideration that the rays arrive from the source to the screen only with small angular deflections from the direction of the optical axis of the entire equipment, then in the case when the diaphragm is outside the pencil of rays the same luminous flux Φ also impinges on the screen. The initial illumination of the screen, whose illuminated area is S' is therefore

$$A_0 = \frac{\Phi}{S'}. \tag{59}$$

Denoting the linear enlargement obtained using the optical system that was described by m, we have $S'/S = m^2$, so that using (58) and (59), we obtain

$$A_0 = \frac{Ebh}{m^2 f_1^2}. \tag{60}$$

The image of the source with the slit in the focal plane of the lens C_2 has the dimensions $h' = h(f_2/f_1)$, $b' = b(f_2/f_1)$, where f_2 is the focal length of lens C_2.

Suppose that the center of one of the longer sides of the (rectangular) source with the slit lies at the focus F_1 of the

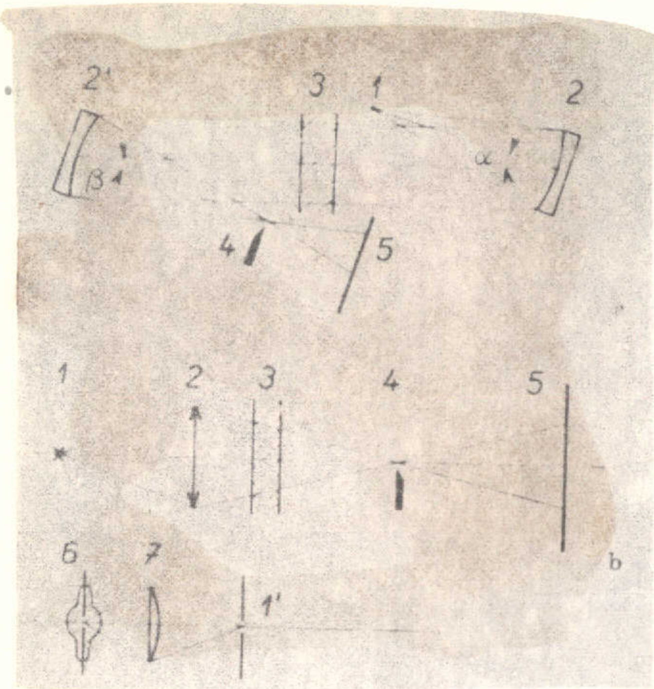

Fig. 70. Simplified schematic diagram of apparatus for diaphragm schlieren method: a) with mirrors; b) with one principal lens (1. light source; 2 and 2'. mirrors or possibly lens; 3. analyzed layer; 4. knife diaphragm; 5. screen).

At the bottom of the diagram is the schematic diagram of the light source in the case when a spark discharge is not used (as for example in Fig. 72 a, b), but an arc lamp or discharge tube is used (6. arc lamp or discharge tube; 7. condenser projecting the luminous discharge into the slit 1', 1' slit at the first focal point of the first mirror or lens; the light area of the slit is considered as the light source for the equipment). The objective is inserted between diaphragm 4 and screen 5, with the aid of which the image of the selected plane in the analyzed layer is formed on the screen or photographic plate.

lens C_1. Then the center of the longer side of the image of the source lies at the focus F_2 of lens C_2, and the image is on the side of the optical axis opposite to the source with the slit. Both sides that were mentioned are parallel.

Now if we shade a part of the image of the source by the knife diaphragm in such a way that the height of the image is equal along the entire length to the distance a of the edge of the diaphgram from the optical axis of the entire equipment (the edge of the diaphragm is parallel to the width b of the source with the slit!) the illumination on the screen is reduced from the value A_0 to the value A for which the relation

$$\frac{A}{A_0} = \frac{a}{h'} = \frac{a f_1}{h f_2},$$

holds, so that in view of (60), we have

$$A = \frac{Eba}{m^2 f_1 f_2}. \qquad (61)$$

If the layer examined has such inhomogeneities that at certain points of the layer the component of the gradient of the refractive index which is perpendicular to the /106 edge of the diaphgram exists and is different from zero (if the edge of the diaphragm is parallel to the Z axis it is the component $\partial n/\partial y \neq 0$), the rays passing through these points will be curved. The rays which leave the layer then are deflected from the original direction by the angle ε whose tangent is equal to the quantity y', which can be expressed either using the first equation in (44) or with the aid of the first equation in (56), obtaining:

$$\tan \varepsilon = y' = \frac{1}{n_0} \int_{x_1}^{x_2} \frac{\partial n}{\partial y} \, dx,$$

where $n = n(y,z)$ is the local refractive index in the layer and n_0 is interpreted as on p. 88, i.e. n_0 is the refractive index of the substance forming the flow medium in the case when the flow does not cause inhomogeneities in it. With regard to the direction of the Y axis it is considered to be the same, so that it is perpendicular to the edge of the diaphragm, i.e. perpendicular to the width d of the light source with the slit to which the edge of the diaphragm is parallel by hypothesis.

The displacement of the ray that has just been considered, which corresponds to a deflection of the ray by the angle ε from the original direction takes place in the plane perpendicular to the edge of the diaphragm, so that the corresponding parts of the image of the source in the focal plane of lens C_2 are shifted in the direction of the Y axis through the distance $\Delta s = f_2 y'$. This, of course, changes the illumination at the corresponding points on the image of the layer of the screen by the amount

$$\Delta A = \frac{f_2 y'}{\frac{f_2}{f_1} h} A_0 = \frac{E b y'}{m^2 f_1}, \tag{62}$$

where the last equality is valid because of (60). The changes in the illumination will again, as before (see p. 93) be evaluated by the relative change in the illumination, the contrast, which we now denote by the symbol B. Using relations (62) and (61) we obtain for the contrast the expression

$$B = \frac{\Delta A}{A} = \frac{f_2 y'}{a} = \frac{\Delta s}{a}. \tag{63}$$

The change in the contrast caused by a unit deflection of the ray is the so-called sensitivity of the equipment C. Hence, according to (63), it is

$$C = \frac{dB}{dy'} = \frac{f_2}{a}, \tag{64}$$

where the first equality holds on the basis of the definition of the sensitivity C that was given. The possibility of increasing the sensitivity by changing the distance of the edge of the diaphragm from the optical axis of the entire equipment which follows from the above is limited due to diffraction phenomena causing changes in the illumination of the screen which do not correspond to the inhomogeneities in the examined layer and also do not correspond to the arguments that have been presented which are based on ray optics. The effect of the diffraction phenomena does not matter during observations of a qualitative nature, so that for these purposes highly sensitive devices can be used; however, the fidelity (accuracy) of the quantitative measurements is reduced (especially those based on the measurement of changes in the illumination) which limits their use to cases in which a lower sensitivity is sufficient [162, 175, 180]. /107

Equation (62) is no longer valid when the image of the source (formed by the lenses C_1 and C_2 in the focal plane of the second lens) or a part of it is shifted entirely outside the diaphragm, or if the entire image is on the diaphragm. If this occurs, the image of the observed field (or a part of it) on the screen will have the illumination A_0 given by equation (60) or the illumination will be zero. This will also occur during larger deflections about which additional information cannot be obtained from the image on the screen. The largest possible shift of the image of the light source (or a part of it) which does not lead to a loss in sensitivity is, for a = h', equal to the height of the image $h' = (f_2/f_1)h$ (Fig. 69). This corresponds to the deflection of the ray

$$y'_{\max} = \frac{h}{f_1}, \tag{65}$$

since

$$f_2 y'_{\max} = \frac{f_2}{f_1} h = h'.$$

Similarly, for $a < h'$, the largest shift of the image of the source (or a part of it) in the direction away from the optical axis toward the edge of the knife diaphragm is a, which corresponds to the ray deflection

$$(y'_{max})_{\text{toward the edge}} = \frac{a}{f_2},$$

since

$$f_2 (y'_{max})_{\text{toward the edge}} = a,$$

and the largest possible shift in the direction away from the edge toward the optical axis in $h' - a$, which corresponds to a the ray deflection

$$(y'_{max})_{\text{from edge}} = \frac{h}{f_1} - \frac{a}{f_2},$$

since

$$f_2 (y'_{max})_{\text{from edge}} = \frac{f_2}{f_1} h - a = h' - a.$$

If the same maximum range must be achieved for both these deflection directions, the diaphragm must be set so that it intercepts exactly one-half of the image of the light source, i.e. we must have $a = h'/2$, or, taking into consideration (65), /108

$$a = \frac{hf_2}{2f_1} = \frac{1}{2} f_2 y'_{\max}. \qquad (66)$$

We then have, for the sensitivity (64),

$$C = \frac{2}{y'_{\max}}. \qquad (67)$$

From the above it follows that the maximum sensitivity that can be achieved for the given deflection range is inversely proportional to this deflection range and that it does not depend, for example, on the intensity of the source, etc. The feasible deflection range can be increased by increasing the height h of the light source with the slit or by reducing the focal length f_1 of the first lens C_1 (or mirror), which follows from equation (65).

Now, substituting z from equation (66) in equation (61) we obtain for the illumination on the screen the relation

$$A = \frac{Eby'_{max}}{2m^2 f_1} = \frac{1}{2} A_0. \qquad (68)$$

The guidelines for the design of the necessary optical equipment follow from the considerations of an approximate character that were given above. The most important parts are the two lenses C_1 and C_2 or the corresponding mirrors. From an optical standpoint, their quality must be high so that the inaccuracies arising during the refraction of light (or reflection in the case when mirrors are used) should not cause deflections of a smaller order of magnitude than the deflections caused by the inhomogeneities that are examined. The spherical and chromatic aberrations in the lens must be corrected as much as possible. The glass must be free of inhomogeneities, since all its local imperfections are observed on the screen. The objective of an astronomical telescope is most suitable for this purpose.

Compared to lenses the advantages of mirrrors are that they do not have a chromatic aberration, that the inhomogeneities inside the glass do not matter and that mirrors with relatively large diameters are cheaper than lenses with the same diameter, since only one surface is treated in a mirror. An aluminum metal plating on the surface of the mirror is better than a silver plating, since it is more durable and the oxidized aluminum layers are transparent.

The focal length of the lens C_1 must be as small as possible, since this increases not only the feasible range, which is evident from equation (65), but also for the given enlargement the initial illumination on the screen, as shown by equations (60) and (68). This will also make it possible to use a large enlargement for the given illumination, which improves observation by the naked eye and facilitates a more precise adjustment of the apparatus. However, the selection of the smallest f_1 is limited by the requirement that a homogeneous pencil of parallel rays be obtained behind the lens C_1. To /109
obtain uniform illumination of the image of the source within 1% limits, the rays must enter the lens C_1 at a vertex angle which is smaller than 8° [171]. A similar limitation also applies to the use of mirrors. This requirement must also be satisfied by the second lens or mirror. A large focal length of the lens C_2 will increase the sensitivity of the equipment as shown by equation (64); however, when the equipment is adjusted

for the maximum possible range it has no effect, according to (68), on the illumination, according to (65) on the range, and according to (67) on the sensitivity. The above gives the conditions for the selection of the lenses (mirrors).

Next, the properties of the light source must be selected so that the necessary enlargement is obtained without exceeding the feasible range. For this purpose, the maximum values of the deflections y', z' which occur in various inhomogeneities in the gas flow must be known. It was established [174-176] that deflections greater than 0.005 rad occur very seldom. This means that if we take the value that was given as a bound, the height h of the source can be calculated from equation (65), since y'_{max} and f_1 have already been selected. The initial illumination on this screen can then be increased by widening the source and also by choosing the smallest enlargement m at which details can still be distinguished.

The requirement of a high value of the initial illumination on the screen is justified by the fact that the observer's eye works in the maximum sensitivity range where it observes the relative changes in the illumination, the contrast. The eye actually reacts to changes in the brightness on the screen and when the basic value of the brightness on the screen is on an order of magnitude less than 3 nt [sic], the sensitivity of the eye to discriminating the contrast drops [174]. Hence, the minimum value of the initial (basic) illumination of this screen will be about 32 lux [174]. From these data and from the previously selected values, the necessary luminous power of the source can be determined, see equations (58) and (61).

When mirrors are used instead of lenses, the fact must be taken into account that both the source and the diaphragm are located outside the optical axis, so that the surface of the mirror should be taken, strictly speaking, as the surface obtained by rotating a parabola about an axis which is not identical with the axis of the parabola. However, normal parabolic and spherical mirrors are also used (with a focal length to aperture ratio greater than 10), since they can be obtained more easily and cheaper. To reduce the defects in the optical equipment when these mirrors are used, the angles α and β are selected as small as possible and equal or nearly equal (see Fig. 70a).

The source and the diaphragm are on opposite sides of the optical axis (of course, very close to it or in its immediate vicinity). This reduces both the astigmatism and the coma. It is advantageous if the equipment is adjusted so that the image of the source is deformed, as a result of the effect of the astigmatism, only in the direction parallel to the edge of the diaphragm.

The distance between the mirrors (or lenses) should be as small as possible to limit as much as possible the effect of the inhomogeneities of the surrounding medium between the mirrors. When mirrors are used, it is of course difficult from a design standpoint to reduce this distance, as in the case of lenses, so that the value of the distance between the mirrors fluctuates around twice the focal length of the mirror.

The light source must be placed exactly in the focal plane of the first mirror or lens. This can be achieved either by measuring the diameter of the pencil of rays between the lenses (mirrors) or the reflected image of the source on the screen placed for this purpose in the immediate vicinity of the source. A plane mirror is used for the reflection, which is inserted between the lenses (mirrors). The diaphragm must also be placed exactly in the focal plane of the second lens (mirror) and it must be positioned so that it can be adjusted exactly with the aid of micrometer screws and the distance a can be measured exactly. The edge of the diaphragm and the edges of the opening (source) must have the smallest possible unevennesses. Similarly, the lens of mirrors must be mounted on suspensions so that their position can be adjusted exactly, and the suspensions must be sufficiently rigid. This entire optical system as a whole must be as rigid as possible to prevent spontaneous changes in the position of its parts. In addition, the possible rotation of the entire optical system or the source together with the diaphragm about the optical axis must be kept in mind. This requirement occurs in certain methods used to obtain quantitative data. /110

The activity of the tunnel can affect the adjustment of the equipment. Therefore, it is sometimes necessary to make the final adjustment under normal operating conditions in the tunnel [5, 5a].

It is important that the axes of the source with the slit and of the diaphragm be parallel. To achieve this, for example, a microscope can be used and the image of the source on the screen can be observed through it, or the image of the source and the diaphragm can be focused with the aid of the modified lens C_3 on the screen (by exchanging it). The normal task of the lens C_3 is to form the image of the inhomogeneity on the screen or the photographic plate or film. In the last two cases, the lens C_3 is the objective of the camera which is focused on the plane which is perpendicular to the light rays and cuts the measurement space in half.

Fig. 71 gives an outline of the equipment that was used successfully, which consists of two systems, a lens and mirror system [174], so that the practical adjustment of the optical /111 equipment for the diaphragm refraction method can be well illustrated on it. The largest linear dimension of the observation field in the tunnel is 22.5 cm. The mirror system has two spherical mirrors with a 23.75 cm diameter and a focal length of 2.7 m, so that the apex angle of the conical pencil of rays is approximately 12°. The lens system which is used to observe details has two lenses with a 5 cm diameter and a focal length of 35 cm and it is mounted on a carriage so that its axis can be adjusted in any position along the measurement space possibly so that the functioning of the mirror system is not disturbed. Both sets of equipment can also be used to obtain photographs with the aid of the shadow method on a photographic plate inserted behind the measurement space in the direction away from the source. The light source used for visual observation is the filament of the projector bulb, and for photography the electric spark discharge with a duration on the order of 10^{-6} sec, obtained by discharging a condenser with a capacity of 0.01 μF charged to 20 kV. Using two different electrode arrangements, a slit and circular (approximately point) light source can be obtained. In the first case, two plane (metal sheet) 1 mm thick electrodes were clamped between two glass plates so that the ends of the electrodes were at a distance of 7 mm from one another, giving the 1 × 7 mm source with the slit drawn in Fig. 72. The arrangement of the electrodes for the point source used to obtain photographs with the aid of the simple refraction method is analogous. This arrangement provides a source with greater luminance than the source with a slit. It is also suitable, when greater sensitivity is required, but mainly for high quality observation, since the width of the image of the source changes during the displacement along the diaphragm, and hence also the sensitivity changes. The possibility of using as the light source a laser is discussed briefly on p. 147.

The equipment used widely in Czechoslovakia is a product of the Zeiss-Jena plant (Schlieren aufnahmegerat 80 [schlieren camera-80]) which can also be used to carry out the measurements using the grid and dye method (see pp. 114 and 119). /112
Here the maximum diameter of the observed field is 80 mm [204] (Fig. 73 a). However, equipment for which the diameter of the observed field is 10 times as large is also being designed [194].

In addition to such types of optical equipment of a basic character, systems which furnish stereoscopic records have also been designed [183, 184]. Such a system consists of two basic mirror systems by means of which the corresponding rays intersect inside the measurement space. The axes of the two systems deviate by a small angle from the perpendicular to the cover glass of the measurement space of the tunnel and lie in the same plane containing this perpendicular. The two corresponding cameras are focused on the plane where the rays from the two systems intersect. Another modification of the basic system makes it possible to determine the measurements in the selected planes of the measurement space through exact focusing [177].

To increase the sensitivity, the instruments were modified for two passages of the rays. It is particularly important to increase the sensitivity of the method during measurements at low pressures. However, it was observed in nitrogen at a density of $1.5 \cdot 10^{-3}$ kg$\cdot$m^{-3} that even at such extremely low values, the shock wave can still be determined by /113
the diaphragm method. At pressures equal to several percent of an atmosphere at which the equipment that was described can no longer be used, the sensitivity can be increased by adding sodium vapors to the air flow [197].

Often it is necessary to obtain simultaneously a record using two cameras or possibly a motion picture camera and also to study the image of the observed field on the screen. This can be achieved not only by splitting the rays immediately behind the light source, but also by having a mirrored surface

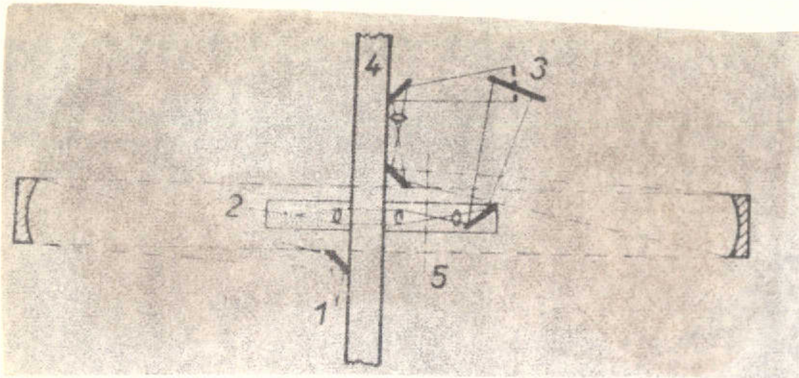

Fig. 71. Schematic diagram of equipment for the diaphragm method, consisting of two systems: a mirror system for the study of the entire cross section of the measurement space, and a smaller system attached to a displaceable optical bench, which is used for the study of details. When the independent mirror system is used, the equipment can also be used for the shadow method, by inserting the screen in the position marked in the diagram by the line 5 (1. light source of mirror system; 2. light source of small instrument; 3. screen, focusing screen or photographic instrument; 4. measurement space).

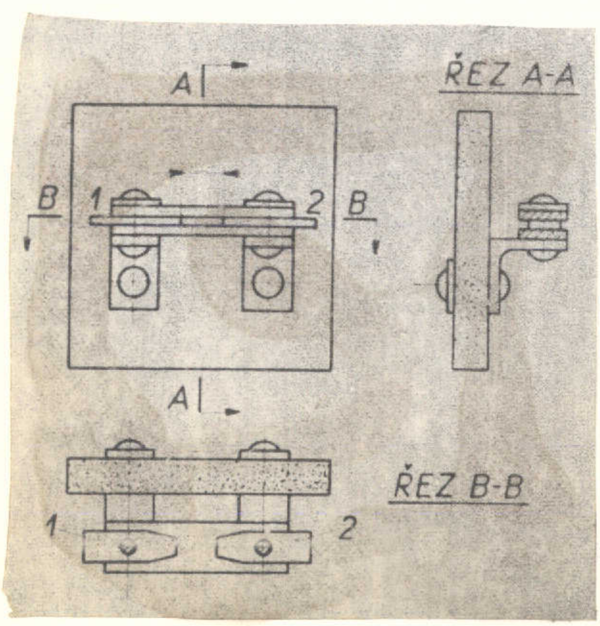

Fig. 72. Schematic diagram of the arrangement of electrodes for spark (discharge) sources of light (1, 2. electrodes).

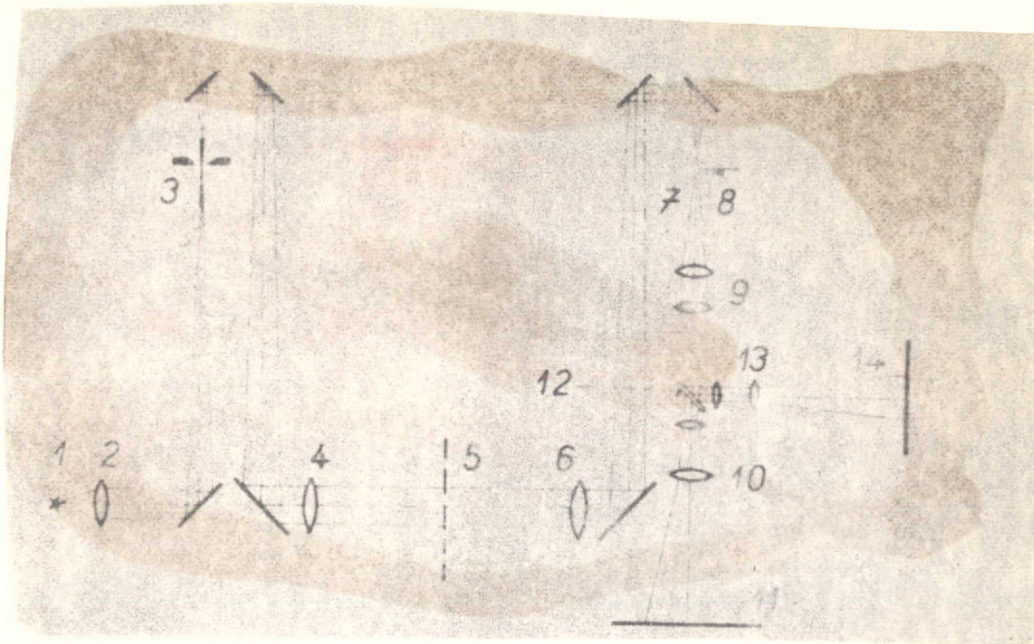

Fig. 73a. Schematic diagram of instrument manufactured by the firm Zeiss-Jena, GDR (Schlierenaufnahmegerat-80 [schlieren camera-80]) used in diaphragm methods [204]. 1. arc lamp or high-pressure mercury discharge tube; 2. condenser; 3. slit at focus of first principal lens; 4, 5. analyzed layer; 6. second principal lens; 7. image focal plane of second principal lens; 8. knife diaphragm; 9 and 10. objectives forming the image of the selected plane 5 in the analyzed layer on the focusing screen 11 of the camera built into the instrument; 12. folding mirror which can be used to reflect the rays through the objective 13 to the screen 14 for visual observation.

The U-shaped arrangement of the optical axis of the instrument with the aid of the plane mirror is of no basic significance. However, much smaller dimensions of the instrument and greater rigidity of the frame are obtained in this manner.

on the knife diaphragm. Additional images are obtained taking advantage of the reflection on the diaphragm [198, 199].

In addition to this more complex equipment, instruments are also used with one principal lens or mirror, in which the rays of the pencil passing through the medium that is examined are not parallel. The light source, its image and also the diaphragm are not in the focal planes (Fig. 73 b). An instrument based on a similar principle with a single mirror has also been used in Czechoslovakia [209].

When we determined quantitatively the requirements on the design of the optical equipment and evaluated the properties of such equipment, we only considered a light source with a slit with a constant height h and a constant width b, which was parallel to the straight line edge of the knife diaphragm. This arrangement by means of which we want to obtain the quantitative data is most suitable for the measurements and therefore has been used most frequently. However, any other shape of the source can be used provided a diaphragm with a corresponding shape is used at the same time, for example, a circular source and a circular diaphragm having the shape of a small opaque disk.

One possible source is a source given by the shape of a filament in a bulb. The corresponding diaphragm for the source is obtained by inserting the photographic plate at the place where the image of the source is formed, i.e. in the focal plane of the second lens or mirror, where it is exposed and, after it is developed, inserted in the same plate where it serves as a diaphragm. Hence this is a procedure with an initial dark field (the dark field on the screen) since only those rays which were not curved in the observed medium pass through the diaphragm (if we ignore diffraction phenomena). /114

Circular shaped sources and diaphragms with a circular aperture with the same diameter as that of the image of the source at the point of the diaphragm have also been used. Hence, during the initial adjustment, the illumination on the screen was at a maximum.

When irregularly shaped sources and the corresponding diaphragms are used, the records obtained on the screen do not correspond to the deflections of the rays only in one direction (as in the case when a light source with a slit and a knife diaphragm are used), but the rays are deflected in different directions when they are formed. Therefore, the evaluation of such records is laborious and difficult. In addition to this, the effect of the astigmatism of the system cannot be eliminated as in a source with a slit.

During the observation of objects with large gradients of the refractive index , a low sensitivity of the equipment must be selected which, however, may not be adequate to record the small gradients that can occur simultaneously in the observed object, or a greater sensitivity can be selected, but on the other hand, the feasible range can be exceeded so that information about points with large gradients is not obtained. The solution (with certain exceptions) can be obtained either on the basis of two photographs obtained with a low

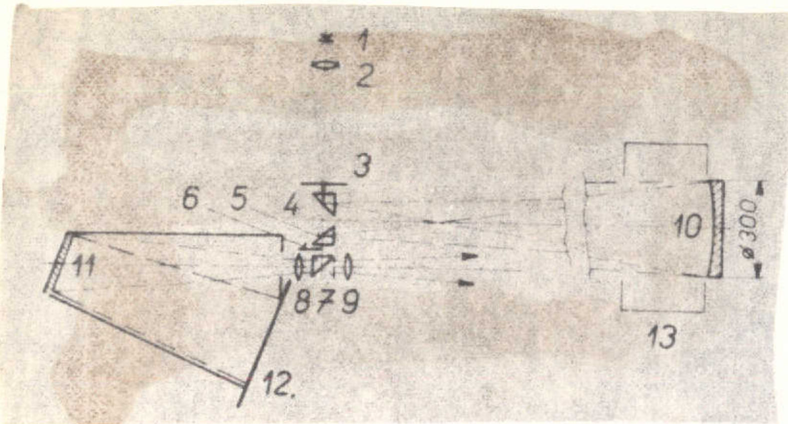

Fig. 73b. Schematic diagram of instrument manufactured by the firm Dätwyler, Switzerland used in the diaphragm method [147, 209]. (1. discharge tube; 2. condenser; 3. slit in first focal plane of mirror 10; 4. prism reflecting beam of rays through analyzed layer 13 to spherical mirror 10; the reflected rays again pass the measured layer and are shifted by prism 5 to the original direction of the optical axis; 6. knife diaphragm placed near image focal plane of the mirror 10; rotary prism reflecting rays either through objective 8 and plane mirror 11 to the screen 12, or through objective 9 to the projection screen).

and high sensitivity, where the observed object must have the same character in both cases, or with the aid of an exponentially expanding slit placed in such a way that the axis of symmetry of its image in the plane of the knife diaphragm is perpendicular to the edge of this diaphragm, or possibly a wedge filter can be used instead of the diaphragm (see p. 122) [178]. An L-shaped source with a slit is also used (two mutually perpendicular slits) and a corresponding L-shaped diaphragm [175]. However, in this case, it is necessary to take into account the fact that sharp images of each arm of the source (for example, the horizontal and vertical arm) are obtained at different distances from the source as a result of the effect of the astigmatism, and therefore the diaphragm must be arranged accordingly. The mutual distance between the two images that were mentioned is on the order of several tenths to 1 mm in the commonly used systems. Sometimes, the diaphragm is replaced by a grid or only a single filament.

Two basic methods can be used to obtain the numerical values of the local refractive index and the local density in the layer that is analyzed with the aid of various types of diaphragm schlieren methods. In the first method, primarily equipment with a source with a slit and a knife diaphragm is used and the calculations are based on equations (44), (48), and (63). The following relations for the relative change in the illumination $(\Delta A/A)_y$ caused by the deflection of the ray in the direction of the Y axis and for the relative change in the illumination $(\Delta A/A)_z$ caused by the deflection of the ray in the /115 direction of the Z axis are obtained from these equations:

$$\left(\frac{\Delta A}{A}\right)_y = \frac{f_2}{a}\frac{x_2 - x_1}{n_0}\frac{\partial n}{\partial y} = k_n \frac{\partial y}{\partial n} = k_n K \frac{\partial \rho}{\partial y} = k_\rho \frac{\partial \rho}{\partial y},$$
$$\left(\frac{\Delta A}{A}\right)_z = \frac{f_2}{a}\frac{x_2 - x_1}{n_0}\frac{\partial n}{\partial z} = k_n \frac{\partial n}{\partial z} = k_n K \frac{\partial \rho}{\partial z} = k_\rho \frac{\partial \rho}{\partial z}. \qquad (69)$$

where K is the constant from equation (47) and $k_n \equiv \frac{f_2}{a}\frac{x_2 - x_1}{n_0}$, $k_\rho \equiv k_n K$ are also constants. Equations (69) imply that the contrast, i.e. the local relative change in the illumination on the screen or photographic plate is proportional to the component of the gradient of the refractive index or the density gradient at the corresponding point of the layer which is perpendicular to the edge of the diaphragm. Hence, if the edge of the diaphragm is parallel to the Z axis, the contrast $(\Delta A/A)_y$ appears on the screen or photographic plate, from which we can determine the y-th component of the gradient of the refractive index and the density gradient, i.e. $\partial n/\partial y$ and $\partial \rho/\partial y$. Now if we rotate the entire optical system about its optical axis through a 90° angle, we will record the contrast $(\Delta A/A)_z$ from which we determine the z-th component of the two gradients, and from the y-th and z-th components of the gradient we can determine the final value of the gradient of the refractive index and the density gradient, and from these, according to equation (45), the field of the refractive index and, from analogous equations for the density, the density field.

When the contrast $\Delta A/A$ is determined, the change in the illumination can be measured point by point with the aid of a modified luxmeter. The disadvantage of this method is that the same luminance of the source must be maintained throughout the entire photometric measurement time, and that the flow studied must be the same, which is almost impossible.

A better solution is to carry out photometric measurements on photographs. Of course, two photographs must be taken for two mutually perpendicular directions of the edge of the diaphragm (the source with the slit is always parallel to the edge of the diaphragm). When these are obtained, the flow need not be exactly the same. For this reason, equipment was built in which the beam from the slit of the source is optically split (through reflection) into two beams which behave like beams which emanated from two mutually perpendicular sources with slits. These two beams pass through the measured layer (the tunnel), and after passage are separated over a greater distance by the mirrors and form in one camera on the same film at the same instant, two separated images. However, before that, each of the two beams passed through one of the two knife diaphragms whose edges are mutually perpendicular [179].

However, it is difficult to obtain photographs on which the blackened contrast is the same as the contrast when the film or photographic plate is illuminated during exposure. This is due to shortcomings in the quality of the photographic material and the imperfections of the photographic technological processes. Therefore, the procedure used introduces into the observed field a reference inhomogeneity (in German: "die Normalschliere") [162, 171]. For example, when the flow around a profile is photographed, a transparent object is inserted at the edge of the light beam at points through which the rays that were not affected by the inhomogeneities in the tunnel pass, whose effect is the same as that of an inhomogeneity with a known gradient of the refractive index (a change in the direction of the rays). Such an object may be, for example, a glass wedge with a very small refracting angle whose effect is the same as that of an inhomogeneity with a constant gradient of the refractive index, or a plane-concave lens with a small curvature of the concave side whose effect is the same as that of an inhomogeneity in which the gradient of the refractive index varies in a certain range. Then in the photograph at the point where the rays that pass through such reference inhomogeneity impinge in a small area whose blackening corresponds to the known gradient of the refractive index in the reference inhomogenity that is used for the comparison. By comparing photometrically the blackening at individual points on the photograph with the blackening on this area, we can then determine the gradients of the refractive index around the streamlined body. It is more convenient to use a lens as the reference inhomogeneity, provided we select its curvature so that it behaves like an inhomogeneity in which the gradient of the refractive index varies in the range of values which apply to the problem under consideration. /116

Another method of obtaining quantitative data may be called the filament or possibly the grid method. Also here the source has a slit, which is as narrow as possible, and instead of a knife diaphragm either a thin filament or several parallel filaments (grid) are inserted in the focal plane of the second lens, and in both cases the filaments are parallel to the axis of the slit. We will first consider only one filament which is placed at the distance a from the optical axis of the equipment in such a way that it is outside the image of the source with the slit, so that if the observed layer has no inhomogeneities, the screen is uniformly illuminated. However, if inhomogeneities are formed in the layer, the rays are deflected from their original direction, and those rays whose angular deflection in the direction perpendicular to the filament is such that its tangent y_a' has the value $y_a' = a/f_2$ are intercepted by the filament (we used the subscript a since we assumed that the filament was at the distance a from the optical axis). Hence, shadows are formed on the screen at those points which correspond to the points in the layer at which, as a result of inhomogeneities, the rays were deflected by y_a'. From equations (44) and (48) it is obvious that the density gradient has at these points the value

$$\frac{\partial \varrho}{\partial y} = \frac{1}{K}\frac{\partial n}{\partial y} = \frac{1}{K}\frac{n_0}{x_2 - x_1} y_a' = \frac{1}{K}\frac{n_0}{x_2 - x_1}\frac{a}{f_2} = k' a, \tag{70}$$

where $k' = \frac{n_0}{K f_2 (x_2 - x_1)}$ is a constant. During the calculations we took in equations (44) $n = n_0$, a possibility we discussed already on p. 90.

If we displace the filament through the distance a' from the optical axis, the dark shadows on the screen will now correspond to those points in the studied layer at which the component of the density gradient which is perpendicular to the direction of the filament has the value $(\partial \rho/\partial y) = k'a'$. Hence, when the filament method is used, the dark shadows on the screen denote those points in the layer that is examined at which the angular deflection of the rays deflected in the direction perpendicular to the filament is the same, and at which the density gradient and the gradient of the refractive index have a constant component in this direction. These dark shadows or lines are called, according to Schardin, isophotes. A narrow slit can also be used instead of a filament. In this case, light shadows are obtained on a light field instead of dark shadows on a dark field. /117

By connecting several filaments into a grid or by using a special grid, isophotes of several orders are obtained in the same photograph. Since the image of the source has a width which is not zero and the shadows obtained are wide, this method does not yield sufficiently accurate results. In addition to this, to obtain a sufficient sensitivity, the grid must be very dense, i.e. the grid spacing must be small, which would lead to diffraction phenomena, which distort the image. Two photographs obtained by the filament or grid method are given in Fig. 74 [1, 174, 180, 181].

The work is more accurate when an arrangement is used where the grid is shifted in front of the image focal plane of lens C_2, see Fig. 75 [186, 147, 191, 175]. If there are no inhomogeneities in this region that is examined, the ray passing through the point P is parallel to the optical axis until the point Q, and then after refraction by lens C_2, impinges at the point S of the image of the slit of the source (of course, before the grid G is inserted) and is then projected through the lens C_3 (projection lens, the objective of the camera) onto the screen T at the point P'. If an opaque strip of the grid G that was inserted intercepts this ray, the point P' and similarly other such points will be dark. Hence the screen will be covered by alternating dark and light lines.

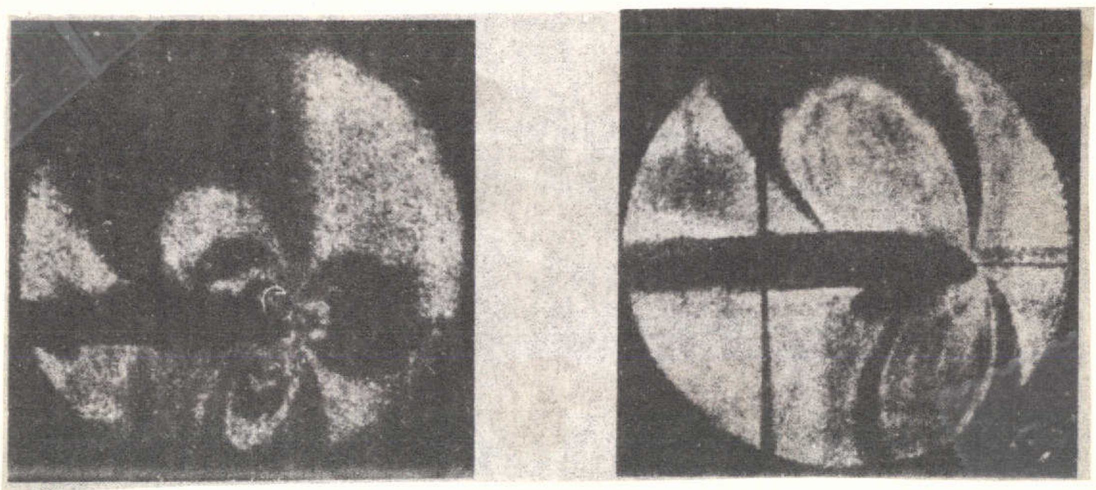

Fig. 74. Samples of images obtained using the filament method [1, 2, 181].

Let us assume now that the layer that is studied has inhomogeneities, so that the ray passing through the point P will now be deflected, say, upward by a small angle ε_P whose tangent has the value $\tan \varepsilon_P = y'_P$ (the subscript P for the point P). This ray will arrive at the point Q' and then, after refraction by lens C_2, at the point R, where $\overline{RS} = f_2 \cdot y_P'$, which can be determined with the aid of the lens equation. Hence, it is obvious that the ray will not pass through the same point of the grid as before, but will be incident on the screen again at the point P', since D and T are conjugate planes which change the illumination on the screen, i.e. in our case, the dark shadow will disappear at the point P' and will be shifted elsewhere. We can find out easily immediately where it is shifted to. /118

Let M denote another point in the inhomogeneous layer that is examined, and let us assume that the ray passing through the point M, which in the case of a homogeneous layer was parallel to the optical axis is deflected from the direction of the optical axis by the small angle ε_M and passes through the points N', A, and V, where $\overline{VS} = f_2 \cdot \varepsilon_M$. When is is intercepted at the point A by an opaque strip of the grid which originally intercepted the ray passing through the point P which was not deflected, this means that the dark shadow which originally passed through the point P' was displaced so that it now passes through the point M' where the distance $\overline{P'M'}$ is equal to the product of the distance $\overline{PM}$ and the enlargement m of the optical system formed by the lenses C_2 and C_3, i.e. $\overline{P'M'} = m \cdot \overline{PM}$.

The distance $\overline{PM}$ which we do not know for the time being will be calculated as follows: from the similarity of the triangles QN'A and SVA, we obtain

$$\overline{QN'} = \frac{f_2 - l}{l} \overline{VS},$$

where $\overline{VS} = f_2 \cdot \varepsilon_M$, as already stated, so that

$$\overline{QN'} = \frac{f_2 - l}{l} f_2 \varepsilon_M$$

and we obtain for $\overline{PM}$ (Fig. 75),

$$\overline{PM} = \overline{QN} = \overline{QN'} + \overline{N'N} = \frac{f_2 - l}{l} f_2 \varepsilon_M + d\varepsilon_M = \varepsilon_M \left(\frac{f_2^2}{l} + d - f_2 \right).$$

With regard to the enlargement m of the system of lenses C_2, C_3, it is

$$m = \frac{f_2}{d - f_2} \frac{b(d - f_2)}{f_2^2} = \frac{b}{f_2},$$

where b is now the distance of the focal plane of the projection lens C_3 from its second principal plane. Hence, we finally obtain for the shift $\overline{P'M'} = m \cdot \overline{PM}$ of the dark shadow under /119 consideration

$$\overline{P'M'} = m\,\overline{PM} = \frac{b}{f_2}\,\varepsilon_M\left(\frac{f_2^2}{l} + d - f_2\right) = k^*\varepsilon_M, \tag{71}$$

where $k^* \equiv \dfrac{f_2 b}{f} + \dfrac{b(d - f_2)}{f_2}$ is a constant for a particular optical system which does not depend on the characteristics of the grid. The displacement $\overline{P'M'}$ of the dark shadow (more precisely, the displacement of the shadow at a given point) is proportional to the error in the angle $\varepsilon \approx y'$ at the point in the examined layer which corresponds to the displaced point of the shadow.

Although at first sight a dense grid should improve the accuracy (a grid with a small grid spacing), this is not the case, since diffraction phenomena interfere considerably. A sensible bound is four opaque strips per 1 mm [146]. The opaque and transparent strips between them usually have the same width; however, it is more advantageous if all opaque strips are narrower than the transparent strips. The same number of strips in the observation field of the screen can be achieved with a sparser grid by increasing the distance l (Fig. 75), which however reduces the sensitivity of the equipment. Hence, the selection of the properties of the equipment must be a compromise between these standpoints [175, 186, 147]. In addition to a source with a slit and a grid formed by parallel straight filaments, a circular source and a circular grid can be used, i.e. a grid in which the transparent and opaque strips have the form of concentric circles.

The use of diaphragm schlieren methods imposes an important requirement on the design of the tunnel, namely that the transparent glasses be plane parallel, without defects and internal strains.

Among all methods in group 3.2 diaphragm schlieren methods /121
are used most frequently, since in comparison with the shadow method, they provide relatively reliable quantitative data about the density fields and, in comparison with interferometer methods, the required equipment is simpler, less sensitive and expensive and much easier to work with.

Figs. 77 through 80 give samples of photographs obtained using the diaphragm schlieren methods. Fig. 81 is a sample of the visualization of a boundary layer, in this case a turbulent boundary layer.

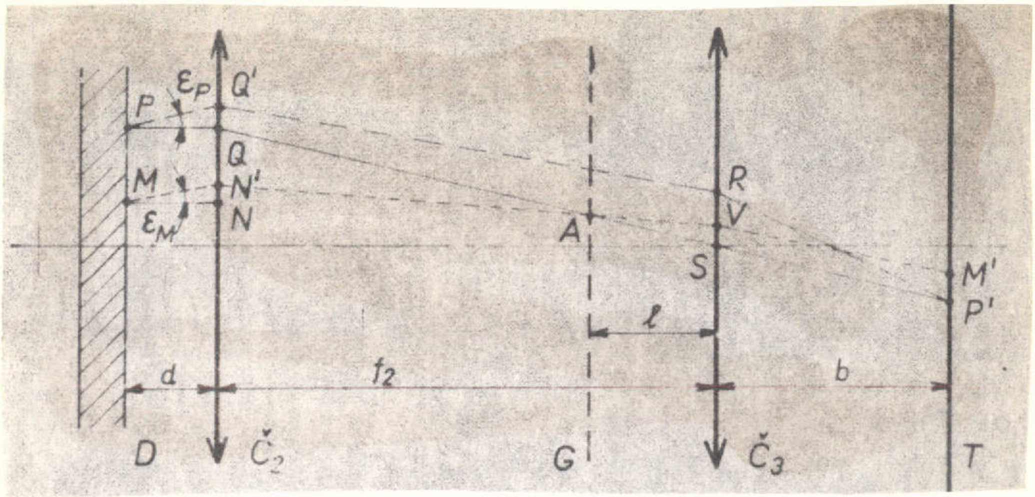

Fig. 75. Diagram illustrating grid schlieren method.

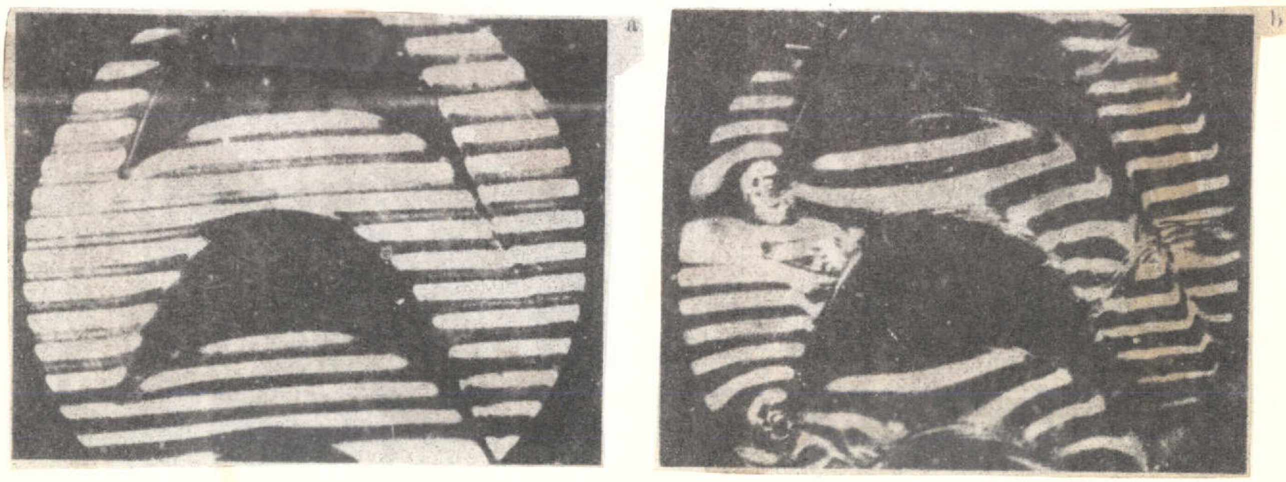

Fig. 76. Sample of images obtained by the grid method with the grid placed in front of the focus of the second lens C_2 (see Fig. 75), a) without flow, b) during flow. The photographs were included with the kind permission of the VZLU [expansion unknown] and the author [147].

3.2.3. Diaphragm Schlieren Methods with a Colored Image /122

The methods that were described in the previous two sections, 3.2.1 and 3.2.2, provide information in the form of white and black phtographs. Hence, in these cases, the eye must

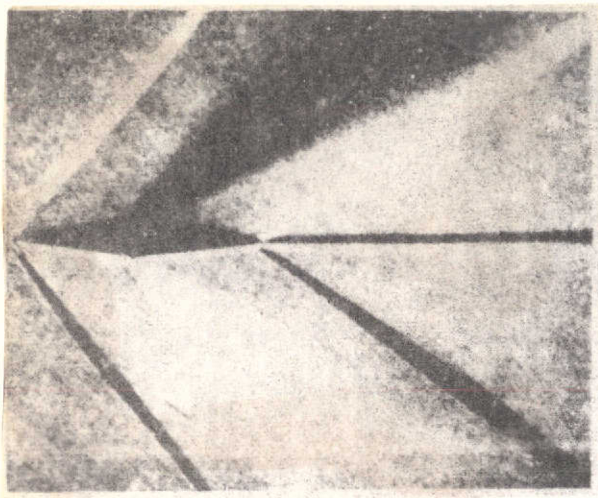

Fig. 77. Photograph obtained using diaphragm method. Flow around a rhombic profile [5].

react to changes in the illumination (unless grid methods are used), an activity for which the eye is not particularly sensitive. A healthy eye records much more easily changes in color so that the observer can observe much more conveniently in the field of view of the appropriate equipment changes in the color of the basic field rather than changes in the illumination. The proposal for and application of the method which is used in this way are not new [162], even though this method has only been used recently in the study of flow [211, 210, 147, 191].

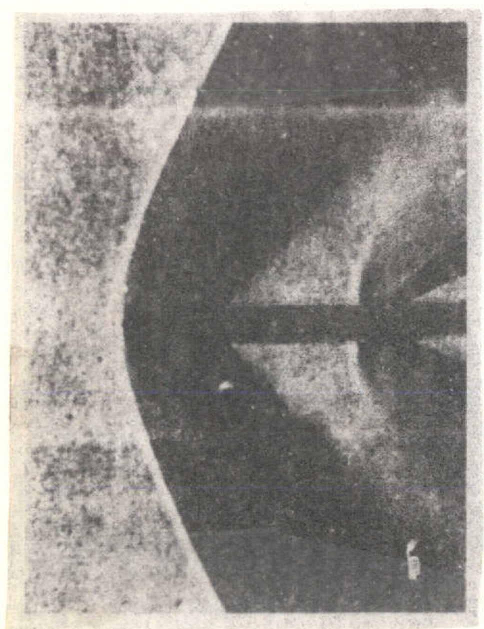

Fig. 78. Front pressure wave visualized by diaphragm method [146].

The principle of the method is such that the normal equipment for the diaphragm schlieren method is used, but a decomposing prism is inserted behind the slit of the white light source (for example, a direct /123
vision prism), which decomposes the white light, and the optical system forms in the plane of the image of the source a spectrum whose image can be intercepted on the screen (Fig. 82). However, if a slit (a slit diaphragm) is inserted in the focal plane of the second lens C_2 (the plane of the image of the source) which is parallel to the spectral lines, the screen will be illuminated only by a part of the spectrum and by choosing appropriately the height of the slit diaphragm and the dimensions of the spectrum, the illumination on the screen will have the same color shade everywhere. This basic color of the illumination on the screen can be selected by choosing the position of this slit and it can also be changed by shifting the slit diaphragm across the spectrum in the direction perpendicular to the width of this slit. When the decomposed light passes through a

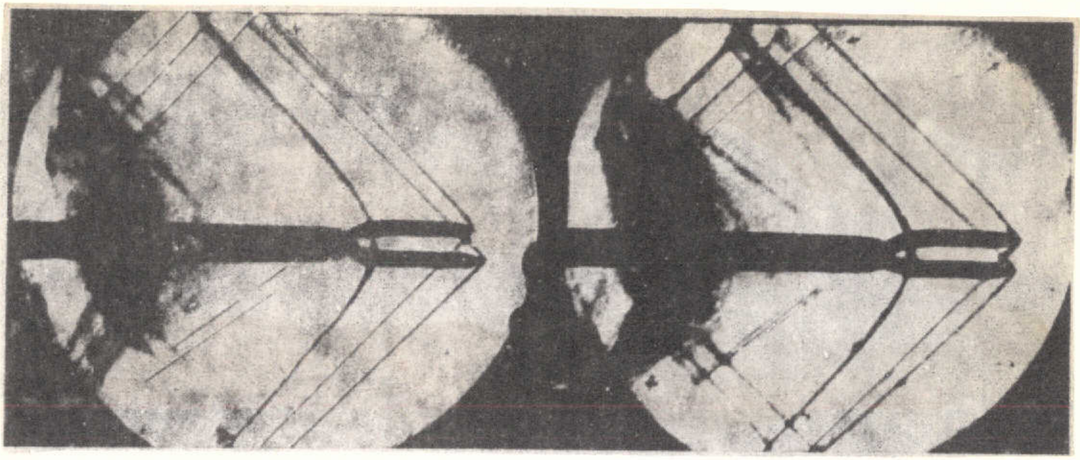

Fig. 79. Images of pressure waves obtained in stereoscopic equipment. The light beams of two independent systems for the diaphragm method intersect at a small angle in the measurement space [183].

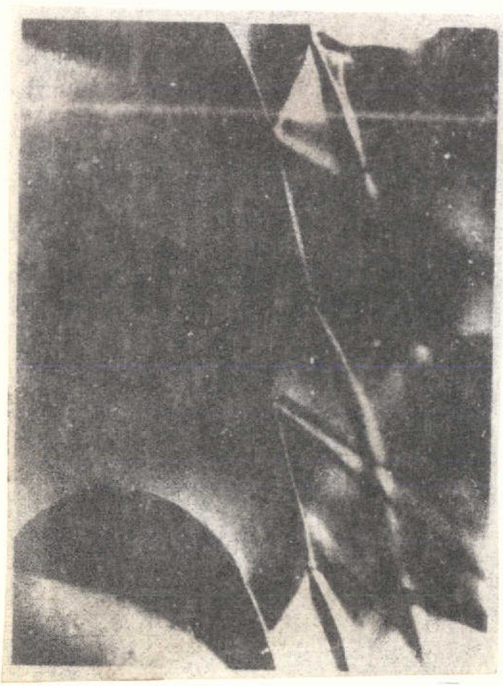

Fig. 80. Image obtained by diaphragm method during the study of flow through a cascade [10].

medium with a density gradient, the rays are deflected from the original direction, from the direction they would have if the density of the medium were constant. The deflected rays are intercepted by the slit diaphragm (i.e. they do not pass through its slit), so that the corresponding point on the screen will be illuminated by rays of a different color. To each color corresponds a certain value of the component of the density gradient which is perpendicular to the slit, which follows from equations (44) and (48).

The dimension (length) of the spectrum must be selected taking into consideration the magnitudes of the density gradient in the medium that is studied and the dimensions of the optical equipment. If the length of the spectrum is too large, the change in the colors is not very noticeable and the sensitivity of the equipment is small. On the other hand, when the length of the spectrum is small, the measurement range of the equipment may be

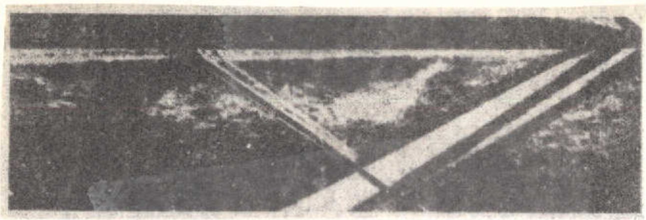

Fig. 81. Visualization of boundary layer with the aid of the diaphragm method.

exceeded and those points on the screen which correspond to the points in the medium that is studied at which the magnitude of the gradient exceeds the measurement range are dark. When the length of the spectrum is properly selected for the study of a particular case, all colors of the spectrum are represented in the image on the screen and no dark unilluminated points must appear on it. This means that the requirements on the design of the parts of the equipment and the manner in which it is constructed are basically the same as those used in the diaphragm schlieren method 3.2.2.

For example, if the basic illumination on the screen when this method is used has a green color, the deflections of the rays in one direction (these deflections lead to an increase in the illumination in the normal diaphragm schlieren method) cause a change in the green color to a color which lies closer to the red end of the spectrum, i.e. depending on the magnitude of the deflection that is considered, the green color changes through yellow to red, and starting with a certain magnitude of the deflection a dark spot appears at the corresponding points on the screen. Deflections in the opposite direction (deflections which in the diaphragm schlieren method lead to a drop in the illumination) result, depending on their magnitude, in a change from the green color through blue to violet.

In addition to a white light source, a source yielding a line /124 spectrum (for example, an iron spectrum) can be used. In this case, both in the spectrum and in the image of the field, lines of various colors separated from one another by dark strips are formed instead of the continuous colored transitions. Images which are similar to those obtained when the diaphragm schlieren method with a grid is used are obtained; however, they are colored, which simplifies considerably their evaluation.

Light sources yielding a system of luminous colored strips obtained by decomposing the light can be replaced by a colored filter strips with selected color strips, which is inserted into the slit of any light source that passes through the filter. The filter can be obtained by photographing the chosen colored sample made from colored paper or by photographing the spectrum on a color print film or plate.

The method that was described only takes advantage of a single color change cycle, which limits either the range or the sensitivity of the method. Several color change cycles

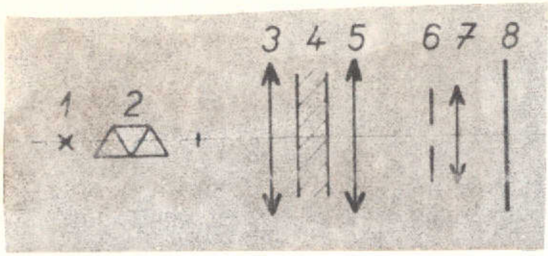

Fig. 82. Schematic diagram of equipment for diaphragm method with colored image (1. light source; 2. decomposing straight vision prism; 3 and 5. principal lenses; 4. analyzed layer; 6. diaphragm; 7. objective; 8. focusing screen or camera.

can be used when the slit diaphragm is replaced by a grid, i.e. by several slits, which increases the range while retaining sufficient sensivity. The width of the transparent and opaque strips in the grid is the same and the grid spacing, in this case, twice the width of a strip in the grid, is approximately equal to the effective width of the image of the source, the spectrum.

Suppose that the image of the source falls onto an opaque strip of the grid so that on both sides of the strip an equal part of the width extends past the edge of the strip, i.e. the red and blue end of the spectrum. In this case, the screen is simultaneously illuminated by red and blue light and appears as a purple color. Now if the beam of light is deflected in the layer that is studied, the image of the source (the spectrum)on the grid is also displaced and more light, for example, from the blue end of the spectrum, will impinge on the screen than from the red end. As the rays are further deflected in the same direction, this relation will continue to change, so that as the deflections of the rays considered increase, the illumination on the screen will change the color from purple through blue, green, yellow, orange, and red, back to purple, which will appear again as soon as the displacement of the image of the source is equal to the grid spacing. Larger deflections will cause additional color change cycles in the illumination on the screen. Deflections of the rays in the direction opposite to that considered until now will cause an alternation of colors in the opposite sequence.

In some cases it is desirable to replace a grid with equally wide parallel strips by a grid in which the transmissive strips widen (Fig. 84), i.e. the width of the strips changes along their length). When such a grid is used the deflections of the rays (components of the density gradient) appear with the color changes on the screen which are perpendicular to the axes of the strips of the grid, whereas the deflections of the rays in the direction of the strips will manifest themselves in changes in the illumination as in the normal diaphgram schlieren method. A further improvement can be obtained with the aid of a grid which has several rows of grid systems with widening strips (Fig. 84). This increases the sensitivity of the equipment to deflections in the direction of the strips [178].

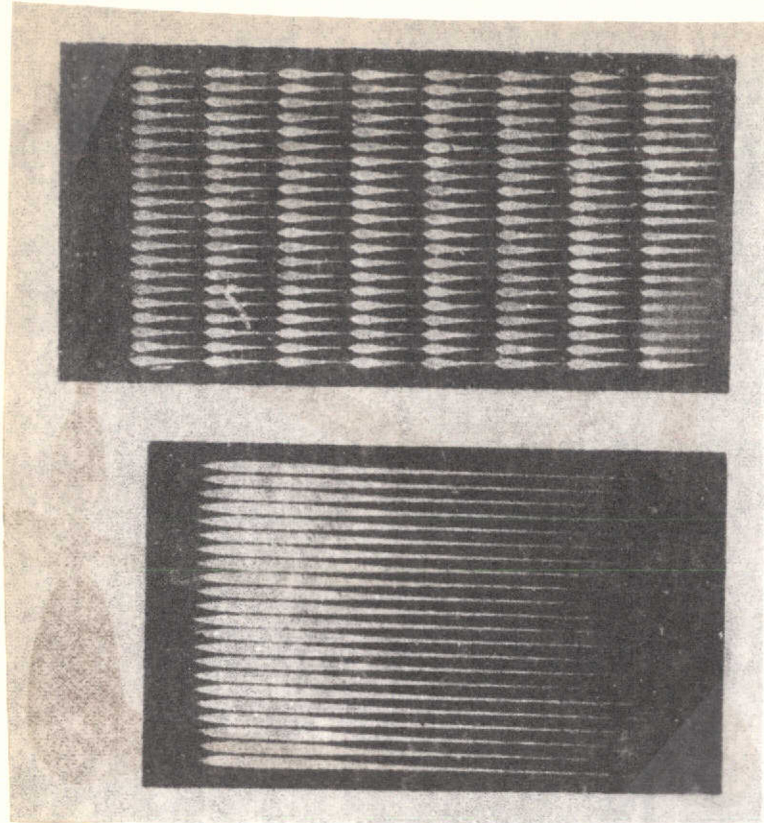

Fig. 84. Grid with widening strips.

A colored image of the inhomogeneities can also be obtained by other methods. The method in which the same equipment is used as in the grid diaphragm schlieren method (see p. 114) is suitable for large inhomogeneities, where the normal grid, located in the focal plane of the second lens, is replaced by a colored grid [162, 191] (see Fig. 85). The principle for other suitable equipment is given in Fig. 86. The middle strip of the plate D which is not cross-hatched radiates white light and the other strips glow in various colors. The size of the layer that is studied must be such that it does not extend past the pencil of rays which radiates from the surface as luminous white light and enters the aperture of diaphram C. If at some point in the layer there is an inhomogeneity deflecting the rays by the angle ε (its tangent was denoted in equation (44) and elsewhere by y'), in the observation field the point illuminated by the light of the same color at which the strip marked in Fig. 8 b by the letter b glows corresponds to this point. Hence, in this method, a certain deflection ε (a particular interval of values of the deflection ε) corresponds to each colored strip. The method is only suitable for large deflections ε and small dimensions of the layer that is studied, since otherwise the distance denoted by l in Fig. 86 is too large [162]. /125 /126

The methods that were described in this chapter are used very seldom even though they yield good results. The reasons are the difficulties which arise when colored photographs are taken and reproduced, since the inaccuracies in the reproduction of the colors in this method reduce considerably the accuracy of the results in the case when the density field is determined quantitatively.

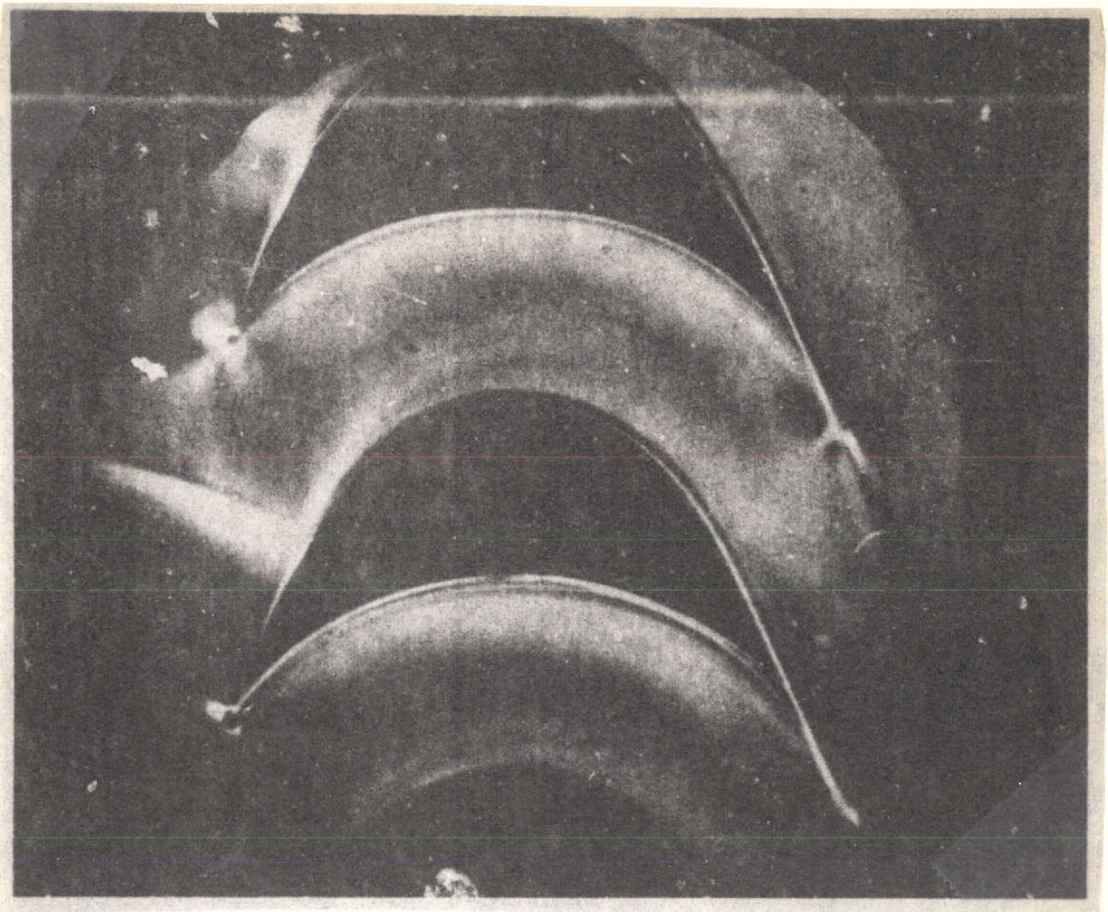

Fig. 85. Photograph obtained during flow through a cascade using colored grid placed in the image focal plane of second lens. The photograph was included with the kind permission of the VZLU [expansion unknown; probably Aviation Research Institute], and the author [191].

3.2.4. Interferometric Methods

The interferometric method requires in comparison with the methods in group 3.2 that were presented much more complex and expensive equipment, and the requirements on the service are also greater. Nevertheless, recently it has been used more and more frequently. The reason for this is that among all the methods in group 3.2 that were presented, it furnishes the most accurate data about the density field in the layer that is studied. These data can also be obtained from the interference images without particular difficulties, even though laboriously, without special instruments.

On p. 84 it was mentioned that if the refractive index of the layer that is studied whose thickness will henceforth be

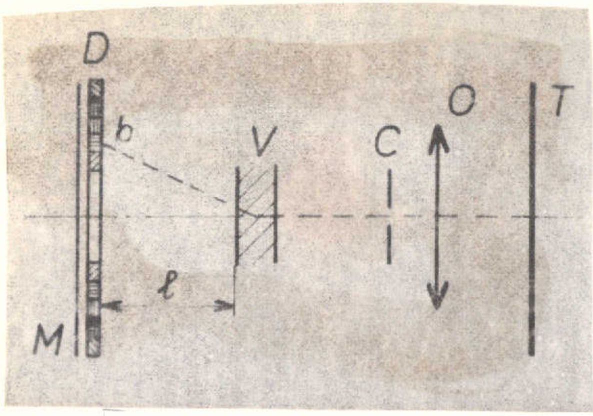

Fig. 86. Schematic diagram of equipment used to obtain colored images of pronounced inhomogeneities (M -- focusing screen; D -- colored grid filter; V -- analyzed layer; C -- diaphragm; O -- objective; T -- focusing screen).

denoted by l (until now in most cases this thickness was denoted by $x_2 - x_1$) changes from the original value n_0 to the value n, in each of these two cases the ray will leave the layer with a different phase. Hence the phase shift of the passing rays corresponds to a change of the refractive index in the layer, and to it, in the surrounding medium with the refractive index n', corresponds the displacement Δs along the trajectory given by the relation

$$\Delta s = \frac{n - n_0}{n'} l, \tag{72}$$

which was given as (50) on p. 89.

When the change in the refractive index in the layer that is studied is not the same everywhere, i.e. if n = n(y,z), the phase and trajectory shift will be a function of the coordinates y, z. This means that by determining the displacement Δs along the trajectories at various points of the inhomogeneous layer, it is possible to obtain data for determining the local values of the refractive index, from which in turn the local values of the density can be determined on the basis of the relation /127

$$\frac{n-1}{\varrho} = \frac{n_0 - 1}{\varrho_0} = K, \tag{73}$$

which we presented as (47) on p. 89.

The shift along the trajectory can be measured using inteference, for example, in the following manner. Two rays are obtained from the same light source, one of which passes through the inhomogeneous layer in which we determine the field of the refractive index, and the other passes through the layer used for the comparison (for example, a layer with the same properties which the layer that is studied had when it had no inhomogeneities, and therefore had the same refractive index n_0 everywhere). If, after passage through the layers, the rays are combined again, they interfere, provided they are coherent. If the trajectory difference at the point where the rays meet again is equal to an odd multiple of half the wavelength λ' of the light used (λ' is the wavelength of the light used in the medium in which interference occurs, which here is the medium which we called the surrounding medium with respect to the layer examined, and whose refractive index we denoted by n'), i.e. if at that point

$$\Delta s = (2k+1)\frac{\lambda'}{2}, \qquad \text{where} \qquad k = 0, 1, 2, 3, \ldots \tag{74}$$

the light will be attenuated at this point, and if the intensities of the two rays are the same the light will vanish. Conversely, the light will be intensified at points where the trajectory difference of the interfering particles is equal to an even multiple of the wavelength, i.e. where

$$\Delta s = 2k\frac{\lambda'}{2} = k \cdot \lambda', \quad \text{where} \qquad k = 0, 1, 2, 3, \ldots \tag{74'}$$

The dark and light fringes that are formed are called interference fringes. The record, a photograph of these interference fringes, serves as the basis for determining the field of the local values of the refractive index in the layer that is examined. This means that the data about the layer that is examined are determined from the shape and grouping of the interference fringes or possibly from their changes.

The images of the phase shifts of the rays, the interference images, are obtained with the aid of interferometers. Hence, in principle, the Michelson (Fig. 87) or Jamin (Fig. 88) interferometers that are known from physics can be used [15, 16]. However, the Michelson interferometer has the disadvantage that the rays in it pass through the layer that is examined twice, which may cause inaccuracies when the records are evaluated. The difficulty in the Jamin interferometer is the small distance of the two separated beams which later interfere with one another, so that its use is limited to cases when one of the transverse dimensions, the dimensions in the directions perpendicular to the direction of the rays of the layer examined, is sufficiently small, as, for example, in the study of a boundary layer. The improper position of the plane in which the interference fringes are formed in another shortcoming in both instruments. The interferometer proposed by Mach, the Mach-Zehnder interferometer, is used exclusively for experimental aerodynamic purposes [223]. A sketch of this equipment /128

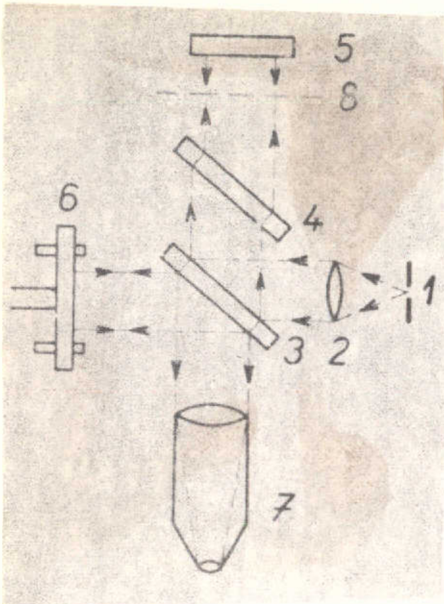

Fig. 87. Schematic diagram of the Michelson interferometer [15, 16]. (1. light source; 2. lens forming parallel pencil of rays; 3. plane parallel glass plate with reflecting semipermeable layer; 4. plane parallel glass plate like 3 without reflecting layer; 5. fixed mirror; 6. displaceable mirror; 7. observation telescope into which luminous rays reflected by the mirrors 5 and 6 enter and interfere 8. image plane of reflecting surface of mirror 6).

(in physics, similar equipment is associated with the name Rozhdestvenskiy) is given in Fig. 89. Compared to the two types that were described, it has the advantage that the light passes through the examined layer only once, and that the separate beams can be separated from one another over a sufficiently large distance so that if necessary, only one beam passes through the measurement space and the other is completely outside this space.

The basic parts in a Mach-Zehnder interferometer are two plane mirrors S_1 and S_2 (Fig. 89) and two plane parallel semipermeable glass plates P_1 and P_2 (a semipermeable plate is a plate which reflects half the incident light and lets the other half through). These four basic parts are located in the instrument in such a way that when their centers are connected a rectangle or square or possibly another parallelogram is formed. The mirrors and glass plates during the measurements are either exactly parallel and subtend with the sides of the rectangle that was mentioned 45° angles, or at least one of these four elements is slightly deflected from the position that was mentioned as a result of a small rotation about the axis that passes through its center, for example, perpendicularly to the plane of the rectangle that was mentioned (for additional details, see p. 133) [226]. /129

Another part of the Mach-Zehnder interferometer is a point source of monochromatic light placed at the focus S of the collimator objective, or possibly the source is projected by the condenser onto the collimator slit which lies at the focus of its objective. Each light ray R emanating from the source S impinges on the plate P_1 which is semipermeable, i.e. it splits the ray R into two parts: the reflected and passing ray, whose intensities

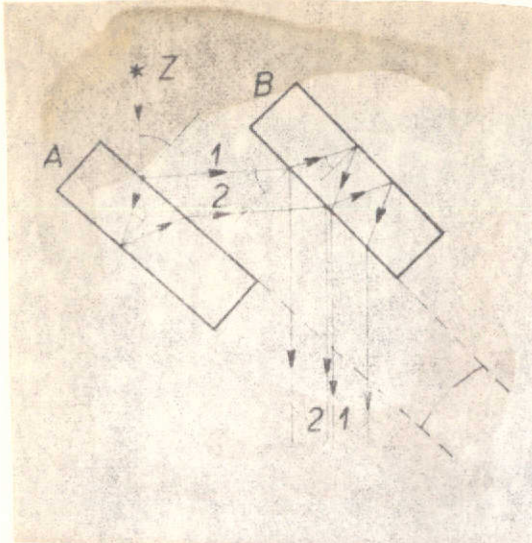

Fig. 88. Schematic diagram of Jamin interferometer [15, 16] (Z -- light source; A and B -- plane parallel glass plates; 1 and 2 -- rays which interfere with one another after reflection on plate B).

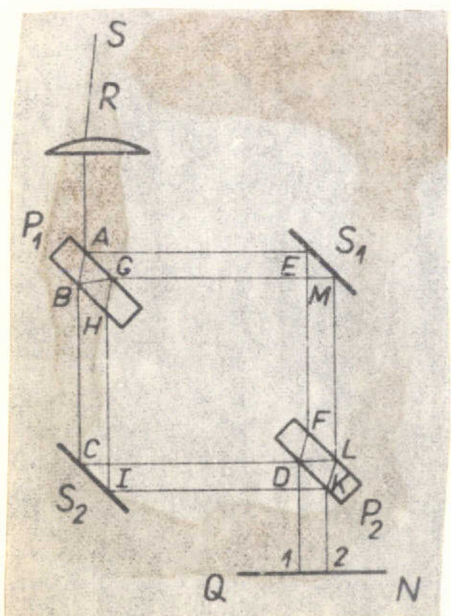

Fig. 89. Schematic diagram of Mach-Zehnder interferometer.

are approximately one-half of the intensity of the incident ray R. If the plate and mirrors are mounted so that they are parallel, the trajectory of the passing ray is determined by the points ABCD1 and the trajecotry of the reflected ray by the points AEFD1. A part of the luminous ray is also reflected at the point B, so that it follows the trajectory ABGMLK2, or, possibly, due to the subsequent reflection at point G, the trajectory ABGHIK2. The reflection may also occur at the point D, so that a part of the original ray may also have the trajectory AEFDLK2. All rays which finally arrive at point 1 will have the same phase at this point, which also applies to the rays arriving at point 2, both of which follow from the assumption that the mirrors and plates are parallel and exactly planar, that the two plates have the same properties and are exactly plane parallel, and that the medium between the plates and mirrors is completely homogeneous. The rays, incident at point 2 (and all similar rays) even though they have, in comparison with the rays arriving at point 1, a very small intensity, can never- /130 theless have a disturbing effect, since the common value of the phase of the rays at point 2 differs from the common value of the phase of the rays at point 1. Therefore, antireflexive layers on the plates are used to prevent them from impinging on the screen. Hence, we may consider only rays which are analogous to the rays passing through point 1 which will illuminate the screen uniformly. This satisfies to a certain extent all the assumptions and requirements made on the properties of the parts of the interferometer which will be discussed later (see p. 140).

Now if in one branch (for example, in the branch AEFD1, see Fig. 89) of the interferometer inhomogeneities are formed as a result of the flow in the air layer that is examined through which the rays from the branch pass, then, for example, the ray of the branch under consideration passing through point 1 will have at the point D a different phase than before. If this phase shift corresponds to a trajectory displacement which is equal to an odd multiple of half the wavelength, a dark spot is formed as a result of interference with the ray ABCD1 at the point D (and also at the point 1 and all points on the segment $\overline{D1}$), since the ray ABCD1 is incident at D with the original phase. Similar pairs of rays will form additional dark spots. On the whole, dark fringes will be formed on the screen (or possibly dark regions which do not have exactly the form of fringes), and at each point of a particular fringe, the phase and hence also the trajectory difference of two rays which at that point are disturbed by interference will have the same value. For various k (k = 0, 1, 2, ...; see equation (74) dark fringes of various orders will be formed.

We will now use (as before in most cases) the following notation:

a) n and ρ are the refractive index and the density at the point of the layer with the inhomogeneities that is examined through which the ray AEFD1 passes; c and λ are the velocity and wavelength of the monochromatic light used during the passage through the layer that is examined;

b) n_0, ρ_0, c_0, and λ_0 are the symbols for the analogous magnitudes in the homogeneous layer used for the comparison which is located in the second branch of the interferometer, through which the ray ABCD1 passed;

c) n', ρ', c' and λ' will denote the analogous magnitudes in the surrounding medium.

The difference of the optical paths of the rays AEFD1 and and ABCD1 (and similar pairs of rays) is

$$\Delta s_{\mathrm{opt}} = (n - n_0)l, \tag{75}$$

since the layer that is examined and the layer used for the comparison have the same thickness l. In the surrounding medium the path difference given by relation (72) corresponds to the above difference. From equations(72) and (74), we obtain for the changes in the refractive index at which the dark interference fringes are formed the relation

$$\frac{n - n_0}{n'} = \frac{1}{l}(2k+1)\frac{\lambda'}{2}, \quad \text{where} \quad k = 0, 1, 2, 3, \ldots, \tag{76}$$

in which we can take, on the basis of (73),

$$n - n_0 = \frac{n_0 - 1}{\varrho_0}(\varrho - \varrho_0), \tag{77}$$

so that we obtain for ρ

$$\begin{aligned} \varrho &= \frac{\varrho_0}{n_0 - 1}\frac{\lambda' n'}{l}\frac{2k+1}{2} + \varrho_0 \\ &= \frac{\varrho_0}{n_0 - 1}\frac{\lambda_v}{l}\frac{2k+1}{2} + \varrho_0, \quad \text{where} \quad k = 0, 1, 2, 3, \ldots \end{aligned} \tag{78}$$

in which the second equality holds because $n' = c_V/c' = \lambda_V/\lambda'$, where λ_V is the wavelength of the monchromatic light used in vacuum and c_V is the velocity of light in vacuum. Since λ_V and l are known and $\rho_0/(n_0 - 1) = 1/K$, according to (73), this fraction has a constant value which we can easily determine in advance (for example, for air we already calculated K on p. 89 and denoted the value by K_0, so that for air the the fraction under consideration will have the value $1/K_0$), and it suffices, obviously, if we determine the density ρ_0 of the layer used for the comparison and determine the order k of the interference fringe. After substitution in (78), we obtain the density along the line in the measurement space, which corresponds to the given interference fringe and hence indicates the points where the density ρ is the same. When the local density is known, additional data can be calculated, data about the local velocity, pressure, the Mach number and temperature [for example, 215, 217, 212, 239, 240, 242 and others].

A procedure which is often used is to determine the density at a point of the layer which corresponds to some point through which the interference fringe in the interference image passes on the basis of the measured static pressure at that point in the layer. This is usually done at several points in the layer. If the observed layer is bounded by glass walls, holes are drilled into them at selected points which are used for measurement of the static pressure. The images of these holes are in the field of view (Fig. 90), so that we can find the interference fringes passing through the centers of these images. If the interference fringe passes through the center of a particular hole, the pressure at these points of the layer which correspond to the interference fringe under consideration may be considered to be equal to the static pressure measured at the point where the hole is located. However, since the pressure is measured at the point where the opening is the inlet into the measurement space, i.e. near the wall of the measurement space, and this pressure is not identical with the pressure at those points in the layer which lie on the line through the center of the opening across the layer, i.e. on the line perpendicular to the walls (cover glasses) of the measurement space, the accuracy of the data that were obtained in affected. Howeven, any other method of measuring the pressure would disturb the flow.

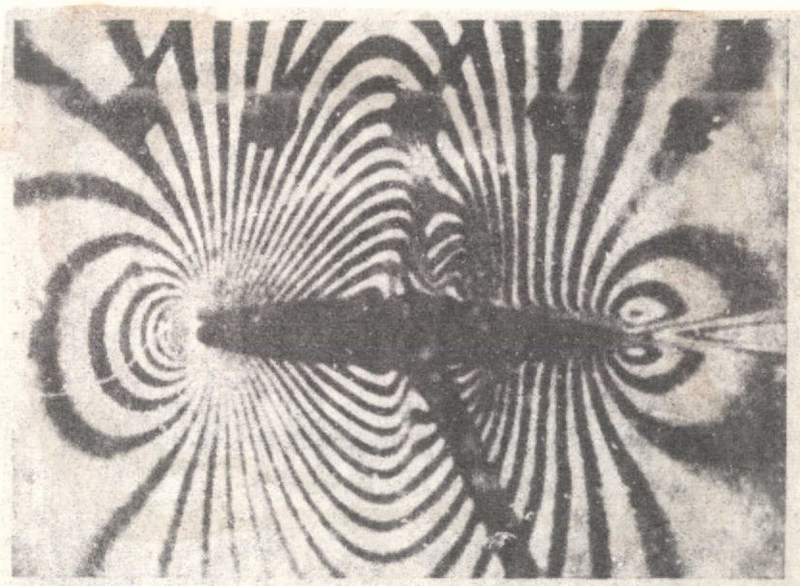

Fig. 90. Interferogram with images of openings used for measurement of static pressure [2]. (Interferometer adjusted for infinite width of fringe.)

The densities corresponding to two neighboring interference fringes differ according to (78) by /132

$$(\Delta \varrho)_1 = \frac{\varrho_0}{n_0 - 1} \cdot \frac{\lambda_v}{l}, \tag{79}$$

so that if we know the density corresponding to a particular interference fringe, we can easily determine the densities corresponding to other interference fringes. Of course, we must know on which side of the interference fringe that was identified the density increases. When k is the order of the identified interference fringe, the fringes whose order is higher than k, and to which, according to (78), correspond higher values of the density are distributed from the fringe that was identified, in the direction toward the point where the velocity on the streamlined body is zero, since, at this point, the pressure is higher than at the points corresponding to the identified fringe. Fringes whose order is lower than k are distributed in the direction from the identified fringe toward the point where the velocity is a maximum (Figs. 91 and 92).

The plotting of interference images in the form of drawings which are later evaluated causes sometimes difficulties because of the great width of the interference fringes. This difficulty can be surmounted by subjecting the photographs to a special photographic process called equidensitometry [21], by means of which two very narrow lines are obtained from one wide fringe.

A Mach-Zehnder interferometer can also be used for the study of inhomogeneous layers in a different manner. By turning a mirror or plate, for example, by rotating the plate P_2 about the axis which passes through its center perpendicularly to /134 the plane given by the centers of the plates and mirrors (the plane in Fig. 89), we obtain a case which is similar to the case in which the light passes through a wedge, in this case an air wedge. We will analyze what happens in such a case. The surrounding medium is considered to be entirely homogeneous and its refractive index is again denoted by n'.

The optical paths of the rays in both branches of the interferometer will now no longer be the same (even though, for the time being, we do not consider the insertion of the examined inhomogeneous layer in one branch of the interferometer and the layer used for the comparison in the other branch!). Their difference depends on the angle of rotation of the plate and on the distance of the ray from the axis about which the plate was rotated. Hence, we may assume that the pencil of rays passing through one branch of the interferometer (for example, the branch in which the measurement space will be inserted must, in comparison with the rays in the other branch, also pass perpendicularly through a wedge with a small refracting angle α, which has a refractive index that will be denoted by n_0). The rays in this branch, unlike the rays in the other branch, will have a trajectory displacement which, in the surrouding medium with refractive index n', has the value

$$\Delta s = \frac{n_0}{n'} d = \frac{n_0}{n'} e\alpha, \tag{80}$$

where d is the thickness of the wedge at the point where the ray studied passes through the wedge and e is the distance of this point from the edge of the wedge.

It is obvious that for some e, conditions (74) will be satisfied after the light disappears. According to (74) and (80), the light will disappear when

$$e = (2k+1)\frac{\lambda'}{2}\cdot\frac{n'}{\alpha n_0} = (2k+1)\frac{\lambda_v}{2\alpha n_0}, \quad \text{where} \quad k = 0, 1, 2, 3, \ldots \tag{81}$$

and where $\lambda_v = \lambda' n'$ is the wavelength of the light that was used in vacuum. Hence, dark interference fringes will be formed in the field of view of the interferometer (Fig. 93) which are parallel to the edge of the wedge (i.e. to the axis about which the plate was turned). The distance b between two neighboring fringes will be the same everwhere and equal to

$$b = e_{k-1} - e_k = \frac{\lambda_v}{2\alpha n_0}(2k+2+1-2k-1) = \frac{\lambda_v}{\alpha n_0}. \tag{82}$$

(If the plate and mirrors are in mutually parallel positions, i.e. if $\alpha = 0$, according to (82), the distance b between the neighboring interference fringes (and their widths) will increase without limit. Therefore, in this case, which we already discussed on pp. 128-132, we talk about adjusting the interferometer to an infinite width of the fringe.)

Now if the inhomogeneous layer with refractive index n and thickness l is inserted in one branch (for example, the branch EF) of the interferometer, the trajectory difference (80) changes by a value which corresponds to the change in the refractive index from the value n_0 to the value n (we assume that in the place where the layer is inserted, the air was originally still, and therefore we use for the original refractive index the same notation as for the refractive index in the wedge considered above, which is also formed in still air). /135
This change in the surrounding medium with refractive index n' is given by the expression $[(n - n_0)/n']l$, so that the total displacement along the trajectory of the ray passing through the branch containing the inhomogeneous layer that is examined, unlike the ray that passes through the second branch of the interferometer, in the surrounding medium with refractive index n', will now be given by the expression

$$\Delta s = \frac{n_0}{n'}d + \frac{n - n_0}{n'}l. \tag{83}$$

instead of expression (80). However, this means that the position of the original dark interference fringes will also change (i.e. those that were formed before the inhomogeneous layer that is examined was inserted in one branch of the interferometer, as a result of turning the plate P_2; see p. 133), since, due to the change in the trajectory difference of the rays, the condition for the vanishing of the light will now be satisfied for a different thickness d' of the wedge, i.e. at a different point e'. From equation (74) and equation (83), in which we will write d' instead of d on the basis of what has just been said, we find that the light will disappear as a result of interference when the condition

$$(2k+1)\frac{\lambda'}{2} = \frac{n_0}{n'}d' + \frac{n-n_0}{n'}l = \frac{n_0}{n'}e'\alpha + \frac{n-n_0}{n'}l, \quad \text{where} \quad k = 0, 1, 2, 3, \ldots$$

is satisfied, where the second equality holds on the basis of the relation $d' = \alpha e'$, where α is the refracting angle of the wedge. From the above, we obtain for e' which gives the new position of the dark interference fringe, using the relation /136
$\lambda' n' = \lambda_v$, the expression

$$e' = (2k+1)\frac{\lambda_v}{2\alpha n_0} - \frac{n-n_0}{\alpha n_0}l, \quad \text{where} \quad k = 0, 1, 2, 3, \ldots \tag{84}$$

When we compare the expression that was just obtained with expression (81) for e which gives the original position of the dark fringe, i.e. its position before the inhomogeneous layer that is examined was inserted in one branch of the interferometer, and also when we compare equations (80) and (83), we find that if $n - n_0$ is positive, the original displacement along the trajectory is increased and the change $\Delta e = e - e'$ in the position of the original interference fringe is in the direction of smaller d, i.e. in the direction toward the edge the wedge (to the axis about which the plate P_2 was turned; see p. 132) and the converse will hold when $n - n_0$ is negative. According to (81) and (84)

$$\Delta e = e - e' = \frac{n-n_0}{\alpha n_0}l, \tag{85}$$

so that we obtain, for the ratio of the change in the position of the fringe to the original distance b between the interference fringes with the aid of equation (82), first

$$\frac{\Delta e}{b} = (n - n_0)\frac{l}{\lambda_v} \tag{86}$$

and, taking into account (77),

$$\frac{\Delta e}{b} = \frac{l}{\lambda_v}\frac{n_0 - 1}{\varrho_0}(\varrho - \varrho_0). \tag{87}$$

This equation determines the relation between the change in the position of the interference fringe and the change in the density. From the above we obtain, for the unknown density,

$$\varrho = \frac{\Delta e}{b}\frac{\varrho_0}{n_0 - 1}\frac{\lambda_v}{l} + \varrho_0 = C_0\,\Delta e + \varrho_0, \tag{88}$$

where

$C_0 \equiv \frac{\varrho_0}{n_0 - 1}\frac{\lambda_v}{bl}$ is a constant; hence for $\Delta\rho = \rho - \rho_0$

we obtain

$$\Delta\varrho = C_0\Delta e. \tag{89}$$

On the basis of expression (88), the density can be determined at any point of the layer that is examined provided we measure the change Δe in the position of the interference fringe as discussed in the next section. The unknown density ρ however is determined, according to (88), as a function of the density ρ_0 in the homogeneous reference layer, for which the surrounding medium can also be used. The original interference image formed by the parallel equidistant fringes with the spacing /137
b given by relation (82) belongs to this reference layer. The reference medium for the density ρ_0 is the surroundind undisturbed atmosphere in the case when the flow around bodies in flight (projectiles, etc.) in the free atmosphere is studied, or during the study of axisymmetric outflow of air from a nozzle into the free atmosphere. During the observation of flow in tunnels, the reference medium is the air in the so-called compensation chamber which is inserted in the branch BC of the interferometer (the measurement space in the tunnel is inserted according to the previous prerequisite in the branch EF) or the undisturbed flow in the tunnel before the part of the measurement space that is examined [212]. In the last case, the

Fig. 91. Interferogram of flow field in a cascade [10]. (Interferometer adjusted to infinite width of fringe.)

rays from both branches of the interferometer pass through the measurement space, i.e. through the same cover glasses. This method is predominately suitable only for supersonic flow when the flow before the shock wave or the front wave of the streamlined body is not disturbed. The compensation chamber is a sealed vessel, whose walls which are perpendicular to the direction of the rays in branch BC, form two parallel glass plates with the same properties as the cover glass of the measurement space. The air inside the chamber is either constantly maintained in the same state, or the chamber is connected by a tube with the opening used for the measurement of the static pressure of the undisturbed flow in the tunnel.

The interference fringes are usually evaluated from photographs. To facilitate this operation, various preparations or apparatus and useful techniques can be used. The basic measurement is the measurement of the distance Δe at the required points. If we want to determine the density ρ at a point M of the layer that is examined, the Δe, which, according to equation (88), must be known, is determined as follows: we find (the shifted) interference fringe which passes in the field of view through the image M' of the point M, and next we find the original position of the same fringe (in this original position the fringe was straight, whereas in the shifted position it is usually not straight), and finally we determine Δe as the perpendicular distance of the point M' on the shifted fringe from the original position of this fringe

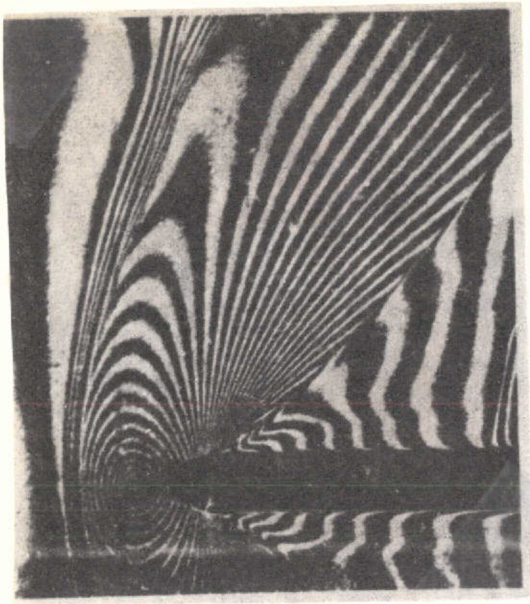

Fig. 92. Interferogram of flow around cylindrical body with conical front part [146]. (Inteferometer adjusted to infinite width of fringe.)

(Figs. 94 and 95). The original position of the fringe is the position which it occupied in the case when the examined layer was either not yet inserted in one of the branches of the interferometer, or when it was inserted there but was not yet homogeneous (for example, because the air did not yet circulate in it or circulated in such a way that the flow field was homogeneous) and had the same density ρ_0 everywhere. For example, a comparator with a reading microscope with a capability for mutually perpendicular shifts is used for the measurement of Δe.

Since, to determine Δe, the original position of the interference fringes must also be known, the original fringes are copied in thin cutouts on the photograph that is evaluated to facilitate the evaluation, or the original positions of the fringes are obtained through extrapolation on the basis of the known behavior of shifted fringes at points (regions) where it can be assumed that the original state did not change, so that the fringes were

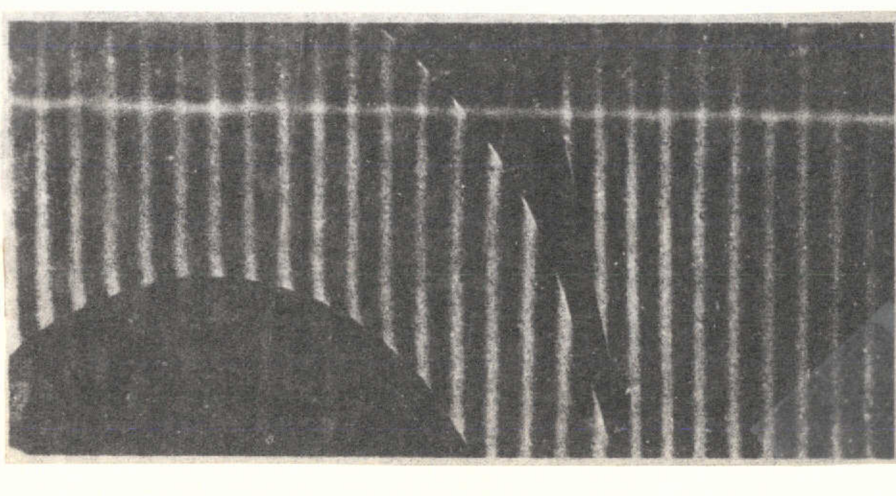

Fig. 93. Interference fringes obtained with the aid of the Mach-Zehnder interferometer adjusted for an infinite width of the fringe. The measurement space is free of inhomogeneities [10].

not shifted at those points. However, this second method may lead to inaccuracies, since the assumption that was made need not be satisfied exactly in the regions under consideration. Although a similar assumption is also used in the mutual pairing of the shifted and original fringes in the first method, the danger of errors is smaller since the original (straight) fringes are copied (in cutouts) on the photograph that is evaluated, so that their direction and positions are known. Another procedure that can be used is that the corresponding grid is prepared in accordance with the original interference image (which was obtained, for example, when the medium in the measurement space was quiescent, the tunnel was blocked), which is copied together with the photograph, or is photographed simultaneously with the flow that is examined (Fig. 96). When photographs of flow fields with large changes in their refractive index are evaluated (for example, at points through which a shock wave passes) the high concentration of the fringes caused by their large shift over a small width causes difficulties. Since, for purposes of accuracy, it is advantageous to adjust the interferometer for very dense interference fringes, in some cases it is not possible to study the interference fringes during the transition through such regions. However, when light which is not perfectly monochromatic is used, usually not all fringes have the same intensity, so that their behavior can be traced more easily in these cases. Mathematical machines, for example, a mechanical analyzer, which calculate and record the pressure distribution from interference images have also been constructed [230]. /138

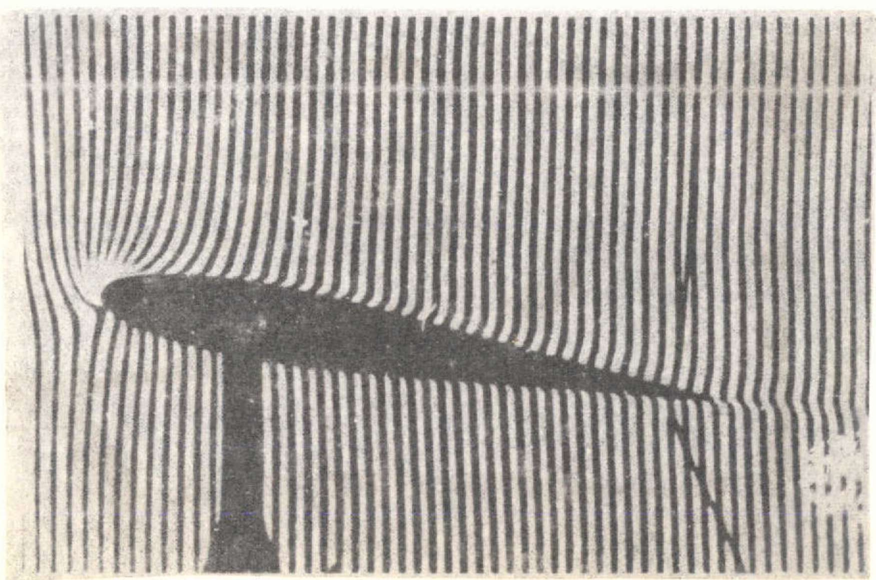

Fig. 94. Interferogram of flow around wing with interferometer adjusted for a finite width of the fringe [5].

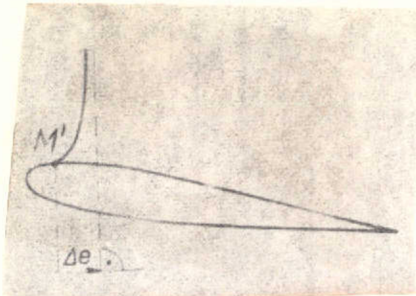

Fig. 95. Diagram for discussion on p. 136.

At first sight, the interferometric method of studying the flow seems to be rather simple. In fact, when the assumed ideal properties of the optical parts are not satisfied and when the disturbing surrounding effects manifest themselves, its use, especially during the adjustment and elimination of disturbing effects by means of various corrections is very laborious and time consuming, which also reduces the accuracy. The inaccuracy of the method itself, when used as described, is sufficiently small when the density is determined and it depends on the type of the flow field that is studied. In the usual cases, it can be held below 3% up to a Mach number 6 [146, 212]. However, the inaccuracies in the equipment and the deviations from the assumptions that were made in the analysis of the method have a substantial effect on the measurement error. Thus, for example, the glass plates and the cover glasses of the measurement space are not exactly plane parallel, homogeneous, and they do not have the same refractive index; hence, they are not completely identical, for instance, also, due to the effect of the temporary birefringence of the glass caused by mechanical stress. Mirrors are never exactly planar. The uneven temperature in the surrounding air through which the /139

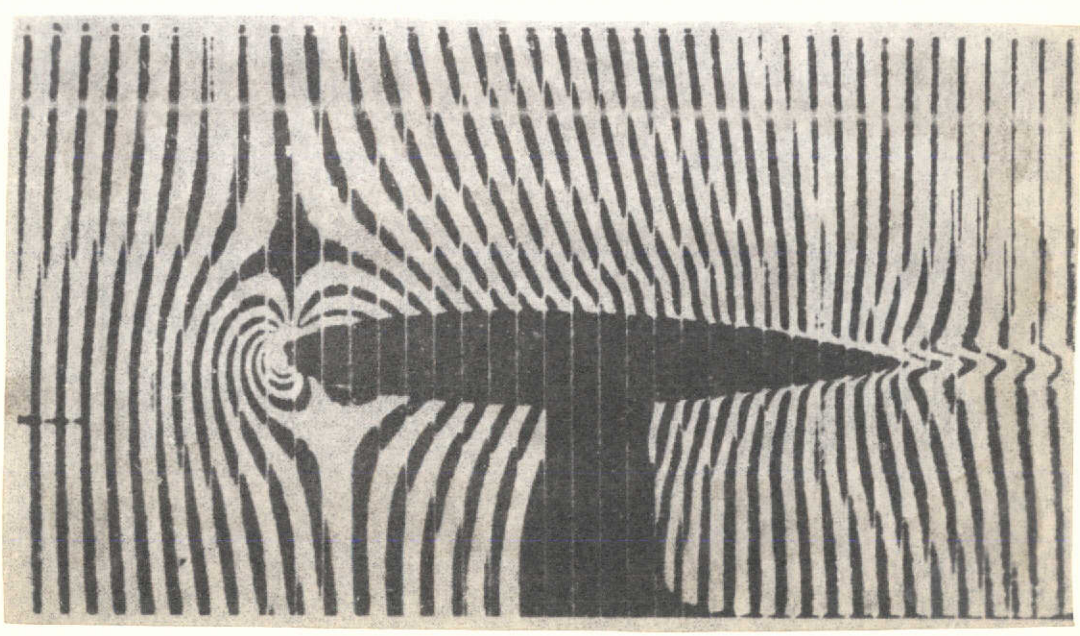

Fig. 96. Interferogram of flow around a wing and grid with original distribution of interference fringes [212].

rays pass, the nonuniform temperature distribution in the glass plates, the vibrations in the entire equipment and the acoustical waves in the tunnel, the effect of the cover glasses of the measurement space on which the existing boundary layer changes the two-dimensional character of the flow, etc. are the disturbing effects which occur most frequently.

Other problems are introduced by the light source which is not exactly monochromatic. The finite width of its spectrum limits the maximum number of fringes that can be obtained, since it limits the smallest possible width of the fringe for which the entire field of view is covered by fringes. For one end /140 of the spectrum of the light that is used (which is roughly, but not exactly, monochromatic) a dark fringe is formed at a certain point, but, for example, a light fringe from the light at the wavelength belonging to the other end of the spectrum of the source is formed at the same point which distorts the interference image. Another limitation on the number of fringes that can be obtained follows from the fact that the light source is not exactly a point source. Therefore, not all rays pass through the glass plates at the same angle, their paths in the plates are not the same, and undesirable phase shifts in the rays are formed.

Light refraction causes difficulties during the observation of strong inhomogeneities in the layer that is examined [215, 219, 239]. The path of the ray is curved during the passage through such a region (see p. 84), which changes the interference image, the fringes cross one another, spread, and sometimes the photographs at such points become unreadable and the data that are obtained (provided that in this case they can be obtained from the photographs) are inaccurate. Hence, on the whole, it is desirable to now discuss the requirements which must be imposed on the properties that will ensure the best functioning of the individual parts of the equipment and of the equipment as a whole.

The typical method used to assemble the equipment is illustrated in the drawing in Fig. 97, and the photograph is given in Fig. 98. The light beam emanating from the source must be converted by the lens C_1, the objective of the collimator, into a parallel pencil of rays which passes through the interferometer and then through the lenses C_2 and C_3 which focus the selected plane U in the measurement space (the examined layer) simultaneously with the interference fringes on the photographic plate or screen (focusing screen). Hence, the mirrors and plates must be adjusted so that the pencils of rays passing through the two branches leave the interferometer at /141 such angles that the unreal image of the interference fringes is formed in the desired plane U of the layer that is studied.

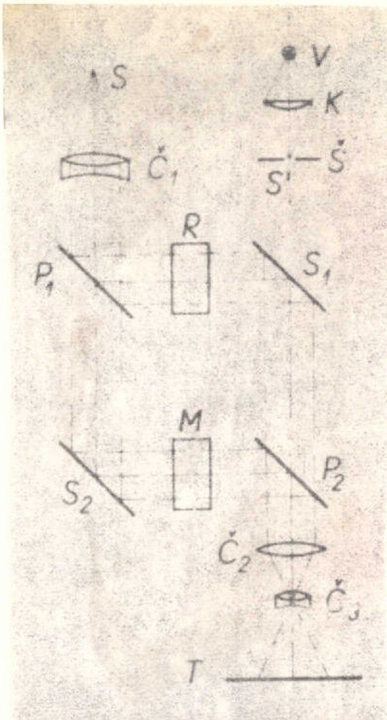

Fig. 97. Schematic diagram of Mach-Zehnder interferometer. (S - light source; C_1- objective of collimator; P_1 and P_2 - semipermeable glass plates; S_1 and S_2 - mirrors; M - measurement space; R - compensation chamber; C_3 and C_2 - lenses forming the image of the plane selected in the measurement space and simultaneously the inferference fringes on the screen, focusing screen or photographic plate; T - screen). Other version exist in which instead of the lenses C_1 and C_3, mirrors are used; see, for example, Fig. 106. The right part of the diagram gives the drawing of a detail in the schematic diagram of the light source (V - discharge tube; K - condenser which projects the glowing dischrage into the slit S of the collimator; the luminous surface S' of the slit represents the light source S of the interferometer).

If the measurement space is covered by glass plates, identical plates must also be inserted in the second branch of the interferometer, of course, as long as the beams in both branches do not pass through the measurement space [213]. This is done in order that the optical paths of the rays in both branches do not differ much. Sometimes, instead of the other plates, a compensation chamber is also used (see p. 136). The arrangement of the plates and mirrors must not always be such that their planes subtend a 45° angle with the direction of the rays.

A requirement on the interferometric equipment which is not easily satisfied is that parallel interference fringes of the same width be obtained during the observation of a homogeneous layer. Some equipment achieves this with a dispersion which is 1/10 of the width of the fringe. It is obvious that it is much more difficult to retain this dispersion value in plates and mirrors whose dimensions are relatively large. It is difficult to manufacture homogeneous glass plates of large dimensions. In addition to this the flexural deformation of the plate has an unfavorable effect in those cases when the plates are not vertical. Similarly as the plates, the cover glasses of the tunnel and the compensation chambers must have excellent optical properties. In order /142

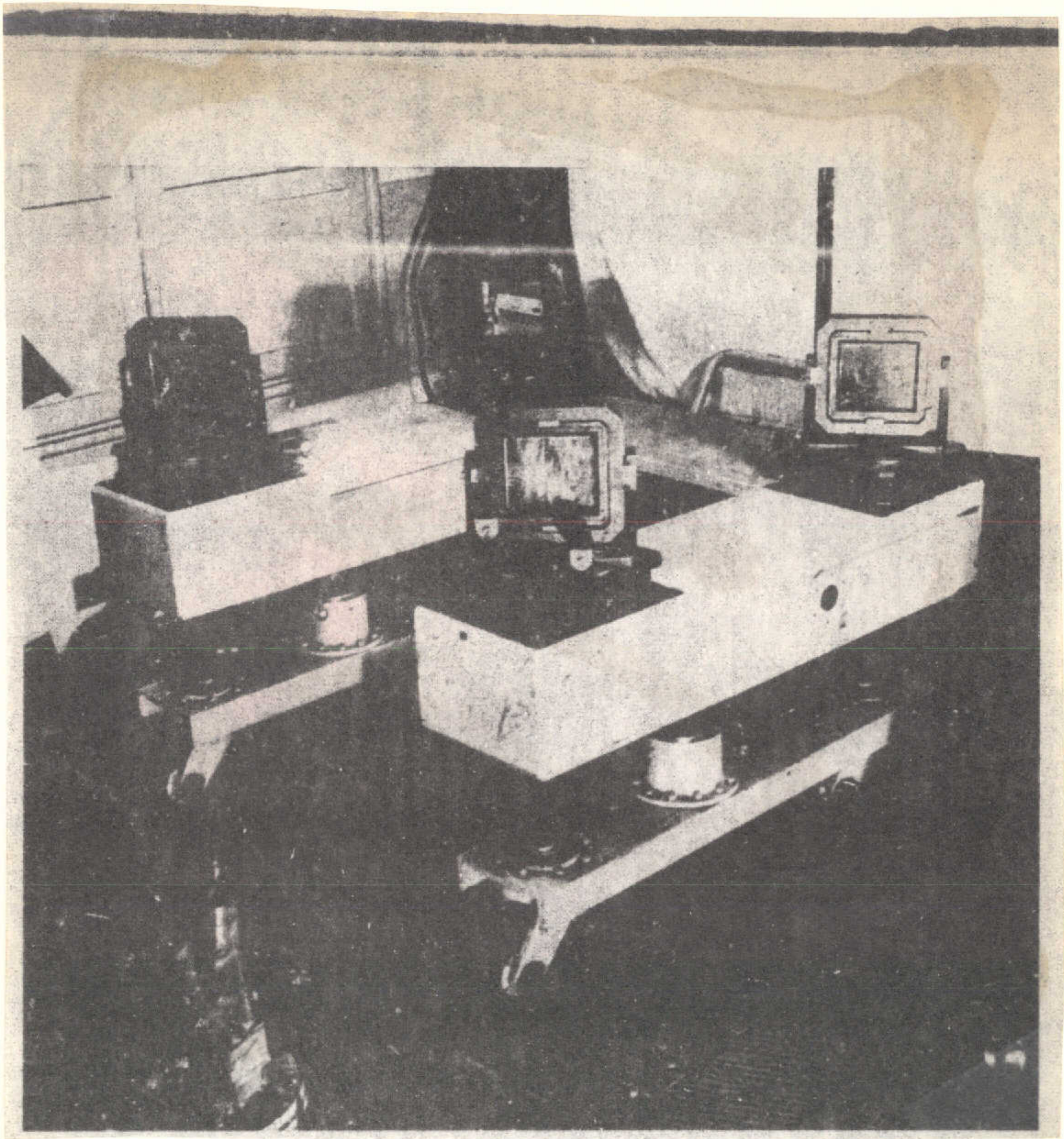

Fig. 98. Mach-Zehner interferometer manufactured in Czechoslovakia, based on a proposal of workers at the VZLU [217]. (The photograph was included with the kind permission of the VZLU management and the author [217].

that the effect of these parts do not cause a distortion in the interference images which is larger than 1/10 of the width of the fringe for green light at wavelength 5000 Å, their refractive index must be constant with a tolerance which is equal to $2 \cdot 10^{-6}$ for 2.5 cm thick plates. The thickness of the plates whose dimensions are larger must of course be greater, the ratio of the thickness to the width (in the case of a circular plate to the diameter) which is required for reasons of strength in operation and manufacturing lies between 1:7 to 1:10. The largest plates used until now had diameters of approximately 30 cm [231].

The thickness of the semipermeable glass plates must not differ by more than 1/12 and the thickness of the cover glasses of the measurement space and the compensation chamber by more than 1/3 of the wavelength of the light that is used. All surfaces reflecting the remaining light must be worked with the same precision. The effect of small local deviations from homogeneity or from a constant thickness of the plates (provided they are not too irregular; hence, for example, in the case of wedges) can be moderated by the mutual turning of the plates about the axes which are perpendicular to their surface, or also be changing very slightly the angle at which the rays are incident to the glass of the compensation chamber, which, in the basic adjustment, is 90°. It also helps when the positives are obtained from the plate or film to incline the plane of the photographic paper so that a positive with parallel fringes corresponding to the still air in the tunnel is obtained. The same inclination must then also be presented when the positives are obtained in the case of an airflow.

The front surface of the glass plates P_1 and P_2 (Figs. 89 and 97) must have an appropriate coating which lets through approximately 50% and also reflects approximately 50% of the intensity of the incident light (among other things, the absorption in such a layer must be very small), and the rear surfaces must have a layer which prevents the formation of undesirable systems of interference fringes from the rays reflected from the rear walls of the plates. The rear walls of the cover glasses and of the lenses must also have such antireflexive layer. Mirrors must reflect more than 90% of the intensity of the incident light [16, 217]. Generally, the absorption in all optical parts must be as small as possible.

All optical parts, especially mirrors and plates must be impeccably clean. Dust, fingerprints or grease spots diffract the rays, whose interference may subsequently form disturbing interference fringes. This danger is great mainly in laser interferometers (see p. 147).

The adjustment of the interferometer requires that it be possible to turn each of the plates P_1 and P_2 about the horizontal and vertical axes, both of which must lie in the plane of the reflecting surface. In addition to this, one of the plates (usually P_2) must be adjusted so that it can move in the direction of the rays, thus changing the relation of the optical paths of the rays in both branches of the interferometer. Therefore, the plates are inserted in frames (in a way which will prevent deformation of the plates even when the inhomogeneities can be corrected by controlling the deformation [213]) and suspended in gimbal suspensions, and the plate P_2 is also mounted on slides. The plates are turned via remote control, since the presence of /143 a person servicing the equipment would raise the local temperature in the equipment and in the air, which are highly unfavorable disturbing effects. Bowden cables, clock electromotors, selsyns, etc., which are connected with multiple gears and can be adjusted so that the position is determined with an accuracy of 1" are used (see Fig. 99) [217, 212, 213, 232]. For a more perfect adjustment (during the setting of a larger initial path difference; see below p. 145), one of the cover plates of the compensation chamber was also turned [215].

Suitable light source are high-performance, high-pressure mercury discharge tubes with input powers raised for a short period up to 10 kW, and spark discharges (see p. 108), Fig. 72). The basic requirements are that the dimensions of the source be small, a high intensity of the light, and the exposure times must be very short, on the order of several microseconds, because of the instability of the flow (especially at high velocities). A certain part of the intensity of the source is lost to the monochromatic filter which is indispensible during the normal use of the method. Recently, experiments were made using a laser as a light source for interferometers. Through the use of lasers, certain difficulties which follows from the fact that classical light sources are not perfect point and monchromatic sources and the the coherence of their rays is only limited to small path differences, roughly to ten wavelengths of the light used, can be eliminated almost completely. All this facilitates considerably the adjustment of the interferometer [237]. /144

The entire optical equipment from the source to the camera must be firmly secured on a sufficiently rigid frame to prevent vibrations of the parts and of the entire equipment. For these reasons, the grips on the frame in the supporting structure are supplemented by vibration dampers (in smaller equipment, by rubber blocks) or possibly suspensions on rubber ropes [215].

These requirements are especially high on the seating of the mirrors and plates in the interferometer itself. The light source, the condenser, the collimator, the objective, and the camera are often located on an independent optical bench which is separated from the frame of the interferometer. This protects the interferometer from possible shocks that arise during the manipulation of the components in the illumination, image-forming or recording unit.

A pentaprism is used most often for the initial adjustment of the interferometer when the plates and mirrors subtend with the incident rays a 45° angle [225], although other methods can also be used [146, 215, 217]. Then the plates (or only one plate) are turned through a small angle until

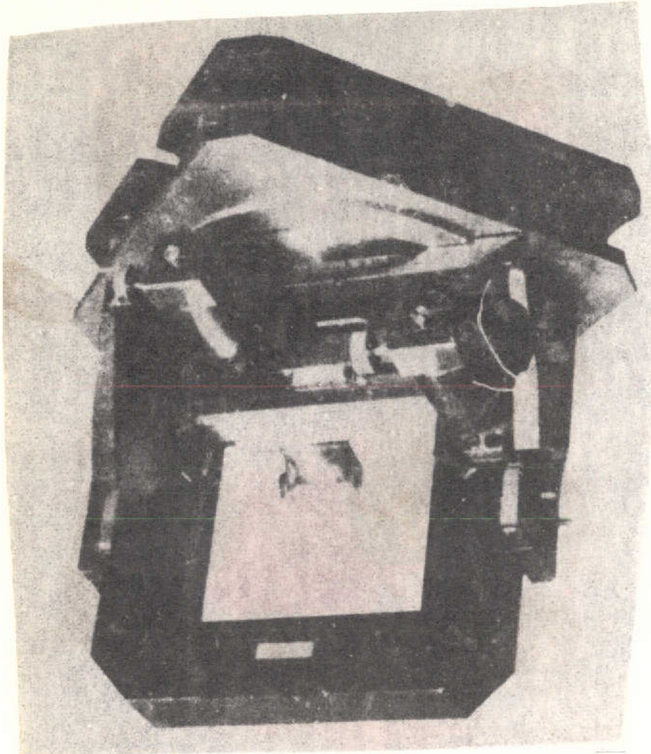

Fig. 99. Plate in gimbal suspension. It is a part in the interferometer in Fig. 98 (the photograph was included with the kind permission of the VZLU and the author [217]).

satisfactory interference fringes are formed. Depending on the axis about which the plates were turned, the fringes that are obtained are either parallel to the plane in which the centers of the plate lie, or the fringes are perpendicular to this plane. Then the equipment must be focused with the aid of the lenses C_2 and C_3 (Fig. 97) on the selected plane in the measurement space and the sharpness and contrast of the fringes must be preserved by turning the plates. The focusing is facilitated by inserting a wire mesh in the selected plane. After the various errors in the equipment, mainly the errors due to the refraction of the rays in the inhomogeneities in the measurement space have been moderated, it is advantageous to focus on the plane in the middle of the measurement space [146, 215]. A monochromatic source with a lower intensity than that used during the measurement is used. Usually, it is a sodium or cadmium lamp. The additional measures that already have been described prove the quality of the initial interference image, i.e. the parallelism of the fringes.

The adjustment of the interferometer to an infinite width of the interference fringes (see p. 133) is even more laborious. The white light (from the bulb) passes through the interferometer with the plates and mirrors adjusted at a 45° angle, and the zero-th order interference fringe (which has the highest intensity) must be spread over the entire field of view until the illumination in the field of view is uniform. This is achieved by shifting the plate P_2 in the direction of one of the light beams without turning the mirrors or planes. Using this method, the result which must be achieved is that the beams in the two branches of the interferometer have the same optical path. After this basic adjustment of the interferometer to an infinite width of the fringe, it is convenient to set a certain selected initial trajectory difference before the measurement. This difference (which is constant over the entire field) must be such that it is roughly compensated by the trajectory difference formed in the flow region which is of greatest interest to us during the measurement. We then obtain in this region much clearer interference fringes than we /145 would have without setting the initial trajectory difference, which is especially evident when a source of light that is not sufficiently monochromatic is used [213, 224, 230, 233, 217, 215, 157].

Hence, three different types of interferometric images of the same flow field can be obtained by different basic adjustments of the interferometer. This is evident from the drawing in Fig. 100. The adjustment method yielding an image of type B' is usually preferred over B", since more data about the shift of the fringes in the vicinity of the leading edge of the profile can be obtained from B', because in the case B' the fringes at this point are denser than in the case B".

Interference images (Fig. 101 c) which are similar to type B in Fig. 100 can also be obtained photographically, by copying on one paper the positive of the image 101 a and the negative of the image 101 b. A photograph of the same flow field obtained with the aid of an interferometer adjusted to an infinite width of the fringe is given in Fig. 101 d for a comparison.

The functioning of the entire equipment depends on the proper choice of the type of tunnel and its dimensions to be used together with the interferometer. For two-dimensional studies, the measurement space should have a rectangular cross section and for the study of flow around axisymmetric bodies, the measurement space should be cylindrical. The tunnel and the measurement space must be adjusted so that the flow in the measurement space is not disturbed. The selection of an open or closed /147 circuit in the tunnel must be considered from several points of view. In a closed circuit it is mainly the disturbing effect of the air which is heated during the flow, and in the measurement space, the disturbing sound waves which propagate from the blower in the direction of the flow or possibly against it. The first unfavorable property of closed circuits can be moderated sufficiently well by cooling; however, the second cannot be moderated easily; the design of the tunnel must be changed. In an open tunnel, these effects are eliminated; however, the condensed vapors in the air have a very unfavorable effect.

The suspension of the model in the tunnel must not disturb the flow. Recently, the ONRA [expansion unknown] magnetic suspension has been used advantageously [202]. When the model is mounted on the pins in the openings of the cover plate of the

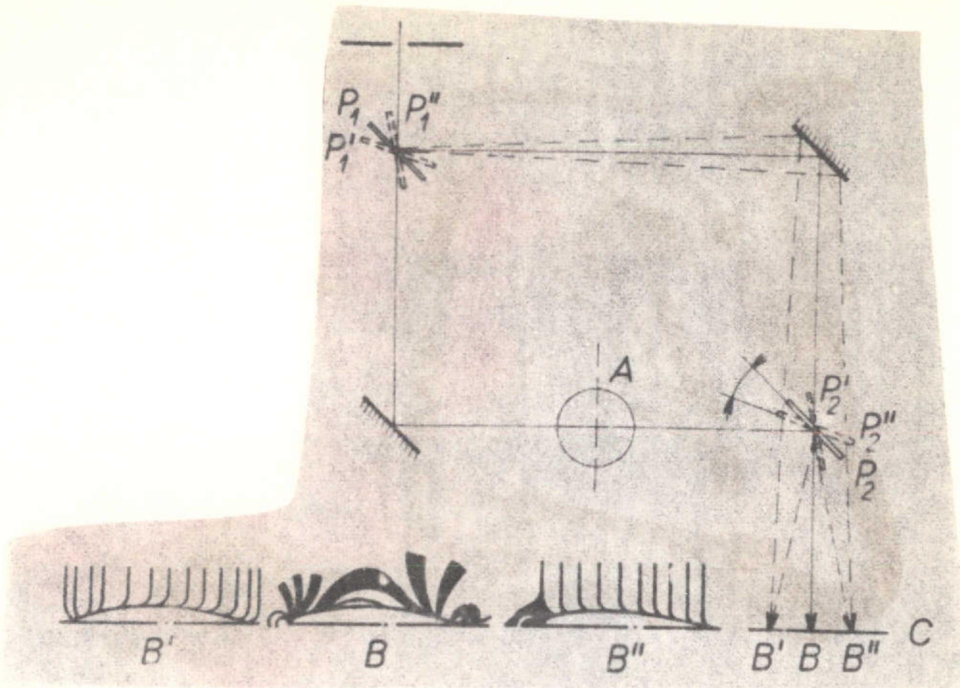

Fig. 100. Principle for various methods used to adjust the Mach-Zehnder interferometer:
B - adjustment to infinite width of fringe;
B', B" - adjustment to finite widths of fringe;
A - investigated layer; C - screen.

measurement space or glued to them, the plates must not be bent as a result of stress. The depth of the measurement space must be selected taking into consideration the processes that will be studied, so that the refracted light does not distort the interference fringes at a great depth. Since the number of fringes also depends on the density in the measurement space, it is convenient to vary the density (tunnels with a variable density of air).

Interferometric methods can be used for the study of a large number of different cases of flows in a wide range of Mach numbers from M = 0.2 up to highly supersonic cases. They can also be used at very low pressures [236], for example, a shock wave was determined in nitrogen already at a density of $1.5 \cdot 10^{-3}$ kg/m^3. Some illustrations which indicate their use have already been presented earlier, and several other illustrations are given in Figs. 102 through 104. Although the boundary layer is very clear in Fig. 104 c, the quantitative evaluation caused problems, since the effect of temperature changes caused by friction also contributes to the shift in the interference fringes. The method is also very suitable for the study of

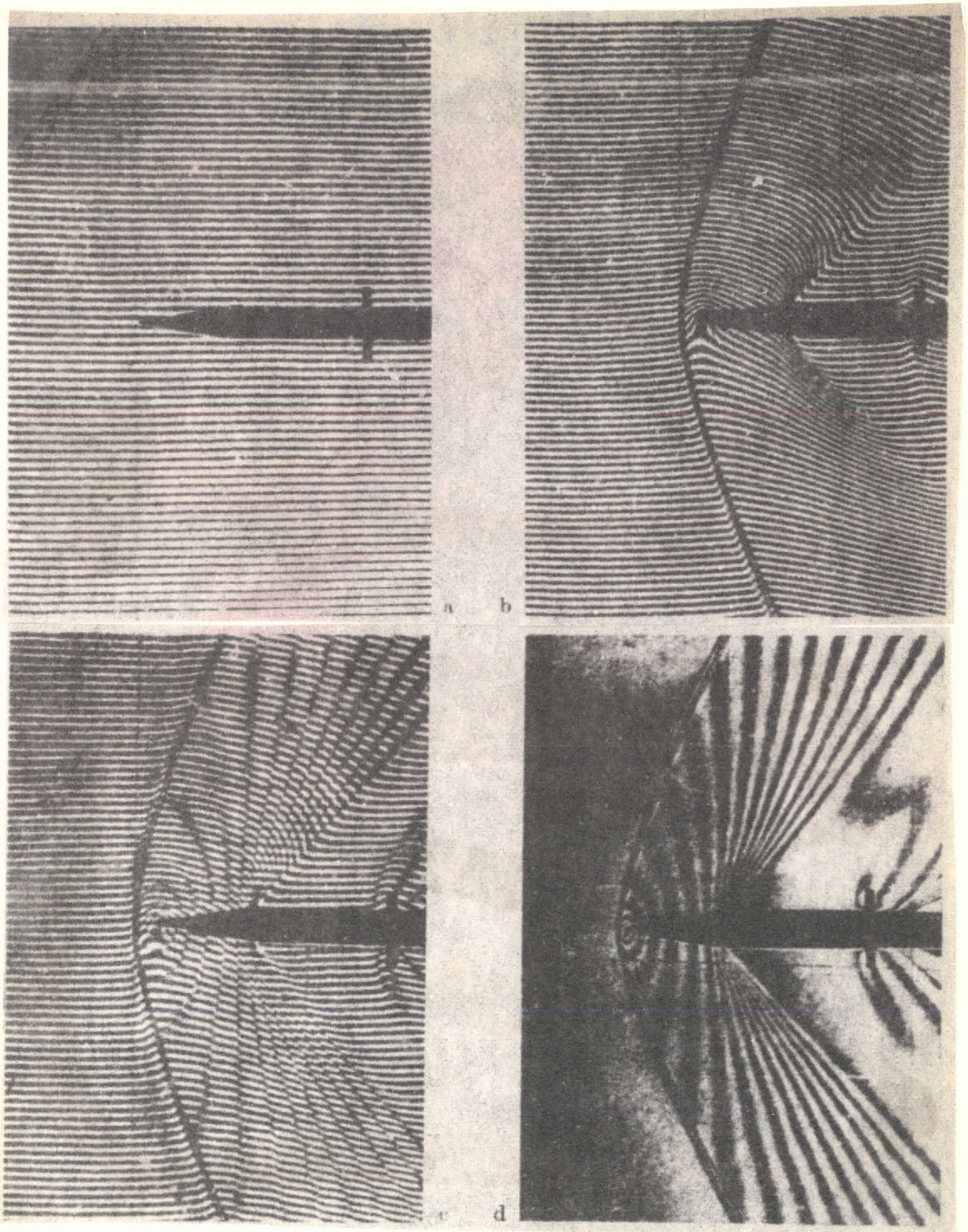

Fig. 101. a) Interferogram of quiescent field (flow field without inhomogeneities). Interferometer adjusted to finite width of fringe. b) Inteferogram of flow field with inhomogeneities (adjusted to finite width of fringe). c) Moaré image resulting from superposition of interferograms of type 101 a and 101 b. d) Inteferogram of the same flow field obtained with the aid of an interferometer adjusted to an infinite width of the fringe [146].

unstable processes. Photographs obtained by the shadow method can also be obtained with interferometric equipment (see p. 154) by stopping down the branch of the interferometer which contains the compensation chamber. Equipment which makes it possible to obtain from the same measurement space simultaneously photographs using the interference method and the diaphragm schlieren method has also been designed (see p. 153). Drawings of these modifications are given in Figs. 105, 106 [146, 159, 218, 219, 220, 221, 238, 242 and others].

The method taking advantage of the interferometric method that was described is used most frequently and yields the best results. In spite of this several attempts were made to use other types of interferometers [227, 228, 230].

In the last few years a laser has been used as the light source for interferometers. Due to the the differences between the properties of a laser light source and the properties of classical sources, the bases for new designs of interferometers for use in the mechanics of fluids have been obtained. For example, a ruby laser can be used for these purposes, which gives single light pulses whose duration is 0.1 microsecond. The coherence of its rays is adequate for use in interferometers; however, the energy of the pulse must be limited so that the optical parts of the interferometer are not damaged during strong pulses, and there is also the danger of injury to the eyes.

The advantages of using a laser are primarily that the time coherence is preserved sufficiently well even when the differences in the trajectory of the particles are large, on the order of several to several tens of centimeters. This eliminates the requirement that the mirrors and plates in the individual branches of the interferometer have the same thicknesses. This fact together with the good spatial coherence of the rays manifests itself in a substantial reduction of the laboriousness with which the Mach-Zehnder interferometer is adjusted. In addition, it also facilitates the assembly of new types of interferometers. In addition to using a laser as the light source in a Mach-Zehnder interferometer when the necessary light beam is formed from the narrow pencil of parallel light rays emanating from the laser with the aid of the lens, simpler interferometric devices can be assembled with the aid of a laser. Advantage is taken of the fact that the ray passing through the second branch of the interferometer can remain very narrow, so that it can pass through the measurement space at a suitably chosen point, or possibly through a certain point in a separate part of the measurement space which represents the compensation chamber. From the narrow beam emanating from the laser, using, for example, a double prism and a diverging lens (Fig. 107), a thin reference ray and a /150

Fig. 102 a, b. Interferograms obtained with interferometer manufactured by the firm Novotechnika, FRG, a) flow through cascade; b) flow through nozzle.

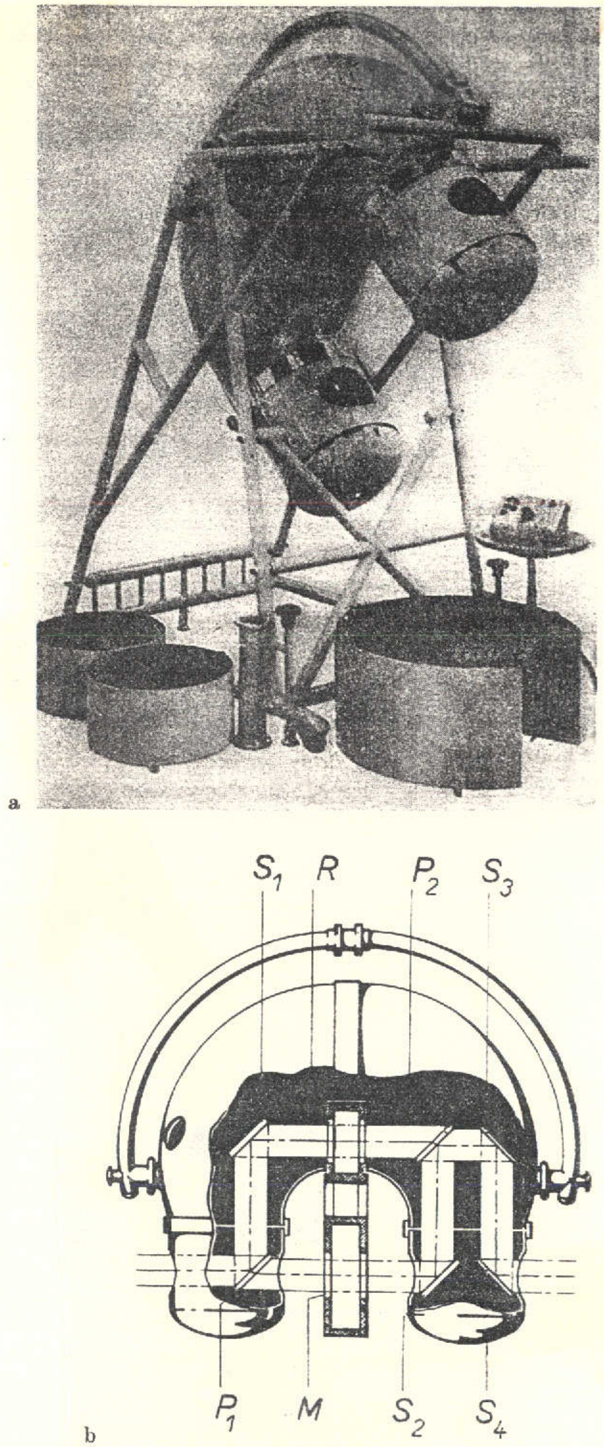

Fig. 103. Interferometer manufactured by the firm Novotechnik, FRG. a) Interferometer in position for basic adjustement. b) Schematic diagram of interferometer. The meaning of the symbols is the same as in Fig. 97. S_3 and S_4 are accessory mirrors forming a periscope whose use is of no essential importance. It is used to achieve the result that the axis of the emanating beam is identical with the axis of the entering beam so that the illuminating and image-forming parts have colinear optical axes.

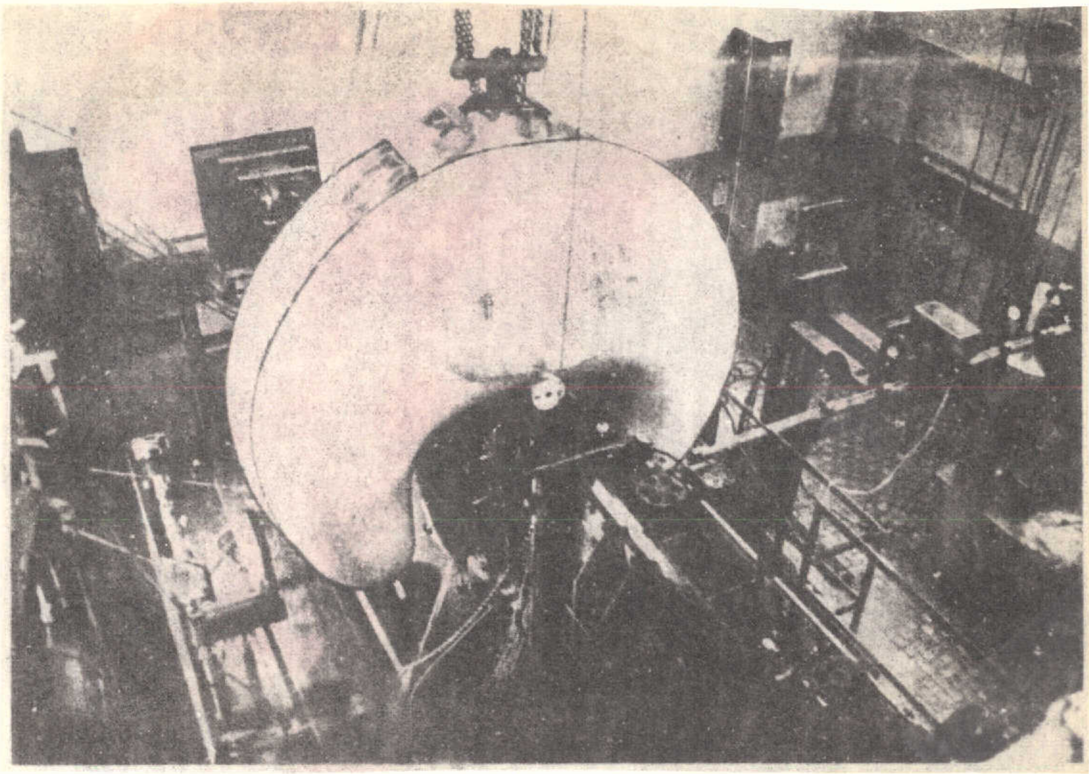

Fig. 103. Interferometer manufactured by the firm Novotechnik, FRG. c) Relatively large type of interferometer manufactured by the firm Novotechnik in operating position near wind tunnel at the Institute of Thermodynamics of the Czechoslovak Academy of Sciences.

diverging beam are formed from which a beam which fills the entire cross section of the measurement space is obtained /153 by a converging lens. The reference ray must pass through the image focal plane of the second lens, outside the area occupied by the principal beam in this plane. The reference beam is spread on the screen (the focusing screen of the camera) with the aid of a small diverging or converging lens placed in this plane so that the areas illuminated by the two beams on the screen cover one another (Fig. 108).

If the reference ray cannot pass through the measurement space, it can be guided outside the measurement space with the aid of of a periscope consisting of four small mirrors or prisms, taking advantage of fiber optics. If, as a result of this measure, the trajecotry difference is large so that, after the two rays are combined, coherence is not preserved, the optical path of the measurement beam must be lengthened and the equipment must be adjusted similarly as the Mach-Zehnder

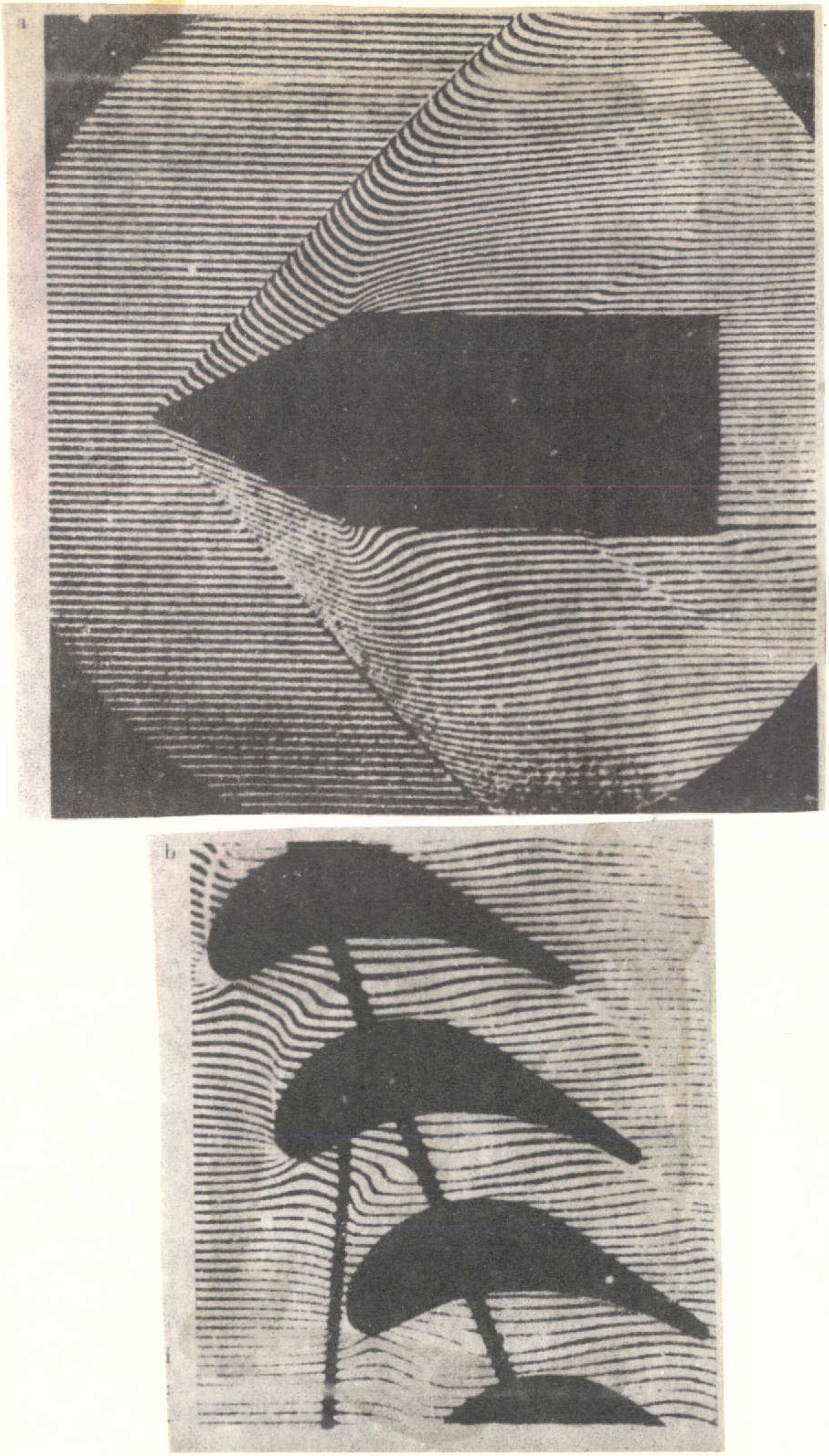

Fig. 104. Interferograms obtained with interferometer adjusted to a finite width of the fringe: a) flow around a projectile [146]; b) flow through cascade.

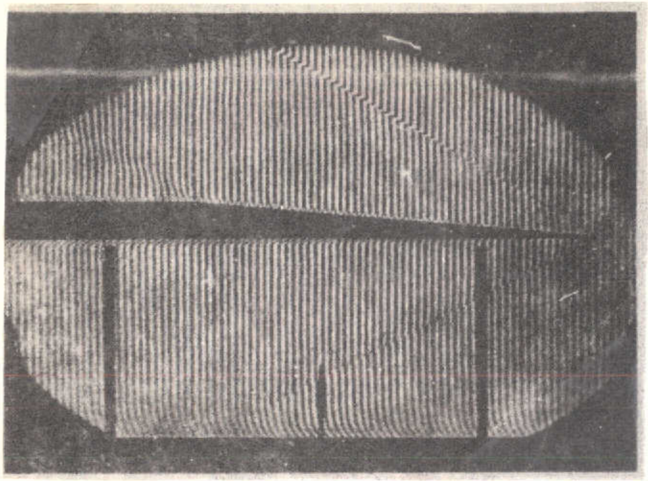

Fig. 104. Interferograms obtained with interferometer adjusted to a finite width of fringe: c) flow around plate with a sharp edge [146].

interferometer. Very small mirrors can be used in the branch of the reference ray in the process.

Hence, interferometers with a laser light source have many advantages. In addition to those that were already mentioned, the additional advantages are the simplicity of the optical equipment requiring a substantially smaller number of high precision optical parts than the Mach-Zehnder interferometer and also the smaller sensitivity to vibrations. On the other hand, however, complications arise during the operation and when the laser is adjusted. The possibility that disturbing interference fringes caused by the interference /154 of the rays reflected from the optical parts or possibly diffracted on the impurities (dust, grease and fingerprints on the optical parts) are also a disadvantage. The possibility that this may happen is considerable due to the high spatial and time coherence of the light from the laser [237].

Attempts were also made to apply a procedure used in holography. The principle of this procedure during the analysis of the density field in the measurement space is as follows: a coherent beam of light with the required cross section is obtained from the laser, for example, with the aid of a lens. It is split by diaphragms into two beams, one of which, the measurement beam passes through the measurement space, and the second, the reference beam passes outside the measurement space. Using a wedge or mirror, etc., the result is achieved that the two beams are mutually incident at some small angle at the photographic plate in whose plane they subsequently interfere. This arrangement represents a simple laser interferometer (Fig. 109).

In the case when both beams consist of parallel rays and there is no inhomogeneity in the measurement space, equidistant interference fringes are formed on the photographic plate /155 after it is developed similarly as in the Mach-Zehnder interferometer adjusted to a finite width of the fringe. If there is an inhomogeneity in the measurement space, we obtain, as a result of interference, an image which records the changes that

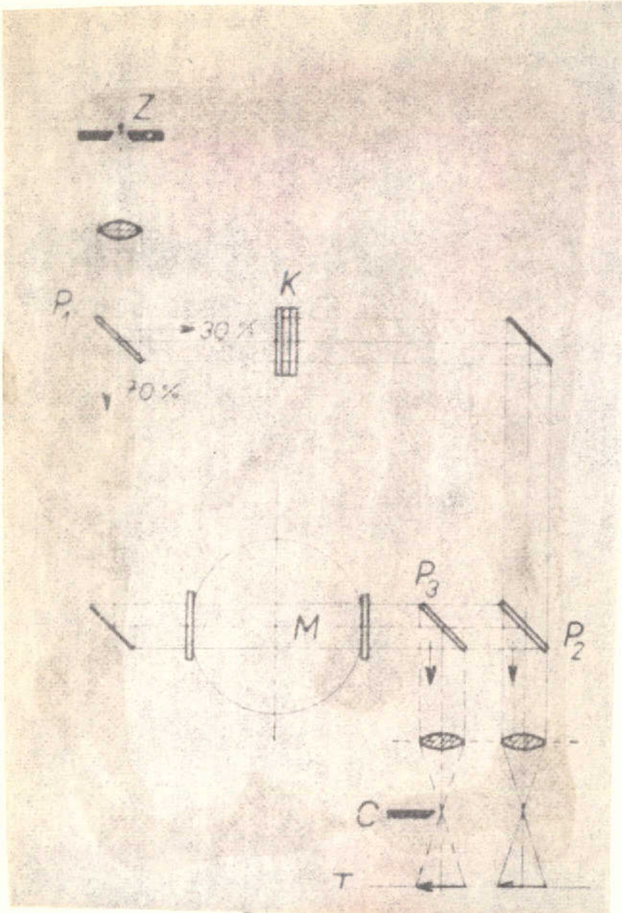

Fig. 105. Schematic diagram of equipment layout for obtaining simultaneously photographs by diaphragm and interference methods (Z - light source; K - compensation plate; M - measurement space; C - knife diaphragm; T - plane of image; the permeability P_1 of the plate is 70%).

occurred in the measurement space. The photographs that are obtained are called holograms, which are analogous to the interference photographs from the Mach-Zehnder interferometer with the exception that no plane in the measurement space is focused on the photographic plate, and also that the maximum density of the interference fringes (the number of intersection points per unit length of the orthogonal) is much higher, up to 100 fringes per 1 mm.

Such a hologram is now inserted in the path of the light beam (the so-called reconstruction beam), which must have the same properties as the reference beam, the same wavelength, the same shape, the same incidence direction as during the hologram exposure (this means that when the hologram was obtained and the reference beam consisted of parallel rays, the rays of the reconstruction beam must be parallel, whereas when the reference beam was divergent, the reconstruction beam must have the same divergence). The hologram represents an optical grid on which the rays of the reconstruction beam diffract and form diffraction maxima. Only first-order maxima can be observed clearly which are given by two images one real and the second unreal. The wave fronts of both maxima are the same as the wave fronts of the measurement beam during the hologram exposure, so that the original wave front of the measurement beam is reconstructed.

Two exposures are made on the same photographic plate (film) produced by two identical light pulses from the laser when the interferograms are obtained from the holograms of the flow fields, the first without the flow field, produced by the

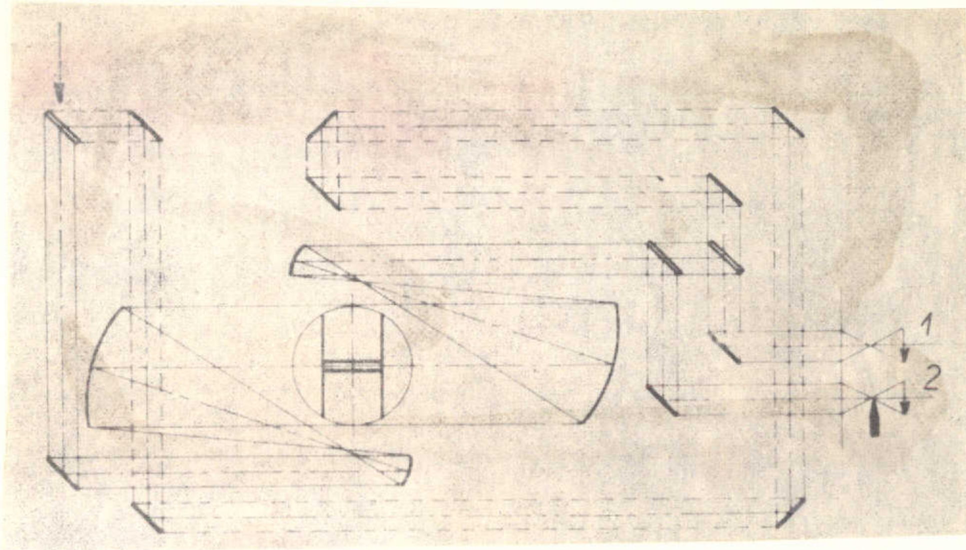

Fig. 106. Schematic diagram of layout for simultaneous analysis by diaphragm and interference methods (1. position of image obtained by interferometer; 2. position of image obtained by diaphragm method).

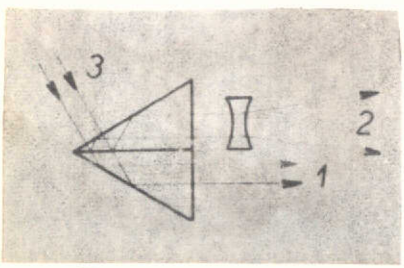

Fig. 107. Schematic diagram for forming the thin reference beam 1 and the diverging beam 2 from beams from the laser 3.

measurement and reference beam, which gives a system of equidistant parallel interference fringes, and the second with the flow field in the measurement space also produced by the reference and measurement beam. After development of the photographic plates that were exposed twice, we obtained the hologram.

Next, by inserting the hologram in the reconstruction beam of light, we reconstruct the wave front which would impinge on the photographic plate during the simultaneous action of the measurement beams from both exposures. After circling out the zero order maximum, we obtain on the next photographic plate (possibly with the aid of a camera) placed behind the hologram the interferogram whose fringes denote the points with the same difference in the optical paths of the rays during both exposures, i.e. an interferogram which is analogous to that which we would obtain from a Mach-Zehnder interferometer when it is adjusted to an infinite width of the fringe.

If the first and second hologram exposures have fringes corresponding to the same inhomogeneity, this inhomogeneity will

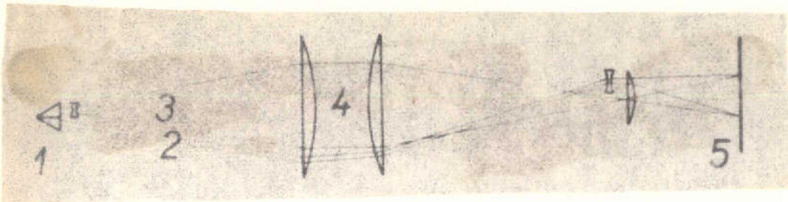

Fig. 108. Schematic diagram of laser interferometer [237] (1. beam from laser; 2. reference beam; 3. measurement beam; 4. measurement space; 5. plane of image).

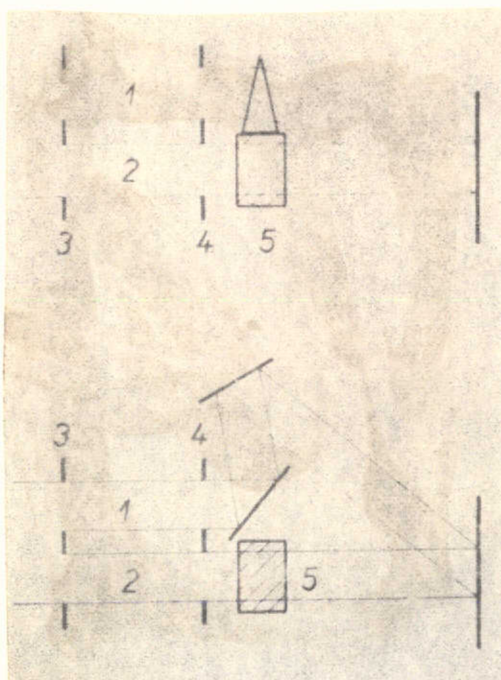

Fig. 109. Schematic diagram of two simple laser interferometers for holography [244] (1 and 2. two coherent beams obtained through separation by diaphragms 3 and 4; 1. reference beam; 2. measurement beam; 5. measurement space).

not appear on the interferogram obtained by reconstruction from the hologram, since here only the differences in the optical paths which occurred between the two exposures will appear. This is the great advantage of this method, since the errors in the optical paths which do not change do not appear on the final interferogram. It is /156 obvious that the configuration of the optical equipment must not change between the two exposures.

Another advantage follows directly from the basic principle of holography. This procedure makes it possible to obtain from the same hologram images of the flow field from different observation directions (in accordance with the position of the photographic plate or camera). The data for an analysis of three-dimensional flow fields can be obtained in this manner [243, 244].

3.2.5. The Method of Phase Contrast

In addition to such classical methods as the diaphragm schlieren method and interferometric methods which have been commonly used for a relatively long period in large aerodynamic laboratories, another new method should also be mentioned, which from the standpoint of adjusting the apparatus, its substance and effectiveness, lies between the two classical methods that were mentioned. This method uses the phase contrast and other modifications of this principle [245, 246, 247, 16].

In this method, which requires the same basic equipment as the diaphragm schlieren method, the differences in the phases of the rays, i.e. the phase difference in the rays passing through undisturbed points in the layer that is examined, and the phases of the rays passing through invisible inhomogeneous layers, i.e. points with a different refractive index than that in their vicinity, are converted into amplitude differences, i.e. for example, into changes in the illumination on the screen. The conversion of the phase differences into differences in the illumination (i.e. contrast) is achieved by the interference of the rays that were deflected by the inhomogeneities in the layer that is examined with the rays that were not deflected in the image plane of this layer. The phase differences are converted into amplitude differences that can be well observed by a phase plate or possibly another absorption plate inserted at the point where the image of the source if formed.

The phase plate has two fields whose optical thickness differs, for example, by a quarter of a wavelength. The adjustment of the plate and the form of the field are such that one field exactly covers the basic image of the light source formed by the beam that was not deflected, and the second field covers the remaining images of the source, the images formed by the beams diffracted by the inhomogeneity. This means that the phase of the rays forming the basic image of the source is shifted by $\pi/2$ which corresponds to a displacement along the trajectory equal to one-fourth of the wavelength of the light used. The absorption plate is similar to the phase plate, and it also has two fields. One of these, however, does not cause a phase shift, but absorbs strongly the light of the beam that was not deflected [16].

The interference images that are obtained provide data about the density field of the object, since they contain lines where the density is constant. (In this case, we have the analogy of the Mach-Zehnder interferometer adjusted to an infinite width of the fringe.) However, systems of fringes can also be obtained along which a particular component of the density gradient is constant, which is the analogy of the diaphragm schlieren method with a grid diaphragm. Next, by /157
using clear diffraction fringes that are formed in the plane of the image of the source when a very narrow source with a slit is used, a system of parallel fringes can be obtained on the screen provided the examined layer is homogeneous (similarly as in the Mach-Zehnder interferometer adjusted to a finite length of the fringes). The density field of the layer is determined from the deformations of these fringes caused by the inhomogeneities.

The necessary equipment for the method of phase contrast and the requirements on it are basically the same as in the diaphragm schlieren method. However, monochromatic light is used. Hence, the equipment is less expensive and less sensitive and it can be adjusted and serviced more easily than the Mach-Zehnder interferometer. The advantage is that the method of phase contrast also records weaker inhomogeneities than those obtained with the aid of the Mach-Zehnder interferometer, provided these are relatively small local inhomogeneities in the center of the undisturbed field. Another advantage compared to the normal diaphragm schlieren method is that the evaluation is based on length measurements in the interference image, and not on sensitive photometric measurements. Finally, the fact that the rays which ultimately interfere with one another are separated directly (immediately) before the image is formed is responsible for the fact that the accuracy of this method is affected much less by the inhomogeneities in the surrounding medium than in other sensitive methods used to determine the inhomogeneities in a transparent medium. Therefore, the acoustical or mechanical vibrations to which the Mach-Zehnder interferometer is very sensitive, do not affect considerably the proper functioning of the equipment. However, compared to the Mach-Zehnder interferometer, the disadvantage of the apparatus that was described is the lower average illumination of the observed field which is due to the use of an absorption plate (Fig. 110).

This method is not widely used insofar as we can base our judgment on the single available published study on this subject, although it can be applied very successfully because of the advantages that were already mentioned [245]. The results that were obtained in this study merit a deeper analysis and a comparison with measurements on a Mach-Zehnder interferometer.

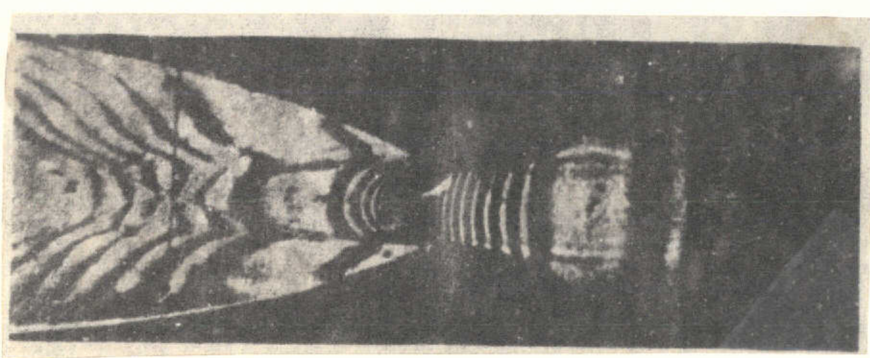

Fig. 110. Visualization of flow in a nozzle using the method of phase contrast [245].

3.2.6. Methods Taking Advantage of the Attenuation of the Electromagnetic or Corpuscular Radiation during Passage Through the Gas Flow

/158

The shadow method, the diaphragm schlieren method, and interferometric methods have by now been developed to a high degree of perfection so that very small differences in the density of the gas in the measurement space of the usual type can be determined by them. However, none of these methods can be used at low density values of the gas that is studied. This limitation becomes clearly evident at pressures below 10 torr, when the optical thickness of the gas layer that is studied in a tunnel with the usual dimensions is no longer adequate for obtaining conclusive results. However, tunnels exist in which the static pressure of the free flow is on the order of 10^{-1} torr. New methods were developed for measurements under these conditions. In addition to the methods that take advantage of luminescence (see p. 56) these methods are mainly based on the attenuation of the radiation passing through the gas flow that is examined caused by the effect of absorption or possibly dispersion. The following are used:

- -- absorption of ultraviolet radiation by oxygen (for wavelengths in the range 1400-1500 Å,
- -- absorption of ultraviolet radiation by ozone (at wavelength 2537 Å),
- -- attenuation of soft X-rays,
- -- attenuation of corpuscular rays (electrons, protons, α particles, potassium atoms).

The attenuation of the radiation during the passage through the measurement space can be described by the well-known relation

$$J(x) = J_0 \exp\left[-\int \mu \varrho(x)\,\mathrm{d}x\right], \tag{90}$$

where J(x) is the intensity of the rays after they have covered the path x in the layer that is examined, J_0 is the original intensity of the rays when they enter the layer that is examined (at the point x = 0), ρ(x) is the density of the gas examined which is a function of x, since generally it varies along the ray, and μ is the attenuation factor which depends on the type of gas, but is independent of the density of the gas and does not change along the ray, i.e. is independent of x.

Using the methods that were presented, the flow field can be analyzed, i.e. the changes in the density ρ caused by the flow. The basic data about these methods are presented in the following table [248].

Type of radiation used	Ultraviolet radiation	Ultraviolet radiation	X-ray radiation	Electron beams
Properties of the radiation (λ = = wavelength	$\lambda = 1470$ Å resonance line Xe	$\lambda = 2437$ Å resonance line Hg	$\lambda \approx 10$ Å	Energy from 4 keV to 60 keV
Type of gas examined	Only O_2	Only O_3	Any	Any
μ Attenuation factor in m^2/kg	$2.5 \cdot 10^4$	$1.7 \cdot 10^4$	79	10^4-10^5
Density of undisturbed flow in kg/m^3	$7.7 \cdot 10^{-4}$	$1.2 \cdot 10^{-3}$	$2.5 \cdot 10^{-1}$	$2 \cdot 10^{-3}$-$2 \cdot 10^{-4}$
p_0 Static pressure in measurement space in torr	0.46	0.7	150	1.2-0.12

Fig. 11 gives the schematic diagram of the equipment for the method taking advantage of the absorption of ultraviolet radiation by oxygen. For example, the image of a shock wave in oxygen in front of the apex of a cone with a 90° apex angle at a Mach number approximately 3.9 was obtained with the aid of this equipment. The diameter of the field that is studied in the measurement space was 3 cm. The source of ultraviolet radiation that was used was an oil-cooled xenon discharge tube with a calcium difluoride window. A pressure below 10^{-4} torr must /159 be maintained in the entire optical equipment. Although the shock wave can be seen on the photograph obtained with the aid of this equipment, it is not possible to obtain conclusive quantitative results by a photographic analysis because of the nonuniformity of the photographic material. These results can be obtained during the study of the measurement space by a narrow pencil of rays from point to point with the aid of a photocell as long as it is possible to maintain a stationary flow during the measurement period [250].

The attenuation of X-rays during the passage through the measurement space was first used to measure the flow field point by point with the aid of a narrow pencil of X-rays with a 0.05 mm diameter. An attempt has also been made to obtain a photograph of the entire flow; however, here basic difficulties arise and for the time being the results are meaningless. This is due to the fact that the photographic film in comparison with chambers and counters is relatively insensitive to X-rays. Since the attainable intensity of the soft rays which are suitable for this method is small, the required phtographic time is large, on the order of 1 min.

The basic scheme for the method which takes advantage of the attenuation of soft X-rays is simple. The X-ray tube and the intensity reader (detector) of the X-rays, hence, for example, an ionization chamber or a Geiger-Muller counter are placed opposite to one another at opposite sides of the measurement space of the wind tunnel. They are positioned so that /160 they can be jointly moved across and around the measurement part of the tunnel. However, they can also be placed in a fixed position and the model can be moved in the tunnel. The emission from the X-ray tube must be high and the anode must have a small surface [248, 252].

The attenuation of electron beams during the passage through the measurement space was used to measure the measurement space first so that the measurements were made from point to point. The density changes in the flow field were determined on the basis of the intensity of the beam current of the electron beams that passed through that were measured, for example, with the aid of an electrometer or photomultiplier.

A numerical comparison of the discrimination boundaries of the interferometric method and the method using the attenuation of electron beams will demonstrate best the advantage of the second method during the study of gas flows at low pressures. We will start out with equation (90) and assume a constant density ρ = const along the ray. Since μ also does not vary, as already mentioned, along the ray, we obtain from equation (90), the relation

$$J = J_0 \exp(-\mu \varrho l), \tag{91}$$

where l is the thickness of the layer that is examined. If we carry out, for the same initial energy of the electrons and the same initial intensity J_0 of the electron beam, two measurements during which we measured the intensity J_1 of the electron beam after passage through the point with density ρ_1, and the intensity J_2 of the same beam after passage through the point with density ρ_2, we obtain, for the difference $\Delta\rho = \rho_1 - \rho_2$ of these two densities from the previous equation, the relation

$$-\Delta\varrho = \frac{1}{\mu l} \ln \frac{J_2}{J_1}, \tag{92}$$

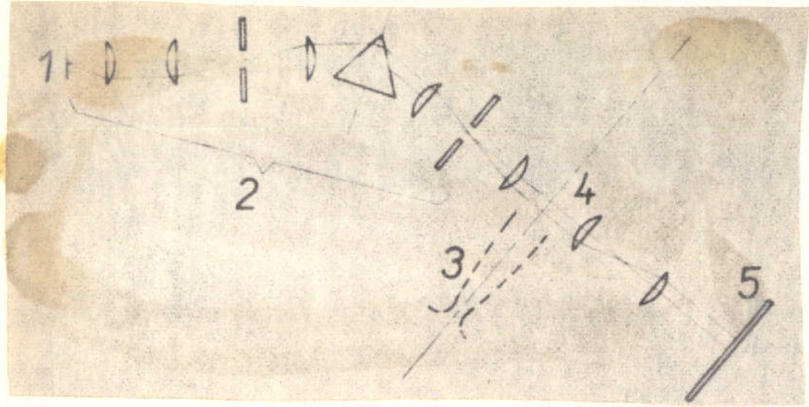

Fig. 111. Schematic diagram of equipment for the visualization method taking advantage of the absorption of ultraviolet radiation by oxygen [250] (1. source of ultraviolet radiation; 2. monochromator; 3. nozzle; 4. measurement space; 5. plane of image).

from which we can clearly write from small changes ΔJ /161

$$-\Delta\varrho = \frac{1}{\mu l}\frac{\Delta J}{J}. \quad (93)$$

Finally, after introducing in this relation the so-called linear attenuation coefficient α defined by the relation $\alpha = \mu\rho$, we obtain:

$$-\frac{\Delta\varrho}{\varrho} = \frac{1}{\varkappa l}\frac{\Delta J}{J}. \quad (94)$$

We will assume for the numerical comparison that the thickness of the layer that is examined is $l = 6$ cm, its density is $\rho = 4.7\cdot10^{-3}$ kg/m^3, which corresponds, in the case of air, to a pressure of 3 torr at a temperature of 25°C, an initial energy of the electrons of 5 keV and an attenuation factor $\alpha = 0.9$ cm^{-1}. Given the high sensitivity of modern instruments for the measurement of electrical current, current intensities on the order of 10^{-9} A can be measured well with a 1% accuracy. Hence, we will determine $\Delta J/J$ with such accuracy. From equation (94) it follows that 0.2% changes in the density can be measured well, so that in our case $\Delta\rho = 9.4\cdot10^{-6}$ kg/m^3, which corresponds to a difference in the pressures of 0.006 torr.

When we use the interferometer, we will distinguish the shift of interference fringes which is 1/10 of the width of the fringe. This shift is caused by a change in the optical path of one of the interfering beams by 1/10 of the wavelength λ of the light that is used, to which corresponds the difference $\Delta n = 0.1\lambda/l$ in the refractive indices. Now, using equation (47) and letting the constant in it be $K_0 = 2.26\cdot10^{-4}$ kg^{-1}m^3 which we calculated for air in the lines following equation (47), we find that the difference $\Delta\rho$ in the density which is equal to

$$\Delta\varrho = \frac{0{,}1\lambda}{lK_0}.$$

corresponds to the difference Δn in the refractive indices that was given. If we also take into consideration that green light at wavelength $\lambda = 5 \cdot 10^{-5}$ cm was used and let, as in the preceding paragraph, $l = 6$ cm, we find that densities greater than $\Delta\rho = 3.6 \cdot 10^{-3}$ kg/m^3 can be measured interferometrically. Hence, the method which takes advantage of the attenuation of electron beams is more sensitive by two orders of magnitude than the interferometric method in the case under consideration.

A further substantial increase in the sensitivity of the method taking advantage of the attenuation of electron beams cannot be achieved sufficiently well by increasing the factor αl in equation (94), since the intensity of the measured electron beam would drop sharply and could not be measured so accurately. This difficulty cannot be eliminated by increasing the input intensity of the beam current, since at higher values of the input intensity of the beam current, the gas is heated. Article [253] states that for an electron probe the heating is negligible at an input intensity of the beam current less than 10^{-7} A. /162

The equipment for the method which takes advantage of the attenuation of electron beams consists of the source of the narrow electron beam and the detector. Diaphragms are placed in front of the detector which prevent the impinging of electrons that were deflected from their original direction. The entire equipment can be placed inside the measurement space [247] where it must be shifted and turned, or the walls of the measurement space must have appropriate windows. Another method was used to record the behavior of the density across a shock wave in the gas flow in a shock tube at a low pressure (0.5 torr) when neither the interferometric method nor the X-ray method could be used [254]. The windows in the shock tube had openings with a 10-15 μm diameter in a platinum foil which was 25 μm thick. The source of the electrons was mounted on a spherical suspension whose center of rotation was in the inlet window, which made it possible to adjust correctly the direction of the electron beam. Other types of corpuscular radiation can be handled similarly.

The disadvantage of the method that was described which takes advantage of the attenuation of the electron beam is that it does not furnish simultaneously the entire image of the flow field. However, since, in comparison with the method taking advantage of the absorption of X-rays the reaction time of the detector is much shorter (on the order of several microseconds) the image of the entire flow field can conceivably be obtained with the aid of a special cathode ray tube.

However, in an attempt to obtain on the fluorescent screen simultaneously the electron shadow image of the entire flow field, experiments were also made with a bundle of diverging electron beams with a larger cross-sectional area of the bundle [254]. When a bundle of parallel electron beams enters a gas, the electrons are deflected from the original direction of motion as a result of diffusion and the bundle widens, acquiring the shape of a spindle, until it occupies roughly a spherical space whose diameter is approximately equal to the range of the electron. The air in the region which the electrons enter has a bluish-violet glow.

The schematic diagram of the equipment that was used in [254] to obtain the electron shadow image of the flow is given in Fig. 112. It consists of an air-tight chamber sealed at one end with a glass window through which the screen is observed or photographed from the outside. The gas flow which is studied enters into the chamber from the sides through a nozzle. The required vacuum is maintained in the chamber with the aid of a vacuum pump which is connected to the neck at the side of the chamber. The source of the electron beams, the electron gun, is inside the chamber. The transparent fluorescent screen on which the bundle of impinging electrons forms a circular luminous trace is placed at the distance s_0 from the gun perpendicularly to the axis of the electron beam. When the input energy of the electrons is in the range 3-25 keV, and the pressure in the chamber in the range 1-20 torr, at a distance s_0 = 65 mm the part of the luminous circular trace at any /163
point of which the luminance can be considered to be the same, has roughly a 20 mm diameter. However, beyond this diameter, the luminance of the trace is reduced considerably. Nevertheless, shadow images can be observed under the conditions that were described even when the diameter of the trace is 40 mm. During visual observation, this attenuation of the luminance of the periphery of the field of view does not cause great difficulties. However, it makes the photography more difficult, since the ratio of the luminance on the periphery of the trace to the luminance at the center of the trace is about 1:10. This shortcoming can be eliminated by using an absorption equalizing filter. It can be obtained by photographing the luminous trace on the screen on a photographic plate on a 1:1 scale when the gas whose flow is to be studied does not enter the chamber. The energy of the electrons and the pressure inside the chamber are adjusted to values at which the gas flow will be studied later. The negative is then used as the base to which a fluorescent layer is applied. A transparent fluorescent screen is obtained in this way which must be inserted in the chamber instead of the screen without the filter.

A field of view with larger dimensions can be obtained by using a magnetic lens which expands the originally narrow beam. From the published photographs of the shadow electron image of an airflow from a cylindrical nozzle with a 1 mm diamter into a chamber in which the pressure was 3.2 torr

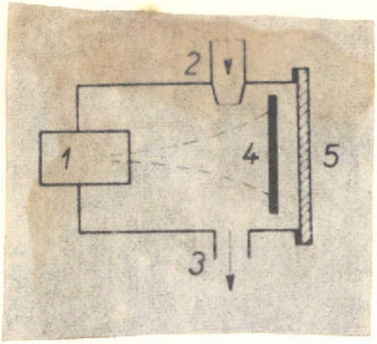

Fig. 112. Schematic diagram of equipment used to obtain the electron shadow image of the flow [245] (1. source of electrons; 2. nozzle; 3. connection for pump; 4. fluorescent screen; 5. glass window).

(the pressure drop on the nozzle was 600 torr) produced by an electron beam with an initial energy of 7.5 keV [254], it can be seen that sufficiently clear images cannot be obtained by this method. Due to this and also due to the entire character of the method, the assertion of the author of the method that quantitative data about the flow field can be obtained with its aid should be accepted with certain reservations. The acquisition of quantitative data would naturally require calibration equipment, i.e. it would require that the relations between the luminance of the trace on the screen, the pressure and the density of the gas layer in the chamber, the thickness of this layer and the deflection of the electron beams from the original direction be determined.

Conclusion

From the survey of the methods that was presented, it follows /164 that the visualization possibilities are far-ranging and that they can be used on a very wide scale. The significance of visualization was already discussed in the introduction. The great number of methods used until now makes it possible to visualize almost any case of flow. Thus, for example, airflow can be visualized from the lowest velocities up to the highest supersonic velocities, by using smoke up to velocities of 30 m/sec, aluminum powder up to velocities of 90 m/sec, and with the aid of interferometric methods, or possibly diaphragm schlieren methods starting with velocities of 60 m/sec, and, finally,for high subsonic and supersonic flows, with the aid of the shadow method. Images of the flow at very low pressures (fractions of a torr) can be obtained, for example, by taking advantage of luminescence exactly like images of the flow of highly viscous fluids by taking advantage of temporary birefringence.

With regard to the cost of the individual methods, the conclusion can be made, on the basis of the survey, that the requirement to obtain quantitative values entails greater expenditures on the equipment. Certain methods in group 3 (the interferometric method and the diaphragm schlieren method) require the most expensive equipment. Further development of methods in this group should be expected in conjunction with the use of laser light sources.

The majority of the methods that were described have already been used many times and in many cases the equipment required for their use has been thoroughly elaborated. On the other hand, very little is known about other newer methods. These are mainly luminescence methods (see p. 56), the temporary birefringence (see p. 75), and the phase contrast methods (see p. 158). For the time being, these methods have not been analyzed and worked out thoroughly, and thus cannot be used on a wider scale.

REFERENCES

General Bibliography

1. Zaks, N. A., Visual'nyye metody izucheniya obtekaniya tel potokom, [Visualization Methods for the Study of Flow around Strealined Bodies], VVIA im. Zhukovskogo, 1949.

2. Zaks, N. A., Osnovy ekperimental'noy aerodynamiky, [Foundations of Experimental Aerodynamics], Oborongiz, 1953.

3. Balint, E., Techniques of Flow Visualization, Aircraft Engng, June 1953.

4. Popov, S. T., Nekotoryye zadachi i metody eksperimental'noy aeromekhaniki, [Some Problems and Methods in Experimental Flight Mechanics], "Gos. isdat. technikoteoreṭich. lit." Press, Moscow, 1952.

5. Pankhurst, R. C., and Holder, D. W., Wind-Tunnel Technique, I. Pitman, London, 1952.

5a. Pankhurst, R., and Holder, D., Tekhnika eksperimenta v aerodinamicheskikh trubakh, [Experimental Techniques in Wind Tunnels] (translation), "Izdat. inostr. lit." Press, Moscow, 1955.

6. Řezníček, R., Výzkum optických vlastností proudících tekutin. Research on Optical Properties of Fluid Flows], Final report on project M-21, Mechanization Department, School of Agriculture, Prague, 1958.

7. Outurquin, R., La visualition au service de l'aeronautique, [Visualization in the Service of Aeronautics], "Technique et Science Aeronautique" Press, 1955.

8. Kurganov, M. M., Vizual'nyye metody issledovaniya potokov [Visualization Methods for the Study of Flows], CAGI [Central Institute of Aerohydrodynamics im. N. Ye. Zhukovskiy], Technical Notes, 1939.

9. Hošek, J., Aerodynamika vysokých rychlostí, [High-Speed Aerodynamics], "Nase vojsko" Press, Prague, 1949.

9a. Hošek, J., Aerodinamika bol'shikh skorostey, [High-Speed Aerodynamics] (translation), "Izdat. inostr. lit." Press, Moscow, 1954.

10. Řezniček, R., Müller, U., and Badin, J., Soubor experimentálních prací v oboru visualisace proudění, prováděných v rámci výzkumné činnosti katedry fyziky VŠZ v Praze [Collection of Experimental Studies in the Field of Flow Visualization Carried Out as Part of the Research at the Physics Department of the School of Agriculture in Prague] (unpublished).

11. Eck, B., Technische Strömungslehre, [Flow Theory in Engineering], "Springer" Press, Berlin, 1954.

12. Brodovicz, K., "Visualization methods applied to the study of media with a nonuniform density distribution," Technika Lotnicza 44 (March-June 1957).

13. Matula, D., "An analysis of methods for the visualization of airflows at low velocities," VZLU, , Letnany, Report, Collection E-70/25-V, 1954.

14. Preston, J. M., "Visualization of boundary-layer flow," Reports and Memoranda 2267 (1946).

15. Horák, Z., and Krupka, F., Fyzika, [Physics], "SNTL/SVTL" Press, 1966.

16. Fuka, J., and Havelka, J., Optika, [Optics], "SPN" Press, Prague, 1961.

17. Brdička, M., Mechanika kontinua, [Continuum Mechanics], "NČSAV" Press, Prague, 1959.

18. Lojcjanskij, L. G., Mechanika kapalin a plynů, [Mechanics of Fluids and Gases], Part I, "SNTL" Press, Prague, 1954.

19. Symposium of Flow Visualization, Collection ASME, 1960.

20. Rektorys, K. et al., Přehled užité matematiky [Survey of Applied Mathematics], "SNTL" Press, Prague 1963.

21. Lau, E., and Krug, W., Die Äquidensitometrie, [Equidensitometry], "Akademie" Press, Berlin, 1957.

22. Lambourne, N. C., and Pusey, P. S. "Some visual observations of the effects of sweep on the low-speed flow over a sharp-edged plate at incidence," Report and Memoranda 3106 (1958). /166

23. Gukosova, Ya. A. et al., Aerodinamicheskoye sovershchenstvovniye lopatochnykh apparatov parovykh i gazovykh turbin, [Aerodynamic Improvement of Bladed Apparatus in Steam and Gas Turbines], "GEI" Press, Moscow-Leningrad, 1960.

Section 1.1.1.

24. Reynolds, O., Papers on Mechanical and Physical Subjects, Cambridge, 1890.

25. Hele-Shaw, H. S., "Experimental Investigation of the motion of a thin film of viscous fluid," Rep. Brit. Assoc. (1898).

26. Hele-Shaw, H. S., "Nature of surface resistance of water and streamline motion under certain experimental conditions," The Engineer (1898).

27. Wortman, F. X., "A method for the observation and measurement of water flows with the aid of tellurium," Zeitschrift für Angewandte Physik 5 (June 1953).

28. Werlé, H., "Nonstationary motion in constant circulation. Results obtained on the basis of hydrodynamic visualization," La Recherche Aeronautique 26 (1952).

29. Werlé, H., "Some experimental results on backswept wings at low velocities obtained in a hydrodynamic tunnel," La Recherche Aeronautique (September-October 1954).

30. "Visualization in a hydrodynamic tunnel," La Recherche Aeronautique (May-June 1953).

31. Jordan, P., "Bouyancy calculations and flow processes when maximum bouyancy is not attained," Luftfahrtforschung 16 (1939).

32. Richardson, "Velocity-gradient methods in rheology," Physics 6 (1935).

33. Van Meel, D. A., and Vermij, H., "A method for flow visualization and measurement of velocity vectors in three-dimensional flow patterns in water models by using color photography," Appl. Sci. Res., Section A 10(2) (1961).

34. Winter, E. F., "Flow visualization techniques applied to combustion problems," J. Roy. Ae. Soc. 62(568) (1958).

35. Myl, J., and Solc, Z., "A method for determining the velocity and direction of streamlines," Chemický průmysl 13(4) (1963).

36. Werlé, H., "Simulation of the effect of the soil in a hydrodynamic tunnel," La Recherche Aerospatiale, No. 95 (1963).

37. Howland, B., and Springer, G. S., "Use of electrochemoluminescence in visualizing separated flows," J. Fluid Mech. 24, 697 (1966).

38. Springer, G. S., "Use of electrochemoluminescence in the measurement of mass transfer rates," Rev. Sci. Instr. 35, 1277 (1964).

39. Goldish, L. H., "Tracer introduction by flash photolysis," Chem. E. Sci. 20, 1011 (1965).

40. McMaster, "Flash photolysis tracer studies," Sen. Project, Rep. University of Delaware, 1964.

41. Allen, M., "Visualization of 3-dimensional flow," Instr. Control system, No. 3, 1966-93.

42. Allen, M., "Better way to trace liquid flow patterns," Ch. Engng 66 (may 1959).

43. Allen, M., "Fluorescent particles for tracing liquids," Chem. Engng. 67 (June 1960).

44. Baker, D. J., "A technique for the precise measurement of small fluid velocities," J. Fluid Mech. 26 (November 1966).

45. Adams, F. G., "A study of the technique of electrochemoluminescence in determining points of separation and transitions," S. M. Thesis, Mass. I. T., 1965.

46. Schiller, T. R., "An apparatus for applying the technique of electrochemoluminescence to boundary layer studies," S.M. Thesis, Mass. I. T., 1964.

Section 1.1.2. /167

47. Relf, E. F., "Photographic investigation of the flow around a model aerofoil," Rep. and Mem. 76 (March 1913).

48. Relf, E. F., Rep. and Mem. 50 (1911-12).

49. Walker, P. B., Rep. and Mem. 1402 (1931-32).

50. Jones, B. M., Farren, W. S., and Lockyer, Rep. and Mem. 1065 (1926-27).

51. Prandtl, L., and Teitjens, O., Applied Hydro- and Aeromechanics, McGraw-Hill, 1934.

52. Prandtl, L., Hydro- und Aeromechanik, [Hydro and Aeromechanics], Vol. II, "Julius Springer" Press, Berlin, 1929.

53. Jerie, J., "Flow through a labyrinth seal," in the collection Výzkum v oboru proudění, [Research in the Field of Flow], Vol. I., "NCSAV" Press, Prague, 1955.

54. Schiegler, L. "The flow process in grate-firing combustion chambers," Z. Ver. Deut. Ing. 82(29).

55. Ahlborn, F., "The hydrodynamic resistance mechanism," Abhandl. geb. d. Naturwiss, Hamburg 17 (1902).

56. Rubach., H., "The origin and motion of a pair of vortices in cylindrical bodies," Forschungshefte des VDI 185 (1916).

57. Timme, A., "The velocity distribution in vortices," Ingenieur-Archiv, No. 1,3 (1957).

58. Pešek, R., "Some results obtained from the visualization of flow," paper read at the scientific conference at the Department of Mechanical Engineering at the Czechoslovak Research Institute for Technology on February 22, 1957.

59. Birkhoff, G., and Caywood, T. E., "Use of air bubbles," J. Appl. Phys. 20, 646 (1949).

60. Caffyn, and Underwood, "An improved method for the measurement of velocity profiles in liquids," Nature (February 9, 1952).

61. Barth, "Application of model experiments to solution of flow problems," Z. Ver. Deut. Ing. 92, 105 (1950).

62. Wuest, W., "Visualization of flows," ATM, No. 329 (1963).

63. Danckwerts, P. V., "Flow visualization by means of a time reaction," J. Fluid Mech., No. 3 (1963).

64. Smith, A.M.O., and Clutter, D. W., "The electrochemical technique of flow visualization," in the collection Symposium on Flow Visualization, ASME, 1960.

65. Schraub, "Use of hydrogen bubbles for quantitative determination of time-dependent velocity fields in low-speed water flows," ASME Paper 64, WA/FE-20.

Section 1.2.1.

66. Preston, J. H., and Sweeting, N. E., "Wood smoke as a means of visualizing boundary-layer flow at high Reynolds number," Rep. and Mem. 2023 (1943).

67. Lippisch, A., "Results from the Deutsche Forschungsanstalt für Segelflug smoke tunnel," J. Roy. Ae. Soc. 43, 93 (1939).

68. Drees, I. J. M., and Hendal, I. W. P., "Airflow patterns in the neighborhood of helicopter rotors," Aircraft Engng 23(266) (April 1951).

69. Salter, C., "Multiple-jet white-smoke generators," Rep. and Mem 2657 (March 1950).

70. "Smoke traces aerodynamic patterns," Aviation Week 64, 12 (1956).

71. Brat, J. S., "Flow patterns in the wake of an oscillating aerofoil," Rep. and Mem. 2773 (March 1950).

72. Brown, F. N., "An American method of photographing flow patterns," Aircraft Engng 24, 280 (1952).

73. Herzig, H. Z., and Hansen, A. G., "Visualization studies of secondary flows with applications to turbomachines," Trans. ASME 77, 3 (1955).

74. Herzig, H. Z., and Hansen, A. G., "Airflow studies in miniature smoke jet wind tunnels," Aero Digest 72, 6 (1956).

75. Brown, F. N., "Fundamental flow patterns," Aircraft Engng. /168
28, 331 (1956).

76. Preston, J. H., and Sweeting, N. E., "An improved smoke generator for use in the visualization of airflow particularly boundary-layer flow at high Reynolds number," Rep. and Mem. 2023 (1943).

77. Farren, W. S. "Airflow with demonstration on the screen by means of smoke," J. Roy. Ae. Soc. 36, 454 (1932).

78. Clark, K. W., "Methods of visualizing airflow with observations on several aerofoils in the wind tunnel," Rep. and Mem. 1552 (1933).

79. Tanner, T., "Movement of smoke in the boundary layer of an aerofoil without and with slot," Rep. and Mem. 1352 (1933).

80. Simons, F. G., and Dewoy, N. S., "Wind tunnel experiments with circular discs," Rep. and Mem. 1334 (1930).

81. Simons, F. G., and Dewoy, N. S., "Photographic records of flow in the boundary layer," Rep. and Mem. 1335 (1931).

82. Simons, F. G., and Dewoy, N. S., "Results from the aerodynamic testing station in Göttingen," Lieferung 2 (1923).

83. Hazen, D. C., "On visual aerodynamics," The Aeroplane (July 15, 1955).

84. Jacobs, E. N., and Sherman, A., "Airfoil characteristics as affected by variations of the Reynolds number," NACA T.R. 586, 1937.

85. Townend, H.C.H., "On rendering airflow visible by means of hot wires," Rep. and Mem. 1349 (1931).

86. Townend, H.C.H., "Hot wire and spark shadowgraphs of the airflow through an airscrew," Rep. and Mem. 1434 (1932).

87. Hampl, J., and Holý, S., "Visualization of flow by means of the shadow method at low velocities," report from SVK [expansion unknown] to the Czechoslovak Technical Research Institute under the leadership of Professor Pesek.

88. Schrüfer, E., "The form of the ray during airflow in a vacuum," Zeit. f. Angewandte Physik 9, 2 (1957).

89. Kunkel, W. B., and Hurlbut, F. C., "Luminescent gas visualization for low-density wind tunnels," J. Appl. Phys. 28, 8 (1957).

90. Fowler, H. S., "A smoke generator for use in wind tunnels," NRC 8225 (research report MET-452), 1964.

91. Hansen, A. G., "Smoke studies of secondary flows in bends, tandem cascades and high turning configurations," NACA Res. Mem.

92. Hansen, A. G., Aero Digest 72(6) (1956).

93. Lippisch, A. M., "Flow visualization," Aero. Eng. Rev. 30(2) (1958).

94. Früngel, F., Impulsetechnik, [Pulse Technique], Leipzig, 1960, p. 378.

95. Bomelburg, H. J., et al., "The electric spark method for quantitative measurements in flowing gases," ZFW 7(11) (1959).

96. Gregore, I. Mc., "The vapor-screen method of flow visualization," J. Fluid Mech. 11(4) (1961).

97. Hall, I. M. et al., "Experiments with inclined blunt-nosed bodies at M_0 = 2.45," Rep. and Mem. 3128 (1957).

Section 1.2.2

98. Bourot, J. M., Chronofotographie des Champs Aérodynamiques, [Chronophotography of aerodynamic fields], "SDITA" Press, Paris, 1949.

99. Bourot, J. M., "Balsa dust shows rotor flow geometry," Aviation Week 53, 1 (1950).

100. Taylor, M. K., "A balsa dust technique for air-flow visualization and its application to flow through model helicopter rotors in static thrust," NACA T.N. 2220, November 1950.

101. Lebouf, R., and Voret, C., "Microphotography of carbide particles pulverized in a combustion chamber," Rech. Aeronautique 45 (1955).

102. Girard, A., and Robert, E., "Stereoscopic chronophotography of particles in a suspension in an aerodynamic flow," Rech. Aeronautique 49 (January, February 1956). /169

103. Townend, H. C., "A method of air cinematography capable of quantitative analysis," J. Ae. Sci. 3 (1936).

104. Townend, H. C., "Visual and photographics methods of studying boundary-layer flow," Rep. and Mem. 1803 (1937).

105. Townend, H. C., "Abstract of a film illustrating the theory of flight," Rep. and Mem. 1767 (1937).

106. Laniece, F., and Tisseau, R., "A study of the aerodynamic field by means of a perturbation method," Rech. Aeronautique 34 (July, August 1953).

107. Tisseau, M., "Measurement of aerodynamic velocities by means of a perturbation method," Rech. Aeronautique 5 (1948).

108. Bird, J. D., "Visualization of flow fields by use of tuft grid technique," J. Ae. Sci. 19, 7 (1952).

109. Kubeš, J., "Flow in a drum blower with blades bent forward," in the collection Výzkum v oboru proudění, [Research in the Field of Flow], Part I, "NČSAV" Press, Prague, 1955.

110. Schlichting, H., "Aerodynamics of the mutual interference of aircraft parts," British R.A.N. Library Transl. 275 (1948).

111. Purser, P. E., Spearman, M. L., and Bates, W. R., "Investigation of low speed of downwash characteristics of small-scale swept-back wings," NACA T.N. NO. 1378, 1947.

112. Kedi, U. M., "Velocity measurement with the aid of illuminated or luminescent particles," article in [146a], p. 147.

113. "Method for the visualization of flows in gaseous media," Die Technik 15(6) (1960).

114. Benetka, J., Cejchováni směrových sond, [Calibration of directional Probes], "VZLU" Press, Letnany, 1964.

115. Maltby, R. L., "Flow visualization in wind tunnels using indicators," AGARDograf 70, 1962.

Section 2.1

116. Main-Smith, J. D., "Chemical solids as diffusible coating film for visual indications of boundary-layer transition in air and water," Rep. and Mem. 2755 (February 1950).

117. Walker, W. P., "Detection of laminar flow on ship models," Trans. Inst. Nav. Arch. (April 1949).

Section 2.2

118. Jaňour, Z., "Experimental analysis of the development of the boundary layer on a profile," Report of the Aeronautical Research Institute, Letňany, No. 6, 1949.

119. Preston, J. H., and Sweeting, N. E., "experiments on the measurement of transition position by chemical methods," Rep. and Mem. 2014 (1945).

120. Owen, P. R., and Ormerod, A. O., "Evaporation from the surface of a body in an airstream," Rep. and Mem. 2875 (September 1951).

121. Richards, E. J., and Burstall, F. H., "The china-clay method of indication transition," Rep. and Mem. 2126 (1945).

122. Holder, D. W., "Transition indication in the National Physical Laboratory 20 in x 8 in high-speed tunnel," Rep. and Mem. 2079 (1945).

123. Gray, W. E., "A simple visual method of recording boundary layer (liquid film)," Tech. Note Aero., RAE 1816 (1946).

124. Jones, B. M., "Airfow about stalled and spinning aeroplanes shown by cinematograph records of the movements of wool tufts," Rep. and Mem. 1494 (1932).

125. Abbot, I. H., and Sherman, A., "Flow observation with tufts and lampblack of the stalling of four typical airfoil sections in the NACA variable density tunnel, " NACA T.N. 672, 1938. /170

126. Smith, A.M.O., "A dust method for locating the separation point," J. Ae. Sci. 22, 4 (1955).

127. Khabinskaya, S. P., Opyty po opredeleniyu oblasti sryva na trokh krylyakh so shchitkami i eleronamy, [Experiments in Determining the Stall Region on Three Wings with Flaps and Ailerons], CAGI [Central Institute of Aerohydrodynamics im. N. Ye. Zhukovskiy], Technical Notes, 1939.

128. Murphy, J. S., "Measurement of wall shearing stress in the boundary layer by means of an evaporating liquid film," J. Appl. Phys. 27(9) (1956).

129. Hignett, E. T., The Use of Dust Deposition as a Means of Flow Visualization, Her Majesty's Office, London, 1963.

130. Hignett, E. T., "Surface flow pattern as visualized by dust deposits on the blades of a fan," J. Roy. Ae. Soc. 67, 633 (1963).

131. Persoz, B., and Gernier G., "Visualization by means of tufts with a fatty base," Rech. Aéron., No. 60 (1957).

132. Garner, H. C., and Bryer, D. W., "Experimental study of surface flow and part-span vortex layer on a cropped arrowhead wing," Rep. and Mem. 3017 (1957).

133. Tigue, J. G. Mc. et al., "Two techniques for detecting boundary layer transition in flight at supersonic speeds and at altitudes above 20,000 feet," NASA T.N. D-18, 1959.

134. Haines, A. B., Some Notes on the Flow Patterns Observed over Various Sweptback Wings at Low Mach Numbers, H. M. Stationary Office, London, 1960.

135. Hopkins, E. J. Et al., "Photographic evidence of streamwise arrays of vortices in boundary-layer flow," NASA, T.N., D-328, 1960.

136. Loving, D. L., and Katzoff, S., "The fluorescent-oil film method and other techniques for boundary-layer flow visualization," NASA Memo 3-17-59 L, 1959.

137. Stalder, J. R., et al., "The use of a luminescent lacquer for the visual indication of boundary-layer transition," NACA T. N. 2263, 1951.

Section 3.1

138. Boeder, P., "Birefringence in flow," Zeitschr. für Physik 75 (1932).

139. Cvětkov, V. N., "Some optical methods for the study of micromolecular structures in solutions," Chemické listy 49, 10 (1955).

140. Wellwer, R., Middlehurst, D. J., and Steiner, R., "The photo viscous properties of fluids," NACA T.N. 841, 1942.

141. Weller, R., "The optical investigation of fluid flow," J. Appl. Mech. 14 (1947).

142. Lindgren, E. R., "Note on the flow of liquids in tubes," Appl. Sci. Research 44 (1954).

143. Leaf, W., "Fluid flow study of locomotive firebox design," Mech. Engng. 67 (1945).

144. Řezníček, R., "The use of temporary birefringence of fluid flows in the visualization of flows," paper read at the scientific conference at the Mechanical Engineering Department at the Czechoslovak Research Institute for Technology on February 22, 1957.

145. Maxwell, I. C., Proc. Roy. Soc. 22 (1873-74).

Section 3.2

146. Landenburg, R. W., Lewis, B., Pease, R. N., and Taylor, H. S., Physical Measurements in Gas Dynamics and Combustion, Princeton Univ. Press, Princeton, 1954.

146a. Ladenburg, R. W., Lewis, B., Pease, R. N., Fizicheskiye izmereniya v gazovoy dinamike i pri gorenii, [Physical Measurements in Gas Dynamics and Combustion] (translation), "Izd. inostr. lit." Press, Moscow, 1957.

147. Kašpar, J., "Application of shadow and mist method to the visualization of density changes in the flow and temperature field," Research report No. V 857/66, VZLU, 1966.

148. Shitov, V. A., and Sokolova, V. A., "Methods for the photography of aerodynamic spectra at supersonic velocities," Trudy VVLA 62 (1940).

149. Horwath, L., Squire, H. B., and Lock, C. N. H., Modern Developments in Fluid Dynamics in High-Speed Flow, Vol. II, Oxford, 1953. /171

150. Lemens, P. et al., "Development of apparatus for a hypersonic ballistic installation..." in the collection Sovremennaya tekhnika aerodinamichekikh issledovaniyi, [Modern Techniques for Aerodynamic Studies], Moscow, 1965, p. 186.

151. Hotz, R., "NACA shows Ames Laboratory progress," Aviation Week 49(4) (1948).

152. Ferri, A., Aerodinamika sverkhzvukovykh techeniy, [Aerodynamics of Supersonic Flows], "Gos. izd. tekhn. teoret. literatury" Press, Moscow, 1953.

153. Chilton, U. F., Aerodinamika bol'shikh skorostey, [High-Speed Aerodynamics], "Izd. inostr. literatury" Press, Moscow, 1955.

154. Wilson, M. R., and Hiemenz, R. J., "High-speed multiple-spark light sources," Rev. Sci. Instr. 29(11) (1958).

155. Kumar, S. S., "A high-intensity spark light source for schlieren and direct shadow photography," NAL Tech. Note, 1964.

156. Ferri, A., "Method for evaluating from shadow or schlieren photographs," NACA Tech. Note 1808, 1949.

157. Price, E. W., et al., "Contrast and color in interference fringes," Rev. Sci. Instr. 24 (1953).

158. Holder, D. W. et al., "A high-speed camera for the photography of shock-wave oscillation in a wind tunnel," Rep. and Mem. 2901 (1949).

159. Seiff, A., and Short, B. J., "An investigation of supersonic turbulent boundary layers on slender bodies of revolution in free flight by use of Mach-Zehnder interferometer and shadowgraphs," NACA Tech. Note, 1958.

160. Sammonds, R. I., "The shock-wave patterns on a cranked-wing configuration," NACA Tech. Note D-346, 1960.

Section 3.2.1

161. Dvorak, V., "A new simple method for schlieren observations," Ann. d. Phys. u. Chem. 9, 502 (1880).

162. Schardin, H., "The schlieren method and its applications," Ergebnisse d. exakten Naturwissenschaften 20 (1942).

163. Hankins, G. A., and Cope, W. F., "The flow of gases at sonic and supersonic speeds," Proceedings of the Institution of Mechanical Engineers, 1946, p. 155.

164. Bukovský, J. J., "Research on cascades in turboengines at high velocities," in the collection Proudění v lopatkových strojich, [Flow in Cascade Machines], "NČSAV" Press, Prague, 1958.

165. Ormerod, A. O., "Note on the use of the three-dimensional shock-wave recorder for studying interference in supersonic wind tunnel," Reports and Memoranda 2798 (December 1950).

166. Kovasznay, L. S. G., Technique for the Optical Measurement of Turbulence in High-Speed Flow, Publications of the Am. Soc. Mech. Engrs., 1949.

167. Petrov, G. I., Primeneniya tenevogo metoda dlya issledovaniya spektrov vozdushnogo potoka, [Application of Shadow Method to the Study of Airflow Spectra], "CAGI [Central Institute of Aerohydrodynamics im. N. Ye. Zhukovskiy], Technical Notes, No. 107, 1936.

168. Lamplough, F. E., "Shock-wave shadow photography in tunnel and in flight," Aircraft Engng (April 1951).

169. Véret, C., "Shadowgraph apparatus for the S2 Modane wind tunnel," La Rech. Aéron. 90 (1962).

170. Love, E. S., "A new shadowgraph technique for the observation of conical flow phenomena in supersonic flow and preliminary results obtained for a triangular wing," NACA Tech. Note 2950, 1953.

Section 3.2.2

171. Schardin, H., "The Töpler schlieren method," VDI Forschungsheft 5, 367 (1934).

172. Schardin, H., Vozmozhnosti eksperimental'nogo issledovaniya snaryadov v polete, [The Possibility of an Experimental Study of Projectiles in Flight], technical translation No. 106, NII-I, 1949.

173. Töpler, A., "Observations based on a new method," Poggendorfs Ann. d. Phys. u. Chem. 127, 128, 131, and 134 (1966-1868) /172

174. Holder, D. W., "The toepler schlieren apparatus," Rep. and Mem. 2780 (April 1950).

175. Speak, G. S., and Walter, D. J., "Optical considerations and limitations of the schlieren method," Rep. and Mem. 2859 (January 1950).

176. Mair, W. A., "The sensitivity and range required in a Toepler schlieren apparatus for photography of high-speed airflow," The Aeronautical Quarterly 4 (August 1952).

177. Kantrowitz, A., and Trimpi, R. L., "A sharp-focusing schlieren system," J. Ae. Sci. 17 (1950).

178. Jeffree, H., "A wide-range schlieren system," J. Sci. Instr. (January 1956).

179. Barry, F. W., and Edelman, G. M., "An improved schlieren apparatus," J. Ae. Sci. 15 (June 1948).

180. Sukhorukikhm V. S., "The functioning of the Töpler apparatus from the standpoint of geometric and wave optics," report No. 231, State Red Banner Scientific Testing Institute of the Air Force, 1944.

181. Tatarenchik, V. S., "Application of the Töpler optical method to a study of flow around airfoils at high subsonic velocities," Report of the State Red Banner Scientific Research Institute of the Air Force, 1944.

182. Sukhorukikh, V. S., "Testing of the Töpler instrument in a high-velocity wind tunnel," Report of the State Red Banner Scientific Research Institute of the Air Force, p. 231.

183. Veret, C., "Stereoscopic schlieren photography," La Recherche Aéronautique (September-October 1952).

184. Picard, C., "Schlieren photographic analysis of three-dimensional supersonic flows," La Recherche Aéronautique (March-April 1953).

185. Barnes, N. F. and Belinger, S. L., "Schlieren and shadowgraph equipment for airflow analysis," J. Opt. Soc. Am. 35, 497 (1945).

186. Ronchi, V., "Optical systems test," Rev. Opt. (Bologna) 5 (1926).

187. Ronchi, V., "Camera catches shock waves in flight," Aviation Week 49 (September 13, 1948).

188. Valensi, J., and Pruden, F. Q., "Some observations on sharp-nosed profiles at supersonic speed," Rep. and Mem. 2482 (May 12, 1947).

189. Hilton, W. F., and Fowler, R. G., "Photographs of shock wave movements," Rep. and Mem. 2692 (Dember 1947).

190. Dunsby, J. A., "Schlieren tests on some conventional turbine cascades," Rep. and Mem. 2728 (September 1949).

191. Kaspar, J., "Visualization of flow in the study of turbine cascades," Die Schwerindustrie der Tschechoslowakei 8 (1966).

192. Kaspar, J., Schlierengërate, [Schlieren Apparatus], Mess 32-280-1 Jena.

193. Brandfield, W. S., and Fish, W. Y., "A high-speed schlieren technique for investigation of aerodynamic transients," J. Ae. Sci. (June 1952).

194. Véret, C., "Schlieren photograph apparatus for the S3 Modane wind tunnel," Rech. Aéron. 78 (1960).

195. Bradfield, W. S., and Sheppard, J. J., "Microschlieren," Aerospace Eng. 18(5) (1959).

196. Thomas, G. M., "Measurement technique for nonequilibrium flow and studies of blast wave propagation," ARS 32(8) (1962).

197. Leonard, D. A., and Keck, J. C., "Schlieren photography of projectile wakes using resonance radiation," ARS 32(7) (1962).

198. Nebbeling, C., "A simple method for simultaneous projection of a schlieren image on a viewing screen and into a camera," J. Roy. Ae. Soc. 67, 631 (1963).

199. Creedon, J. E., and Sterling, J., "Multiple simultaneous imaging schlieren system," J. Roy. Aer. Soc. 68(2) (1964).

200. Creedon, J. E., and Sterling, J., "Photographs obtained with the schlieren No. 80 photographic equipment on microfilm," Janaer Rundschau 9(2) (1964).

201. Lawrence, L. F. et al., "A self-synchronizing stroboscopic schlieren system for the study of unsteady air flows," NACA Techn. Note 2509, 1951.

202. Dubois, G., "A method for visualizing supersonic flows," Rech. Aéron., No. 53 (1956). /173

203. Vas, I. E., "An experimental investigation of the flow over simple two-dimensional and axial symmetric bodies at hypersonic speeds," Jet Propulsion 28(2) (1958).

204. Nebe, V., "Schlieren photographic equipment NO. 80, universal equipment for optical studies," Jenaer Rundschau 3, 4(1958).

205. Grubman, D. H., "Method of determining boundary layer thickness from schlieren photographs," ARS 32(8) (1962).

206. "Basic optical studies of the change in the boundary layer of a supersonic airflow," Feingerätetechnik 11(12)(1962).

207. "Optical schlieren observations in heat flows," Jenaer Rundschau 8(3)(1963).

208. Earnshaw, K. B., and Benedict, Ch. M., "An ultra-high speed image dissecting camera for photographing strong shock waves," Eng. and Instr. 66C(4) (1962).

209. Lebduška, J., "Experimental methods for a high-speed tunnel," in the collection Výskum v oboru proudění [Research in the Field of Flow], Part I, "NCSAV" Press, Prague, 1955.

210. Surget, J., "Quantitative schlieren photography with a color grid with multiple input slits," Rech. Aérospat., No. 97 (1963).

Section 3.2.3

211. Holder, D. W., and North, R. J., "Color in the wind tunnel," The Aeroplane (January 4, 1952).

Section 3.2.4.

212. Hutton, S. P., "The use of interferometers in aerodynamics at the L.F.A Brunswich, Germany," Rep. and Mem. 2366 (July 1946).

213. Ashkenas, H. I., and Bryson, A. E., "Design and performance of a simple interferometer for wind-tunnel measurements," J. Ae. Sci. 18 (February 1951).

214. Zobel, Th., Hochgeschwindigkeitskanal der Luftfahrtforschungsanstalt Braunschweig und seine Messeinrichtungen, [The High-Speed Wind Tunnel of the Braunschweig Aeronautical Research Facility and Its Measurement Apparatus], German Academy for Aeronautical Research, Berlin, 1944.

215. Mokrý, M., "Aerodynamical measurements using the Mach-Zehnder interferometer," report No. Z-239/67 of the Thermomechanics Institute at the Czechoslovak Academy of Sciences, 1967.

216. Zeiss, C., "Mach-Zehnder interferometer," Report G-41-270-1, Jena.

217. Kašpar, J., "Mach-Zehnder interferometer," VZLU Report No. V 784/65, 1965; also published in Zpravodaj VZLU 3, 51 (1965) and in Trojnický cåsopis SAV 17(1) (1965).

218. Faulders, C. R., "An interferometric study of the boundary layer on a turbine nozzle blade," Transactions of the ASME 76 (January 1954).

219. Bershader, D., "An interferometric study of supersonic channel flow," Rev. Sc. Instr. 20 (1949).

220. Bryson, A. E., "An experimental investigation of transonic flow past two-dimensional wedge and circular section using a Mach-Zehnder interferometer," NACA report 1094, June 1, 1951.

221. "Interferometric analysis of airflow about projectiles in free flight," J. Appl. Phys. 23 (April 1952).

222. Eckert, E., Strömungsuntersuchungen in Turbomaschinen, [Studies of Flow in Turboengines], German Academy for Aeronautical Research, Berlin, 1944.

223. Mach, L., "An interference refractometer," session on report to the Academy of Sciences, Math., Natural Science Department, Section 2A, 102, 1035-1056 (1893) 101, 5-10 (1892).

224. Bouniol, F. and Chevalierias, R., "Interferometer with large field for a supersonic blower," La Recherche Aéronautique, No. 30 (1952).

225. Lamla, E., "Adjustment of the Mach-Zehnder interferometer," Z. Instrumentech. 62 (1942). /174

226. Kinder, W., "Theory of the Mach-Zehnder interferometer and a description of apparatus with a single mirror adjustment," Optik 1 (1946).

227. Kraushaar, R., "A diffraction grating interferometer," Opt. Soc. Amer. 40 (1950).

228. Sterret, J. R., "Investigation of a diffraction grating interferometer for use in aerodynamic research," NACA Tech. Note 2827, 1952.

229. Schardin, H., "Theory and application of the Mach-Zehnder interference-refractometer," Z. f. Instrumentenk. 53 (1933).

230. Tanner, L. H., The Design and Use of Interferometers in Aerodynamics, H.M. Stationary Office, London, 1959.

231. Richter, W., Interferenzgeräte grosser Speigelabmessungen für optische Strömungsuntersuchungen, [Interference Devices for Large Mirror Measurements for Optical Flow Studies], Jahrbuch WGL, 1958.

232. Constans, M., "Causes of errors in interferential interferometry and schlieren photography, Rech. Aéron., No. 86 (1965).

233. Johnstone, R. K. M. et al., "A design for a 6 in. field Mach-Zehnder interferometer," J. Sci. Instr. 42(4) (1965).

234. Motyčka, J., Interferometry a fotoelectrické přístroje, [Interferometers and Electric Photographic Instruments], "CVUT"Press, Prague, 1965.

235. Dubois, G., and Rugué, C., "A method for measuring base pressure," Rech. Aéron., No. 79 (1960).

236. Philbert, M., and Dubois, G., "The visualization of aerodynamic flows at low densities," Rech. Aéron., No. 81 (1961).

237. Tanner, L. H., "The design of laser interferometers for use in fluid mechanis," J. Sci. Instrum., 43(12) (1966).

238. Wood, G. P. et al., "Investigation with an interferometer of the flow around a circular-arc airfoil at Mach numbers between 0.6 and 0.9," NACA Tech. Note 2693, 1952.

239. Howes, W. L. et al., "A theory and method for applying interferometry to the measurement of certain two-dimensional gaseous density fields," NACA Tech. Note 1693, 1952.

240. Zobel, Th., "Flow measurement by means of light interference," NACA Tech. Note 1253, 1949.

241. Werner, F. D., and Leadon, B. N., "Very accurate measurements of fringes shifts in an optical interferometer study at gas flow," Rev. Sci. Instr. 24 (1953).

242. Guinne, P., and Bouniol, F., "Determination of the velocity field in front of a shock wave on the basis of an interferogram," Rech. Aéron., No. 53 (1956).

243. Tanner, L. G., "Some applications of holography in fluid mechanics," J. Sci. Instrum. 43(2) (1966).

244. Helfinger, L. O., et al., "Holographic interferometry," J. Appl. Phys. 37(2) (1966).

Section 3.2.5

245. Erdmann, S. F., "A new very simple interferometer for obtaining flow images that can be evaluated quantitatively," Appl. Sci. Research B2 (1951).

246. van der Vorren, A. I., "Theory of the Erdmann interferometer for investigation of compressible flows," Appl. Sci. Research B3 (1952).

247. Saunder, M. J., and Smith, A. G., "Phase contrast observations," J. Appl. Phys. 27 (1956).

Section 3.2.6

248. Hurlbut, F. C., Techniques of Flow Visualization Applicable on Low Density Fields (see [19]).

249. Dimeff, J., et al., "X-ray instrumentation for density measurements in supersonic flow field," NACA Tech. NOte 2845, 1952. /175

250. Shermann, P. M., "Visualization at low-density flows by means of oxygen absorption of ultraviolet radiation," J. Ae. Sci. 24(2) (1957).

251. Evans, R. A., "A new visualization method in wind tunnels at low densities," Voprosy raketnoy tekhniki 8(4) (1958).

252. Winkler, E. M., X-Ray Technique (see [146 and 146a]).

253. Grün, A. E. et al., "Electron shadowgraphs and afterglow pictures of gas jets at low densities," J. Appl. Phys. 24 (1953).

254. Schumacher, B., "Images of gas flows obtained by electron beams," Ann. Physik, Ser. 6 (1953).

255. Venable, D., and Kaplan, D., "Electron beam method of determining density profiles across shock waves in gases at low densities," J. Appl. Phys. 26 (1955).

The literature that was presented in this bibliography can also be obtained, with certain exceptions, in our libraries, namely in

1. the State Technical Library in Prague,
2. the VZLU Library in Letnany
3. the Mathematics-Physics Department Library at Charles University in Prague.